DROUGHT IN LUVUVHU RIVER CATCHMENT – SOUTH AFRICA: ASSESSMENT, CHARACTERISATION, AND PREDICTION

Fhumulani I. Mathivha

Student Number: 11560876

A thesis submitted to the Department of Hydrology and Water Resources, School of Environmental Sciences at the University of Venda in fulfilment of the Requirements for the Degree of Doctor of Philosophy in Environmental Sciences (Hydrology).

Promoter **: Prof H. Chikoore**

Co-Promoters **: Dr C. Sigauke**

: Prof J.O. Odiyo

September 2020

DECLARATION

I, **Fhumulani Innocentia Mathivha** hereby declare that the Ph.D. thesis titled **"Drought in Luvuvhu River Catchment: Assessment, Characterisation and Prediction"** submitted to the Department of Hydrology and Water Resources at the University of Venda in fulfillment of a Ph.D. degree in Environmental Sciences (Hydrology) under the supervision of Prof H. Chikoore, Dr. C. Sigauke and Prof J.O. Odiyo is my work and has never been submitted to the University of Venda or any other institution of higher learning for the fulfilment of the requirements of a Ph.D. degree. All the referenced material contained have been duly acknowledged.

08-09-2020

SIGNATURE DATE

Fhumulani Innocentia Mathivha

ABSTRACT

Demand for water resources has been on the increase and is compounded by population growth and related development demands. Thus, numerous sectors are affected by water scarcity and therefore effective management of drought-induced water deficit is of importance. Luvuvhu River Catchment (LRC), a tributary of the Limpopo River Basin in South Africa has witnessed an increasing frequency of drought events over the recent decades. Drought impacts negatively on communities' livelihoods, development, economy, water resources, and agricultural yields. Drought assessment in terms of frequency and severity using Drought Indices (DI) in different parts of the world has been reported. However, the forecasting and prediction component which is significant in drought preparedness and setting up early warning systems is still inadequate in several regions of the world. This study aimed at characterising, assessing, and predicting drought conditions using DI as a drought quantifying parameter in the LRC. This was achieved through the application of hybrid statistical and machine learning models including predictions via a combination of hybrid models.

Rainfall and temperature data were obtained from South African Weather Service, evapotranspiration, streamflow, and reservoir storage data were obtained from the Department of Water and Sanitation while root zone soil moisture data was derived from the NASA earth data Giovanni repository. The Standardised Precipitation Index (SPI), Standardised Precipitation Evapotranspiration Index (SPEI), Standardised Streamflow Index (SSI), and Nonlinear Aggregated Drought Index (NADI) were selected to assess and characterise drought conditions in the LRC. SPI is precipitation based, SPEI is precipitation and evapotranspiration based, SSI is based on streamflow while NADI is a multivariate index based on rainfall, potential evapotranspiration, streamflow, and storage reservoir volume. All indices detected major historical drought events that have occurred and reported over the study area, although the precipitation based indices were the only indices that categorised the 1991/1992 drought as extreme at 6- and 12- month timescales while the streamflow index and multivariate NADI underestimated the event. The most recent 2014/16 drought was also categorised to be extreme by the standardised indices. The study found that the multivariate index underestimates most historical drought events in the catchment. The indices further showed that the most prevalent drought events in the LRC were mild drought. Extreme drought events were the least found at 6.42%, 1.08%, 1.56%, and 4.4% for SPI, SPEI, SSI, and NADI, respectively. Standardised indices and NADI showed negative trends and positive upward trends, respectively. The positive trend showed by NADI depicts a decreased drought severity over the study period.

Drought events were characterised based on duration, intensity, severity, and frequency of drought events for each decade of the 30 years considered in this study i.e. between 1986 – 1996, 1996 – 2006, 2006 – 2016. This was done to get finer details of how drought characteristics behaved at a 10-year interval over the study period. An increased drought duration was observed between 1986 - 1996 while the shortest duration was observed between 1996 - 2006 followed by 2006 - 2016. NADI showed an overall lowest catchment duration at 1- month timescale compared to the standardised indices. The relationship between drought severity and duration revealed a strong

linear relationship across all indices at all timescales (i.e. an R^2 of between 0.6353 and 0.9714, 0.6353 and 0.973, 0.2725 and 0.976 at 1-, 6- and 12- month timescales, respectively). In assessing the overall utilisation of an index, the five decision criteria (robustness, tractability, transparency, sophistication, and extendibility) were assigned a raw score of between one and five. The sum of the weighted scores (i.e. raw scores multiplied by the relative importance factor) was the total for each index. SPEI ranked the highest with a total weight score of 129 followed by the SSI with a score of 125 and then the SPI with a score of 106 while NADI scored the lowest with a weight of 84. Since SPEI ranked the highest of all the four indices evaluated, it is regarded as an index that best describes drought conditions in the LRC and was therefore used in drought prediction.

Statistical (GAM-Generalised Additive Models) and machine learning (LSTM-Long Short Term Memory) based techniques were used for drought prediction. The dependent variables were decomposed using Ensemble Empirical Mode Decomposition (EEMD). Model inputs were determined using the gradient boosting, and all variables showing some relative off importance were considered to influence the target values. Rain, temperature, non-linear trend, SPEI at lag1, and 2 were found to be important in predicting SPEI and the IMFs (Intrinsic Mode Functions) at 1-, 6- and 12- month timescales. Seven models were applied based on the different learning techniques using the SPEI time series at all timescales. Prediction combinations of GAM performed better at 1- and 6- month timescales while at 12- month, an undecomposed GAM outperformed the decomposition and the combination of predictions with a correlation coefficient of 0.9591. The study also found that the correlation between target values, LSTM, and LSTM-fQRA was the same at 0.9997 at 1- month and 0.9996 at 6- and 12- month timescales. Further statistical evaluations showed that LSTM-fQRA was the better model compared to an undecomposed LSTM (i.e. RMSE of 0.0199 for LSTM-fQRA over 0.0241 for LSTM). The best performing GAM and LSTM based models were used to conduct uncertainty analysis, which was based on the prediction interval. The PICP and PINAW results indicated that LSTM-fQRA was the best model to predict SPEI time-series at all timescales. The conclusions drawn from drought predictions conducted in this study are that machine learning neural networks are better suited to predict drought conditions in the LRC, while for improved model accuracy, time series decomposition and prediction combinations are also implementable. The applied hybrid machine learning models can be used for operational drought forecasting and further be incorporated into existing early warning systems for drought risk assessment and management in the LRC for better water resources management.

Keywords: Decomposition, drought, drought indices, early warning system, frequency, machine learning, prediction intervals, severity, water resources.

ACKNOWLEDGEMENTS

First and most importantly the Lord, who gave me the strength, wisdom, and ability to complete the Ph.D. Thesis.

Secondly, I would like to express my sincere gratitude and thanks to the following people and institutions for their assistance and support in making this study possible:

- My promoter, Prof Hector Chikoore, for his supervision, guidance, encouragement, and mentorship throughout the process of undertaking this study. Although he came into the work after two promoters left, he quickly familiarised himself with my work and he offered much-needed guidance to move the Ph.D. forward. His patience and courage to commit to supervising a full-time employed student were instrumental in the success of this study. I appreciate him for believing that I could see this through.

- The co-promoters of this work, Dr. C. Sigauke, and Prof J.O. Odiyo are acknowledged for their guidance and valuable comments in the different sections of the work that helped to improve and shape this Ph.D. thesis.

- My gratitude goes to Dr. M.E. Abdelatif; a Senior Lecturer at Liverpool John Moores University who gave me the courage and motivated me to conduct a study that seeks to predict future hydrological conditions. Her mentorship and guidance during my Ph.D. exchange programme at Liverpool John Moores University were instrumental in shaping this Ph.D. thesis idea.

- Dr. N.B. Mbatha from the Department of Geography at the University of Zululand is highly acknowledged for assistance with MERRA-2 modeled soil moisture data, forecasting model introduction in *R* packages and *Matlab*, and statistical training and guidance.

- Prof A. Taigbenu, Head of School of Civil Engineering, Wits University in his capacity as my mentor in the nGAP programme. His advice and constant availability have been invaluable throughout the Ph.D. study. He always made himself available even with a busy schedule.

- The DHET nGAP program for having afforded me the opportunity of employment and assistance in funding part of the Ph.D. study is also highly acknowledged. The NRF development grant is also acknowledged for its funding at the inception of this study. The AESOP Erasmus Mundus is acknowledged for providing funding for the Ph.D. mobility that was taken up in the Liverpool John Moores University. The University of Venda RPC for funding the Ph.D. study.

- Liverpool John Moores University Civil engineering Ph.D. candidates, in particular, Dr. Salah L. Zubaidi for spending his time introducing me to the fundamentals of MATLAB language.

- Mr. Tendani Mutavhatsindi for his assistance with Pythons *jupyter notebook* training and the introduction to LSTM forecasting.

- Ms. M. Nkosi for her assistance in the literature search and making sure I always smile throughout her stay as an NRF intern under my mentorship. I am very thankful for the light mood she always brought during the darker days of putting this document together.

- Mr. S.M. Matimolane for his assistance with literature that I could not access while not connected to the university server. This helped strengthen the literature presented in the thesis document.

- The South African Weather Services and Department of Water and Sanitation are highly acknowledged for providing the data used in this study.

- I am thankful to my family, grandmother (N.J. Mathivha), my mother (M.J. Mathivha) and siblings Zwidofhela & Masindi, my nephew (Thendokhae Mashudu JNR Mulaudzi), my sisters, Mondi Maisa & Tsireledzani Ragwala and my brother, Mukoma Ragwala, who have provided me with much needed moral and emotional support throughout the study. Their prayers and constantly believing that I can complete the Ph.D. studies are much appreciated.

- The Free United Church in South Africa (Tshalovha) under the leadership of Bishop P.S. Sitholimela. Their prayers and words of encouragement at every congregation went a long way in giving me the strength to see this Ph.D. study through. May God continue to give them strength and wisdom to keep the righteous work going.

- My psychologist, Mme Priscilla Mulaudzi, who enabled me to maintain good mental health during the period of my Ph.D. studies. In the darkest days, she would avail herself and give me much needed support. God can only reward her action during this time of my life as words are not enough.

- I will remain eternally grateful for the love and support of the late Dr. Avhasei "Seimaan" Mudau for his constant belief in my academic ability to carry out this Ph.D. work. For his constant reminder on how it is not easy to attain the highest level of academic status but with that comes a great reward at the end of the tunnel. Dr. Mudau would check on my progress each week either by a phone call if away or just a walk past my office. May his soul Rest in peace.

- Mrs. O.S. Ibeh who came into my life when I was seeking direction spiritually and with my Ph.D. work. Her words of encouragement and prayers are nothing short of God's glory in my life.

- My dogs (Mondi-Superman and Mario-Batman), that were my constant companions and securities through all the sleepless nights I endured while working on this thesis.

- And to all the people I have crossed path with during my Ph.D. journey, those that have supported me directly or indirectly during the compilation of this thesis document.

Thank you for all your encouragement!

DEDICATION

This Ph.D. thesis is dedicated to my late Great grandmother (Musundwa Mukulumedzi Nditsheni Mabogo) who valued education although she was not afforded the opportunity to gain one herself.

And

My guardian Angel ("Mukonanyi wa vhathu")

LIST OF PUBLICATIONS

Fhumulani Mathivha, Hector Chikoore, Caston Sigauke, and John Odiyo (**2020**) Short-Term and Medium-Term Drought Forecasting Using Generalized Additive Models, *Sustainability*, 12, 4006; doi:10.3390/su12104006.

Mathivha, F.I., Mawada A. and Al Kadar, R. (***under review***) Drought assessment using SPI and SPEI over north-eastern South Africa, Jàmbá: *Journal of Disaster Risk Studies, Manuscript no 769.*

Mathivha, F.I. and N.B. Mbatha (*Manuscript in preparation*) MERRA-2 and NDII soil moisture data performance in calibrating NADI.

Mathivha, F.I., Mbatha, N.B and Sigauke, C. (*Manuscript in preparation*) Drought forecasting using Deep learning techniques.

TABLE OF CONTENTS

LIST OF FIGURES

LIST OF TABLES

LIST OF APPENDICES

LIST OF ACRONYMS

AD	Anderson Darling
ADAS	Atmospheric Data Assimilation System
ADI	Aggregated Drought Index
AFRA	Association for Rural Advancement
AGCM	Atmospheric Global Circulation Models
ANN	Artificial Neural Networks
ARIMA	Autoregressive Moving Average
ASALs	Arid and Semi-Arid Lands
CDF	Cumulative Density Functions
DEA	Department of Environmental Affairs
DEAT	Department of Environmental Affairs and Tourism
DI	Drought Index
DMSNN	Direct Multi-Step Neural Networks
DWA	Department of Water Affairs
DWAF	Department of Water Affairs and Forestry
DWS	Department of Water and Sanitation
EEMD	Ensembled Empirical Mode Decomposition
EMD	Empirical Mode Decomposition
EPS	Ensembled Prediction System
EWT	Empirical Wavelet Transform
FANN	Fast Artificial Neural Network
FAO	Food and Agricultural Organisation
FFT	Fast Fourier Transform
GAM	Generalised Additive Model
GLUE	Generalised Likelihood Uncertainty Estimation

GIS	Geographical Information System
GoF	Goodness of Fit
IMFs	Intrinsic Mode Functions
ITCZ	Intertropical Convergence Zone
KNP	Kruger Nation Park
KS	Kolmogorov -Smirnov
LNN	Linear Neural Network
LRB	Limpopo River Basin
LRC	Luvuvhu River Catchment
LSTM	Long Short-term Memory
MAE	Mean Annual Evaporation/ Mean Absolute Error
MAP	Mean Annual Precipitation
MAPE	Mean Absolute Percentage Error
MCS	Monte Carlo Simulation
MERRA	Modern-Era Retrospective analysis for Research and Application
MOS	Model Output Statistics
MSE	Mean Square Error
NADI	Non-Linear Aggregated Drought Index
NASA	National Aeronautics Space Agency
NDDI	Normalised Difference Drought Index
NDVI	Normalised Difference Vegetation Index
NDWI	Normalised Difference Water Index
NLPCA	Non-Linear Principal Component Analysis
PCs	Principal Components
PCA	Principal Component Analysis
PDF	Probability Density Function

PDSI	Palmer Drought Severity Index
PET	Potential Evapotranspiration
PHDI	Palmer Hydrological Drought Index
PICP	Prediction Interval Coverage Probability
PINAW	Prediction Interval Normalised Width
RBFNN	Radial Basis Function Neural Network
RMSE	Root Mean Square Error
RMSNN	Recursive Multi-Step Neural network
SADC	Southern Africa Development Community
SARMA	Seasonal Autoregressive Moving Average
SAWS	South Africa Weather Services
SOM	Self-Organising Map
SPEI	Standardised Precipitation Evapotranspiration Index
SPI	Standardised Precipitation Index
SRI	Standardised Runoff Index
SSI	Standardised Streamflow Index
STOMSA	Stochastic Streamflow Models
SWAT	Soil Water Assessment Tool
SWD	Surface Water Drought
SWSI	Surface Water Supply Index
UN	United Nations
UNDP	United Nations Development Programme
UNESCO	United Nations Educational Scientific and Cultural Organisation
VCI	Vegetation Condition Index
WSVI	Water Supply Vegetation Index

1 INTRODUCTION

Background, Motivation for the study, Research objectives, Research contribution to knowledge, Thesis outline

1.1 Background

Drought is a critical natural hazard, adversely impacting on communities' livelihood, ecosystems, river basins, the environment, and water resource systems (Jahangir *et al*., 2013). It is multi-dimensional and characterised by stochastic processes that are usually related to each other (Shiau *et al*., 2012). For improved planning and management of water supplies, irrigation systems, crop and food security programmes, hydropower generation, and water quality management, drought assessment becomes critical (Abad *et al*., 2013). On a global scale, demand for water resources has been on an increase and this is compounded by population pressures and related developments. Drought-induced water scarcity has affected numerous sectors of the economy; thus, effective management of drought-induced water deficit is of significance. The resulting drought impacts are severe on arid and semi-arid areas than in humid environments (UNDP, 2012). Management of droughts has become an important matter in the world. Its assessment in terms of frequency, duration, and severity using Drought Indices (DI) in different parts of the world has been reported (e.g. Mishra and Singh 2010; Barua, 2010; Belayneh and Adomowski, 2013; FAO, 2004). However, the forecasting and prediction components which are an important aspect of drought preparedness, drought risk assessment, and setting up early warning systems is still inadequate in many regions of the world, including the Limpopo River Basin (LRB) in southern Africa.

On a global scale, drought events have become more frequent and severe due to climate variability and change, with different regions experiencing droughts at varying scales and times (Naumann et al., 2018). Therefore, the global impacts of drought on the environment, agriculture, and socio-economic aspects require attention. Meteorological, agricultural, hydrological and socio-economic droughts are recognised drought types. Drought have either direct or indirect impacts on river basins, including degradation of water resources (Van Vlient, 2015; Safavi and Malek Ahmadi, 2015), reduced crop productivity (Karl et al., 2009; Olesen et al., 2011), increased livestock and wildlife mortality rates, increased land degradation (Inbar,

2017) and increased plant diseases (UN, 2008; Scheffran *et al*., 2012). The indirect impacts include reduced income, reduced tax revenues, increased food prices, unemployment, and increased migration of people and animals. More than 11 million people have died worldwide since 1900, resulting from negative drought impacts (Emergency Event Database; EM-DAT, 2010). This is in addition to a population of two billion that has been adversely affected by the impacts of drought since 1900 (FAO, 2013). Shortages of water resources during drought periods result in ill health, famine & malnutrition, and this remains one of the critical drought challenges (UN, 2008).

African countries are among the most vulnerable to impacts of drought consequences, changing climate, and its variability. Estimates show that about 30% of Burundi, Rwanda, Burkina Faso, Lesotho, and South Africa land areas are severely affected by drought (UNESCO, 2007). The impacts are often adversely affected by social factors such as poverty and diseases. The demand for water, food, and livestock forage on the African continent over time is expected to increase (UNDP, 2012). Drought assessment studies provide an understanding of trends in drought frequency, severity, magnitude, and their associated impacts. Such studies yield information for informed decision making by authorities on support programmes for communities affected by drought. Damages caused by drought because of inadequate water resources may lead to famine due to lower agricultural yields, humanitarian crises, and rationing of water supply.

To cope with the challenges of drought occurrence, its evaluation, prediction, and forecasting are crucial, to formulate effective mitigation measures (Sharda *et al*., 2012). Preparedness of drought is of fundamental importance to effectively mitigate impacts, especially through water resources management under different climate change scenarios. Different techniques are used to assess (i.e. standardised indices, threshold level method, rainfall anomaly index, and deciles index) and predict (regression analysis, stochastic, probabilistic, artificial intelligence-based, hybrids, and dynamic modeling) drought conditions with regards to their spatial and temporal domains. Evaluation and prediction of drought conditions are important to formulate effective drought risk measures in the Luvuvhu River Catchment (LRC).

1.2 Motivation for the study

Drought is a normal feature of the climate and is quite common in southern Africa. The frequency of weather and climate-related disasters have increased in Africa since the 1970s,

with southern Africa reported having become drier between 1974 and 2003 (e.g. Engelbrecht et al., 2009; Lukamba, 2010; Malherbe et al., 2013). Unganai (1994) found that drought is a prevalent natural disaster in southern Africa due to the climatic nature of the region, while according to Ngaka (2012), drought is the most common type of disaster experienced in South Africa. About 65% of South Africa receives rainfall of less than 500 mm/annum (DWAF, 1994; Nyakudya and Stroosnijder, 2011; Dallas and Rivers-Moore, 2013) indicating that agriculture in the country is practiced under arid and semi-arid conditions (Wilhite 1993; Mavhura et al., 2015). Levubu Valley in the LRC is one of the largest agricultural producers in Limpopo Province, thus drought-induced water deficit in the LRC poses a major challenge in the agricultural sector. The LRC is found in a summer rainfall region where agricultural production will be affected by the projected 5% to 10% reduction in annual rainfall (DEAT, 2004; Nyakudya and Stroosnijder, 2011). During drought periods dam water levels drop, i.e. during the 2014/2015 drought (Hawker, 2015). Studies have shown that up to 30% drop in dam levels across South Africa can be realised if a drought event is followed or preceded by a dry year (Vogel, 1994). This severely stresses the water supply systems and communities that depend on such surface water resources for domestic use and subsistence farming as is the case in the LRC.

There exist serious ecological and economic consequences due to drought in the study area which exacerbates existing challenges of communities with global climate change (Maponya and Mpandeli, 2012). The increase in the frequency and intensity of drought in the Limpopo River Basin region have been reported (Biggs *et al*., 2004; Engelbrecht et al., 2015; Gebre and Getahun, 2016; Mosase and Ahaiblame, 2018), which is due to the wide projection of a warm planet, climate and weather variability (Thornton et al., 2014). Kiem and Austin (2013) attributed this to the increased frequency, intensity, and duration of droughts to anthropogenic climate change and further stressed the importance of robust drought adaptation strategies. Climate change emanating from reduced precipitation negatively affects the hydrology and water resources of an area (Singh, 2006). This subsequently reduces runoff and water resource availability. Global trends in precipitation, humidity, drought, and runoff are indicated to be on a negative trajectory in southern Africa (Kundzewicz et al., 2007).

North-eastern South Africa, within which the catchment under study is found in a drought corridor (an area prone to dry spells) which lies between 20° to 25°S in southern Africa (Usman and Reason, 2004). Predictions provide information for better preparedness and developing

better early warning systems for adoption purposes (Panu and Sharma, 2002). Few early-warning systems are implemented since municipalities' disaster management programmes are limited to reacting after disasters (Musyoki *et al*., 2016). There has been a culture of crisis management in many areas around the world, with communities experiencing one disaster after another without or with little risk reduction. Reactive measures do not deal with the root cause of the vulnerability and therefore cannot contribute to drought risk reduction of future drought events (Sifundza et al., 2019; Baudoin et al., 2017; De Stefano et al., 2015). If drought conditions are detected early on, this has the potential to reduce impacts and the need for the government to intervene (Panu and Sharma 2002; Wilhite, 2005). Therefore, there is a need to apply and develop forecasting and prediction methods and techniques that have the potential to determine onset and recovery points of drought, (Mishra and Desai, 2005) especially at catchment level where water resources are managed. Although major drought drivers act over relatively large geographic distances through large-scale atmospheric motions, which are generally forced by SST (Sea Surface Temperature) anomaly, land surface interactions, as well as other external factors superimposed on natural climate variability (Schubert et al., 2016), drought studies at catchment level where water is managed, is also of significance.

To effectively mitigate adverse drought impacts, timely detection, quantification, evaluation, and prediction is critical. There are currently drought forecasting and prediction techniques used in South Africa. The South African Weather Service (SAWS) maintains two separate seasonal forecasting systems, one is dynamic and the other a statistical approach. These are dynamical global Ensemble Prediction System (EPS) using the ECHAM4.5 Atmospheric General Circulation Model (AGCM), and a statistical prediction system based on a Model Output Statistics (MOS) approach (Landman et al., 2012). Department of Water and Sanitation (DWS) determines long-term assurance of supply through a stochastic approach based on historical flow data using marginal distribution, cross-correlation, and serial correlation in the Stochastic Streamflow Model (STOMSA) (DWS, 2013) which is integrated into the Water Resources Yield Model. These models are applied at a regional and national level and therefore cannot account for finer catchment characteristics and the resulting community-level impacts.

Several drought studies have been conducted in the catchment, such as Usman and Reason (2004); Kabanda (2004); Kagoda *et al*. (2010); Maponya and Mpandeli (2012), and Mpandeli and Maponya (2013). Most of these studies focused on drought characterisation, assessment of drought conditions, and impacts of drought. However, Kagoda *et al*. (2010) successfully

performed a one-day forecast of streamflow using Radial Basis Function Neural Network (RBFNN). Although the study was not on hydrological drought forecasting, streamflow can also act as an indicator of hydrological drought, and therefore successful streamflow forecasting can assist in drought planning management. Trambauer *et al*. (2015) conducted a study in the LRB that aimed at seasonal forecasting of hydrological drought at 3, 4, and 5 months' lead times. This study found that the Seasonal Forecasting System (FS_S4) and Forecasting System Conditional Streamflow Prediction Approach (FS_ESPcond) have the potential to forecast seasonal hydrological drought in the LRB.

The current study differs from Kagoda *et al*. (2010), Trambauer *et al*. (2015), and the forecasting system currently in use by SAWS and DWS in that it proposes to predict drought using a multiscalar drought index (drought quantifying parameter) in statistical and deep learning Artificial Neural Network (ANN) models coupled with Empirical Mode Decomposition (EMD) technique. Given that the study area is located in a drought corridor, it is important to carry out drought prediction studies in such areas to ensure proper mitigation measures for water resources management. This will ensure that communities and industries are provided with water during drought events. Although currently, drought prediction exists in South Africa, Mishra and Singh (2010) indicated that it is important to test different forecasting and prediction approaches to have area-specific drought prediction models. The latter is further motivated by the fact that drought in itself is relative; therefore, a drought prediction model for tropical catchment might not be the same for arid catchments.

1.3 Objectives

The main objective of the study is to predict drought by coupling Ensemble Empirical Mode Decomposition with deep learning Artificial Neural Network and statistical models in north-eastern South Africa.

The specific research objectives are to:

i) detect and assess historical drought using drought indices (i.e. SPI, SPEI, SSI, and NADI) over the study area,
ii) characterise drought in the LRC based on duration, intensity, severity & frequency and evaluate the performance of drought indices,
iii) apply hybrid drought prediction models based on deep learning neural networks and statistical learning for the study area.

1.4 Research Hypothesis

i) A multivariate drought index best describes drought conditions in the LRC.

ii) Drought severity increases with timescales.

iii) Hybrid models effectively predict drought conditions in the LRC.

1.5 Research contribution to knowledge

There have been drought studies conducted in the catchment (e.g. Mpandeli and Maponya, 2013; Maponya and Mpandeli, 2012; FAO, 2004, Kagoda *et al*., 2010). Most of these studies only assessed the impacts of drought. It was the study by Kagoda and Ndiritu (2011) that successfully forecasted streamflow time series using ANN at the catchment level. The focus of Kagoda and Ndiritu (2011) was to use the Radial Basis Function Neural Network (RBFNN), which is a type of ANN to account for the uncertainty inherent in hydrological modeling and not to predict drought. The current study aims at applying hybrid models to predict drought making use of a suitable drought index. Although there have been previous studies (e.g. Mishra et al., 2007) that have developed hybrid drought prediction models, the approach used in this study start by determining a suitable index to assess drought in the study area as well as the type of hybrid model's applied. The thesis contributions to knowledge are the following:

- The determination of a suitable drought index to detect and assess drought historical conditions in the LRC. This is because the indices currently used in the catchment have not been tested for their suitability.
- The evaluation of ANN (LSTM) and GAM models to predict drought in the catchment. This has never been attempted in the selected study area in the past making use of a drought index.
- The application of hybrid models to predict drought conditions in the catchment, these types of hybrid models have not been well documented in drought forecasting and prediction literature.

1.6 Thesis outline

The thesis structure is presented in Figure 1.1, clearly showing the seven chapters contained herein. The first chapter looks at the background of the subject matter tackled in this thesis, the motivation behind the study as well as the significance and the contribution to knowledge. A detailed review of literature on drought as a natural hazard with emphasis on hydrological

drought, drought characterisation, assessment, and prediction methodologies is carried out in the second chapter. Chapter 3 details the study area characteristics, its importance, and the datasets used in the study including the sources of the data. The formulation of four selected drought indices is carried out in the fourth chapter. The fifth chapter characterises drought (in terms of frequency, magnitude, and severity) and an evaluation of the selected drought indices based on Keyentash and Dracup (2004) is also done. The sixth chapter details the hybrid drought model applications for the LRC together with their performance evaluation and the best model(s) for this study. A synthesised summary of the thesis findings, the main conclusions are drawn and the recommendations emanating from the study are presented in the seventh chapter.

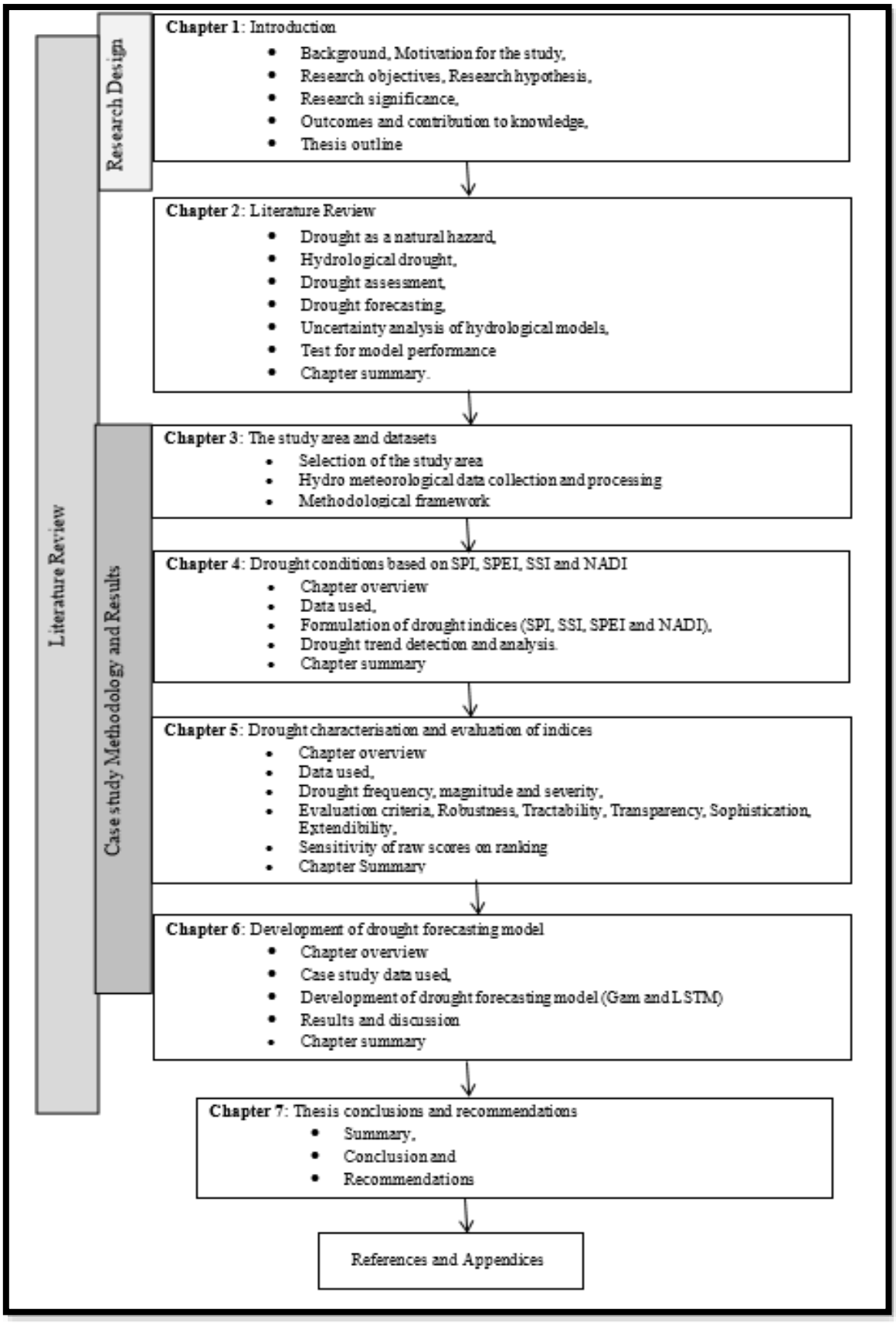

Figure 1.1: Thesis outline

2 LITERATURE REVIEW

Chapter overview, Drought as a natural hazard, Hydrological drought, Drought assessment, Drought prediction, Uncertainty analysis of hydrological models, Summary

2.1 Chapter overview

The chapter reviewed literature associated with drought as a hydrological extreme and the review further informed the types of methodologies and techniques employed in drought science. This chapter reviews the literature on the nature of the South African climate and its variability. The concept of drought as a hazard and how it impacts communities' livelihoods with more emphasis on the Limpopo River Basin are discussed. Drought assessment techniques in the form of drought indices (meteorological, hydrological, and agricultural) are also reviewed. The concepts of drought prediction and forecasting and different techniques used to achieve this, which are the focus of this study are also reviewed in detail. The prediction aspect is reviewed as a scientific technique, its importance in hydrological extremes, and the different methodologies used.

2.2 Climate variability and Climate change

There has been a chain of evidence that support the increased global mean surface temperature and rainfall over the past half-century, with anthropogenic drivers being largely responsible for the warming of the planet (e.g. Alexander et al., 2006; Trenberth et al., 2007; Sánchez-Lugo et al., 2018). Climate change from increased greenhouse gas emissions threatens global services that are closely related to the climate by increasing temperature, changes in the amount and intensity of precipitation, and therefore affecting the variability of climate variables (i.e. temperature, precipitation) (IPCC 2007, 2013). Since internal climate variability is manifested through preferred modes of atmospheric circulation and decadal sea surface temperature variability modulating temperature trends globally (Thompson et al., 2009; Foster and Rahmstorf 2011), regional climate change pace will be modified, which in the coming several decades will potentially obscure anthropogenic-forced regional change (e.g. Deser et al. 2012) and is, therefore, a source significant of near-term regional climate projections uncertainty (Hawkins and Sutton 2011).

A reliable and adequate supply of potable freshwater is necessary for the survival of living organisms on earth and the maintenance and sustainability of terrestrial biotic systems throughout the world (Cook, 2007). However, population increase stresses available water supplies even without the anticipated impacts of climatic variability and climate change. Although there have been improvements in understanding the dynamics of climate variability on a large-scale, much needs to be done on its cascading effects to hydrology, quantity, and quality on catchment for water resources and sustainability (Peng *et al*., 2013). The hydrological cycle and associated extremes (i.e. drought) have been strongly associated with climate variability and change (Mishra et al., 2009). Drought directly reduces crop production since it threatens the water supplies for irrigation (Rana et al., 2016).

The variability and change in climate regimes result in hydrological variability that tends to affect water supply for domestic, industrial, agricultural purposes. For instance, before 2016, 2005 was found to have recorded the warmest global mean annual temperature departure (0.84°C), with 1.08°C the warmest annual temperature departure in the Northern Hemisphere which is comparable to the 1998 annual departure in the Southern Hemisphere annual temperature departure (0.57°C) (Lugina *et al.,* 2006). Global mean temperatures over 2015 and 2016 showing to be the highest compared to all instrumental records (Berger *et al*., 2017). Consequently, such changes directly or indirectly alter the hydrological response of a catchment. Climatic variability plays a key role in the modification of spatial-temporal patterns of precipitation. For instance, Ma *et al*. (2009) indicated that climate variability has altered the hydrological processes, reduced glaciers, and water supply downstream of the Himalaya's catchment.

Various approaches have been used to study changes within different basins. Hydro-meteorological variables and the application of Remote Sensing (RS) and Geographical Information Systems (GIS) techniques have been widely used to detect the effects of climate variability at the catchment level. With population increase throughout the world, food security has also become a major challenge of the 21st century. Historically, when irrigated agriculture was established, competing water users such as domestic and industrial supply were often virtually non-existent (Solomon, 2010; Reisner 1986). In addition, environmental water requirements were given little attention. It becomes important to evaluate how hydrological variability impacts on agricultural yields at the catchment scale for food security given the increasing population.

2.3 Drought occurrence

Drought phenomena are characterised by water scarcity that falls below normal or defined threshold levels. The different application defines the term drought differently (UNDP, 2012), and a universal definition does not exist. However, drought is expressed in terms of precipitation deviation from the normal, soil-water deficit, low flows, reservoir levels, and groundwater level. For example, a hydrological-drought occurs when the river and/or groundwater levels are relatively low (Van Loon, 2013). In addition, water-resources drought occurs when a river basin experience low flow, reduced reservoir volume, and groundwater levels which affects water intense activities.

Water-resources drought is influenced by climatic and hydrological variables, water resource system characteristics, and the basin drought management practices (Van Loon, 2013). Hydrological-drought mainly deals with low streamflow which adversely affects various aspects of communities' livelihood such as food security, water supply, and hydropower generation (Karamouz *et al*., 2009; Belayneh and Adamowski, 2013). The recurrence of droughts may result in the desertification of vulnerable semi-arid and sub-humid environments. Drought occurrence further compromises these fragile ecosystems, resulting in critically degraded water resources, soil structure including soil fertility (El-Jabi *et al*., 2013).

There four main categories of droughts as described by Wilhite and Glantz 1(985); Tallaksen and Van Lanen (2004); Mishra and Singh (2010); Sheffield and Wood (2011); Zoljoodi and Didevarasl (2013), i.e. Meteorological, Hydrological, Agricultural and Socio-economic droughts as depicted in Figure 2.1. The propagation of hydrological and agricultural drought originates from meteorological droughts which emanate from the changes within the hydrological cycle.

- Meteorological drought refers to a precipitation deficiency, possibly combined with increased potential evapotranspiration, extending over a large area and spanning an extensive period.
- Agricultural drought, also referred to as the soil moisture drought occurs when there is deficit soil moisture which reduces the moisture for crop growth and is strongly linked to crop failure (Van Loon, 2013).
- Hydrological drought is associated with the effects of below-normal precipitation on the surface and sub-surface water resources. Its characteristics which are defined by

magnitude, severity, duration, and frequency can be studied at a basin scale. Hydrological drought may be divided into surface and groundwater droughts which are defined separately. Groundwater drought can be defined as below-normal groundwater levels (Peters, 2003; Hisdal *et al*., 2004; Peters *et al*., 2006; Mishra and Singh, 2010) while surface water drought is below-normal river discharge (Stahl and Demuth, 1999; Smakhtin, 2001; Fleig *et al*., 2006; Feyen and Dankers, 2009). The Surface Water Drought (SWD) is as a result of direct reduction in precipitation that subsequently leads to low surface runoff and consequently results in below-normal river discharge and reduced water levels in reservoirs and lakes.

- Socio-economic drought emanates from the impacts of the three-above-mentioned drought (i.e. hydrological, agricultural, and meteorological). This may result from the failure of water resources systems to meet the demands and ecological or health-related impacts of drought (Van Loon, 2013).

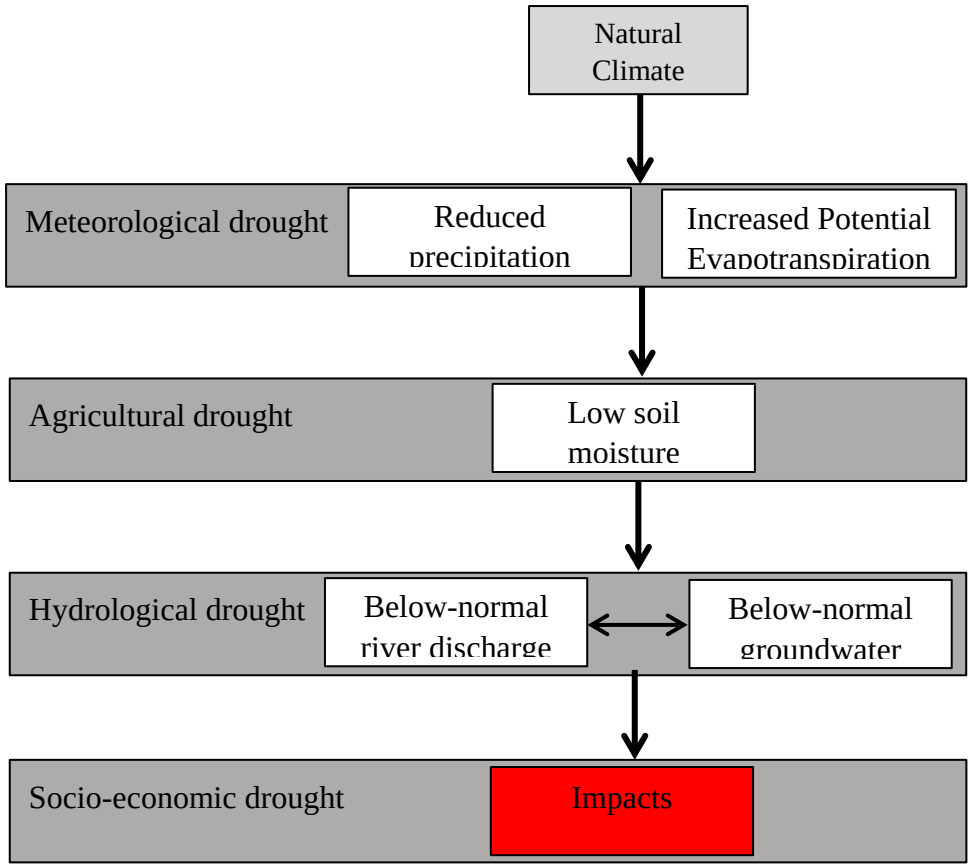

Figure 2.1: Categories of drought and their development (Peters, 2003; Van Loon, 2013).

2.3.1 Hydrological drought processes

Reduced runoff and shortage of streamflow and groundwater resources are a result of hydrological drought (Tallaksen and van Lanen 2004) and may result in dry river beds (Shaw 1994; Hisdal *et al*., 2004). Drought in the hydrological cycle is dependent on natural climate variability (Sheffield and Wood, 2011). Generally, hydrological drought develops differently in relative constant climate as compared to climates with strong seasonality (Van Loon, 2013). The main factor for drought development in constant climates is below-normal precipitation while in warm seasonal climates, most of the recharge is received over the wet season.

Hydrological drought is not solely dependent on atmospheric circulation, but also hydrological processes that add moisture to the atmosphere providing water and runoff to streams play a significant role (Mishra and Singh, 2010). Catchment characteristics i.e. climate, topography, geological condition, and land use/land cover, etc., also play a role in the occurrence of hydrological drought. Vegetation cover reduces streamflow and promotes infiltration whilst human activities i.e. stream diversions and abstractions of surface water and irrigation has the potential to influence the quantity of water in streams (Tallaksen and van Lanen, 2004). Hydrological drought is not solely dependent on the onset and cessation of meteorological drought such that it may persist even after a meteorological drought ends (Heim, 2002).

The rate of climate water deficit giving rise to hydrological drought is dependent on the catchment response. Water may feed the streams quickly as a response to rainfall or melting snow or it may recharge an extended groundwater system leading to a slow response to precipitation (Van Lanen *et al*., 2004). The water pathway in the catchment should be known. This is because not only water deficits have to be considered, but also water surpluses to fully understand drought development (Van Lanen *et al*., 2004).

2.4 Drought in South Africa

Rainfall variation at both temporal and spatial scales is of significance in southern Africa (Tyson, 1986; Nicholson and Entekhabi, 1987; Lindesay, 1988). Increasing trends of rainfall have been reported for some locations over South Africa (Mason *et al*., 1999; Easterling et al., 2000; New et al., 2006; Kruger, 2006). However, Mosase and Ahiablame (2018) cautioned that although this may suggest an increase in water resources availability, the increasing population, land use changes coupled with the intensification of agricultural activities exert pressure on

water resources. The variability of rainfall coupled with the nature of the South African climate (arid to semi-arid climate), makes the country prone to natural hazards such as droughts and floods. Droughts events occur frequently in South Africa's arid and semi-arid rangelands and with severe ecological and economic consequences (Vetter, 2009). The chronic nature of drought disasters in the region further affects negatively on social, economic, and environmental aspects (Gommes, 2006). Mosase and Ahiablame (2018) found an increasing trend of annual maximum temperatures in the Limpopo River Basin. Increased temperatures exacerbate drought characteristics (i.e. frequency, duration, and severity) (Vicente-Serrano *et al*., 2014) since there exists a positive linear relationship between temperature and evapotranspiration.

Southern Africa's summer climate is characterised by recurrent and features of prolonged droughts (Lindesay 1998; Rouault and Richard, 2005) and threaten vulnerable communities (most of which are rural) of the region. Droughts have occurred over South Africa regularly throughout the twentieth century (Vogel, 1994). About 60% of Sub-Saharan Africa is vulnerable to drought, with 30% being highly vulnerable (Benson and Clay, 1998). Southern Africa Development Community (SADC) region has been a victim of several major droughts, notably in the years 1982/83, 1987/88, 1991/92, and 1994/95 (FAO, 2004) and 2005/06 (Mosase and Ahiablame, 2018). It was estimated that the 1991/92 drought resulted in 50 000 job losses in the agricultural sector in South Africa, which affected over 250 000 citizens (Association for Rural Advancement; AFRA, 1993). More recently, the country experienced two consecutive droughts, the 2014/2015 and 2015/2016 which resulted in severe water shortages in the Western Cape Province (DEA, 2017).

Extreme drought has been recorded for more than a century at intervals of 10–20 years and has been reported to be a regular phenomenon in the Limpopo River Basin (FAO, 2004). Limpopo region, located in northern South Africa, is prone to extreme events (i.e. drought and flood events) as a result of significant intra-seasonal variability during the core rainy season (December–February) (Levey and Jury, 1996; Tennant and Hewitson, 2002; Cook *et al*., 2004). Although the LRC has a substantial flow of water derived from the mountainous area at its source, during drought season water resources become inadequate to meet the ecological reserve and domestic water supply (DWA, 2004). According to the State of the River Report (2001), the 1993 drought-affected upstream activities due to low flows and resulted in the death

of much riparian vegetation. Masupha *et al*. (2016) found severe drought occurrences at various rainfall regions over the LRC between 1975 and 2014.

2.5 Drought characterisation

The diverse definitions of drought are one of the principal obstacles to investigating drought (Yevjevich, 1967). Wilhite and Glantz (1987) distinguished between conceptual and operational droughts. The conceptual drought definition relates to those stated in relative terms while operational drought definition seeks to identify the onset, severity, and termination of a drought period (Wilhite and Glantz, 1987). Therefore, the understanding of drought duration, frequency, and severity to characterise the probability of occurrence at various magnitudes is of significance. The occurrence of any drought in terms of magnitude, duration, and severity may be determined by defining its threshold or truncation level. Panu and Sharma (2002) showed that for hydrological drought, the threshold can be defined based on flow characteristics or the water demand scenario of a catchment under consideration. The threshold level of any drought is based on the theory of crossing method where the properties of runs above and below a truncation level are determined (Tallaksen, 2000). A run is defined as a portion of a time series of drought variable X_t, in which all values are either below or above the selected threshold level of X_0; accordingly, it is called either a positive run or a negative run (Figure 2.2) (Mishra and Nagarajan, 2011). When drought data is plotted and falls below the threshold value, a drought event starts, and when it rises above the threshold, the drought event ends. Therefore, the onset and termination point of drought is defined.

Apart from the run theory-based methodology (Yevjevich, 1972; Chung and Salas, 2000), Panu and Sharma (2002) listed drought identification and prediction methods as; frequency (probability) based methods (Tate and Freeman, 2000; Kjeldsen *et al*., 2000; Dalezios *et al*., 2000), regression-based methods (Kumar and Panu, 1997), group-based methods (Kumar and Panu, 1994; Shin and Salas, 2000), PDSI based methods (Lohani and Lognathan, 1997) and the moisture adequacy index methods that measure the degree of soil moisture available for plant growth (Kumar and Panu, 1997).

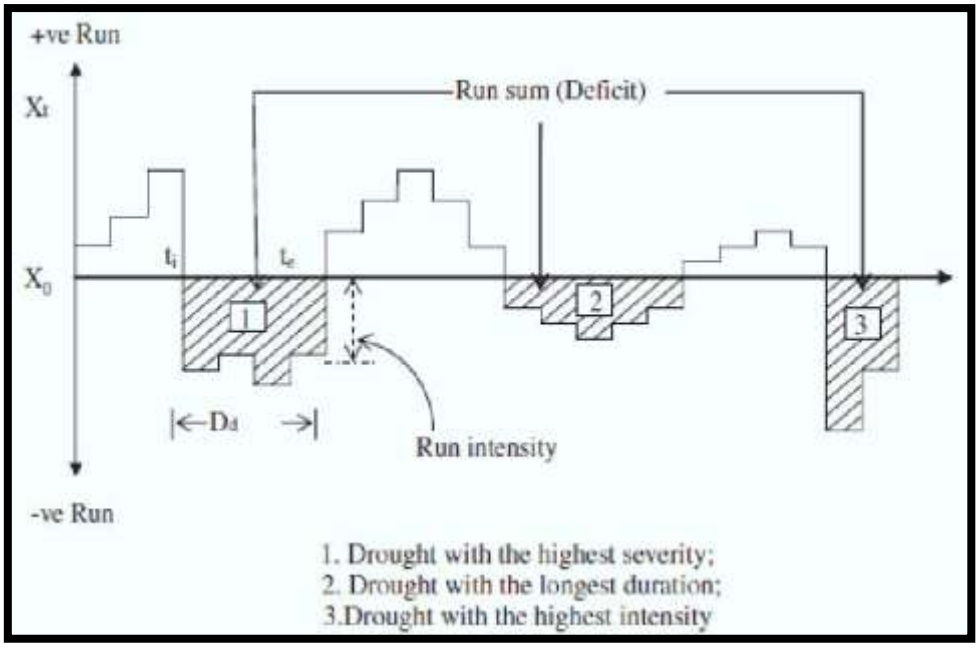

Figure 2.2: Drought characteristics using the run theory for a given threshold level (Mishra and Nagarajan, 2011)

2.6 Drought indices

Drought indices assimilate data on rainfall, snowpack, streamflow, and other water supply indicators into a comprehensible picture (Monacelli, 2005). Although none of the major indices is inherently superior to the rest in all circumstances, some indices are better suited than others for specified uses. Two categories of drought indices, namely: satellite-based and data-driven drought indices. Examples of some satellite drought indices are the Vegetation Condition Index (VCI), Normalised Difference Vegetation Index (NDVI), Normalised Difference Water Index (NDWI) (Gao, 1996), Water Supply Vegetative Index (WSVI), and Normalised Difference Drought Index (NDDI). Examples of some data-driven drought indices are the Standardised Precipitation Index (SPI) (McKee *et al*., 1993), Standardised Precipitation Evaporation Index (SPEI), Standardised Runoff Index (SRI), Palmer Drought Severity Index (PDSI) (Palmer, 1965), Surface Water Supply Index (SWSI) (Shafer and Dezman, 1982) and Aggregated Drought Index (ADI) (Keyantash and Dracup, 2004).

2.6.1 Standardised Precipitation Index

The Standardised Precipitation Index (SPI) was developed by Mckee *et al*. (1993). This index was developed to quantify the rainfall deficit and monitor drought conditions within Colorado, USA. To successful formulation of SPI, a long-term historical precipitation record of at least 30 years is integrated into a probability distribution function which is then transformed into a

normal distribution. The index is characterised by fewer input data (precipitation data) compared to most drought indices and therefore makes it flexible for a wide range of applications (Edwards and Mckee, 1997; Bacanli *et al*., 2008).

The SPI has several advantages, making it more applicable in many different river basins around the world. The index requires precipitation only as input data and thus makes it ideal for river basins that do not have extensive hydrological data records. It is a standardised index, and this makes it independent of geographical location as it is based on average precipitation values derived from the area of interest. Further to this, the SPI exhibits statistical consistency and can present both short-term and long-term droughts over time scales of precipitation variation (Belayneh and Adamowski, 2013). The SPI can be used to present significant drought conditions within a river basin. However, to identify key dry periods, it is important to analyse data for time scales greater than 6 months. This is because of the high frequency of SPI values at shorter time scales conceal the critical dry periods. For time-scales shorter than 6 months, there is insignificant autocorrelation while for time scales greater than 6 months, the autocorrelation increases significantly (Awass, 2009).

The SPI has some disadvantages in its use as a drought assessment tool. First, it is not always easy to find a probability distribution function to fit and model the raw precipitation data. Secondly, most river basins do not have reliable time-series data to generate the best estimate of the distribution parameters. In addition, the application of SPI in arid and semi-arid lands of time-series of less than three months may give inaccurate values. To overcome the challenge of simulating and modeling the data for SPI outputs, the application of different probability distribution functions may be employed. These include gamma, Pearson type III, lognormal, extreme value, and exponential distribution functions (Cacciamani *et al*., 2007).

2.6.2 Standardised Precipitation Evapotranspiration Index

First introduced by Vicente-Serrano *et al*. (2010a), Standardised Precipitation Evaporation Index (SPEI) was developed to account for the effect of potential evapotranspiration (PET) that lacked in the SPI. Due to its multi-scalar nature, SPEI enables the identification of different drought types and the resulting impacts emanating from such droughts. SPEI has been widely applied in different drought studies (i.e. drought analysis, climate change, drought impacts, and drought monitoring amongst others) over the past years (Lorenzo-Lacruz *et al*., 2010; Vicente-

Serrano *et al.*, 2010b; Allen *et al.*, 2011; Li *et al.*, 2012; Sohn *et al.*, 2013; Mosad and Alazba, 2015 in Beguer´ıa *et al*., 2013). SPI has been widely used in South Africa and is considered as the basis for drought assessment, forecasting, and prediction for the entire country. Although the SPI is quite popular in South Africa, SPEI has just started gaining popularity, as it is relatively a new index with the incorporation of PET in its computations. Edosaa *et al*. (2016) made a comparison of SPEI and PDSI while testing the applicability of the self-calibrating Palmer Drought Severity Index (PDSI) in the Free State Province and found that the relationship between the two meteorological indices improves an increases SPEI timescale. Botai *et al*. (2016) explored and characterised historical drought evolution variation using SPI and SPEI in Free State and North West Provinces in South Africa and reported that SPEI suggested that the severity and frequency of drought were more pronounced in Free State Province while drought intensity in the Northwest Province was higher between 1985 and 2015. Masih *et al*. (2014) reviewed drought in the African continent based on SPEI. This study found that between 1900 and 2013, drought events have intensified regarding their frequency, severity, and geospatial coverage.

2.6.3 Palmer Drought Severity Index

The Palmer Drought Severity Index (PDSI) was developed based on a criterion for determining the beginning and end of drought or wet period spell (Palmer, 1965). It is a simple monthly water balance model that requires rainfall, temperature, and catchment soil moisture content as input parameters. This tool applies a concept of supply and demand over a two-layer model. In this concept, the difference between the quantity of precipitation needed to maintain a natural water balance level and the actual precipitation is determined. The index does not consider streamflow, reservoir water balance, and other hydro-meteorological variables that influence drought (Karl and Knight, 1985; Yan *et al*., 2013).

The original PDSI has been modified to yield Palmer Hydrological Drought Index (PHDI) and the Palmer Modified Drought Index (PMDI) (Palmer, 1965; Karl, 1986; Heddinghaus and Sabol, 1991). The original PDSI does not take into account the human-induced impacts on water balances such as irrigation. However, the new version is a model mainly for the evaluation and monitoring of water supply. PDSI and its variations have been applied at the catchment level for detecting and planning of drought relief programmes (Karl and Heim, 1990; Dai *et al*., 2004; Loucks and Van Beek, 2005; D'Arrigo and Wilson, 2008).

The PDSI has some limitations or disadvantages as a drought index. In some regions, the PDSI assumes that all the precipitation is rain (Fuchs *et al*., 2012). This may result in misleading values in regions that experience winter season rainfall and in high elevation areas. In addition, it under-estimates runoff since it assumes that overland flow occurs after all soil layers have been saturated. The other disadvantage is that PDSI responds slowly to the development or cessation of a drought event (Mishra and Sigh, 2010). While the original model is more suitable for agricultural drought, the choice of the selected time series can also assess other types of droughts i.e. hydrological and meteorological drought.

The major advantages of the original PDSI as indicated in Fuchs *et al*. (2012) are that the index provides decision-makers with measurement of abnormality of recent weather conditions for a basin or region. It provides an opportunity to place current drought conditions on a historical perspective and can express historical drought conditions on the spatial and temporal domain. PDSI is sensitive to potential evapotranspiration (PET) equations and calibration periods, as well as the lack of precise spatial comparability (Alley, 1984; Karl, 1983; Karl, 1986; Guttman, 1991; Guttman *et al*., 1992). Potential evapotranspiration in PDSI is computed based on Thornthwaite method, which is a poor method of estimating the variable and the original tools considered coarse resolution of land use and land cover parameters of 700 to 100 000 km^2 yet the land-use changes within such a large area may be significant.

2.6.4 Surface Water Supply Index

Surface Water Supply Index **(**SWSI) was developed for Colorado USA, as an indicator for surface water or moisture levels (Shafer and Dezman, 1982). The index requires input variables which include; snow water content, streamflow, rainfall, and storage reservoir volume. Normally the snow water content, rainfall, and storage reservoir volume are used for computing the SWSI values for the winter season. However, during the summer season, streamflow substitutes snow water content. Further, the study area is located in the tropics and therefore not affected by snowfall. At a basin scale, SWSI values are determined from monthly catchment average values of rainfall, reservoirs, snow water content and, stream flows measured at stations within the catchment. One of the advantages of the SWSI is that it gives a representative measurement of surface water supplies across the river basin. The SWSI is unique for specific basins or regions. It requires long-term record data for its calibration and thus may be limited in basins that lack sufficient data. Another limitation of the SWSI is that

any additional change in the water management within a basin calls for modification of its algorithm. The change may be due to the addition of new water reservoirs and flow diversions that based on their weights, require to be accommodated in the algorithm (Barua, 2010). Thus, it is difficult to have a homogeneous time series of the index for numerous basins.

2.6.5 Aggregated Drought Index

The Aggregated Drought Index (ADI) is used for the determination of three categories of drought; hydrological, agricultural, and meteorological droughts. The specific drought is determined by selectively inserting input variables required into the model. This index can use the following input variables; rainfall, streamflow, potential evapotranspiration, soil moisture content, snow water content, and reservoir storage volume (Keyantash and Dracup, 2004).

Principal Component Analysis (PCA) is used as a numerical method for the construction of ADI using input data sets. The PCA is used to transform spatially correlated series data from a basin into two sets of orthogonal and uncorrelated functions. The principal components are used to express the original p-variable data set in terms of uncorrelated component $Z_j (1 < j \leq p)$. The p-mode is used where the analysis explains temporal fluctuations of the input variables of a basin. The calculation of principal components involves the construction of a $p \times p$ symmetric correlation matrix C_x. The matrix gives the correlation between the original data where p is the number of variables. This matrix is expressed using the relation:

$$C_x = E\{(x - u_x)(x - u_x)^T\}, \quad (2.1)$$

where; C_x= covariance matrix, x = vector of observed data, u_x = mean value of x and T denotes the transpose. The covariance matrices developed undergo PCA via the application of eigenvectors. The eigenvectors are unit vectors that establish the relationship between the principal components and standardised data. A unit vector may be derived from the relation:

$$Z = X \times E, \quad (2.2)$$

where; $Z = n \times p$ matrix of principal components, $X = n \times p$ matrix standardised observation data and $E = p \times p$ matrix of eigenvectors. The first Principal Component (PC) to represent ADI is determined and normalised by use of its standard deviation function defined by:

$$ADI_{i,k} = \frac{Z_{i,l,k}}{\sigma_k}, \quad (2.3)$$

where; $ADI_{i,k} = ADI$ value for month k in year i, $Z_{i,l,k}$= the first PC for month k in year i and σ_k= the sample standard deviation overall years for month *k*. To determine ADI thresholds, the empirical cumulative distribution of the above ADI values is constructed. The ADI thresholds are then calculated using empirical cumulative distribution function and used to classify drought conditions based on the thresholds.

2.6.6 Normalised Difference Water Index

Normalised Difference Water Index (NDWI) is determined based on leaf water content and vegetative type. Its value ranges from -1 to +1. The higher the NDWI value the higher the vegetative water content and the higher the proportion of vegetative cover. The values of NDWI are computed by processing the satellite data in which green and near-infrared bands are used as per the relation:

$$NDWI = \frac{G-NIR}{G+NIR}, \quad (2.4)$$

where; NDWI=normalised difference water index, G=green band, and NIR=near infrared band. The NDWI is very sensitive to soil moisture content, vegetation covers, and leaf moisture content (Tychon *et al*., 2007). Although NDWI is used for drought detection, it is sometimes affected by land cover and pests and diseases on vegetation. However, it has the advantage of detecting drought more effectively as compared to the Normalised Difference Vegetation Index (NDVI) (Gu *et al*., 2007).

2.7 Drought forecasting and prediction

2.7.1 The different forecasting and prediction techniques

Developments in forecasting and early warning of the drought phenomenon are increasingly being applied in many regions in the world. This is being done to help mitigate the consequences of drought in vulnerable river basins. Different drought modeling, forecasting, and prediction techniques are currently in use. Some of the common models include; Autoregressive integrated moving average (ARIMA) and its many variations, the Adaptive Neuro-fuzzy inference system, Markov chain model, Log-linear model, Ensemble Empirical Mode Decomposition (EMD), Empirical Wavelet Transform (EWT), and Artificial Neural Network (ANN) model among others.

2.7.1.1 Empirical Mode Decomposition (EMD)

First introduced by Huang *et al*. (1998) EMD is a self-adaptive and empirical technique that can break down a time series and can be utilised to examine non-linear and non-stationary hydro-meteorological data (Tang *et al*., 2012). The technique has been proven to be quite effective in extracting signals from data generated in noisy non-linear and non-stationary processes and has been successfully applied in many areas, such as engineering (fault diagnosis, computer image processing) (Xu *et al*., 2010) solar cycle, seismic waves, crude oil price analysis, speaker identification system (Coughlin and Tung 2004; Huang and Wu, 2008; Wu and Tsai, 2011; Zhang *et al*., 2008).

Time series decomposition utilising wavelet and wavelet packet transforms has been known to improve the prediction ability of conventional data-driven models (Amiri and Asadi, 2009; Adamowski and Sun, 2010; Gokhale and Khanduja, 2010; Kisi *et al*., 2011; Nourani *et al*., 2012; Ravikumar and Tamilselvan, 2014; Seo, 2015; Seo *et al*., 2015). Since hydro-meteorological time series are characterised by linearity and stationarity (Karthikeyan and Kumar, 2013), EMD can, therefore, be utilised in analysing the non-linear nature of such time series (Huang et al. 2009; Sang *et al*., 2012). The idea of EMD is to decompose a time series into a sum of oscillatory functions which is called intrinsic mode functions (IMFs) (Abadan and Shabri, 2014). Each IMF must satisfy two conditions which are: a) In the whole data set, the number of extrema (maximum and minimum) and the number of zero-crossings must either equal or differ at most by one and b) At any point, the mean value of the envelope defined by the local maxima and the envelope defined by the local minima is zero. For an original time series $x(t)$ $(t = 1, 2, \ldots, m)$, the main steps of EMD are as follows;

Step 1: Identify all local maxima and minima points for a given time series $y(t)$;

Step 2: Connect all local maxima points to form an upper envelope $e_{max}(t)$ and all minima point to form a lower envelope $e_{min}(t)$ with spline interpolation, respectively;

Step 3: Calculate the mean $a(t)$ between two envelopes;

$$a(t) = \frac{e_{max}(t)+e_{min}(t)}{2} \tag{2.5}$$

Step 4: Extract the mean from the time series and calculate the difference of $y(t)$ and $a(t)$ as $h(t)$;

$$h(t) = y(t)/a(t), \tag{2.6}$$

Step 5: If *h(t)* meets the two conditions of IMFs according to stopping criterion, *h(t)* is denoted as the first IMF [written as $c_1(t)$ and 1 is its index]; If *h(t)* is not an IMFs, y*(t)* is replaced with *h(t)* and iterate steps 1–4 until *h(t)* meets the two conditions of IMFs.

Step 6: The residue $r_1(t) = y(t)-c_1(t)$ is then treated as new data subjected to the same shifting process as described above for the next IMFs from $r_1(t)$. Finally, the shifting procedure can be stopped, when the residue *r(t)* becomes a monotonic function or at most has one local extreme point from which no more IMF can be extracted (Huang *et al*., 2003).

Then the original series *y(t)* can be expressed as the sum of these IMFs and a residue,

$$y(t) = \sum_{i=1}^{N} imf_i(t) + r(t), \qquad (2.7)$$

where; N is the number of IMFs, and *r(t)* is the final residue. Research has shown that EMD has a shortcoming from the mode mixing (MD) e.g. Wu and Huang (2009). Lei *et al*. (2009) defined MD as a single IMFs consisting of components of widely disparate scales, or a component of a similar scale residing in different IMFs. This shortcoming, however, can be accounted for by the Ensembles Empirical Mode Decomposition (EEMD) (Wu and Huang, 2009). In the EEMD method, the added white noise would fill in the whole time-frequency space uniformly, which facilitates a natural separation of the frequency scales and reduce the occurrence of mode mixing. As per the properties of the previous EMD method, the procedure of EEMD can be described as follows (Wu and Huang 2009 in Huang *et al*., 1998):

- **Step 1**: Add a white noise series to the targeted data;
- **Step 2**: Decompose the data with added white noise into IMFs;
- **Step 3**: Repeat step (1) and step (2) again and again, but with different white noise series each time; and
- **Step 4**: Obtain the (ensemble) means of corresponding IMFs of the decompositions as the result.

2.7.1.2 Empirical Wavelet Transform (EWT)

The main idea of building an adaptive wavelet is to extract the different modes of signals by designing an appropriate wavelet filter bank which leads to a new wavelet transform called the Empirical Wavelet Transform (EWT) (Gilles, 2013). EWT has strong mathematical support and is more robust compared to EMD (Liu *et al*., 2016). Literature has well documented the

efficiency of EWT to perform time series analysis as compared to EMD (Kedadouche et al., 2016; Hu et al., 2017; Zheng *et al*., 2017; Liu *et al*., 2018). Kedadouche *et al*. (2016) compared the computing time between EMD, EEMD, and EWT and observed that EWT reduced computation time by 95.96% compared with EMD and 98.91% compared with EEMD. Since the advantage of EWT is based on computation time, EMD can therefore not be fully disregarded for performing decomposition of a time series.

Wavelet analysis is suitable for investigations involving multi-time scales or variance trends (Torrence and Compo, 1998), it has been widely used in drought analysis as well as drought prediction. Morlet Wavelet function successfully characterised drought conditions in the Jilin Province of China (Chen *et al*., 2014) while Nury and Hasan (2016) used wavelet transforms to analyse drought using SPI as a drought indicator. Khan *et al*. (2018) developed a wavelet-based ANN for predicting meteorological and hydrological drought. They found that the application of wavelet for pre-processing the raw data in the developed W-ANN models achieved higher correlation coefficients. A wavelet fuzzy logic model proved superior compared to an uncoupled fuzzy logic and ANN in long lead-time forecasting (Ozger *et al*. 2011). Adamowski and sun (2010) coupled a continuous wavelet transform with neural networks for streamflow forecasting in a semi-arid watershed. The study determined that the developed model showed promise for short-term river forecasting. The application of the EWT has not been extensively reported in drought assessment, characterisation, and prediction and its application in this study adds to the body of knowledge. Detailed computational formulation of EWT can be obtained in Gilles (2013). The objective of EWT is to extract different modes by building adaptive wavelets using the following steps;

Step 1: Apply Fast Fourier Transform (FFT) to the signal *f(t)*, where *f(t)* is a discrete signal, $t=\{t_i\}_{i=1,2,\ldots,M}$, where M is the number of samples. To obtain the frequency spectrum $X(w)$ and find the maxima, $M=\{M_i\}_{i=1,2,\ldots,N}$ in the Fourier spectrum and deduce their corresponding frequencies $w=\{w_i\}_{i=1,2,\ldots,N}$. Here, N is the number of maxima and the number of filter banks is introduced hereinafter.

Step 2: Obtain proper segmentation of the Fourier spectrum and the set of boundaries. Define the boundaries Ω_i of each segment as the centre of two consecutive maxima:

$$\Omega_i = \frac{w_i + w_{i+1}}{2}, \quad (2.8)$$

where w_i and w_{i+1} are two frequencies and the set of boundaries is $\boldsymbol{\Omega}=\{\Omega_i\}_{i=1,2,\ldots N-1}$.

Step 3: Define a bank of N wavelet filter composed of one low-pass filter and N-a bandpass filter based on the boundaries. The expressions for the Fourier transform of scaling $\phi_1(w)$ and the empirical wavelets $\psi_i(w)$ are given by:

$$\phi_1 = \begin{cases} 1 & |w| \leq (1-\gamma)\Omega_1 \\ \cos\left(\frac{\pi}{2}\alpha(\gamma,\Omega_1)\right) & \left((1-\gamma)\Omega_1 < |w| \leq (1-\gamma)\Omega_1\right) \\ 0 & \end{cases}, \quad (2.9)$$

Otherwise,

$$\psi_i = \begin{cases} 1 & \left((1+\gamma)\Omega_i < |w| < (1-\gamma)\Omega_{i+1}\right) \\ \cos\left(\frac{\pi}{2}\alpha(\gamma,\Omega_{i+1})\right) & \left((1-\gamma)\Omega_{i+1} \leq |w| \leq (1+\gamma)\Omega_{i+1}\right) \\ \sin\left(\frac{\pi}{2}\alpha(\gamma,\Omega_i)\right) & \left((1-\gamma)\Omega_i \leq |w| \leq (1-\gamma)\Omega_i\right) \\ 0 & \end{cases}, \quad (2.10)$$

Otherwise,

where $\alpha(\gamma,\Omega_{i+1}) = \beta\left(\left(\frac{1}{2\gamma\Omega_i}\right)(|w| - (1-\gamma)\Omega_i)\right)$, γ is the parameter that ensures no overlap between the two consecutive transitions and $\beta(x)$ is an arbitrary function defined as

$$\beta(x) = \begin{cases} 0, & x \leq 0 \\ 1, & x \geq 1 \\ \beta(x) + \beta(1-x) = 1, & x \in (0,1) \end{cases}, \quad (2.11)$$

Step 4: Perform scaling and wavelet functions to extract the components of different modes. Therefore, the approximate coefficients can be expressed by the inner product of analysed signal *f* with the empirical scaling function

$$W_f(1,t) = (f,\phi_1) = \int \overline{f(\tau)\phi_\iota(\tau - t)d\tau}, \quad (2.12)$$

Similarly, the detailed coefficients are obtained by the inner product of analysed signal *f* with empirical wavelets

$$W_f(i,t) = (f,\psi_i) = \int \overline{f(\tau)\psi_\iota(\tau - t)d\tau}. \quad (2.13)$$

Here, $W_f(i,t)$ denotes the detailed coefficients for the i^{th} filter bank at time t.

2.7.1.3 Seasonal Autoregressive Integrated Moving Average

The seasonal autoregressive integrated moving average model (SARIMA) is a time series analysis tool. Time series events re-occur in every given number of observations (Chatfield, 2003). For monthly measurements, the recurrence of a year of twelve months, it is expected that the recurring value (x_t) depends on values that are based on annual lags. These lags are defined by x_{t-12} or x_{t-24}. It may be influenced by recent non-seasonal values. The ARIMA model has been generalised to deal with seasonality as defined by the relation given is below:

$$u_t = x_t - x_{t-\omega}, \tag{2.14}$$

where; u_t= seasonal value representing seasonality, ω = the period for monthly series, typically of multiples of 12 and x_t=recurring value. To achieve stationarity, the seasonal difference can be repeated D times. For instance, if D = 2 and D =12, then the following function which is called SARIMA model results:

$$\omega_t = u_t - u_{t-12} = (x_t - x_{t-12}) - (x_{t-12} - x_{t-24}) = x_t - 2x_{t-12} + x_{t-24}\ , \tag{2.15}$$

where; x_t=recurring value, $x_{t-\omega}$ =annual lag and u_t=seasonal value representing seasonality.

SARIMA has been used to develop an SPI drought forecasting model (Mishra and Desai, 2005; Durdu, 2010). Both the latter studies found that it was possible to forecast 2-months lead time (short term) while making use of the SARIMA model.

2.7.1.4 Markov chain model

Markov chains have greatly been used in the stochastic characterisation of drought (Cancelliere and Salas, 2004). For instance, an early warning system using the Markov chain model in conjunction with PDSI based on probabilistic severity, duration, and return period of drought may be developed (Shatanawi *et al*., 2013). Drought has also been characterised in terms of probabilistic occurrence by combining the Markov chain model with SPI for short term drought prediction within a period of 1 to 3 months lead time (Paulo *et al*., 2005; Paulo and Pereira 2007; 2008). The Markov chain model has two main applications; modeling stochastic characteristics of drought and forecasting future series of drought using historical data sets. Markov chain model exhibits a discrete stochastic process where drought state (x) at a future time step (t+1) is dependent upon the present state x_t and independent of previous states X_{t-1}, X_{t-2},...,X_{t-n}. The P_{ij} may be used to denote transitional probabilities from state i to stage j. The

P_{ij} can be represented in the form of $n\times$n matrix. Entries of such a matrix defined as P may be computed from several transitions n_{ij} from state i to next state j using the relation:

$$P_{ij} = \frac{n_{ij}}{\sum_{i=1}^{k} n_{ij}} \quad , \tag{2.16}$$

where; p_{ij} = the probability of moving from state i to stage j, n_{ij}=the entries of the P matrix. The following summation holds for the matrix,

$$\sum_{i=1}^{k} P_{ij} = 1 \, , \tag{2.17}$$

The transitional matrix at any given time step is calculated using the function:

$$P^{t+1} = P^{t} \times P^{t+n-1} \tag{2.18}$$

where; P^{t+1}=transition matrix at any given time, P^{t}=transition matrix at initial time, P^{t+n-1}=transition matrix of previous time step. The Markov chain attains a steady-state after several time steps. It is thus possible to define a stationary matrix π as the eigenvector of P^{t} using the relation:

$$\pi = P \times \pi \tag{2.19}$$

Since π_j is a stationary probability for state j, thus,

$$\sum_{j=1}^{k} \pi_j = 1. \tag{2.20}$$

The persistence and recurrence time can be presented using two main terms of the Markov chain. The first is the probability that the system will retain the same state in a subsequent time step called persistence. The persistence probability P_r is defined using the relation:

$$P_r = \sum_{j=1}^{k} P_{ij} \times \pi_j. \tag{2.21}$$

On the other hand, the recurrent time is defined as the average time for a system to transit from a certain state j and then back to the same state j and is computed using the function:

$$t_{ij} = \frac{1-\pi_j}{(1-\hat{P}) \times \pi_j}. \tag{2.22}$$

The time required for a system to be transformed for the first time from state i to j is called first passage time (t_{ij}) and is computed using the relation:

$$t_{ij} = 1 + \sum_{k=j} P_{ik} \times t_{kj}. \tag{2.23}$$

2.7.1.5 Artificial Neural Network (ANN)

A neural network consists of computational units or nodes that are linked where the output of a neuron can be an input to the next neuron. The most commonly used neural network architecture is one with three layers, comprising an input layer, a hidden layer, and an output layer (Ripley, 1994). The number of units in the input layer and those in the output layer depend on the problem being analysed. The number of units or neurons within the hidden layer is selected by trial and error to best describe the input-output relationship. A general recommendation is that the number of hidden units should be half the sum of the number of units in the input and output layers (Ripley, 1994).

Although parametric statistical protocols and deterministic models have been the traditional approaches to forecasting water quality variables in streams, many recent efforts have shown that when explicit information of hydrological sub-processes are not needed Artificial Neural Networks (ANN) can be more efficient and effective (Maier, *et al.*, 2010). One of the advantages of the ANN modeling technique is that the definition of physical processes need not be done (Morid *et al*., 2007; Tran *et al*., 2009). This property makes it appropriate in processing large and complex data sets, including that of drought prediction. Numerous activation equations or functions can be used within the neurons. The most common functions used in the ANN models include; the step-function, non-linear sigmoidal, hyperbolic tangent, and linear activation functions (Maier and Dandy, 2000; Mishra and Dessai, 2006).

ANN modeling approach has been used for drought prediction and forecasting in many regions of the world, e.g. (Ochoa-Rivera, 2008; Cutore *et al*., 2009; Barau, 2010; Le et *al*., 2016). For instance, it has successfully been used in India to forecast drought in Kansabati River Basin (Mishra *et al*., 2007) and Yara River Catchment in Victoria, Australia (Barau, 2010). For the Kansabati basin, two ANN models were applied and included the Recursive Multi-Step Neural Network (RMSNN) and the Direct Multi-Step Neural Network (DMSNN). These were used to forecast SPI values across the river basin. The results showed that the RMSNN performed best in 1-month lead time forecasting while the DMSNN was the best in 4-month lead time forecasting (Mishra and Desai, 2006). Barau (2010) successfully predicted a 6-month lead time NADI values for the Yara River Catchment making use of ANN (DMSNN and RMSNN).

Long Short-term Memory (LSTM) is a Recurrence Neural Network (RNN) first introduced by Hochreiter and Schmidhuber (1997) as an RNN architecture designed to model temporal sequences in a time series data. LTSM can sort error backflow problem so that this algorithm only uses the error feedback that can make a more accurate prediction, this makes it better than the conventional RNN. LSTM allows the network to capture information from inputs for a long time using a special hidden unit called an LSTM cell instead of an RNN unit in the hidden layer (Kong *et al.*, 2018).

2.7.1.6 Generalised Additive Models

Generalised additive models (GAMs) proposed by Hastie and Tibshirani (1986; 1990) are used in modeling predictors in regression-based models as a sum of smooth functions. They use automatic smoothness selection methods to determine the complexity of fitted trends and further allows for potentially complex, non-linear trends, proper accounting of uncertainty models, and the identification of periods of significant temporal changes (Simpson, 2018). Figure 2.3 gives an insight into various regression-based models and highlights the model advantages over the others. This figure further illustrates that GAMs are a combination of Generalised Linear Models (GLM) and Additive Models (AM).

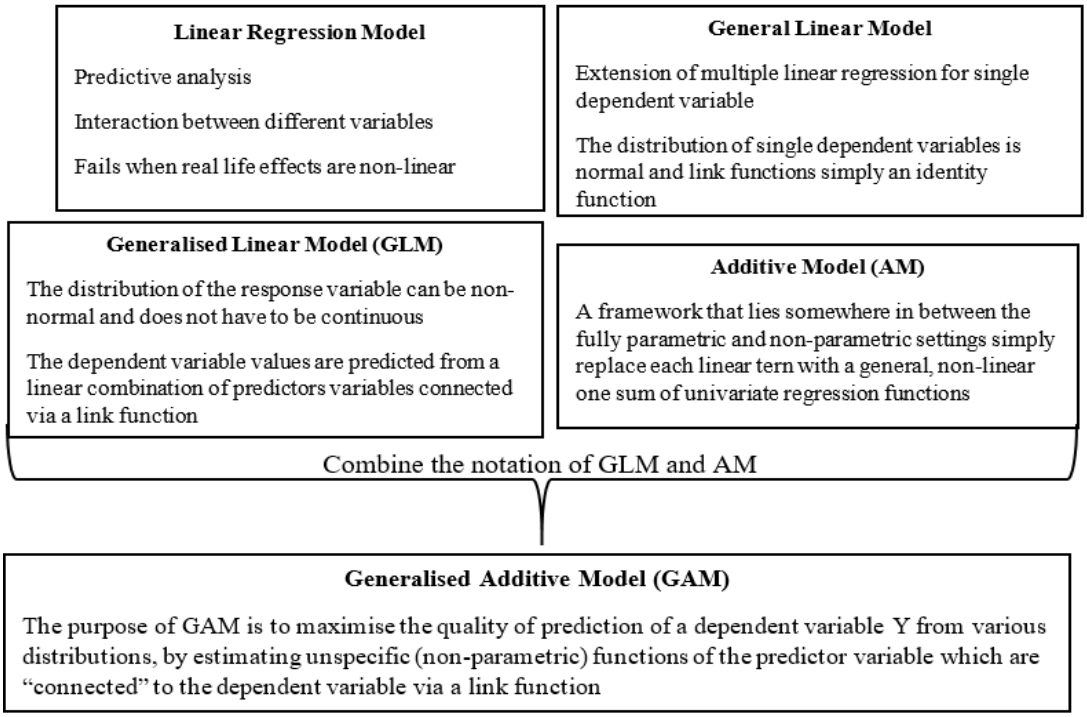

Figure 2.3: Overview and linkages between regression-based models (Ravindra *et al.*, 2019)

The GAM family models have been extensively applied with different loss and smoothing functions in time series prediction studies. Studies such as Chikobvu and Sigauke (2012); Sigauke and Chikobvu (2012); Wood *et al*. (2015) and Sigauke *et al*. (2018) amongst other have used GAMs in electricity load forecasting in South Africa and the United Kingdom while Ma *et al*. (2013) and Ravindra *et al*. (2019) applied these models to environmental time series. Ma *et al*. (2019) found that a mixed GAM gave good prediction, which reported an R^2 of 0.875 and 0.859 in the training and testing data respectively and Ravindra *et al*. (2019) found that GAM with reasonable spline and valid degrees of freedom has proved a robust method for the environmental datasets.

2.7.1.7 Hybrid models

The development of hybrid models combining various statistical approaches and data-driven models has been increased for improving the efficiency of conventional prediction models (Seo and Kim, 2016). Mishra *et al*. (2007) further indicated that the basic idea for combining models for drought forecasting and prediction is that the unique strength of each model can be employed to capture a different pattern in the data. Therefore, this makes hybrid models more efficient as compared to using stochastic or deterministic models alone. Experimental results with real data sets indicate that the hybrid models can be an effective way to improve prediction accuracy achieved by either of the models used separately (Xu *et al*., 2010). Despite many attractive features of prediction models (i.e. single/stand-alone and hybrid models), some drawbacks can lead to an over-parameterized model and thus, poor generalization ability (Falla *et al*., 2018). For the case of hybrid models, the latter authors further outline the limitation of some development hybrid models as shown in Table 2.1.

Table 2.1: Limitations of some hybrid models (Falla *et al*., 2018)

Hybrid model type	Limitation
ANN-k-shape clustering	The unknown optimal number of clusters
ANN-WT	Only frequency resolution
NF	The unknown optimal number of clusters
SVM-FOA	Complicated architecture
SVM-HS	Complicated architecture

*ANN- k – Artificial Neural Network with a clustering algorithm, ANN-WT – Artificial Neural Network-Wavelet transform, SVM-FOA – Support Vector Machine with Fruit Fly Optimisation Algorithm and SVM-HS – Support Vector Machine – Harmony Search Algorithm.

Forecasting future conditions using hybrid models have been extensively applied in the field of econometrics and have been gaining popularity in the field of engineering including

hydrology. Hydrological studies that developed hybrid models include but are not limited to; i.e., Zhang (2003); Mishra *et al*. (2007); Di *et al*. (2014); Seo and Kim (2016). These studies achieved time series forecasting using ARIMA and ANN, ARIMA/SARIMA and ANN, EMD-EEMD-RBFNN-LNN, and EEMD-FANN respectively. Pan *et al*. (2013) developed a hybrid model by combining empirical mode decomposition (EMD) with a multi-layer perception MLP-NN (EMD-NN) and compared these models to the MLP model and a SARIMA model. The study found that EMD-NN was more stable than the other techniques and in volatile situations.

2.8 Test for model performance

The goodness of Fit (GoF) of a statistical model describes how well it fits into a set of observations (Maydeu-Olivares and Garcia-Forero, 2010). GoF tests can be reliably used in climate statistics to assist in finding the best distribution to use to fit the given data. These tests cannot be used to pick the best distribution, rather reject possible distributions. These tests calculate test-statistics, which are used to analyse how well the data fits the given distribution. They describe the differences between the observed data values and the expected values from the distribution being tested. The null hypothesis is that the empirical data is approximately normally distributed. The null hypothesis is rejected if the significance level is greater than the p-value. The Anderson-Darling (AD), Kolmogorov-Smirnov (KS), and Chi-Squared (X^2), Mean Absolute Error (MAE), and Root Mean Square Error (RMSE) tests are used to test the goodness of fit. For a detailed discussion of these statistical tests, see Solaiman (2011) among others.

2.8.1 Kolmogorov-Smirnov Test

The Kolmogorov-Smirnov test statistic is based on the greatest vertical distance from the empirical and theoretical CDFs. Like the AD test statistic, a hypothesis is rejected if the test statistic is greater than the critical value at a chosen significance level. For the significance level of α=0.05, the critical value calculated is 0.12555. The samples are assumed to be from a CDF $F(x)$. The test statistic (D) is:

$$D - \max(F(x_i) - \frac{i-1}{n}, \frac{i}{n} - F(x_i)). \qquad (2.24)$$

2.8.2 Anderson-Darling Test

The Anderson-Darling (AD) test compares an observed Cumulative Density Function (CDF) to an expected CDF. This method gives more weight to the tail of the distribution than the KS test, which in turn leads to the AD test being stronger and having more weight than the KS test. The test rejects the hypothesis regarding the distribution level if the statistic obtained is greater than a critical value at a given significance level (α). The significance level most commonly used is α=0.05. This number is then compared with the test distributions statistic to determine if it can be rejected or not. The AD test statistic (A^2) is:

$$A^2 = -n - \frac{1}{n}\sum_{i=1}^{n}(2i-1)\times[lnF(x_i) + ln(1-F(x_{n-i+1}))]. \quad (2.25)$$

2.8.3 Chi-Squared Test

The Chi-Squared test is used to determine if a sample comes from a given distribution. It should be noted that this is not considered a high-power statistical test and is not very useful (Cunnane, 1989). The test is based on binned data, and the number of bins (k) is determined by:

$$k = 1 + \log(N). \quad (2.26)$$

where N is the sample size and the test statistics is expressed as:

$$X^2 = \sum_{i=1}^{k}\frac{(O_i - E_1)^2}{E_1} \quad (2.27)$$

where O_i is the observed frequency, E_1 is the expected frequency, $E_1 = F(x_2) - F(x_1)$ and x_1 and x_2 are the limits of the i^{th} bin. The significance level, α=0.05 gives a critical value of 12.592 which is used in this report. Again, if the test statistic is greater than the critical value, the null hypothesis is rejected.

2.8.4 Root Mean Square Error

The Root Mean Square Error (RMSE) is the standard deviation of the residual (Barnston, 1992). The residuals are a measure of how far from the regression line data points are located, thus, RMSE is a measure of how spread out these residuals are. It has been used as a standard statistical metric to measure model performance in meteorology, air quality, and climate research (Chai and Braxler, 2014). In the field of geosciences, many present the RMSE as a standard metric for model errors (e.g. McKeen *et al*., 2005; Savage *et al*., 2013; Chai *et al*.,

2013). On the reliability of RMSE, Willmott and Matsuura (2005) have suggested that the RMSE is not a good indicator of average model performance and might result in a misleading indicator of average error and proposed that the MAE would be a better metric for that purpose. However, Chai and Draxler (2014) reported that the RMSE is more appropriate to represent model performance than the MAE when the error distribution is expected to be Gaussian. They also showed that the RMSE satisfies the triangle inequality requirement for a distance metric whereas Willmott *et al*. (2009) indicated that the sums-of-squares-based statistics do not satisfy this rule. RMSE can be computed from Equation 2.28 below:

$$RMSE = \sqrt{\frac{1}{n}\sum_{j=1}^{n}(y_j - \hat{y}_j)^2}. \qquad (2.28)$$

where RMSE is the Root Mean Square Error, n is the sample size, y_j and $\hat{y}_j$ are the observed and forecasted values respectively. Smaller RMSE reflects greater accuracy; however, there is no absolute criterion for an ideal value for RMSE, because it depends on the scales of the measured variables and the size of the sample (Li, 2012).

2.8.5 The correlation coefficient

The correlation coefficient (R) is used to determine the statistical relationship between the observed and the predicted conditions in a given scenario. The fundamental function will be customised to the respective variable and will take the following general form:

$$R = \frac{\sum_{i=1}^{n}(x_{obs}-x_{for})(x_{for}-x_{obs})}{\sum_{i=1}^{n}\sqrt{(x_{obs}-x_{for})(x_{for}-x_{obs})^2}} \qquad (2.29)$$

where R is the correlation coefficient, X_{Obs} is the observed value of the drought index, X_{For} is the forecasted value of the drought index and n is the number of data points considered. The R is a measure of the strength of the linear relationship between observed and forecasted X values. It varies from -1 to 1. The values of -1 and 1 indicate a strong negative and positive forecasting capability of the model respectively.

2.8.6 Nash–Sutcliffe efficiency

The Nash–Sutcliffe Efficiency (NSE) statistical approach has been used effectively to evaluate measured and predicted hydrologic data including drought (Nash and Sutcliffe, 1970; Biamah *et al*., 2002). The NSE will be used to indicate how well the plot of observed versus simulated data fits the 1: 1 line: Its value ranges from $-\infty$ to 1.0. The NSE is given as:

$$NSE = \frac{\sum_{i=1}^{n}(DI_i^{obs} - DI_i^{for})^2}{\sum_{i=1}^{n}(DI_i^{obs} - \overline{DI})^2}. \quad (2.30)$$

where *NSE* is the Nash–Sutcliffe Efficiency, DI_i^{obs} is the observed value of the drought index, DI_i^{for} is the forecasted value of the drought index, $\overline{DI}$ is the mean value of the drought index and *n* is the total number of observations. The resulting values of NSE will then be compared with those given as acceptable levels of efficiency (Nash and Sutcliffe, 1970).

2.9 Uncertainty analysis

Identification, quantification, and reporting of the different sources of errors in a modeling process constitute an uncertainty analysis (McIntyre et al., 2002; Refsgaard and Henriksen 2004; Refsgaard et al., 2007). The efficient application of any model depends on the accuracy and reliability of its output. However, because all models are imperfect abstractions of reality and precise input data are rarely available, all output values are subject to imprecision (UNESCO, 2005). Input data errors and modeling uncertainties are not independent of each other but can interact in various ways. This gives rise to the significance of model uncertainty not only in hydrological systems but to a bulk of models that are developed and applied in other fields of study. In hydrology, uncertainties impact all facets of hydrologic data collection and modeling, i.e. (a) conceptual and numerical model development, (b) estimation of model parameters, and (c) quantification of historical and future model stresses (Mishra and Singh, 2009). Uncertainties in hydrology arise due to the nature of hydrological models, which often contain many parameters that describe important characteristics of the catchment sub-surface and hydrological processes (Zhang *et al*., 2014).

Mishra and Singh (2009) outlined the key elements of a systematic framework to consider while dealing with uncertainty in hydrological modeling, i.e. (a) uncertainty characterisation, (b) uncertainty propagation), and (c) uncertainty importance assessment. Bayesian and non-Bayesian based techniques are used to determine the uncertainty of model outputs. Vallam *et al*. (2014) adopted a simplified Bayesian method, the Generalised Likelihood Uncertainty Estimation (GLUE) to determine the parametric uncertainty in hydrological modeling. Mishra and Singh (2009) presented two case studies of uncertainty and sensitivity analysis using MCS and other techniques that complement MCS. The MCS complementing techniques include first-order second-moment analysis, point estimate method, logic tree analysis, and first-order

reliability method. Although MCS can be data-intensive in its computation, the fact that it is more general and requires fewer assumptions makes it the strategy of choice compared to other Bayesian techniques in the literature. A detailed methodological approach of the MCS technique can be obtained in Mishra and Singh (2009).

An example of non-Bayesian based techniques is the bootstrap method. Bootstrap is a statistical method that requires no assumptions concerning the distributions of the model parameters or their errors. Zhang *et al*. (2014) compared the model-based and block bootstrap methods while analysing the impact of parameter uncertainty on the overall uncertainty of model simulation in the case of the SWAT model applied to a hydrological simulation of the Dongliao River Watershed. The study found that the uncertainty ranges of parameters acquired by the block bootstrap were narrower as compared to those acquired by model-based bootstrap.

Prediction Intervals (PI) is a statistical measure of confidence used to explore the behaviour of predictive models. A PI is concerned with the accuracy of prediction outputs by focusing on the distribution of the quantity (Mazloumi *et al*., 2011). Therefore, a PI value expresses the uncertainty of the prediction. Hyndman and Athanasopoulos (2018) indicated that point forecasts are of no value, however by producing PI, they account for uncertainty associated with each prediction. Prediction intervals increase in size as the forecast horizon increases therefore, more uncertainty is associated with the increased forecast length (Hyndman and Athanasopoulos, 2018).

2.10 Chapter summary

Drought as a hydrological extreme event has been of interest in many regions of the world due to its impact on several sectors of the economy and communities' livelihoods. In southern Africa, drought is a frequent phenomenon with notable drought years being 1982/83, 1987/88, 1991/92, 1994/96, 1997/98, 2001/02, 2005/06, 2014/15, and the 2015/16. Literature has shown that any major drought is a result of climate variability which may be exacerbated by climate change. For the case of hydrological drought (the focus of this study), the literature review showed that catchment characteristics (climate, topography, geological conditions, land use/ land cover) also play a major role in its development. Therefore, an index-based assessment of hydrological drought should consider catchment characteristics with more than one input variable i.e. a multivariate drought index. The increase in frequency and severity of drought around the world due to climate change impacts have seen frequent studies in forecasting and

prediction. The main objective is to aid the timely development of an early warning system and preparedness measures to be put in place. This further makes a community recover faster from a drought event before another one strikes. The following table show some of the most prominent drought forecasting and prediction studies:

Author(s)	Drought forecasting and prediction study
Yan et al. (2017)	Probabilistic drought forecasting framework (dynamic and statistical ensemble).
Crochemore et al. (2017)	Forecasted seasonal streamflow using eight ensembled GCM's.
Hao et al. (2016)	Toward a categorical drought prediction system based on U.S. Drought Monitor (USDM) and climate forecast.
Hao et al. (2016)	An integrated package for drought monitoring, prediction and analysis to aid drought modeling and assessment
Hao et al. (2016)	A general framework for the multivariate multi-index drought prediction based on multivariate ensemble streamflow predictions (ESP)
Humprey et al. (2016)	Made use of a hybrid approach (GR4J conceptual rainfall-runoff models and Bayesian ANN statistical forecasting model) to forecast streamflow.
Huang et al. (2016)	Research to advance national drought monitoring and prediction capabilities, NOAA Interagency Drought Task Force.
Trambauer et al. (2015)	Successfully conducted a seasonal forecast of hydrological drought at 3-, 4- and 5- month lead time in the Limpopo River Basin making use of a Seasonal Forecasting System (FS_S4) and Forecasting System Conductions Streamflow Prediction Approach (FS_ESPcond).
Hao et al. (2014)	Global integrated drought monitoring and prediction system.
Barua (2010)	Forecasted a multivariate drought index (NADI) using the ANN technique over the short and medium-term.
Cutore et al. (2009)	Forecasting Palmer Index using neural networks and climatic indexes.
Ochoa-Rivera (2008)	Prospecting droughts with stochastic artificial neural networks.
Mishra et al. (2007)	Drought forecasting using hybrid stochastic and neural network models.
Mishra and Desai (2006)	Drought forecasting using stochastic models.

Literature has shown that hybrid models (that combines statistical and data-driven approaches) can increase the efficiency of conventional prediction models. Many drought studies in South Africa have focused on the assessment of drought, their nature, and impacts at regional, national, provincial, and catchment scales. This study, therefore, applied hybrid drought prediction model(s) for the Luvuvhu River Catchment in north-eastern South Africa making use of a multivariate drought index.

3 THE STUDY AREA AND DATASETS

Chapter overview, Selection of the study area, Hydrometeorological data, Methodological framework, Summary.

3.1 Chapter overview

This chapter details the selection of the study area and characteristics of the Luvuvhu River Catchment (LRC) that relate to drought. The significance of the catchment under study is also discussed. Description of the datasets used in drought assessment, characterisation, and prediction are discussed. Sources of the data, collection process and the length of each hydro-meteorological variable are discussed. GIS maps depicting the Luvuvhu River system and its tributaries, the elevation of the catchment, location of rain gauges, major reservoirs, weather stations, and streamflow stations are also presented in this chapter. In the case where hydro-meteorological data for a certain variable was not available, methods are presented on how the estimation was carried out. The chapter concludes with a methodological framework depicting the sequence of drought assessment, characterisation and prediction followed in this study.

3.2 Selection of the study area

The LRC is located between latitudes 22°17'33.57" S and 23°17'57.31" S and longitudes 29°49'46.16" E and 31°23'32.02" E in the Vhembe District of Limpopo Province in South Africa (Figure 3.1). The catchment covers an area of approximately 5 941 km^2 and is situated between 202 to 1 506 meters above sea level. It consists of a relatively rolling landscape, which gives rise to shallow storage dams that have large water surfaces exposed to evaporation. The catchment lies at the periphery of the southernmost position of the Intertropical Convergence Zone (ITCZ) during the southern summer with an average January position at about 15°S. The river rises as a steep mountain stream in the southern slopes of the Soutpansberg Mountain complex range, which features the west-east direction, flows through Kruger National Park (KNP) (an important conservation and ecotourism area) and empties into the Limpopo River at the border with Mozambique and Zimbabwe.

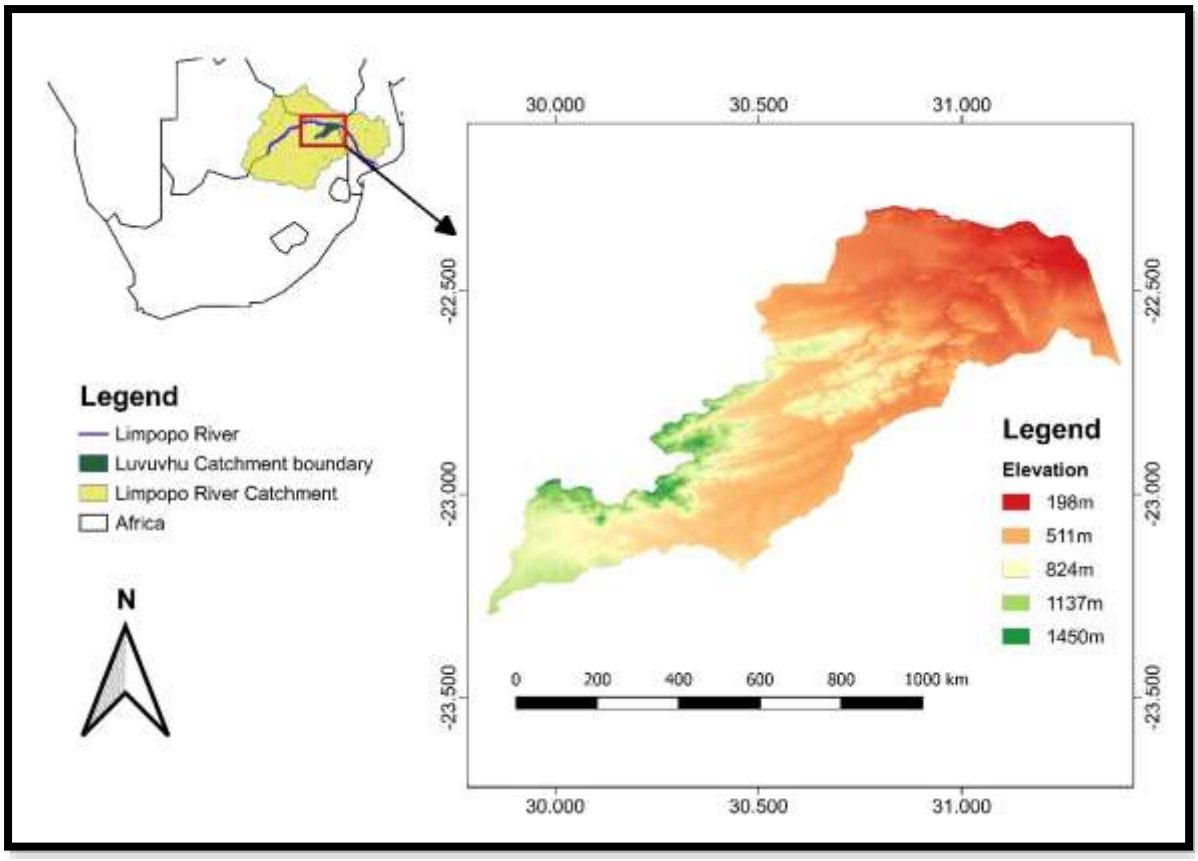

Figure 3.1: The study area (Luvuvhu River Catchment) showing the main river system and elevation.

The highest rainfall is received in the upper reaches (of high altitudes) while the lower reaches around the Kruger National Park receive the lowest rainfall during the rainfall season. The upper reaches Mean Annual Precipitation (MAP) is approximately 1800 mm/a while the low lying is characterised by low rainfall with a MAP of 400 mm/a (Ramulifho *et al*., 2019). The mean annual rainfall is 608 mm and the mean annual run-off is 520 x 10^6 m^3 (Odiyo *et al*., 2015). LRC falls within the eastern summer rainfall region of southern Africa and receives peak rainfall during the summer months of December to February. Distribution of rainfall through the year is highly seasonal with 95% of the rainfall occurring during the summer months (October and March) (M'Marete, 2003). The lower rainfall area in the catchment tends to experience greater variability than the higher rainfall areas.

Local towns such as Thohoyandou experience daily maximum temperatures from about 25˚C to 40˚C in summer and between 22˚C and 26˚C in winter (Mzezewa *et al*., 2010). The high temperatures in the catchment create favourable conditions for increased evaporation. Evaporation increases gradually from 1 400 mm to 1 900 mm per annum (State of Rivers

Report, 2001) with 1 678 mm Mean Annual Evaporation (MAE) showing a high spatial and temporal variation with the highest rainfall and lowest evaporation over the Soutpansberg mountain range and lowest rainfall with the highest evaporation to the Kruger National Park (DWAF, 2004).

LRC consists of a fragile ecosystem threatened by drought, as the region is in an arid to semi-arid climatic zone. LRC is predominantly rural, with a community that is highly dependent on commercial and subsistence agriculture. Because the Levubu valley (an agricultural economic backbone of the Vhembe District) is located in this catchment, a timely early warning system would aid in better preparedness and reduction of drought risk to the fragile industry that is heavily dependent on water availability. There have been 8 notable historical droughts that have affected the catchment which results in far-reaching impacts on all sectors of society.

3.3 Regional climate and hydrology

The regional climate within which the LRC is found ranges from tropical rain in the coastal plains of Mozambique to tropical dry savannah and tropical desert further inland, south of Zimbabwe (Zhu and Ringler, 2012). The mean spatial pattern of summer rainfall over southern Africa depicts a strong gradient that increases from west to east (Chikoore, 2016). Limpopo River Basin annual precipitation varies between 250 mm to 1 050 mm in the hot, dry western and central areas in the high-rainfall eastern escarpment areas respectively (Zhu and Ringler, 2012).

The region experiences high variability between extreme wet and dry seasons, which Mulenga et al. (2003) suggest makes the region vulnerable to extreme events such as droughts and floods. The nature and pattern of inter-annual variability of precipitation are crucial as the variation exerts long-term control on water resources, affects plant growth, and the biogeochemical cycle while moderating extreme events such as droughts and floods (Fatichi *et al*., 2012). Limpopo Valley (20 – 25^0S) possess the highest variability in southern Africa (Chikoore, 2016) which agrees with reports by Usman and Reason (2004) and Kabanda (2004). Figures 3.2 and 3.3 show the inter-annual variability of rainfall and streamflow in the LRC for over 57 and 53 years respectively. The inter-annual variability plots depict a strong seasonal variation in the study area. Makarau (1995) determined that the rainy season of the region is characterised by alternating wet and dry spells. Both variables showed a positive trend over the

sampling period considered, although streamflow (with an R^2 of 0.0661) was more significant compared to rainfall (with an R^2 of 0.0064). The significance of streamflow may be influenced by recharge from groundwater, since streamflow are controlled by the variability of antecedent groundwater recharge (Stahl et al.,2012; van Lanen et al., 2013) and not only reliant of rainfall for replenishment. The wet and dry alternating results obtained in this study are comparable with those obtained by Chikoore (2016) over southern Africa. This notable rainfall and streamflow positive trends may be due to the catchment recovery after each dry period such as the extreme event of February 2000.

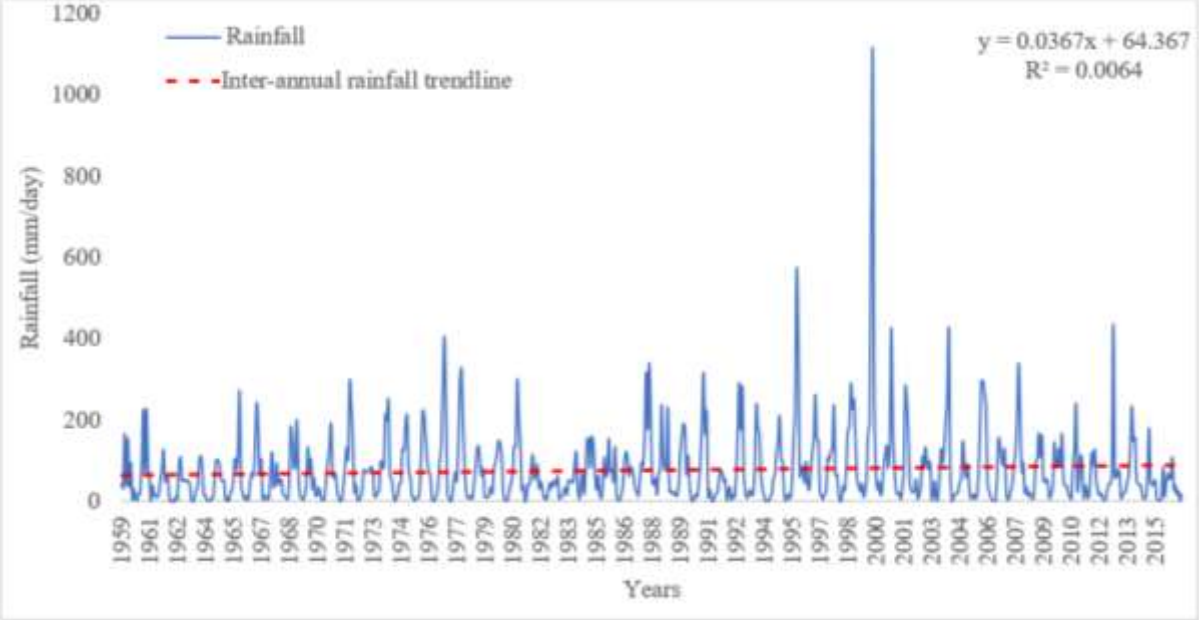

Figure 3.2: Interannual variability of mean rainfall over the study area.

The two figures depict the negative departure from the mean between the 1980s and 1990s, Kabanda (2004) reported a declining trend over the study area during the decade while Chikoore (2016) reported a high interannual variability of mean rainfall with drier years (negative departures) during the same period. Rainfall increased in 1995/96, which resulted in increased streamflow in 1996/97. This event was followed by above-normal rainfall received over southern Africa in 2000 as a result of tropical cyclone Eline which produced 25% of mean rainfall over a few days in the year 2000 (Reason and Keibel, 2004). The latter two periods indicate that the system was on partial recovery. These findings are comparable with Chikoore (2016) although studies such as New *et al*. (2015) reported a continued drying trend.

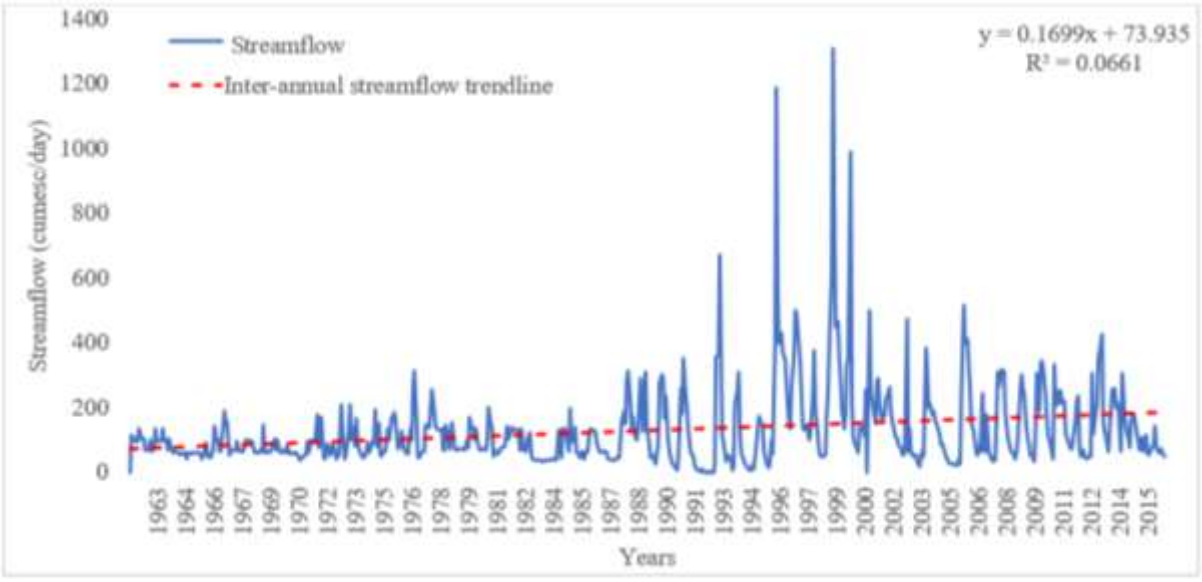

Figure 3.3: Interannual variability of mean streamflow over the study area.

3.4 Hydro-meteorological data requirements, collection and quality control

Data requirements to compute drought indices and predict drought for the LRC include; rainfall, evapotranspiration, temperature, streamflow, reservoir storage volume, soil moisture data. Data for 30 hydrological years spanning from September 1986 to August 2016 were considered for the study. Although studies such as Tadross *et al*. (2007) and Tshililo (2017) defined onset as the first day after the 1st October over summer rainfall season such as in the study area, this study further accounted for false onset and therefore included the month of September. Figures 3.4 and 3.7 show the location of rain gauges, reservoirs, weather stations, and streamflow gauges within the catchment, respectively. Data sets are available in different time scales. However, for operational purposes, Barua (2010) showed that a monthly time scale is preferred as its sensitivity is lower or has low observational errors. Drought studies often use monthly datasets as the shorter periods (i.e. hour or day) fail to reflect drought. Sherval et al. (2014) indicated that drought occurs over some time, such as months or years. This study, therefore, considered monthly timescale for the computation of drought indices and prediction of drought.

Missing data are often identified as a major problem in many hydrological studies. Kang and Yusof (2012) attributed missing data in hydrology to erroneous sampling, insufficient samples obtained, or problems in recording. Missing hydro-meteorological data in this study was imputed through Self Organising Maps (SOM) CRAN Package “class” in R. SOMs are neural networks are multivariate methods capable of modeling multivariate non-linear systems,

therefore, providing possibilities to estimate missing environmental data, considering interactions between variables in the vector-profile of the datasets (Folguare et al., 2014). These neural networks have seen many diverse applications in a broad range of fields, however, for imputation Fessant and Midenet (2002) described the process as follows:

1. Presentation of an incomplete observation on the input layer;
2. Selection of the image-node by minimising the distance between observation and prototypes in the available dimensions only: $\sum_{ilX^i_{exists}}(X^i - W^i_j)^2$. The other dimensions corresponding to missing values are simply ignored during the image-node determination;
3. Selection of the activation group composed of image nodes neighbours in the map;
4. Determination of the value given to the missing item based on the weights of the activation group's nodes in the missing dimensions.

While making use of the SOMs, Folguare et al. (2014) found that there were no statistically significant differences from estimates results from professional criteria and SOM, thus proving to be a suitable time-saving imputation method. For a detailed description of the SOM properties and applications, see Kohonen (2001).

Due to the nature of indices to be computed, data averaging was conducted. Individual station data were used in the formulation of the SPI, SSI, and SPEI for the LRC. For the case of NADI, data from the selected stations of rainfall, streamflow, and temperature were averaged using the arithmetic mean method. One advantage of this method is that it makes use of every value in the data and therefore making it a good representative of the data (Manikandan, 2011). Barua (2010) compared arithmetic mean and Theissen Polygon and reported that both averaging methods gave similar results. Glaser (2000) further indicated that mean is the measure of central tendency that best resists the fluctuation between different samples.

Datasets selected (i.e. rainfall, temperature, and rainfall) for use in the study area were checked for consistency using the double mass curve analysis and the results of this are shown in Figure 3.4. The double-mass analysis assumes a linear relationship between hydrological tine series (Dahmen and Hall, 1990). The method has been extensively applied in testing the consistency of hydrological data and showed good results (e.g. Wijesekera et al., 2012; Peng et al., 2018; Pirnia et al., 2019). Cumulative data (i.e. rainfall, temperature) for each station was plotted against the mean cumulative data of the rest of the stations. A 45^0 line was introduced to the

scatterplot, and if the point falls within this line then the data did any adjustment. For the case of rainfall, the point falling off the line might be an outlier in the data.

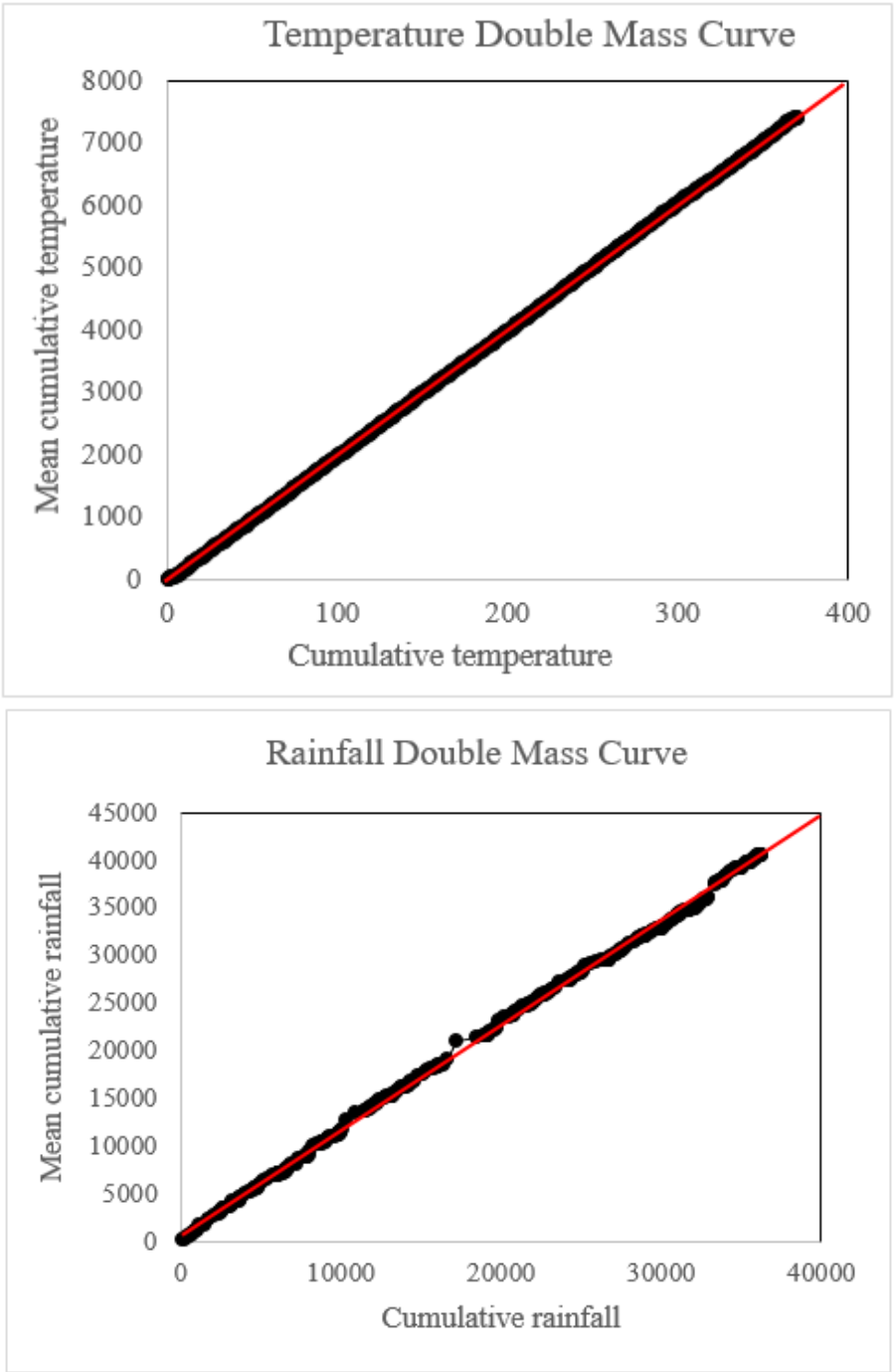

Figure 3.4: Double mass curve analysis for rainfall and temperature for the selected stations in the study area.

3.4.1 Rainfall

Rainfall is one of the fundamental components of the hydrological cycle and acts as an important indicator of the development of drought conditions. Data on rainfall over South

Africa is measured at a daily time scale, however, monthly means and totals are also made available by South African Weather Services (SAWS). Monthly rainfall data from eight weather stations in the LRC were collected from the SAWS. Table 3.1 shows the station names and numbers and the data span in each respective station selected to be used in this study while Figure 3.5 shows their location in the study area. There is a paucity of weather observations in the drier lower catchment of the LRC.

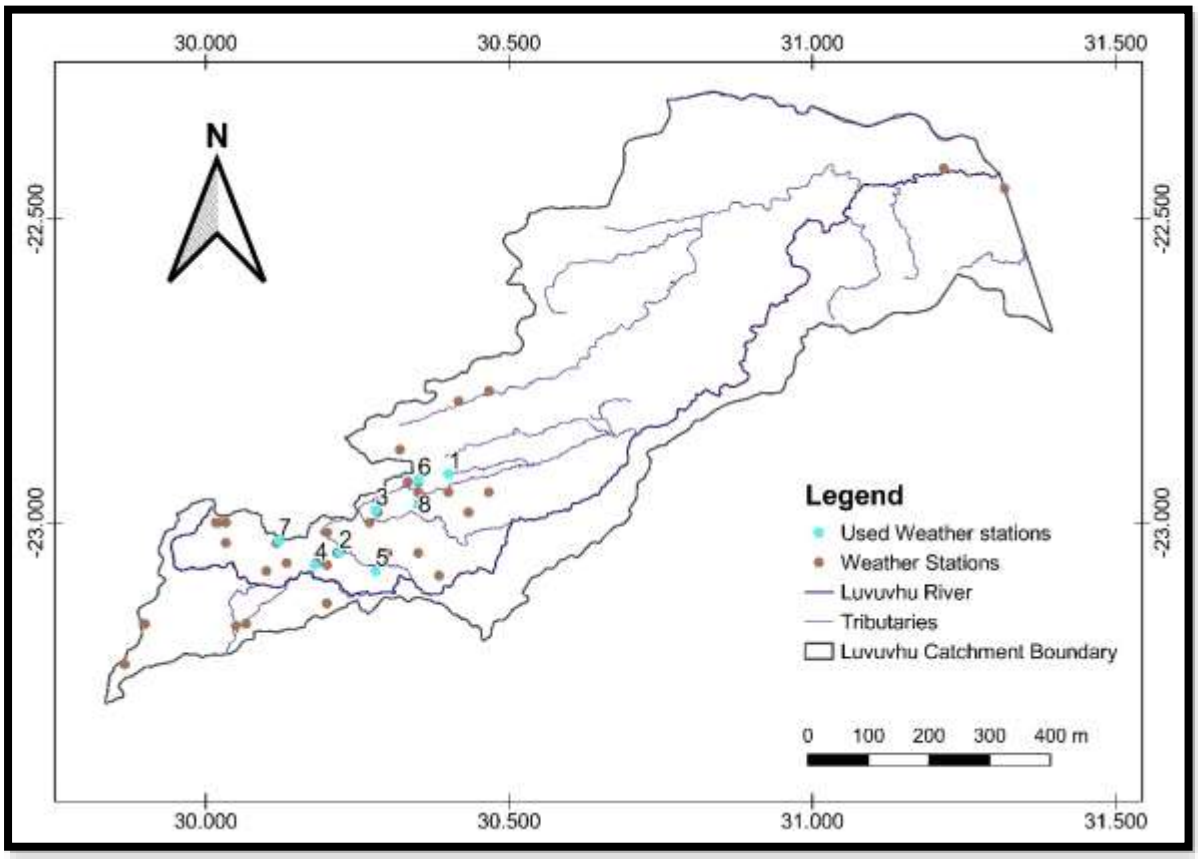

Figure 3.5: Location of weather stations in the LRC used in this study.

Table 3.1: Weather stations in the study area.

	Station name	Station number	Data span	Data length (years)
1	Mukumbani	0766715	1956-2016	60
2	Klein Autsralie	0723363 X	1959-2016	57
3	Matiwa	0766509 9	1959-2016	57
4	Nooitgedatch	0723334 X	1959-2016	57
5	Levubu	0723485A0	1964-2016	54
6	Vondo Bos	0766596 9	1963-2016	53
7	Shefera	0723182 6	1948-2016	68
8	Tshivhase	0766628 W	1986-2016	30

3.4.2 Potential Evapotranspiration

Potential Evapotranspiration is the idealized quantity of water evaporated per - unit area, per unit time from an idealized, extensive free water surface under existing atmospheric conditions (Shuttleworth, 1993). There is one evaporation station in the entire LRC (Albasini) and is located in the upper reaches of the catchment. Due to the lack of evaporation data in the LRC, potential evapotranspiration (PET) for the catchment was estimated from the temperature-based method. Daily minimum and maximum temperatures from three weather stations (Levubu, Mukumbani, and Tshivhase stations) were collected from SAWS (Table 3.1). Hargreaves and Samani temperature-based method was used to estimate PET in the study area using Equation 3.1.

$$PET = 0.0023 \times R_a \times (T_{max} - T_{min})^{0.5} \times (T + 17.8), \quad (3.1)$$

where, R_a is the solar radiation (MJ/m^2/day), which was measured following the procedure outlined in Allen et al. (1998), T_{max} and T_{min} are the maximum and minimum temperatures (°C), respectively and T is the mean air temperature (°C). Figure 3.6 shows the correlation between the estimated PET and the measured evaporation in the upper reaches of the catchment and Figure 3.7 shows how the estimated PET compared with the catchment temperature. An R^2 of greater than 0.5 shows that a positive linear relationship exists between two variables, therefore the R^2 of 0.56 between the estimated PET and measured evaporation from the Albasini Dam depicts a good comparison.

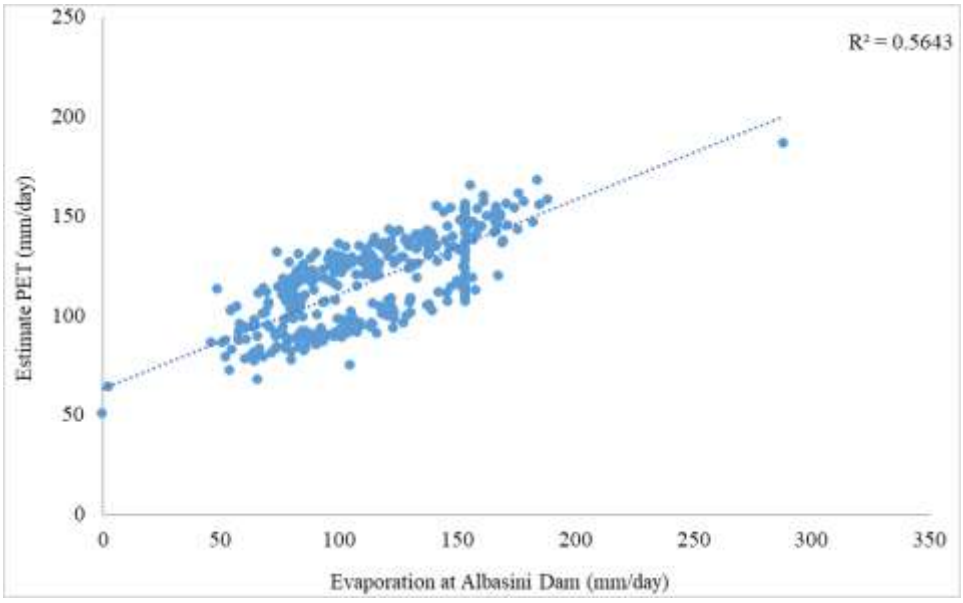

Figure 3.6: Correlation of Hargreaves estimated PET and measured evaporation.

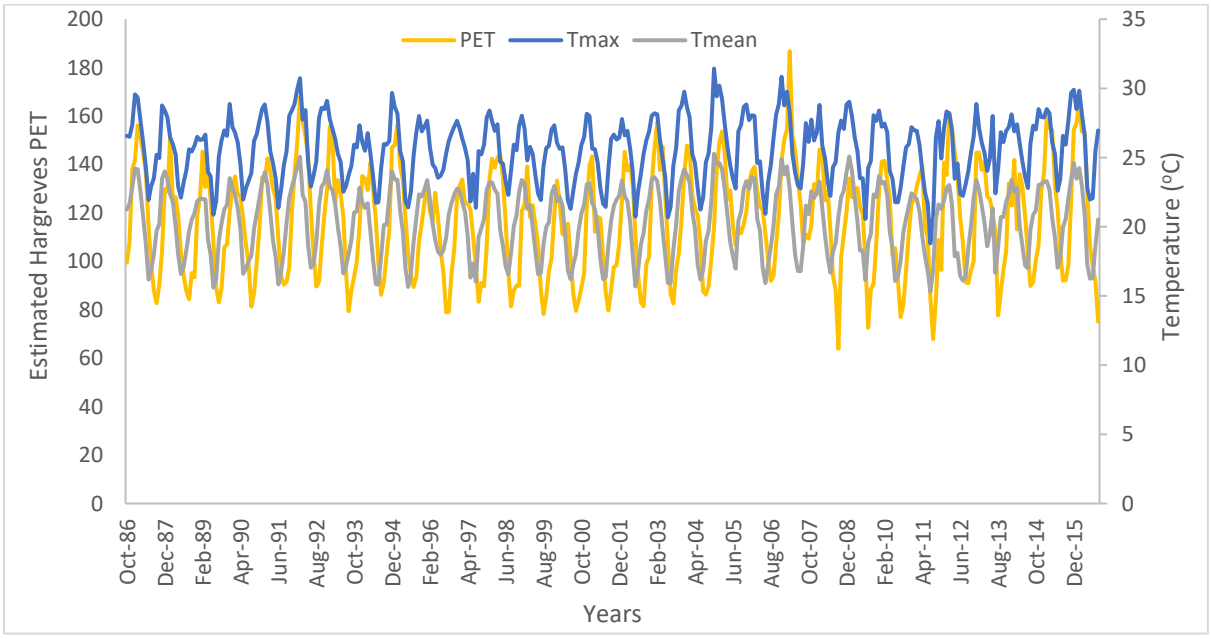

Figure 3.7: Comparison of Hargreaves estimated PET and LRC temperature.

3.4.3 Streamflow

There are approximately 26 streamflow monitoring stations in the LRC, located in the main river system and the major tributaries (Figure 3.8). Most of these stations do not have continuous data with some having large amounts of missing data. Of the 23 streamflow stations, three stations (A9H006, A9H012, and A9H013) with sufficient data were considered in this study. Streamflow data from the selected stations had data between 40 to 54 hydrological years. Measured streamflow data for the entire South Africa is available from the Hydrological

Information Services (HIS) (DWAF, 2003) and therefore data used in this study was obtained from the DWS HIS repository. Table 3.2 and Figure 3.8 show the detailed information on the selected streamflow stations and their location within the study area, respectively.

There are three types of flow gauging structures used in South Africa; namely, Crump weir, Sharp-crested weir, and the Sluicing flumes. The selected streamflow stations are gauged using the sharp-crested weir and the sluicing flume. A comprehensive overview and the calibration theories and techniques as applied in South African rivers are given in Wessels and Rooseboom (2009a); Wessels and Rooseboom (2009b).

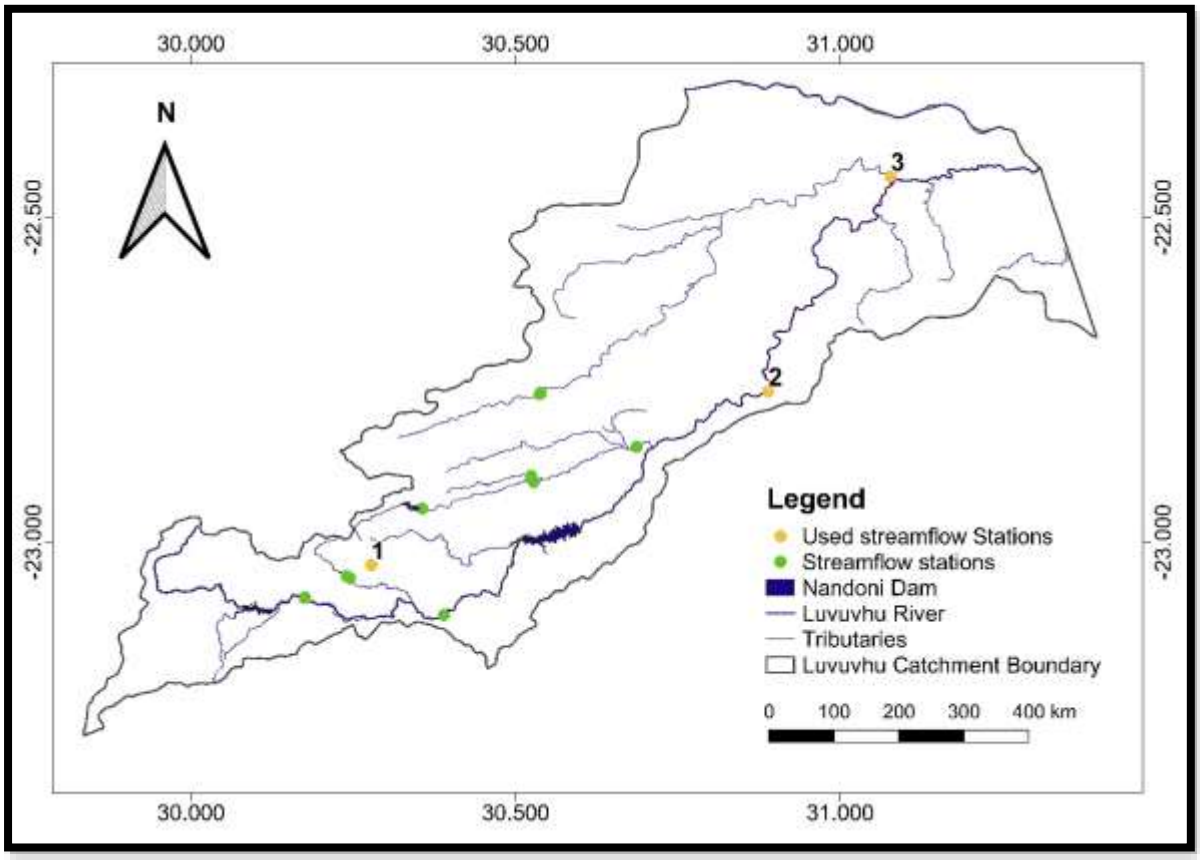

Figure 3.8: Location of streamflow gauging stations and the main reservoir in the LRC.

Table 3.2: Streamflow stations in the study area.

	Station number	Station name	Data span	Data length
1	A9H006	Livhungwa at Barotta	1961 – 2018	57
2	A9H012	Luvuvhu River at Mhinga	1987 – 2018	31
3	A9H013	Mutale River at KNP	1988 – 2018	30

3.4.4 Reservoir storage

There exist three major reservoirs in the LRC, namely; Albasini, Vondo and, Nandoni dams (Figure 3.8). Nandoni Dam only became operational in 2006 and the length of data available was considered not sufficient to meet the objective of the study. Albasini is the oldest of the three reservoirs with a record of 34 years while Vondo had 30 years' record. Reservoir data from Vondo Dam was considered for this study as it had sufficient data of over 30 years and Albasini Dam, although located within the LRC, does not supply the catchment with water. The dam was constructed to supply water to the Makhado Municipality town of Louis Trichardt. The monthly storage time series for Vondo Dam data were obtained from DWS HIS repository. The storage-area relationship for Vondo Dam was used to determine the area inundated for each monthly water level, which was multiplied by the area inundated to obtain reservoir storage.

3.4.5 Soil Moisture

Root zone soil moisture was considered for this study because it plays a significant role in the regulation of water and energy fluxes at the soil–vegetation–atmosphere interface through evaporation processes of the uppermost surface soil layer and plant transpiration (Shukla and Mintz 1982). In situ soil moisture data over many regions of Africa are not available due to the cost of setting up, operating and maintaining dense soil moisture networks. Consequently, soil moisture is often estimated indirectly, using both remote sensing and hydrological models (Myeni et al., 2019). This study, therefore, made use of the Modern-Era Retrospective analysis for Research and Applications version 2 (MERRA-2) as a soil moisture proxy for the study area for the period considered. MERRA-2 is a NASA atmospheric reanalysis for the satellite era using the Goddard Earth Observing System Model, Version 5 (GEOS-5) with its Atmospheric Data Assimilation System (ADAS), version 5.12.4. The MERRA project focuses on historical climate analyses for a broad range of weather and climate time scales and places the NASA EOS suite of observations in a climate context. A detailed description of the

MERRA-2 observation system can be obtained in Reichle (2012). Monthly root zone soil moisture time series from September 1986 to August 2016 were downloaded from the Giovanni website (*https://disc.gsfc.nasa.gov/datasets?keywords=%22MERRA-2%22&page=1&source=Models%2FAnalyses%20MERRA-2*) from the bounding box (Figure 3.9). The MERRA-2 uses the finite-volume dynamical core of Lin (2004) at a horizontal resolution of 0.5° × 0.625° in latitude and longitude, respectively, and 72 hybrid-eta levels from the surface to 0.01 hPa. Figure 3.10 shows the moderate correlation relationship between rainfall in the catchment and the satellite-derived root zone soil moisture. An r^2 of 0.475 at a 90% confidence interval shows that there exists a positive linear relationship between the two variables. Ratner (n.d) showed that correlation coefficient values between 0.3 and 0.7 indicate a moderate positive linear relationship via a fuzzy-firm linear rule. MERRA derived surface soil moisture was reported to correspond positively with in situ observations (R = 0.53±0.01, $p < 0.001$) in the mid-latitudes, where its accuracy was directly proportional to the quality of precipitation (Yi et al., 2011).

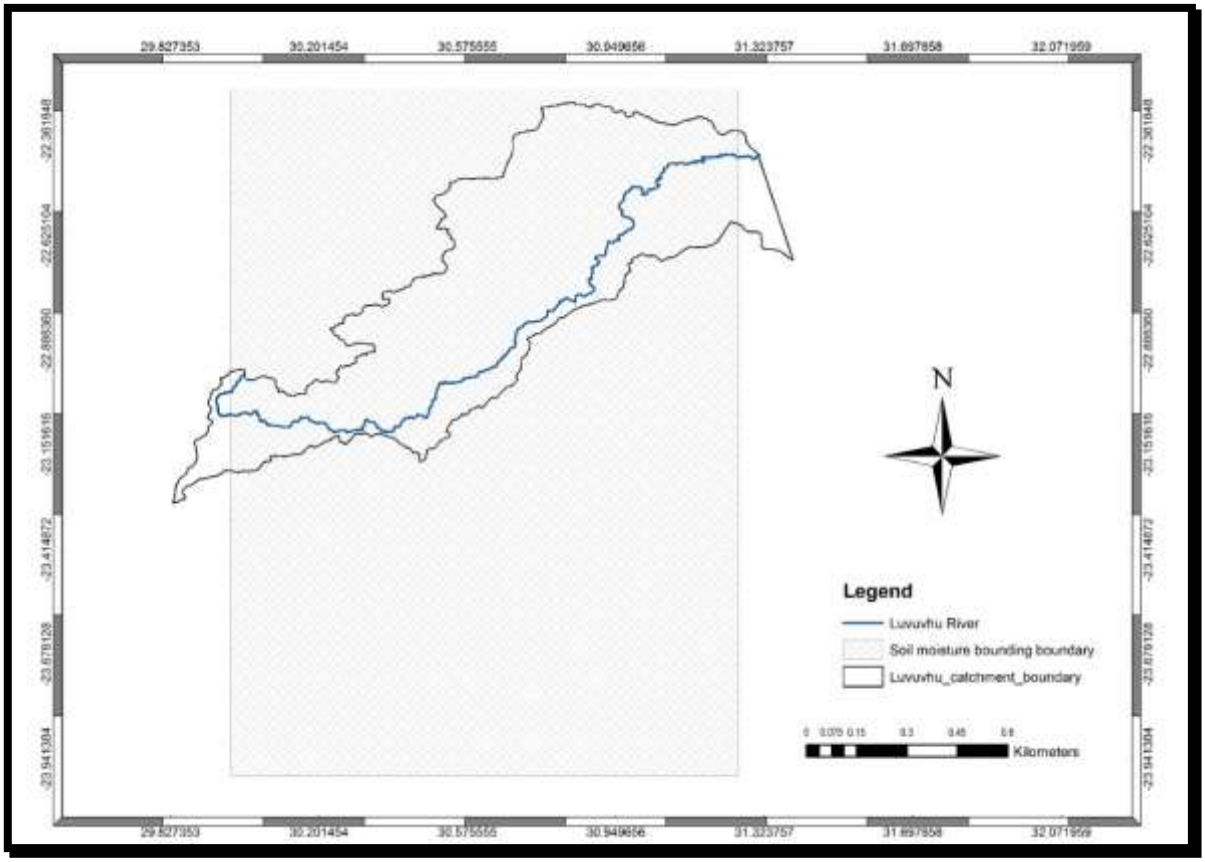

Figure 3.9: MERRA-2 root zone soil moisture bounding box.

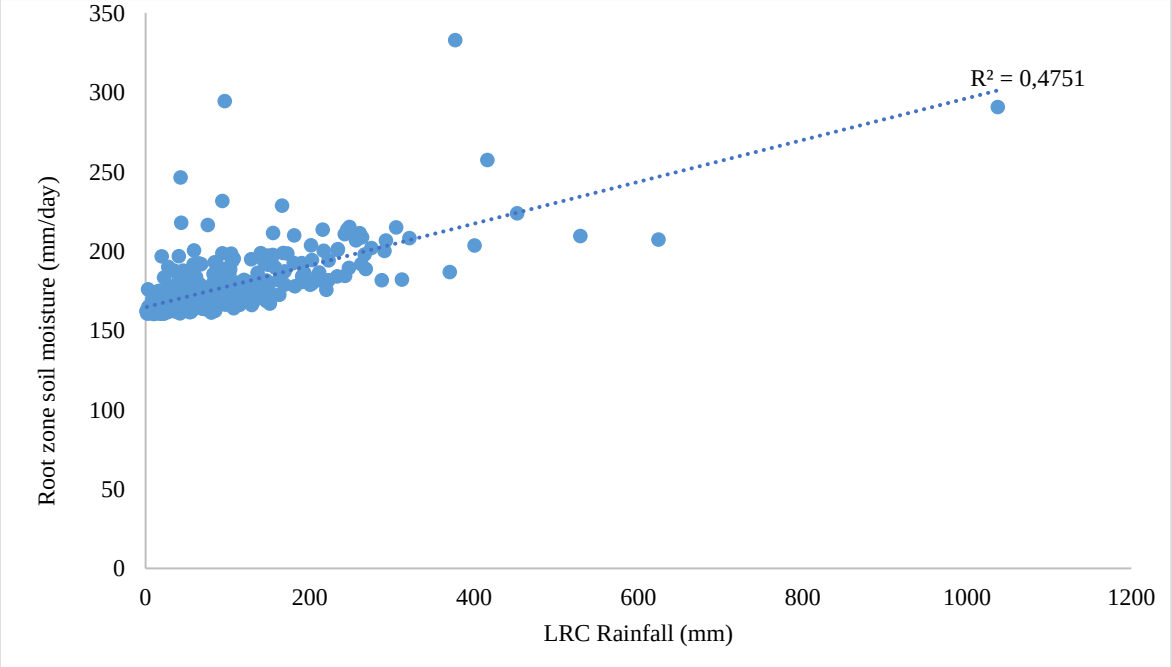

Figure 3.10: Correlation of rainfall and satellite-derived root zone soil moisture.

3.5 Methodological framework

The methodological framework for drought prediction in the LRC is depicted in Figure 3.11. The framework was developed sequentially in-line with the objectives of the study. The study is structured to start with drought assessment where all the four drought indices were applied in this exercise to determine which index best detects historical drought conditions in the study area. The second step was to characterise drought conditions in the catchment. The selected indices were again used for this exercise to determine which index best characterises historical drought. The latter two steps were important as they yield important information in terms of index strength to detect and characterise drought conditions in a place. The following step in the methodological framework was to apply a hybrid drought prediction model that incorporates decomposition, statistical, and artificial neural network methodologies. Then following the application of the models, an uncertainty analysis was carried out to determine the level of reliability of the model.

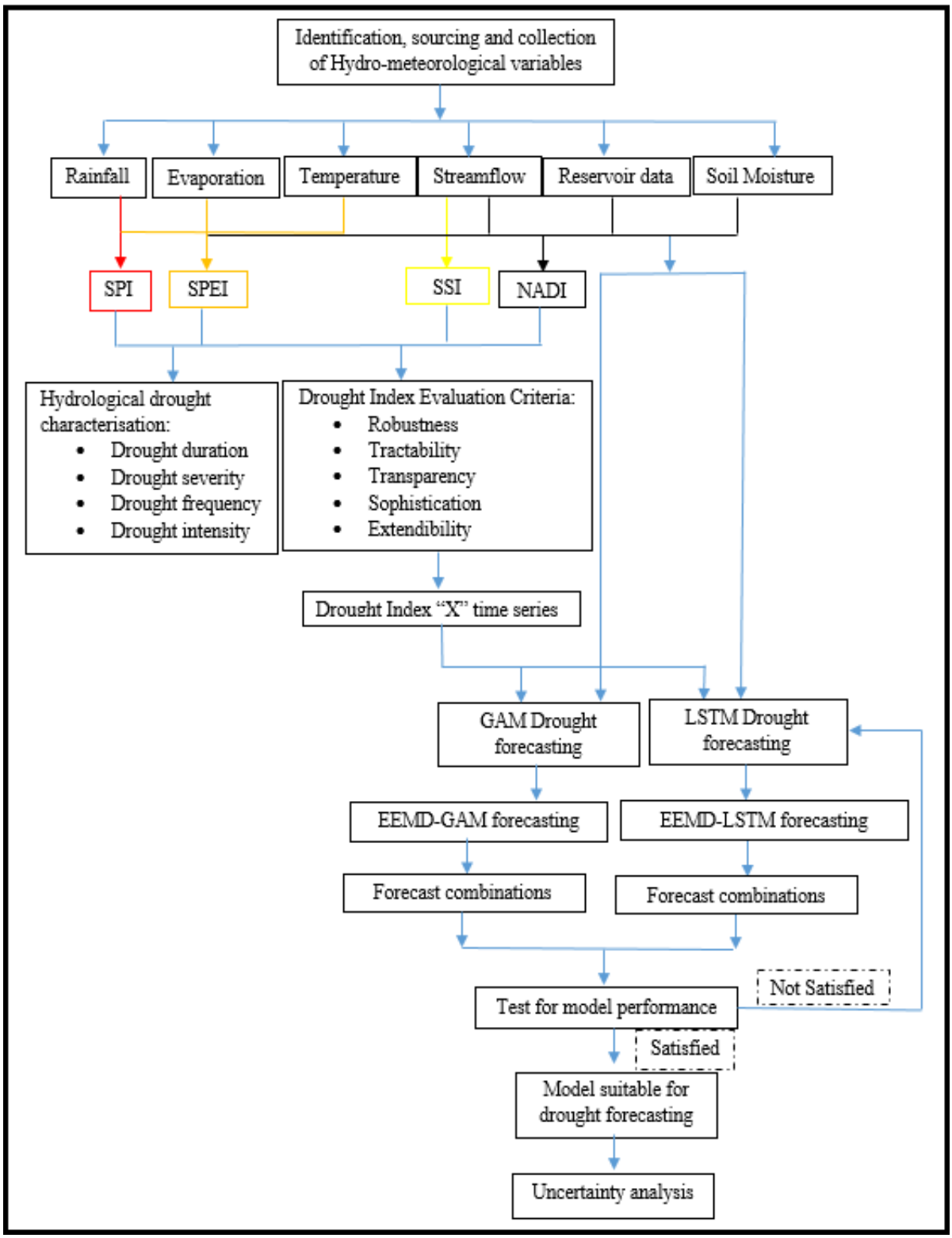

*__GAM__ – Generalised Additive Models, __EEMD__ – Ensemble Empirical Mode Decomposition, __NADI__ – Non-linear Aggregated Drought Index, __LSTM__ – Long Short-term Memory, __SPI__ – Standardised Precipitation Index, __SPEI__ – Standardised Precipitation Evaporation Index, __SSI__ – Standardised Streamflow Index.

Figure 3.11: Methodological framework for drought prediction for LRC.

3.6 Chapter summary

The LRC is an important catchment in the Limpopo Province as it is home to the Levubu valley (an agricultural economic backbone of the Vhembe District). Rainfall in this region of southern Africa is highly influenced by the ITCZ and tropical temperature troughs. The nature of the topography in the study area also influences rainfall distribution. Most of the rainfall is received on the western side of the catchment where the Luvuvhu River rises within the Soutpansberg Mountain range and decreases to the east towards the Kruger National Park. Temperature also increases from the mountainous areas to the lower reaches of the catchment. By its position, the LRC is prone to extreme hydrological events. The region has been found to have witnessed an increase in drought frequency over the past decade. Considering the position of the catchment and its economic importance, such a study is of significance.

Hydro-meteorological variables (i.e. rainfall, evaporation, temperature, streamflow, reservoir storage, and soil moisture) from September 1986 to August 2016 (30 years) were obtained or estimated for the LRC. Hydro-meteorological data is no stranger to gaps, missing data in this study were imputed using Self Organising Maps. Evapotranspiration was estimated using a temperature-based method (Hargreaves) while root zone soil moisture was obtained from the NASA earth data repository. MERRA-2 data were selected since they had data for the required study period. All the datasets obtained or estimated were on a monthly timescale, since they have low observational errors. The datasets were collected or estimated and analysed for the specific purpose of this thesis for the use in the LRC to achieve the objectives of the study. A sequential methodological framework was further depicted in this chapter, this entailed the drought characterisation, assessment, application of drought prediction models, and the analysis of the uncertainty of the applied models.

4 DROUGHT CONDITIONS BASED ON SPI, SPEI, SSI, AND NADI

Chapter overview, Formulation of drought indices, Results, and discussions, Summary

4.1 Chapter overview

Four drought Indices [Standardised Precipitation Index (SPI), Standardised Precipitation Evaporation Index (SPEI), Standardised Streamflow Index (SSI), and the Nonlinear Aggregated Drought Index (NADI)] that describe drought are formulated at different time scales for the LRC. The 1-, 6- and 12- month timescales were adopted in this case study as the formulation of SPI, SPEI, and SSI while 1- month time scale was only applied for NADI. A timescale is the time allowed for or taken by a process or a sequence of events. For example, SPI was designed to quantify the precipitation deficit over multiple timescales which reflect drought impacts on different water resources. The 3- month SPI reflects short- and medium-term moisture conditions and provides a seasonal estimation of precipitation, while information from a 6- month SPI may also be associated with anomalous streamflow and reservoir levels, depending on the region and time of year [World Meteorological Organisation (WMO, 2012)]. The 12- month up to 24- month SPI reflects long-term precipitation patterns and usually associated with streamflow, reservoir levels, and even groundwater levels on longer timescales.

The objective of this chapter is to detect and assess historical hydrological drought conditions in the LRC. The methodology followed in formulating each respective index together with the case study results and discussions is presented. The assessment of drought for this case study focused on each index capability to detecting notable historic drought as reported in literature within the catchment, how each index categorised historical drought events and which category was more prevalent was also discussed. Mann-Kendall trend test was also utilised to detect drought trends and their significance in the LRC. The catchment spatial variability maps were generated for the LRC to show the locations which are most affected by drought in the catchment.

4.2 Formulation of drought indices methodology

Four indices have been selected to assess and characterise drought conditions in the study area. Although (Hayes et a., 2010) indicated that there seems to be a scientific consensus that there

is no best hydrological drought index, this study selected for instance SPI based on a recommendation by the WMO (2009). Both SPI and SPEI have been widely used in drought assessment (Masih et al., 2014; Botai et al., 2016; Edossa et al., 2016; Masupa et al., 2016; Kolusu et al., 2019) and prediction (Mishra et al., 2006; Maca and Pech, 2016; Le et al., 2016; Mulualem and Liou, 2020) studies. NADI is a relatively new index based on the linear ADI and accounts for all components of the hydrological cycle. Therefore, indices were selected based on their different input variables and their application in different drought studies.

4.2.1 Standardised Precipitation Index

The SPI was utilised to quantify the rainfall deficit within the LRC. The procedure involved fitting the rainfall data into a Probability Density Function (PDF). A gamma distribution function was adopted as it fits well in rainfall time series data (Sometz et al., 2005). The gamma distribution is expressed in terms of its PDF as:

$$f(x;\alpha,\beta) = \frac{1}{\beta^{\alpha}\Gamma(\alpha)} x^{\alpha-1} e^{-x/\beta} \quad \text{for } , \alpha,\beta > 0, \tag{4.1}$$

where α is the shape parameter, β is the scale parameter, x is the rainfall amount (mm), $\Gamma(\alpha)$ is the value taken by the Gamma function and $\bar{x}$ is the mean rainfall (mm). The $\Gamma(\alpha)$ is the value defined by a standard mathematical equation called the Gamma function. This is given by Cacciamani et al. (2007) as:

$$\Gamma(\alpha) = \int_0^{\alpha} x^{\alpha-1} e^{-y} dx, \tag{4.2}$$

where $\Gamma(\alpha)$, x, and α are defined in Equation (4.1). The above Gamma function was then evaluated both by the numerical method and the use of tabulated values depending on the value taken by the shape parameter α. A maximum probability is used to estimate the optimal values of α and β using the function given in the Equations: (4.3) and (4.4) respectively:

$$\alpha = \frac{1}{4A}\left(1 + \sqrt{1 + \frac{4A}{3}}\right), \tag{4.3}$$

$$\beta = \frac{\bar{x}}{\alpha}, \tag{4.4}$$

where α *is* the shape parameter, β is the scale parameters, $\bar{x}$ is defined above and A is the sample statistic. The sample statistic is defined as:

$$A = \ln(\bar{x}) - \frac{\ln x}{n}, \quad (4.5)$$

where n is the number of observations. The calculated values are then used to compute the cumulative probability for non-zero rainfall using Equations (4.6) and (4.7), respectively:

$$f(x;\alpha,\beta) = \int_0^x f(x,\alpha,\beta)dx = \frac{1}{\beta^{\alpha}\Gamma(\alpha)}\int_0^x x^{\alpha-1}e^{-x/\beta}\ dx \quad (4.6)$$

Equation 4.6 parameters are defined in Equation 4.4.

$$f(x;\alpha,\beta) = \frac{1}{\Gamma(\alpha)}\int_0^x t^{a-1}e^{-t}dt \text{ for } t = \frac{x}{\beta}, \quad (4.7)$$

where *Γ(α)*, *x*, and *β* are defined above in Equation 4.1 and 4.4 respectively while *t* is the time. The gamma function applies for values of rainfall $x > 0$ for the rainfall time series of the basin under study. In the case of non-zero values, there was a need to compute the cumulative probability of both zero and non-zero values. This probability is represented by a function *H(x)* defined as:

$$H(x) = q + (1-q)f(x;\alpha,\beta), \quad (4.8)$$

where *H(x)* is the cumulative probability and q is the probability of zero rainfall. If m is the number of zeroes and n the number of observations in the rainfall time series, then q is estimated by the ratio n. The cumulative probability is transformed into a standard normal distribution in such a way that the mean and variance of the *SPI* are zero and one respectively. To carry out this step, an approximate transformation as per Mishra and Desai (2006) was adopted. This is achieved as follows:

$$SPI = k - \frac{C_0 + C_1 k + C_2 k^2}{1 + d_1 k + d_2 k^2 + d_3 k^3} \quad (4.9)$$

The value of *k* in Equations (4.9) was determined from the functions given below:

$$k = \sqrt{ln\left(\frac{1}{1-H(x)^2}\right)}, \quad (4.10)$$

where C_0 is 2.515517, C_1 is 0.802853, C_2 is 0.010328, d_1 and is 1.432788, d_2 is 0.189269 and d_3 is 0.001308 (Bezdan *et al*., 2019) and these are constants values for computing the SPI. The SPI uses a classification system whereby wet conditions are indicated by positive values and

negative values represent dry conditions (Table 4.1). This study only makes use of negative values as they indicate drought.

Table 4.1: SPI drought classification (McKee *et al*., 1993).

SPI Values	Drought category
0 to -0.99	Mild/ Near normal
-1.00 to -1.49	Moderate
-1.50 to -1.99	Severe
≤ -2.0	Extreme

4.2.2 Standardised Precipitation Evaporation Index

The SPEI is based on the computation procedure of the original SPI. The index makes use of either monthly or weekly difference between precipitation and Potential Evapotranspiration (PET) (Vicente-Serrano *et al*., 2010a). Due to the complex computation of the PET which involves numerous parameters, including surface temperature, air humidity, soil incoming radiation, water vapour pressure, and ground-atmosphere latent and sensible heat fluxes (Allen *et al*., 1998), this study made use of Hagreaves and Samani temperature-based method for PET estimation. The latter approach has the advantage of only requiring data on monthly-mean temperature. The SPI methodology was modified by replacing the two-parameter distribution with a three-parameter distribution (i.e. SPEI requirement) (Vicente-Serrano *et al*., 2010a). The latter suggested getting the best fit three-parameter distribution from L-moments and the detailed methodology for achieving this can be obtained in Hosking (1990). Following the classical approximation of Abramowitz and Stegun (1965), SPEI is given as:

$$SPEI = W - \frac{C_0 + C_1 W + C_2 W^2}{1 + d_1 W + d_2 W^2 + d_3 W^3}, \qquad (4.11)$$

where $W = \sqrt{-2\ln(P)}$ for $P \leq 0.5$ and P is the probability of exceeding a threshold value denoted by D value, $P = 1 - F(x)$. If $P > 0.5$, then P is replaced by $1 - P$ and the sign of the resultant SPEI is reversed. The constants C_0, C_1, C_2, d_1, d_2, and d_3 are as defined in Equation (4.9). For this study, SPEI was computed using a CRAN Package "spei" in R. The SPEI drought classification is similar to that of SPI, therefore Table 4.1 was adopted to classify drought categories for the case of SPEI.

4.2.3 Standardised Streamflow Index

For determining the SSI, this study followed the procedure as outlined in Faragman and Aghakouchak (2015), which derived marginal probability of (i.e. precipitation and streamflow) using the empirical Gringorten plotting position (Gringorten, 1963) as shown in Equation (4.12).

$$P(x_i) = \frac{i-0.44}{n+0.12}, \quad (4.12)$$

where; n is the sample size, i denotes the rank of non-zero streamflow data from the smallest, and $P(x_i)$ is the corresponding empirical probability. Making use of such an empirical approach, the original distribution (two-term gamma probability density function and the cumulative gamma distribution function) used in SPI for instance are not required to derive the parametric probabilities. Following the classical approximation as described by Abramowitz and Stegun (1965); Entekhabi *et al*. (1996); Edwards and McKee (1997), SSI is computed as follows:

$$SSI = t - \frac{C_0+C_1t+C_2t^2}{1+d_1t+d_2t^2+d_3t^3}, \quad (4.13)$$

The constants C_0, C_1, C_2, d_1, d_2, and d_3 are as defined in Equation (4.9), while t is given by Equation (4.14).

$$t = \sqrt{ln\frac{1}{P^2}}, \quad (4.14)$$

Since SSI is a standardised index, the SPI classification as described by McKee *et al*. (1993) is adopted to categorise the different drought events in the study area.

4.2.4 Formulation of NADI for the LRC

NADI for the LRC was formulated using five hydro-meteorological variables (i.e. precipitation, potential evapotranspiration, streamflow, storage reservoir volume, and soil moisture content). These variables have been discussed in detail in Chapter 3. The formulation of NADI steps followed in this study was adapted from Barua (2012) as shown in Figure 4.1. NADI represents an overall catchment water availability as opposed to the standardised indices considered which can be computed for the catchment and on a station to station basis.

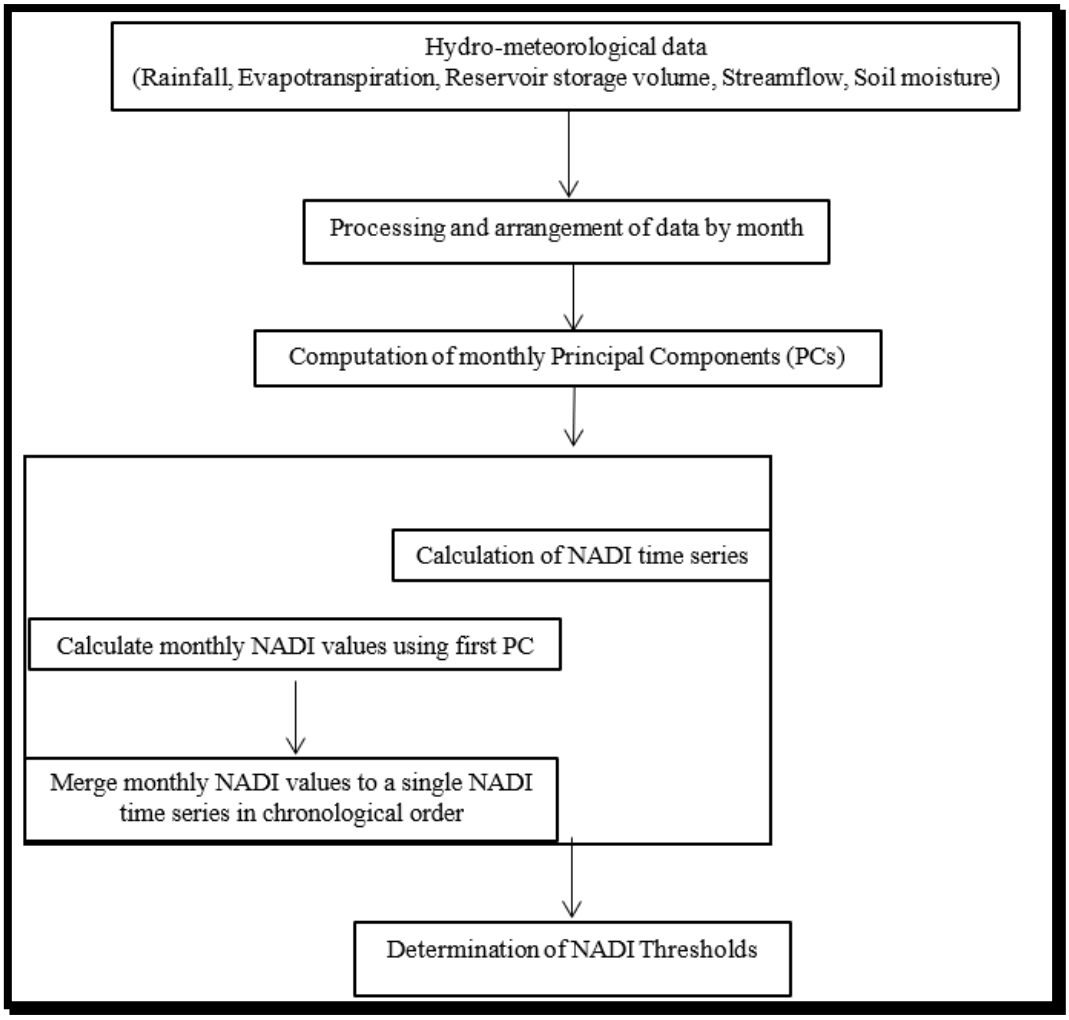

Figure 4.1: Process for NADI formulation (Adopted from Barua, 2010).

4.2.4.1 Computation of Principal Components using NLPCA

Although NLPCA is widely used as a data redundant technique (Kramer, 1991; Monahan, 2000, 2001; Linting *et al*., 2007), in this study, however, it was utilised to aggregate hydrologic information from the five hydro-meteorological variables (rainfall, evapotranspiration, streamflow, reservoir storage, and soil moisture) that resulted in the NADI time series. The NLPCA is like linear PCA, the difference is that in PCA, PCs are obtained through a linear combination of variables while in the NLPCA, PCs are obtained through a linear combination of transformed variables (Barua, 2010). Linting *et al*. (2007) reported that PCs obtained through NLPCA capture the nonlinear relationship between hydro-meteorological variables and account for more variance compared to the linear PCA. The variable transformation is achieved through NLPCA using an iterative process. A detailed discussion of the iterative process can be obtained in Barua (2010).

4.2.4.2 Computation of NADI time series

To compute the NADI time series for the duration considered in this study, only PC1 was utilised. This is because PC1 explains the largest fraction of variance of a standardised sample data, like the case of ADI. Since PCs are orthogonal vectors, it is not mathematically proper to combine them into a single expression. Keyantash and Dracup (2004) suggested that only the dominant mode be adopted to describe water anomalies. Hence the adoption of PC1 in the NADI computation. Considering 12 months, PC1 obtained through NLPCA described a data set variance of 70%. To represent a normalised expression of variability for the computed NADI, PC1 is standardised using Equation (4.18). Keyantash and Dracup (2004) indicated that in the absence of standardisation, months that routinely possess a higher degree of hydrologic variability result in a chronological plot of NADI values to predictably jump.

$$NADI_{i,x} = \frac{P_{i,1,x}}{\sigma_x}, \tag{4.18}$$

where $NADI_{i,x}$ is the NADI value for the x^{th} month in i^{th} year, $P_{i,1,x}$ is the PC1 during the i^{th} year for the x^{th} month while σ_x is the standard deviation of $P_{i,1,x}$ over all the years for x^{th} month. Following the computation of NADI values for each month for all the year under consideration using Equation (4.18), the individual month NADI is reorganised chronologically in a single NADI time series.

4.2.4.3 Example of NADI calculation at the beginning of the hydrological year

The example discussed here considers the computation of NADI for September. The 30 years of observed monthly data for rainfall (*R*), evaporation (*E*), streamflow (*S*), reservoir storage volume (*RS*), and root-zone soil moisture (*SM*) are arranged into a [30 x 5] matrix. The monthly data of *R, E, S, RS,* and *SM* were used in their original units of millimetres, cubic meters per second, cubic meters per day, a cubic meter of water per cubic meter of soil respectively in $\mathbf{O}_{September}$ (Figure 4.2). The differing units of measurements do not have any impact on the results as the non-correlation-based NLPCA approach was used to standardise the data and its un-impacted by units of measurements. Matrix $\mathbf{O}_{September}$ was then used in CAPTCA module of SPSS to generate another [30 x 5] matrix $\mathbf{T}_{September}$ (Figure 4.3) which contain optimally transformed variables and [5 x 5] matrix eigenvectors. However, since PC1 describes the greatest variance, only [5 x 1] matrix containing eigenvectors related to PC1 $\mathbf{P}_{September}$ (Figure 4.4) is utilised in NADI computation.

$O_{september}$ =

12.978	18.282	99.45	8.985	162.785
10.11	95.745	90.196	6.138	171.397
20.048	73.364	95.197	14.019	169.153
5.468	41.855	105.699	10.148	160.629
3.6	13.809	99.526	4.61	161.292
10.329	17.495	97.532	5.63	160.436
0.296	11.682	105.826	1.939	160.495
7.758	19.318	93.557	10.515	161.097
1.215	20.918	102.513	5.224	160.756
2.858	8.673	108.415	3.432	161.144
40.819	27.477	95.089	27.506	168.369
29.504	96.818	89.703	40.133	166.133
10.957	79.982	90.098	26.062	161.173
27.129	20.745	95.72	32.236	162.576
27.893	76.536	89.13	68.52	169.348
33.734	25.909	97.627	67.104	162.628
15.605	38.082	98.867	55.654	162.854
4.287	51.173	103.474	30.103	162.549
26.24	23.182	100.984	41.354	161.758
4.447	10.318	115.493	20.986	160.618
12.476	3.064	107.109	33.519	160.532
7.414	84.682	109.309	22.812	162.203
10.948	6.855	101.562	17.305	164.219
9.285	20.1	90.659	13.753	161.908
13.243	10.5	96.453	17.932	160.817
14.437	8.882	108.863	27.496	170.027
11.178	28.495	96.43	19.435	168.13
13.498	28.065	96.287	55.882	162.299
23.927	7.782	100.681	64.999	161.468
23.318	78.082	98.456	52.627	173.542

Figure 4.2: Observed data matrix for September.

$\mathbf{T}_{september}$ =

0.095	-0.669	0.17	-1.254	0.085
-0.704	2.003	0.054	-1.254	2.109
0.796	1.398	0.17	-0.524	1.395
-1.029	0.154	0.17	-0.524	-0.643
-1.029	-0.669	0.17	-1.254	-0.643
-0.704	-0.669	0.17	-1.254	-1.345
-1.029	-0.669	0.17	-1.254	-0.643
-0.704	-0.669	0.054	-0.524	-0.643
-1.029	-0.669	0.17	-1.254	-0.643
-1.029	-1.005	0.17	-1.254	-0.643
1.91	0.154	0.17	0.171	1.395
1.363	2.003	0.054	0.756	0.763
-0.704	1.398	0.054	0.171	-0.643
1.363	-0.669	0.17	0.171	-0.643
1.363	1.398	0.054	1.933	1.395
1.91	-0.669	0.17	1.933	-0.643
0.095	0.154	0.17	1.249	0.085
-1.029	0.853	0.17	0.171	-0.643
1.363	-0.669	0.17	0.756	-0.643
-1.029	-0.669	0.17	-0.524	-0.643
0.095	-1.005	0.17	0.756	-0.643
-0.704	2.003	0.17	0.171	-0.643
-0.704	-1.005	0.17	-0.524	0.085
-0.704	-0.669	0.054	-0.524	-0.643
0.095	-0.669	0.17	-0.524	-0.643
0.095	-0.669	0.17	0.171	2.109
-0.704	0.154	0.17	-0.524	1.395
0.095	0.154	0.17	1.249	-0.643
1.363	-1.005	0.17	1.933	-0.643
1.363	1.398	0.17	1.249	2.109

Figure 4.3: Matrix **T** containing optimally transformed variables.

$\mathbf{P}_{september}$ =

0.828
0.598
0.214
0.742
0.648

Figure 4.4: Matrix **P** containing eigenvectors related to PC1.

The [30 x 1] matrix of PC1 ($|\boldsymbol{X}_{September}$) is then computed for September using Equation (4.19). This equation relates the optimally transformed data to the respective PCs. Figure 4.5 is the example computation for September.

$$X = TP, \tag{4.19}$$

$$\mathbf{X}_{september} = \mathbf{T}_{september} \cdot \mathbf{P}_{september} =$$

0.095	-0.669	0.17	-1.254	0.085			-1.16
-0.704	2.003	0.054	-1.254	2.109			1.065
0.796	1.398	0.17	-0.524	1.395			2.047
-1.029	0.154	0.17	-0.524	-0.643			-1.529
-1.029	-0.669	0.17	-1.254	-0.643			-2.562
-0.704	-0.669	0.17	-1.254	-1.345			-2.748
-1.029	-0.669	0.17	-1.254	-0.643			-2.562
-0.704	-0.669	0.054	-0.524	-0.643			-1.777
-1.029	-0.669	0.17	-1.254	-0.643			-2.562
-1.029	-1.005	0.17	-1.254	-0.643			-2.764
1.91	0.154	0.17	0.171	1.395	0.828		2.74
1.363	2.003	0.054	0.756	0.763	0.598		3.394
-0.704	1.398	0.054	0.171	-0.643	0.214	=	-0.025
1.363	-0.669	0.17	0.171	-0.643	0.742		0.474
1.363	1.398	0.054	1.933	1.395	0.648		4.314
1.91	-0.669	0.17	1.933	-0.643			2.233
0.095	0.154	0.17	1.249	0.085			1.188
-1.029	0.853	0.17	0.171	-0.643			-0.595
1.363	-0.669	0.17	0.756	-0.643			0.908
-1.029	-0.669	0.17	-0.524	-0.643			-2.021
0.095	-1.005	0.17	0.756	-0.643			-0.343
-0.704	2.003	0.17	0.171	-0.643			0.362
-0.704	-1.005	0.17	-0.524	0.085			-1.481
-0.704	-0.669	0.054	-0.524	-0.643			-1.777
0.095	-0.669	0.17	-0.524	-0.643			-1.091
0.095	-0.669	0.17	0.171	2.109			1.209
-0.704	0.154	0.17	-0.524	1.395			0.062
0.095	0.154	0.17	1.249	-0.643			0.716
1.363	-1.005	0.17	1.933	-0.643			1.579
1.363	1.398	0.17	1.249	2.109			4.295

Figure 4.5: Matrix of the first Principal Components (PC1) for September.

The NADI values for September for 30 years are computed using Equation 4.18. The 30 years' standard deviation of the 1st PC for September is computed as 2.09. Figure 4.6 shows the NADI time series for September. The NADI time series for the remaining months are also computed similarly to the September example outlined in the section.

$NADI_{September} = X_{september}/STDEV = 1/2.09 =$	-1.16	=	-0.556
	1.065		0.511
	2.047		0.981
	-1.529		-0.733
	-2.562		-1.228
	-2.748		-1.317
	-2.562		-1.228
	-1.777		-0.852
	-2.562		-1.228
	-2.764		-1.325
	2.74		1.313
	3.394		1.627
	-0.025		-0.012
	0.474		0.227
	4.314		2.068
	2.233		1.07
	1.188		0.569
	-0.595		-0.285
	0.908		0.435
	-2.021		-0.969
	-0.343		-0.165
	0.362		0.173
	-1.481		-0.71
	-1.777		-0.852
	-1.091		-0.523
	1.209		0.579
	0.062		0.03
	0.716		0.343
	1.579		0.757
	4.295		2.059

Figure 4.6: Computed NADI values for September between 1986 and 2016.

4.2.4.4 Determination of NADI threshold

As shown in Figure 4.1, the last step is to rearrange NADI into a single time series in chronological order. NADI threshold values are calculated probabilistically for a study area using an empirical CDF. The SPI threshold was used to generate the NADI threshold, SPI dryness thresholds are Gaussian variates -2, -1.5, -1, and 1 standard deviation which corresponds to 2.3rd, 6.7th, 16.0th and 84.0th percentiles in the SPI cumulative distribution. The NADI threshold corresponding to the latter percentiles for the LRC are; -2.05, -1.42, -1.09, and 1.01 respectively (Figure 4.7). Table 4.2 relates the NADI threshold to the relevant drought

classification in the LRC, as shown in Figure 4.7, a threshold is considered zero. This is because NADI drought classes are obtained using the SPI dryness threshold and this considers a drought event to occur anytime when SPI values are continuously negative (McKee *et al*., 1993). Therefore, although the near normal or mild drought condition classification is between -1.09 and 1.01, the study only considered drought when NADI values were continuously negative.

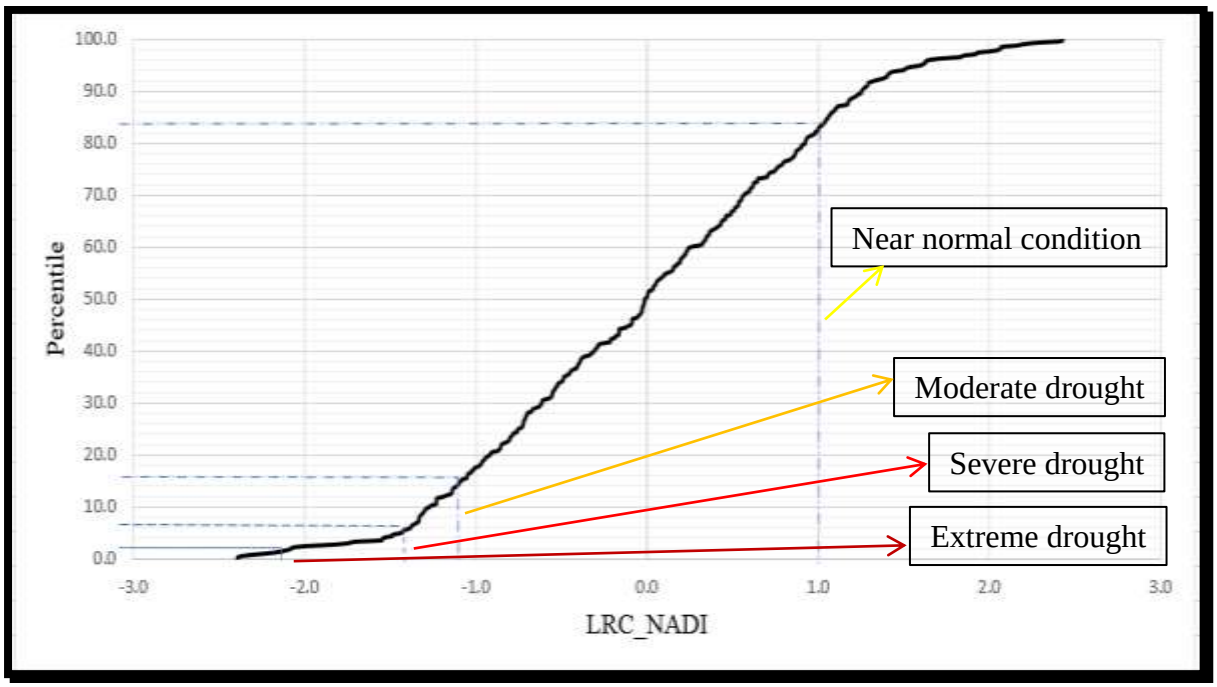

Figure 4.7: Computed NADI threshold for the Luvuvhu River Catchment.

Table 4.2: Drought classification based on the NADI threshold for the LRC.

SPI	NADI	Drought category
0 to -0.99	**0 to -1.09**	Mild/Near normal
-1.00 to -1.49	**-1.10 to -1.41**	Moderate
-1.50 to -1.99	**-1.42 to -2.04**	Severe
≤ -2.0	**≤ -2.05**	Extreme

4.3 Determination of drought trends in the study area

The Breaks for Additive Seasonal and Trend (BFAST) Equation (4.20) method is applied to decompose the drought index time series to obtain the trend variations in the study area.

$$y_t = m + T_t + S_t + R_t \,, \qquad (4.20)$$

where, m is the constant, T is the trend component value, S is the seasonal component, and R is the random component at time step t. Mann-Kendall (M-K) non-parametric trend test is

utilised to detect hydrological drought trends for the four drought indices formulated for the LRC. M-K is recommended by WMO as an approach for calculating the trend of hydro-meteorological time series (Mann, 1945; Kendall, 1976). The MK test statistics ***S*** is expressed as;

$$S = \sum_{i<j} sgn(x_j - x_i) \ , \tag{4.21}$$

where, n is the number of data points, x_i and x_j are the data values in time series i and j, $i < j$, respectively and $sgn(x_j - x_i)$ is the sign function given as:

$$sgn(x_j - x_i) = \begin{cases} 1 & x_j > x_i \\ 0 & x_j = x_i \\ -1 & x_j < x_i. \end{cases} \tag{4.22}$$

The variance of ***S*** is computed as;

$$Var(S) = \frac{n(n-1)(2n+5)}{18}, \tag{4.23}$$

where, n is the length of the data points. In cases where the sample size $n > 10$, the standard-isation test statistic is computed by;

$$Z = \begin{cases} \frac{S-1}{Var(S)} & S > 0 \\ 0 & S = 0 \\ \frac{S+1}{Var(S)} & S < 0. \end{cases} \tag{4.24}$$

Positive values of Z indicate an increasing trend while a negative value of Z indicates a declining trend. When the null hypothesis is rejected a significant trend exists in the time series. S is obtained from the standard normal distribution with an exceeding probability of $\alpha/2$. This study set the significance levels α at 0.05 corresponding to a Z value 2.38. Assigning a small value of significance level gives a small chance of rejecting the null hypothesis if it is true (Ross, 2017). Further, a 5% significance level has become common in practice.

4.4 Results and discussions

4.4.1 Index based historical drought detection

4.4.1.1 SPI

SPI time series were analysed at three timescales (1-, 6- and 12- month) and further used to detect historical drought in the LRC for the duration of 30 hydrological years (September 1986 to August 2016). As indicated in Chapter 3, notable historic droughts i.e. 1987/88 (SPI of -1.2), 1991/92 (SPI of -1.46), 1994/96 (SPI of -1.14), 2001/02 (SPI of -1.54), and 2014/16 (SPI < -2), were the focus regarding the historical assessment of drought in the catchment. Figure 4.8 shows the SPI drought time series at 1-, 6- and 12- timescales for station KA. For SPI figures of all the other stations computed for the LRC, see Appendix A (Figures A1, A2, and A3). The analysis of all SPI time scales successfully detected all the notable drought years as reported in the literature (Glantz *et al*., 1997; Mason and Tyson, 2000; Vogel *et al*., 2000; FAO, 2004; Chikoore, 2016) and further detected more drought years as depicted in Figure 4.8. Although the drought was detected in all months of the year, the majority were between September and March and this may be due to the fact that; this is the period the study area received its rainfall. The LRC is one of the summer rainfall regions in South Africa. The mean rainfall in the study area onset is September and cessation is in March of the subsequent year.

Although literature (e.g. Mason and Tyson, 2000; Vogel *et al*., 2000; Chikoore, 2016) reported the 1991/92 drought as the most extreme in the region, resulting in major economic losses, only two stations (KA and VB) could detect this extreme event at 6 and 12-time scales. The most extreme drought cases across all stations and time scales are between 2012 and 2015, with Lev station reporting 35 drought months at 12- month timescale. The 35 drought months correspond to 20.61% (see Table 4.3) in that station. Table 4.3 shows historical drought categories percentages of occurrence. Mild droughts are more dominant in the catchment with all stations reporting their occurrences at over 60% except for Mat station at 6- month timescale, which showed an occurrence of 55.43%. Moderate drought ranged between 7.88% and 27.05% while severe cases ranged between 0.36% and 16.77%. Extreme drought was the least found and ranged between 0% and 21.61%. This study found that increased SPI time scales increase with drought severity, this is because, and the majority of extreme droughts were shown at 6- and 12- month timescales.

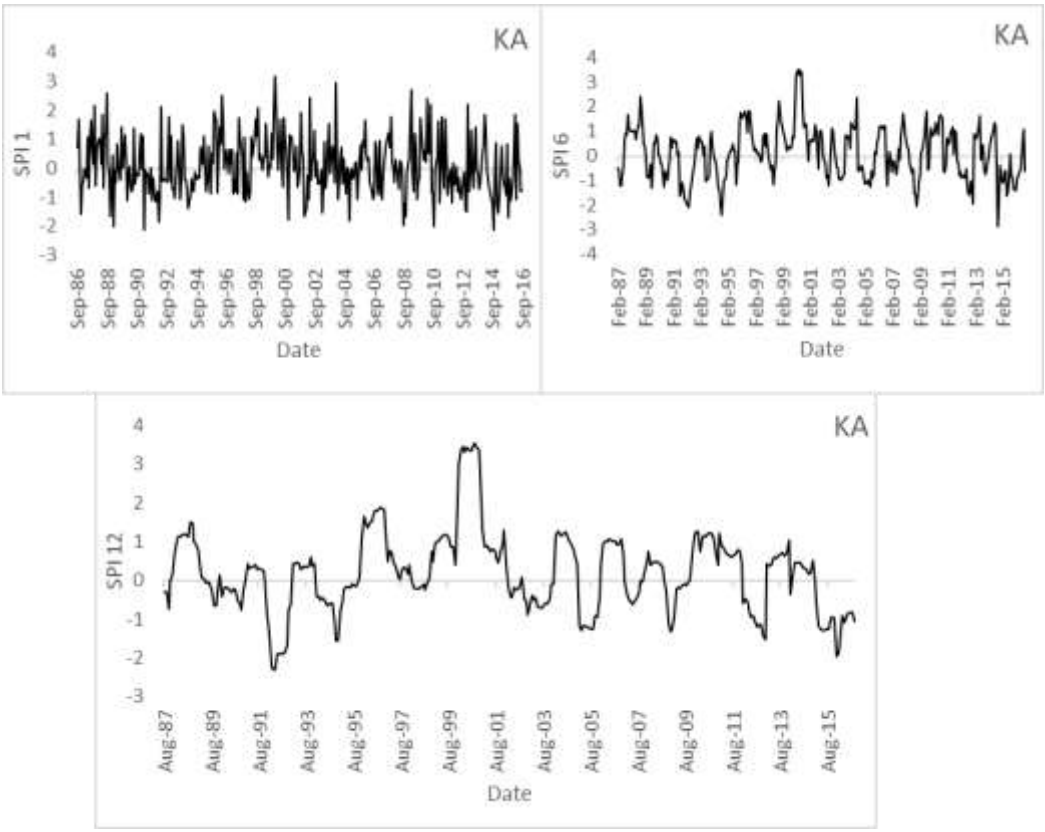

Figure 4.8: SPI time series for KA station at 1-, 6- and 12- timescales.

Table 4.3: Analysis of SPI historical drought categories.

Station	Timescale	Mild (%)	Moderate (%)	Severe (%)	Extreme (%)
KA	1	76.6	14.89	6.38	1.6
	6	68.78	19.88	7.83	3.61
	12	73.75	16.25	7.5	1.88
Lev	1	71.08	18.63	9.8	0.49
	6	67.03	9.89	11.54	11.54
	12	68.49	**7.88**	3.03	**20.61**
Mat	1	61.62	24.75	12.12	1.52
	6	**55.43**	21.2	11.41	11.96
	12	60.77	18.79	8.29	12.16
Muk	1	82.26	10.75	6.45	0.54
	6	65.22	15.53	9.94	8.7
	12	61.49	13.51	**14.87**	10.14
Nooit	1	**82.81**	10.94	5.21	1.04
	6	62.84	27.87	7.65	1.64
	12	65.56	26.67	7.78	0
Shef	1	73.08	21.15	5.29	0.48
	6	69.56	**27.05**	2.9	0.48
	12	80.51	15.9	**0.36**	**0**
Tshi	1	78.95	10.53	8.77	1.75
	6	73.41	14.45	5.78	6.36
	12	66.46	11.18	16.77	5.59
VB	1	71.67	18.33	7.78	2.22
	6	73.14	14.29	6.86	5.71
	12	79.16	11.31	4.76	4.76

Figure 4.9 shows the spatial variability of SPI at the study timescales. This study made use of station data and thus, the stations with quality data were concentrated in the upstream of the catchment. Therefore, the variability in the lower reaches of the catchment is not discussed in this study. SPI 6- (ranged from -0.7425 and -1.027) showed the greatest variability followed by 12- (ranged from -0.6996 and -0.9895) and the 1- (ranged from -0.6346 and -0.8248). This study found that the variability was greatly influenced by the average station data. Upper reaches showed the least drought severity at 1- and 12- month timescales while 6- month timescale showed greater severity. The upper reaches of the LRC receive higher amounts of precipitation compared to the middle and lower reaches and this is can be seen in the variability as shown in Figure 4.9.

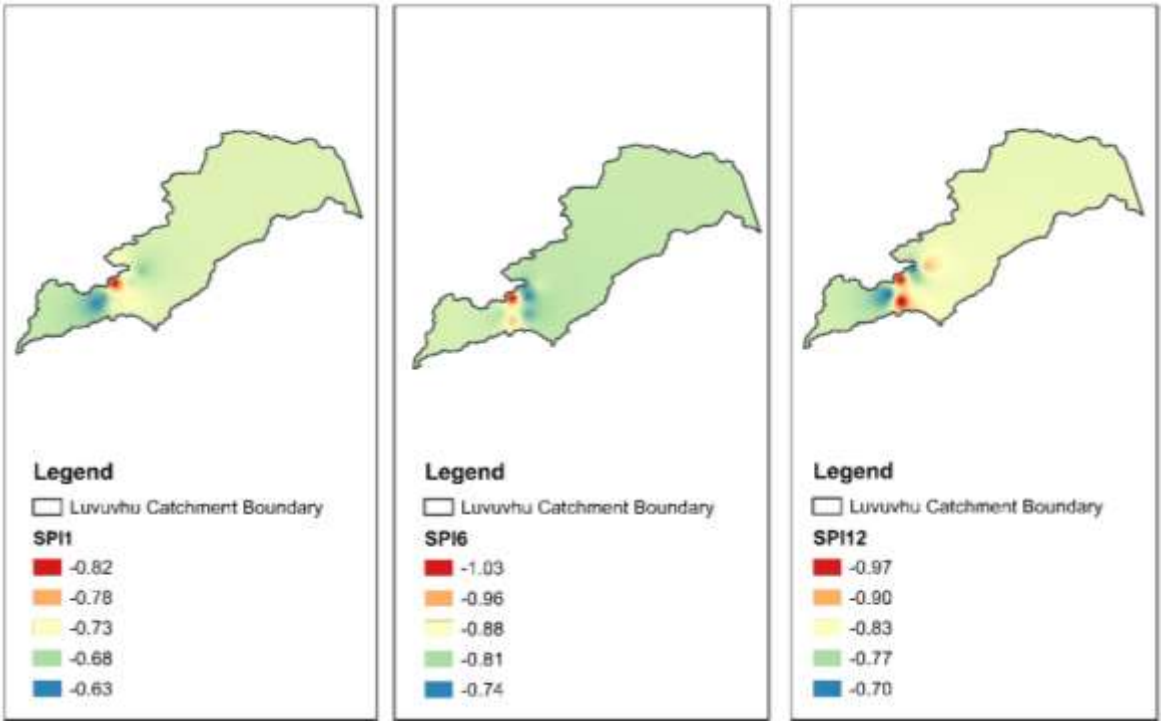

Figure 4.9: Spatial variability of SPI at 1-, 6- and 12- month timescales in the LRC.

4.4.1.2 SPEI

The SPEI time series which depicts drought at different timescales are shown in Figure 4.10 for KA station [for all stations figures, see Appendix A (Figures A4, A5, and A6)]. Considering the notable historical drought reported in the literature, SPEI detected all the drought years as in all the stations at different SPEI time scales. SPEI results indicate that drought is prevalent over the same months (September of the former year to March of the subsequent year) which is consistent with SPI finding and the hydrological year of the catchment. Like SPI, SPEI

managed to detect the 1991/92 drought as the most extreme over the study period at 6- and 12-month timescales and this was showed by VB station only. The 2014/16 drought dominated the severe category in most stations at 6- timescale and showed to be more severe than the 1991/92 in most the stations across all the timescales. The deviation from the literature may be since the studies that classify 1991/92 as extreme made use of different drought quantifying parameters as the one considered in this study.

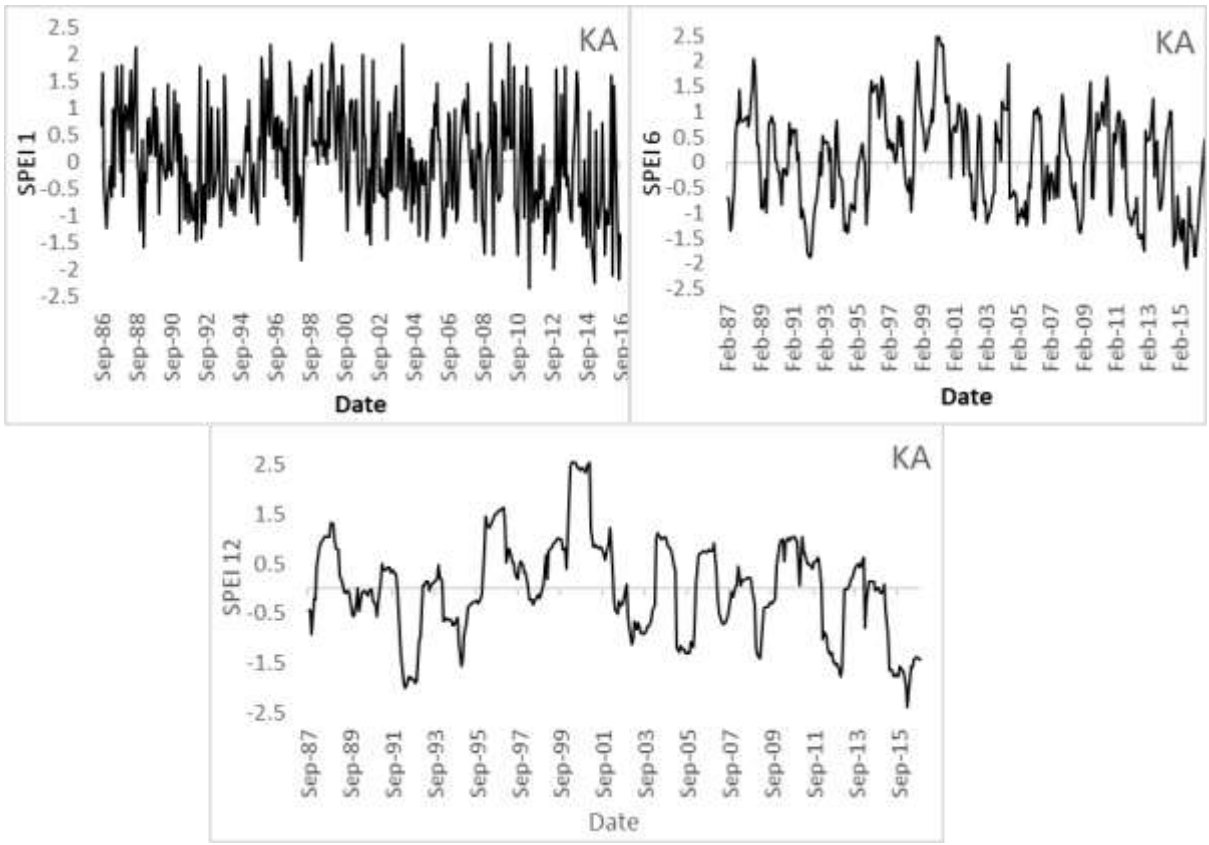

Figure 4.10: SPEI time series for KA station at 1-, 6- and 12- timescales.

Table 4.4 shows the different drought categories percentages of occurrence of historical drought for all the stations at different timescales. Mild, moderate, severe and extreme droughts conditions ranged between 63.28% - 71.88%, 12.65% - 27.59%, 4.2% - 21.69% and 0% - 6.65% respectively, in all stations and considering the respective timescales considered in the study. Station VB, Muk, and Mat showed the highest percentages of extreme droughts at 6.14% for both and 6.65% for VB at 12- month timescale. This, however, is still lower than the percentage of extreme events shown by SPI at the same timescale. This may be attributed to the inclusion of evapotranspiration as an input in the formulation of SPEI. The relationship between increased drought category and timescale as shown by SPI is also seen in Table 4.4 on SPEI. The spatial variability of SPEI at 1-, 6- and 12- month timescales is presented in

Figure 4.11. The variability shows that SPEI 12- was found to be of greater severity compared to 1- and 6- month timescales in the middle reaches while the upper reaches 12- showed the least drought severity compared to SPEI 1- and 6-. Higher temperatures are experienced in the middle and lower reaches of the LRC around the KNP, and since the increased temperature is associated with increases evapotranspiration, it, therefore, explains SPEI 12- showed the least drought severity in the upper reached of the catchment.

Table 4.4: Analysis of SPEI historical drought categories.

Station	Timescale	Mild (%)	Moderate (%)	Severe (%)	Extreme (%)
KA	1	68.28	23.66	5.91	0.02
	6	63.79	27.59	8.05	0.575
	12	65.68	17.16	15.98	1.18
Lev	1	65.91	22.35	2.24	0.56
	6	66.67	16.67	16.67	0
	12	65.66	12.65	21.69	0
Mat	1	67.9	26.84	5.26	0
	6	65.35	25.57	8.52	0.57
	12	69.14	14.2	10.49	6.14
Muk	1	68.42	23.68	7.37	0.53
	6	65.36	25.7	6.7	2.23
	12	69.33	14.11	10.42	6.14
Nooit	1	66.86	24	7.43	1.14
	6	63.28	25.42	10.72	0.57
	12	61.15	23.08	14.2	1.18
Shef	1	68.51	21.55	7.74	2.21
	6	68.36	23.72	6.21	1.7
	12	70.88	21.43	6.05	1.65
Tshi	1	70.97	23.12	4.2	1.61
	6	68.11	21.08	10.27	0.54
	12	65.06	19.88	15.06	0
VB	1	71.73	19.9	6.81	1.57
	6	71.51	18.99	6.7	2.79
	12	71.88	15.63	6.65	6.65

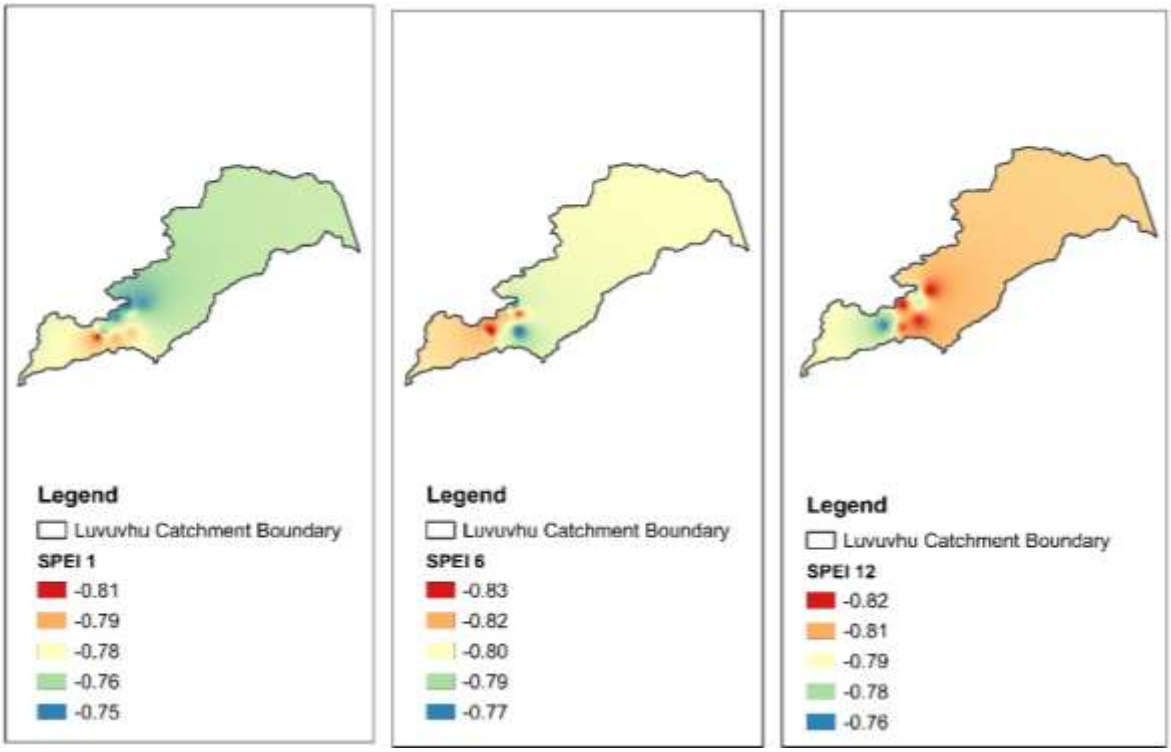

Figure 4.11: Spatial variability of SPEI at 1-, 6- and 12- month timescales in the LRC.

4.4.1.3 SSI

The SSI drought time series for all the streamflow stations (i.e. A9H006, A9H012, and A9H013) at 1-, 6- and 12- month timescales are shown in Figure 4.12. A9H006 is located upstream while A9H012 is in the middle reaches and A9H013 is in the downstream of the LRC. Like the SPI and the SPEI, SSI has managed to detect the reported historical drought events. The index showed an average of 151, 150, and 182 drought months at 1-, 6- and 12-timescales, respectively throughout the study in the LRC. The SSI quite notably depicted the 1991/92 drought in all stations; however, SSI categorised these drought events as extreme on record as opposed to severe categorisation by the precipitation based indices (SPI and SPEI). This may be attributed to the fact that SSI is based on streamflow, and as a surface water body is highly affected by evaporation. Both precipitation based indices showed that the 2014/16 drought was the most extreme drought over the study period. The behaviour of SSI compared to the precipitation-based indices might be due to the fact that streamflow is dependent on precipitation, therefore there is a lag between precipitation deficiency and reduced streamflow. Streamflow and base flow drought occurs around 7 and 11 months respectively after the end of meteorological drought (Yang *et al*., 2017). The extreme case of 2014/16 can, therefore, be noticed in the 2016/17 in the LRC, however, the current study period does not include.

The index categorised between 54.76% to 93.758 as mild, 5.7% to 31.84% as moderate, 0.52% to 12.41% as severe, and 0% to 8.7% as extreme drought across the stations at different timescales over the period considered in this study (see Table 6.5). The middle reaches of the catchment showed the highest extreme compared to the further downstream station with extreme percentages below 4% for all time scales. The extreme classification may have been exacerbated by abstraction from the Mhinga weir for domestic and agricultural use to the villages around the middle reaches of the LRC. Comparing SSI to the other standardised indices that have been discussed in the earlier sections (4.3.2.1 and 4.3.2.2), the index ranked second highest extreme droughts after the SPI at 12- month timescale. The results of this index still do not indicate that the catchment experiences extreme drought as up to 93.78% of the drought events were categorised as mild. The findings of SSI agree with SPI and SPEI in that the mild droughts are the most dominant in the catchment across all time scales over the study period.

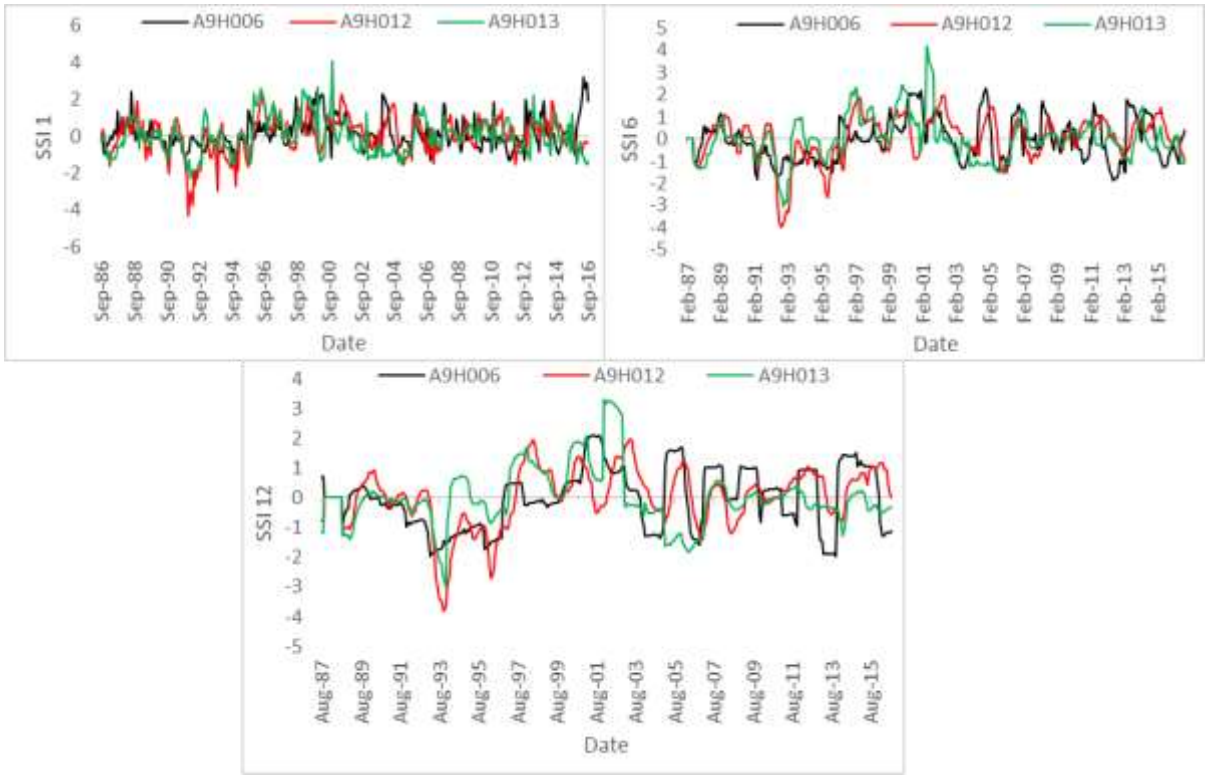

Figure 4.12: SSI time series for stations A9H006, A9H012 and A9H013.

Table 4.5: Analysis of SSI historical drought categories.

Station	Timescale	Mild (%)	Moderate (%)	Severe (%)	Extreme (%)
A9H006	1	93.78	5.7	0.52	0
	6	68.02	24.27	7.61	0
	12	**54.75**	**31.84**	**12.41**	0
A9H012	1	69.94	13.5	10.43	6.14
	6	73.91	14.29	3.11	**8.7**
	12	69.23	18.59	3.85	8.33
A9H013	1	70.05	23.35	6.09	0.51
	6	68.06	25.66	3.14	3.14
	12	78.67	11.85	7.11	2.27

The spatial variability of drought as shown by the SSI are presented in Figure 4.13 at 1-, 6- and 12- month timescales. Like the SPI at 1- and 12- month showed a much lower variability of drought severity compared to SSI 6- month timescale. However, it should be taken into account that unlike precipitation based indices, streamflow stations considered in this study, covers the upper, middle, and lower reaches of the study area. At 12- month timescale, the upper reaches showed that the highest drought severity (-0.871), however, this was less than the severity experiences in the middle reaches as shown by an SSI at 6- month timescale of -1.66. Streamflow in the upper and middle reaches of the LRC at 1- and 6- month timescales depict low drought severity and this correlates with the low maximum temperatures experienced in these parts of the catchments compared to the lower reaches which are characterised by high temperatures which translated to increased evaporation from open water bodies.

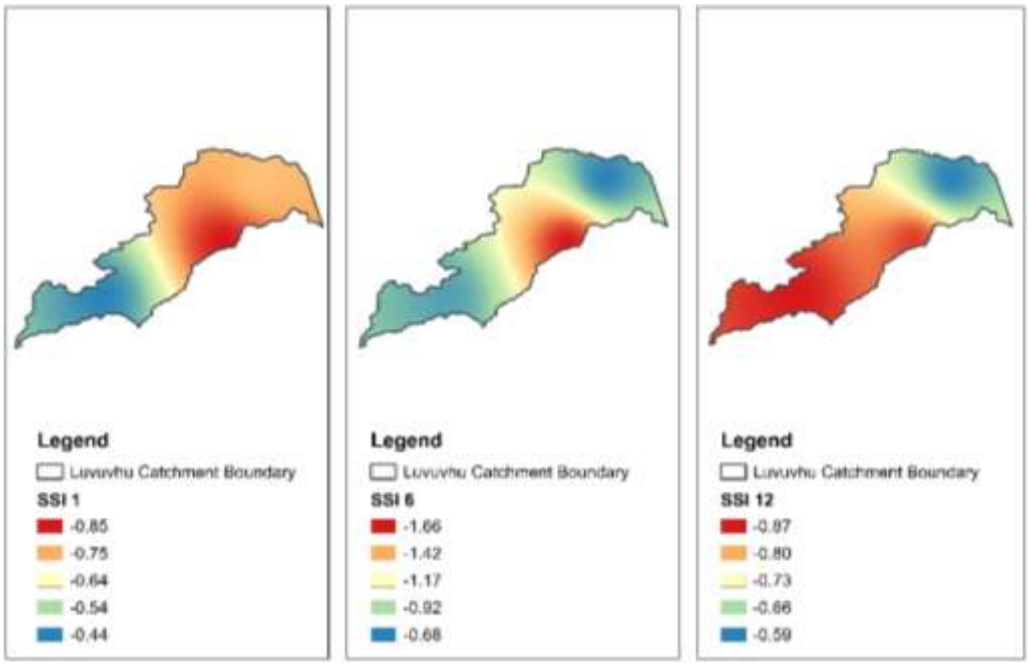

Figure 4.13: Spatial variability of SSI at 1-, 6- and 12- month timescales in the LRC.

4.4.1.4 NADI

Figure 4.14 shows drought events as depicted by NADI. The index categorised 120, 30, 22, and 3 drought months as mild, moderate, severe, and extreme drought, respectively. The index managed to depict the major notable droughts events in the study area (i.e. 1991/92, 1994/96, 2001/02, and 2014/16). NADI underestimated the severe drought reported in the literature (1991/92 and 2014/16 drought) and by the standardised indices. This may be due to the nature of the index since it considers all the components of the hydrological cycle which standardised techniques fall short of. Barua *et al*. (2012) reported that NADI considers a broad perspective of dryness within a catchment rather than just the traditional meteorological drought conditions. Three extreme droughts were found in December 1987, October 1988, and February 1996 with the NADI also value of -2.68, -2.22, and -2.09, respectively. The NADI found 1.71% drought events compared to the overall drought events in the study area. The most recent drought event (2014/16) was also classified as severe with the lowest NADI of -1.45 found for the multi-year drought. These findings agree with those obtained by the standardised indices as they also detected and categorised the latter drought (2014/16) as severe to extreme. A total of 12.57%, 17.14%, and 68.57% drought events were categorised as severe, moderate, and mild respectively. Like the standardised indices, NADI showed that the most prevalent historical drought events were in the mild category.

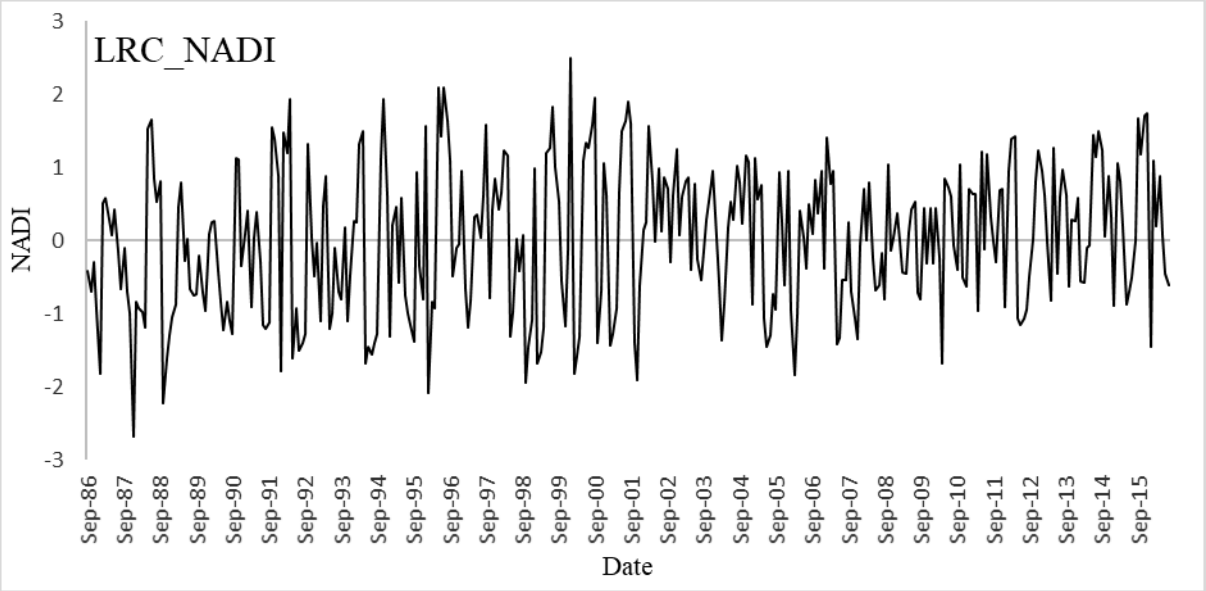

Figure 4.14: NADI time series for the study area.

4.4.2 LRC drought trends and their significance

MK non-parametric trend test was conducted to detect drought trends as shown in Tables 4.6., 4.7, 4.8, and 4.9 for SPI, SSI, SPEI, and NADI respectively. These are conducted on all historical drought events detected by all the stations and across the different timescales (i.e. 1-, 6- and 12- months) considered in the study area. The SPI, SPEI, and SSI rejected the null hypothesis that there was no monotonic trend drought in the LRC. All standardised indices rejected the null hypothesis that there was no monotonic drought trend in the time series data at 95% confidence level. SPI drought trends were found to be negative (decreasing) in all stations across all timescales with exception of Tshi and Shef at 12- and 6- months' timescales, respectively. About 50% of the negative SPI drought trend was found to be both significant and insignificant and the positive (increasing) drought trends report the same.

SPEI showed a significant negative trend in the time series in all the stations and time scales with exception of Lev station at 6- month time scale for the period considered in this study. For the case of SPEI, 13.64% of the negative drought trend was shown to be insignificant with 86.36% significance. For the positive drought trends, SPEI showed that all were significant while SSI found a 55.56% positive trend for station A9H012 at all timescale and station A9H012 at 1- and 6- months timescale. About 75% of the negative drought trend was shown to be insignificant and 25% was significant while the positive drought trend dominated with 60% insignificant and 40% significant drought trend. Of all the indices formulated for the LRC in this study, NADI is the only index that showed a positive drought trend in its time series. The index time series reported a significant positive drought trend at a 95% confidence interval. This may be attributed to the multivariate nature of the index, as it considers all components of the hydrological cycle.

Table 4.6: SPI MK statistics for all the stations considered in this study.

Index	Time scale	S	z	P_value	alpha	Test Interpretation	Trend	Significant
KA	1	-9.87e+2	-1.155	0.248	0.05	H_a	-ve	No
	6	-5.3e+2	-0.74	-0.46	0.05	H_a	-ve	No
	12	-2.5e+3	-3.68	0.00023	0.05	H_a	-ve	Yes
Lev	1	-4.54e+3	-4.91	9.01e-7	0.05	H_a	-ve	Yes
	6	-4.82e+3	-5.86	4.59e-9	0.05	H_a	-ve	Yes
	12	-6.24e+3	-8.79	<2.2e-16	0.05	H_a	-ve	Yes
Mat	1	-5.75e+3	-6.17	6.81e-10	0.05	H_a	-ve	Yes
	6	-4.05e+3	-4.84	1.27e-6	0.05	H_a	-ve	Yes
	12	-4.54e+3	-5.57	2.53e-8	0.05	H_a	-ve	Yes
Muk	1	-2.51e+3	-2.95	0.003	0.05	H_a	-ve	Yes
	6	-4.25e+3	-6.21	5.44e-10	0.05	H_a	-ve	Yes
	12	-2.43e+3	-4.02	5.75e-5	0.05	H_a	-ve	No
Nooit	1	-1.47e+3	-1.65	0.098	0.05	H_a	-ve	No
	6	-4.58e+2	-0.55	0.58	0.05	H_a	-ve	No
	12	-2.62e+3	-3.24	0.0012	0.05	H_a	-ve	Yes
Shef	1	-1e+1	-0.009	0.99	0.05	H_a	-ve	No
	6	**1.1e+3**	**1.10**	**0.27**	**0.05**	**H_a**	**+ve**	**No**
	12	-1.52e+3	-1.67	0.096	0.05	H_a	-ve	No
Tshi	1	-7	-0.015	0.99	0.05	H_a	-ve	No
	6	-1.1e+3	-1.95	0.15	0.05	H_a	-ve	No
	12	**3245**	**4.74**	**2.11e-2**	**0.05**	**H_a**	**+ve**	**Yes**
VB	1	-9.02e+2	-1.12	0.27	0.05	H_a	-ve	No
	6	-1.5e+5	-1.95	0.052	0.05	H_a	-ve	No
	12	-3.55e+3	-4.866	1.14e-6	0.05	H_a	-ve	Yes

*-ve (negative) represents a decreasing trend while +ve (positive) represents an increasing trend.

Table 4.7: SSI MK statistics for all the stations considered in this study.

Station	Time scale	S	z	P_value	alpha	Test Interpretation	Trend	Significant
A9H006	1	-1.05e+3	-1.167	0.24	0.05	H_a	-ve	No
	6	-1.08e+3	-1.186	0.236	0.05	H_a	-ve	No
	12	-1.91e+3	-2.384	0.017	0.05	H_a	-ve	Yes
A9H012	**1**	**2.59e+3**	**3.709**	**0.00021**	**0.05**	**H_a**	**+ve**	**Yes**
	6	**2.24e+3**	**-1.186**	**0.236**	**0.05**	**H_a**	**+ve**	**No**
	12	**1.93e+3**	**-1.476**	**0.0033**	**0.05**	**H_a**	**+ve**	**Yes**
A9H013	**1**	**1.08e+3**	**1.17**	**0.242**	**0.05**	**H_a**	**+ve**	**No**
	6	**1.47e+3**	**1.668**	**0.095**	**0.05**	**H_a**	**+ve**	**No**
	12	-1.5e+3	-1.476	0.14	0.05	H_a	-ve	No

*-ve (negative) represents a decreasing trend while +ve (positive) represents an increasing trend.

Table 4.8: SPEI MK statistics for all the stations considered in this study.

Index	Time scale	S	z	P_value	alpha	Test Interpretation	Trend	Significant
KA	1	-2.78e+3	-3.277	0.0011	0.05	H_a	-ve	Yes
	6	-3.07e+3	-4	6.24e-5	0.05	H_a	-ve	Yes
	12	-3.6e+3	-4.896	9.8e-7	0.05	H_a	-ve	Yes
Lev	1	-4.67e+3	-5.82	5.77e-9	0.05	H_a	-ve	Yes
	6	**06.97e+3**	**-8.6**	**<2.2e-16**	**0.05**	**H_a**	**+ve**	**Yes**
	12	-7.491	-10.46	<2.2e-16	0.05	H_a	-ve	Yes
Mat	1	-4.33e+3	-4.82	1.45e-6	0.05	H_a	-ve	Yes
	6	-4020	-5.14	2.7e-7	0.05	H_a	-ve	Yes
	12	-3.96e+3	-5.73	1.007e-8	0.05	H_a	-ve	Yes
Muk	1	-2.09e+3	-2.385	-0.017	0.05	H_a	-ve	Yes
	6	-3.04e+3	03.79	0.0002	0.05	H_a	-ve	Yes
	12	-3.93e+3	-5.67	1.42e-8	0.05	H_a	-ve	Yes
Nooit	1	-2.78e+3	-3.59	0.0003	0.05	H_a	-ve	Yes
	6	-2.25e+3	-2.85	0.004	0.05	H_a	-ve	Yes
	12	-4.24e+3	-5.77	8.12e-9	0.05	H_a	-ve	Yes
Shef	1	-2.17e+3	-2.66	0.0078	0.05	H_a	-ve	Yes
	6	-8.44e+2	-1.07	0.285	0.05	H_a	-ve	No
	12	-4.9e+3	-4.98	6.38e-7	0.05	H_a	-ve	Yes
Tshi	1	-1.87e+2	-0.22	0.827	0.05	H_a	-ve	No
	6	-1.13e+3	-1.34	0.18	0.05	H_a	-ve	No
	12	-3.75e+3	-5.23	1.69e-7	0.05	H_a	-ve	Yes
VB	1	-2.07e+3	-2.34	0.019	0.05	H_a	-ve	Yes
	6	**1701**	**-2.12**	**0.034**	**0.05**	**H_a**	**+ve**	**Yes**
	12	-2.28e+3	-3.37	0.0008	0.05	H_a	-ve	Yes

*-ve (negative) represents a decreasing trend while +ve (positive) represents an increasing trend.

Table 4.9: NADI MK statistics.

Time scale	S	z	P_value	alpha	Test Interpretation	Trend	Significant
1	2.34e+03	3.039	0.0011	0.05	H_a	+ve	Yes

* +ve (positive) represents an increasing trend.

Figures 4.15, 4.16, 4.17 and 4.18 depict the BFAST extracted drought non-linear trend from the SPI, SPEI, SSI, and NADI drought time series respectively at 1-, 6- and 12- month timescales. For the case of standardised indices, only station KA results are presented, all the stations considered in this study results are found in Appendix A (Figures A7, A8, A9, A10, A11, A12, and A13). In the case of drought as depicted by an index, a downward trend signifies an increase in the severity of the drought. From the BFAST extracted trends, the trend is observed to decrease with increasing timescale. The standardised indices showed an increasing drought trend across all time scales while NADI showed a decreasing drought trend. As depicted in Figure 4.15, there is a notable negative trend that may be attributed to the severe

drought that was categorised by the index in 1986/87. NADI time series trend depicted a decreasing drought trend from the year 2000. The increasing trend indicates that drought events over the study period as detected by the SPI, SPEI, and SSI are increasing which indicates that drought events are becoming more severe. This supports the argument that over the study period drought severity has increased in the study area. Further to the increase in drought severity, the findings of the standardised indices are consistent with rainfall and temperature trends as reported over north-eastern South Africa by e.g. McKellar *et al*. (2014); Kruger and Nxumalo (2017).

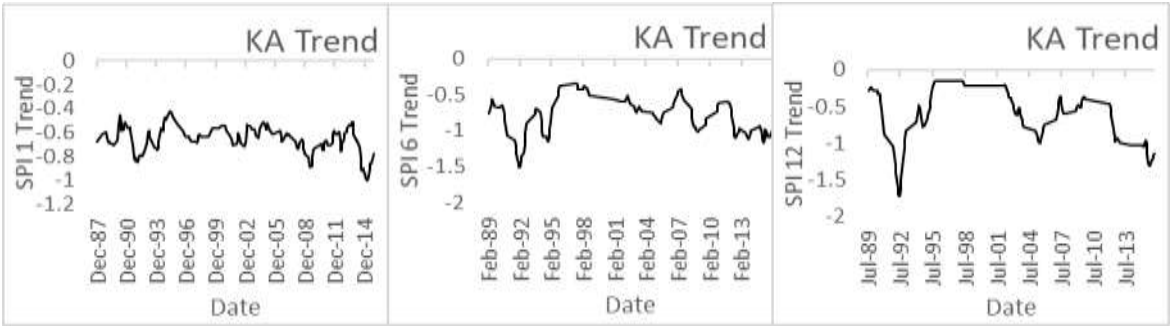

Figure 4.15: SPI drought trend at all timescales.

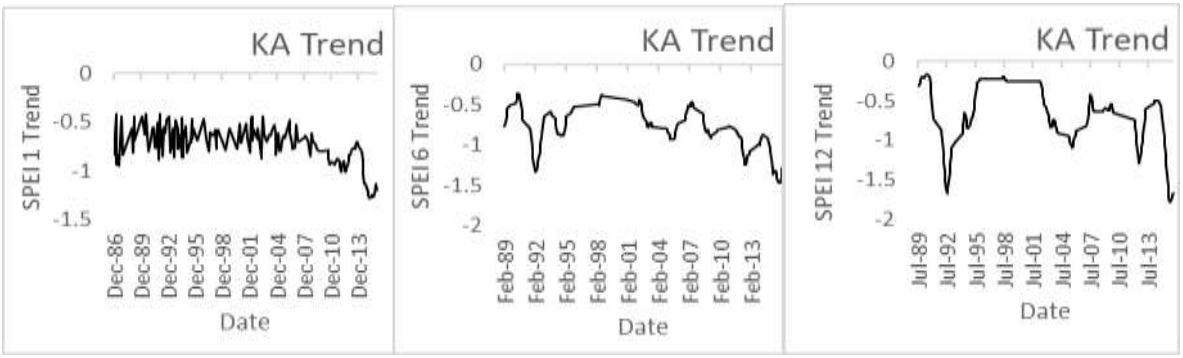

Figure 4.16: SPEI drought trend at all timescales.

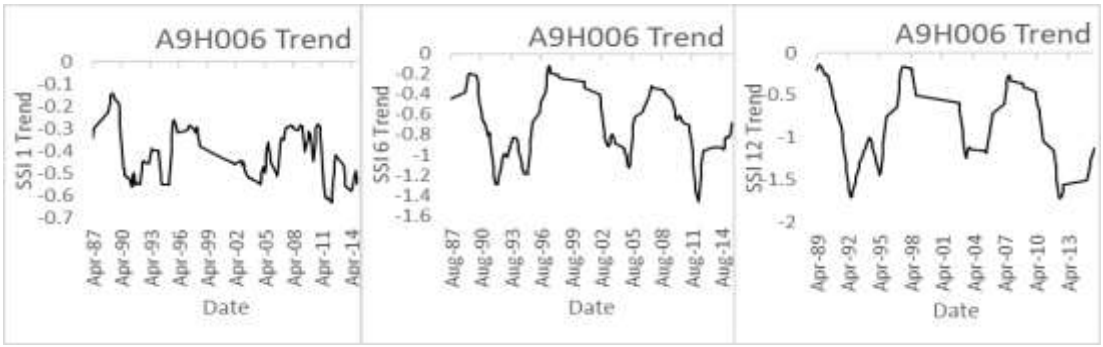

Figure 4.17: SSI drought trend at all timescales.

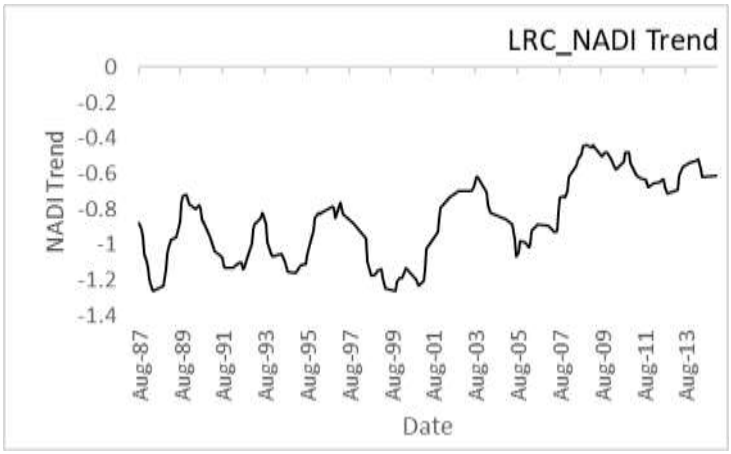

Figure 4.18: NADI drought smooth trend.

4.5 Chapter summary

The chapter aimed at assessing historical drought events in the LRC from 1986 to 2016 using three standardised indices and the non-linear aggregated drought index. All the indices managed to detect major historical drought events that have been found to have occurred in the study area, although the precipitation based indices were the only indices that categorised the 1991/92 drought as extreme at 6- and 12- month timescales in two stations while the streamflow index and multivariate NADI underestimated the event. All the selected indices further showed that the most prevalent drought event in the LRC was mild drought. Extreme drought events were the least shown at 6.42%, 1.08%, 1.56%, and 4.4% for SPI, SPEI, SSI, and NADI respectively. Considering the MK trend test, the standardised indices detected a negative trend that showed that drought severity increased in the study area throughout the study period while NADI showed a positive upward trend which depicts a decreased drought severity throughout the study period. The MK trend result for standardised indices and NADI may be due to the fact that the latter present overall water resources in the catchment while the former are either rainfall or streamflow based. There is therefore a need to further characterise the drought events in terms of magnitude, duration, frequency, and severity as detected by these indices to get a better understating of their performance in detecting and assessing drought conditions in the study area. In Chapter 5, drought events are then characterised based on the aforementioned characteristics and then further evaluated for their suitability to assess drought in the catchment under consideration.

5 DROUGHT CHARACTERISATION AND COMPARATIVE INDEX EVALUATION

Chapter overview, Drought characterisation, Drought indices evaluation, Summary

5.1 Chapter overview

This chapter presents drought characterisation and an analysis of the comparative evaluation of the drought indices. The characteristics of drought discussed include; drought duration (the total time is taken by a drought event), intensity (ratio of drought severity to duration), severity (the relationship between duration and Intensity), and drought frequency. An analysis of severity-duration-frequency and severity-area-frequency is also conducted. The latter is presented as part of the characterisation of drought based on the four drought indices considered. The evaluation of drought indices is done according to the evaluation criteria previously applied by Keyantash and Dracup (2002). The goal of index evaluation is to come out with an index that best describes drought in the LRC.

5.2 Methodology

5.2.1 Drought characterisation

To characterise historical hydrological droughts in the study area, 1-, 6- and 12-months timescales for SPI, SPEI and SSI are utilised while NADI was characterised at 1-month timescale. Drought characteristics analysed include drought duration, severity, intensity, and frequency (see Figure 5.1). Drought duration (*d*) of drought events is the number of months between the start (included in the computation) and end month (not included) of a drought event (Tan *et al*., 2015). Drought severity (S_e) is defined as the absolute value of the sum of index values during a drought event and is given by the following equation:

$$S_e = \left|\sum_{j=1}^{m} index_j\right|_e , \quad (5.1)$$

where *e* is the drought event, *j* is the month, $index_j$ is the index value in month *j*.

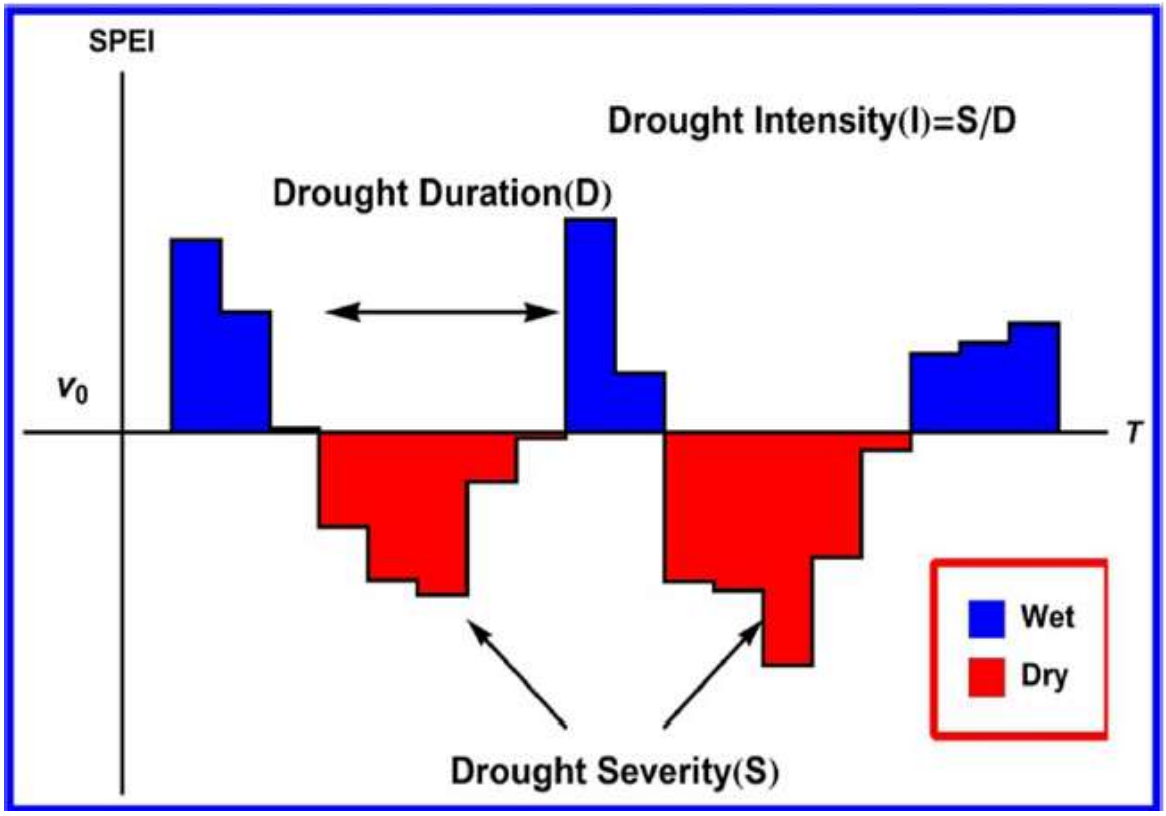

Figure 5.1: Relationship between drought duration, intensity, and severity.

Drought intensity (DI_e) of any drought event is given by the drought severity divided by the drought duration. The larger the drought intensity value, the more severe the drought. Drought intensity is calculated using Equation (5.2).

$$DI_e = \frac{S_e}{d}, \tag{5.2}$$

where, m, S_e and DI_e are the drought duration, severity, and intensity of a drought event *e* respectively. Drought Frequency (Fs) was used to assess drought liability during the study period (Wang *et al*., 2014). The frequency over a long time series gives the frequency of drought occurrence over the study area and this is achieved by:

$$F_s = \frac{n_s}{N_s} \times 100\% , \tag{5.3}$$

where, n_s is the number of drought events, N_s is the total number of years for the study period and *s* is the station under study.

5.2.2 Drought indices evaluation

Redmond (1991) proposed several desirable properties while judging the overall usefulness of DIs. Keyantash and Dracup (2002) made use of six decision criteria from these desirable

properties, namely *robustness*, *tractability*, *sophistication*, *transparency*, *extendibility*, and *dimensionality*, for evaluating some of the DIs used in the United States. To determine whether a DI satisfied desirable properties and is useful in drought detection in the catchment, a decision criterion by Keyantash and Dracup (2002) was utilised. This study employed only five decision criteria to determine the most suitable drought index for hydrological drought assessment in the study area. This was informed by Keyantash and Dracup (2002) as a recommendation since dimensionality is mostly covered by the transparency criteria while Barua (2010) also made use of the same decision criteria. Although the Simos Procedure for multi-criteria outranking suggested by Simons (1990) and revised by Figueira and Roy (2002) is more objective and has been applied in the field of water resources. Studies such as Kodikara *et al*. (2010) successfully determined the weights for a multi-objective urban water supply operation. The outranking procedure, however, has never been applied in this type of study. The latter therefore resulted in the choice of the decision criteria by Keyantash and Dracup (2002).

In assessing the overall utilisation of an index, the five decision criteria were assigned a raw score of between one and five. As stated in Barua (2010), the individual raw scores are based on the qualitative and quantitative assessment of each index. The quantitative assessment is based on how well the index modeled historical drought while qualitative assessment is based on findings of previous studies on evaluating indices and the computational aspects of the index. The sum of the weighted scores (i.e. raw scores multiplied by the relative importance factor) was the total for each index. The current study adopted the relative importance factor from Keyantash and Dracup (2002) which regard robustness as the most important factor with a relative importance of 28% and a weight of eight followed by tractability with 21% with a weight of six and transparency and sophistication equally at 17% with a weight of five. Since dimensionality is covered under extendibility, this study will, therefore, add the relative importance of dimensionality to extendibility bringing it 17% with a weight of five. Therefore, extendibility, transparency, and sophistication are of the same relative importance in this study. The relative importance scoring by Keyantash and Dracup (2002) was selected because the catchment is diverse (i.e. it is an economic hub with irrigated agricultural activities and densely populated in the middle reaches) and therefore an index with a wide range of application would be more useful, therefore the robustness criteria are ranked higher. The sum of the weighted scores is then used in the comparative evaluation for the respective indices in the LRC. The sensitivity analysis was not conducted for this study since the index raw scoring was compared to those assigned by Barua (2010).

5.3 Results and Discussions

5.3.1 Drought duration, frequency, intensity, and severity

Drought characteristics (duration, frequency, intensity, and severity) were analysed in this study for the four respective indices based on the run theory analysis (Yevjevich, 1967; Dracup et al., 1980; Mishra and Desai, 2005) at the standard truncation level of 0. The standard truncation level adopted for this study was also used by Al-Tamimi and Al-Jiboori (2014) in index-based drought assessment in Iraq. Since the SPEI and SSI are both standardised indices, the NADI threshold was obtained using the SPI dryness threshold, the standard truncation level of 0 was therefore used uniformly for all the four indices at 1-, 6-, and 12- month timescales for all the weather and streamflow stations considered in the study.

Drought characteristics were analysed for the three decades considered in this study i.e. between 1986 – 1996, 1996 – 2006, 2006 – 2016 years. Table 5.1 shows the duration, intensity, and severity of drought for SPI, SPEI, SSI, and NADI at the standard truncation level in all the timescales considered. The results presented in Table 5.1 are for station KA for SPI and SPEI and A9H006 for SSI, for all other station results, see Appendix B (Table B1). For the case of standardised indices, the length of drought duration varied from station to station for all timescales. The SSI showed the longest average drought duration between 1986 – 1996, 1996 – 2006, and 2006 – 2016 followed by SPI and then SPEI over the same periods. The period between 1986 – 1996 showed the longest duration followed by 2006 – 2016 while 1996 – 2006 showed the shortest duration under the period considered in this study. Drought duration was generally seen to increase with an increasing timescale in the LRC. NADI showed an overall catchment lowest duration in all the decades at 1- month timescale compared to the standardised indices. Like the standardised indices, NADI also showed that the longest duration between 1986 – 1996.

Drought severity for the LRC generally exhibited the same behaviour over the three decades. However, the highest severity was observed between 1986 – 1996 followed by 2006 – 2016 with the least severity observed between 1996 – 2006. In a study of drought in southern Africa, Chikoore (2016) found severe and extreme droughts during 1991 and 1992, which falls within the 1986 – 1996 period. SPI showed the strongest severity in 2006 – 2016 and followed by the SSI between 1986 – 1996. Severity was found to increase with increasing timescale. A study conducted in Bali, Java, and Nusa Tenggara Islands, Adhyani *et al*. (2017) reported similar

findings in their study on the exposure of drought that longer timescale correlates positively with increased drought duration. This, therefore, indicates that should the LRC experience drought over a prolonged period, communities are likely to be affected by server water shortages which will also affect the agricultural sector. The NADI showed the strongest severity between 1986 – 1996, which was higher than the average shown by the standardised indices at the same timescale. This is consistent with NADI categorising the 1987/88 drought as severe over the study period in Chapter 4, section 4.5.1.4. Greater drought intensity was found between 2006 – 2016 while the lowest was between 1996 – 2006. For the case of the standardised indices, SPEI showed the highest intensity followed by SPI and then the SSI. NADI intensity ranged from -0.89 to -1.19. The intensity of drought was seen to generally increase with an increased timescale and this was evident between 2006 – 2016 (72.2%) with the other periods showing 50% and 44%. The severity of the drought is highly dependent on the relationship between drought duration and severity. Because high intensity corresponds to higher severity (Dayal *et al*., 2017), SPEI showed the highest severity followed by SPI, SSI, and NADI.

Drought frequency was found to be higher between 2006 – 2016 followed by 1986 – 1996 and the lowest was showed between 1996 – 2006 with an average of 21.2%, 18.4%, and 12.0% respectively. For detailed drought frequency results, see Appendix B (Table B2). The frequency of drought increased with an increasing timescale, which varied between 3.7% at 1-month timescale and 75.9% at 12- month timescale across the stations. The SSI showed the highest frequency compared to the rest of the indices over all the periods, followed by SPEI and SPI. This, therefore, shows that; streamflow drought occurs more often in the LRC. The NADI at 1- month timescale showed the lowest frequency (7.5%, 4.1%, and 4.2% between 1986 – 1996, 1996 – 2006, and 2006 – 2016, respectively) compared to the standardised indices at the same timescale.

Table 5.1: Duration, severity, and intensity of drought events for SPI, SPEI, SSI, and NADI.

			1986-1996						1996-2006						2006-2016					
Station	Drought indicator		Longest		Strongest		Highest		Longest		Strongest		Highest		Longest		Strongest		Highest	
			Year	D	Year	S	Year	I	Year	D	Year	S	Year	I	Year	D	Year	S	Year	I
KA	SPI	1	1994	11	1991 - 1992	-6.37	2015	-1.26	2004 - 2005	6	2002	-4.35	2002	-1.088	2012	8	2012	-6.43	2008	-1.042
		6	1992 - 1995	13	1994 - 1995	-13.23	1994 - 1995	-1.-012	2004 - 2006	13	2004 - 2006	-11.61	2004 - 2006	-0.89	2011 - 2012	15	2011 - 2012	-14.7	2014 - 2015	-1.156
		12	1989 - 1990	19	1991 - 1993	-21.14	1991 - 1993	-1.409	2002 - 2004	24	2002 - 2004	-10.2	2002 - 2004	-0.427	2015- 2016	21	2015- 2016	-22.85	2005	-1.092
	SPEI	1	1994	13	1992 - 1992	-7.609	1991	-1.322	1998 + 2003	5	2002	-4.278	2005	-1.329	2012	8	2012	-9.233	2015	-1.858
		6	1991 - 1992	15	1991 - 1992	-17.846	1991 - 1992	-1.19	2004 - 2005	16	2004 - 2005	-13.693	2004 - 2005	-0.856	2014 - 2016	22	2014 - 2016	-28.476	2014 - 2016	-1.347
		12	1994 - 1995	23	1994 - 1995	-13.803	1994 - 1995	-0.6	2003 - 2004	16	2003 - 2004	-12.084	2006	-1.173	2015 - 2016	20	2015 - 2016	-31.49	2015 - 2016	-1.575
A9H006	SSI	1	1991 - 1995	58	1991 - 1995	-25.98	1990	-0.634	2004 - 2005	15	2004 - 2005	-7.29	2000	-1.17	2011 - 2012	17	2011 - 2012	-10.44	2010	-0.87
		6	1990 - 1996	69	1990 - 1996	-64.33	1990 - 1996	-0.932	2004 - 2005	14	2004 - 2005	-14.27	2004 - 2005	-1.019	2014 - 2016	21	2014 - 2016	-13.7	2011 - 2012	-1.186
		12	1989 - 1995	82	1989 - 1995	-78.02	1989 - 1995	-0.952	1996 - 1998	22	2002 - 2004	-16.62	2005	-1.159	2015 - 2016	14	2011 - 2012	-20.67	2011 - 2012	-1.723
	NADI	1	1987 - 1988	9	1987 - 1988	-9.734	1995	-1.16	2005	5	2005	-4.95	1999	-1.19	2008	5	2007	-3.4	2007	-0.89

*D-Duration, S-Severity, I-Intensity, KA-Klein Austraile, SPI-Standardised Precipitation Index, SPEI- Standardised Precipitation Evaporation Index, NADI-Non-linear Aggregated Drought Index

Figure 5.2 depicts the relationship between drought duration, intensity, and severity. The results depicted in Figure 5.2 are for station KA for standardised rainfall based indices and streamflow station A9H006 for the SSI, at 1-, 6- and 12- month timescale. For all the station results, see Appendix B (Figures B1, B2, B3, and B4). At 1- month timescale, the standardised indices showed a strong correlation between drought severity and intensity. A similar relationship between drought duration, severity, and intensity in the standardised indices was shown in the NADI. It was found that, at greater duration (e.g. 10 years going forward), the severity tends to increase while the intensity decreases and this is seen for stations VB, Tshi and Mat at all timescales for SPI and SPEI while for the SSI, station A9H013 showed the same relationship between severity and intensity. Other stations' relationship of severity-intensity with duration fluctuated and did not follow a distinct pattern and this can be seen in station KA at 12- month timescale.

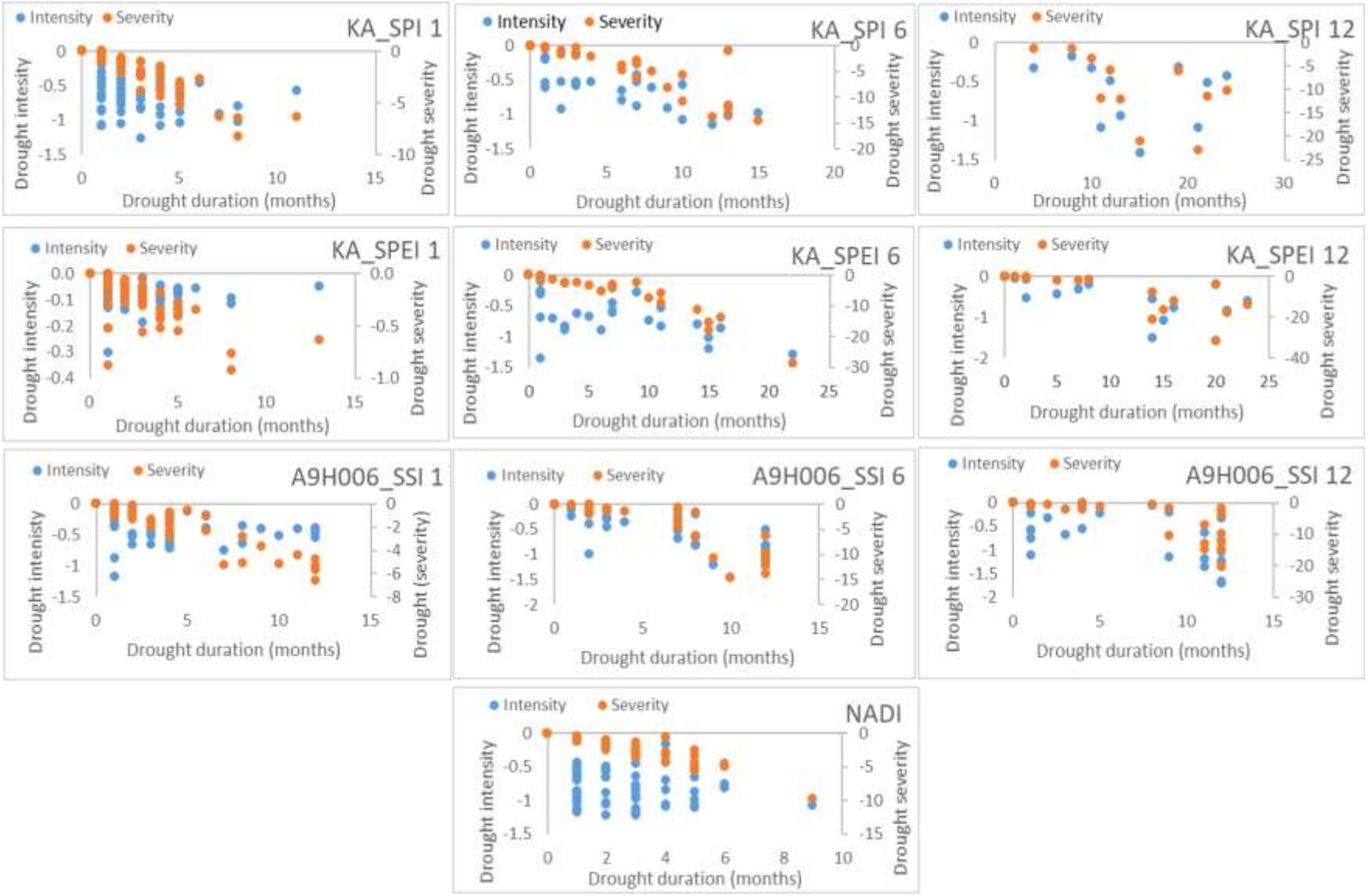

Figure 5.2: Drought duration-intensity-severity relationship.

Generally, it was found that drought intensity and severity both decreases with increased duration, and these were observed mainly at the 6- month timescale. This study observed that most low drought severity corresponded to a much-reduced drought intensity. Figure 5.3 shows some results of the relationship between drought duration and severity for SPI, SPEI, and SSI at all timescales. NADI at 1- month timescale results are also included in Figure 5.3. All other results are found in Appendix B (Figure B5, B6, B7, B8, B9, B10, and B11). An R^2 of between 0.6845 and 0.9714 was found at 1- month timescale for standardised indices and the NADI. At 6- month timescale the standardised indices had a correlation coefficient between 0.6353 and 0.973 while at 12- month, an R^2 between 0.2725 and 0.9761 was found. All the indices depict a strong linear relationship between duration and severity at all timescales. However, some weak correlations of 0.3216 and 0.2725 are realised at 12-month timescale. These results, therefore, show that generally, the severity of drought increases with an increased duration as can be seen in Figure 5.3. However, Van Loon and Laaha (2015) indicated that although hydrological drought duration and deficit are related, their relationship is not linear since the deficit accumulates throughout a drought event. The results obtained from this study differ from Van Loon and Laaba (2015) at shorter timescales (i.e. 1- and 6- month) while at 12- month timescale, a weak linear relationship was found in some stations as already indicated above. One reason for the linear relationship between drought duration and severity may be due to the fact that the study by Van Loon and Laaha (2015) used streamflow as an indicator of hydrological drought whilst the current study uses standardised drought indices.

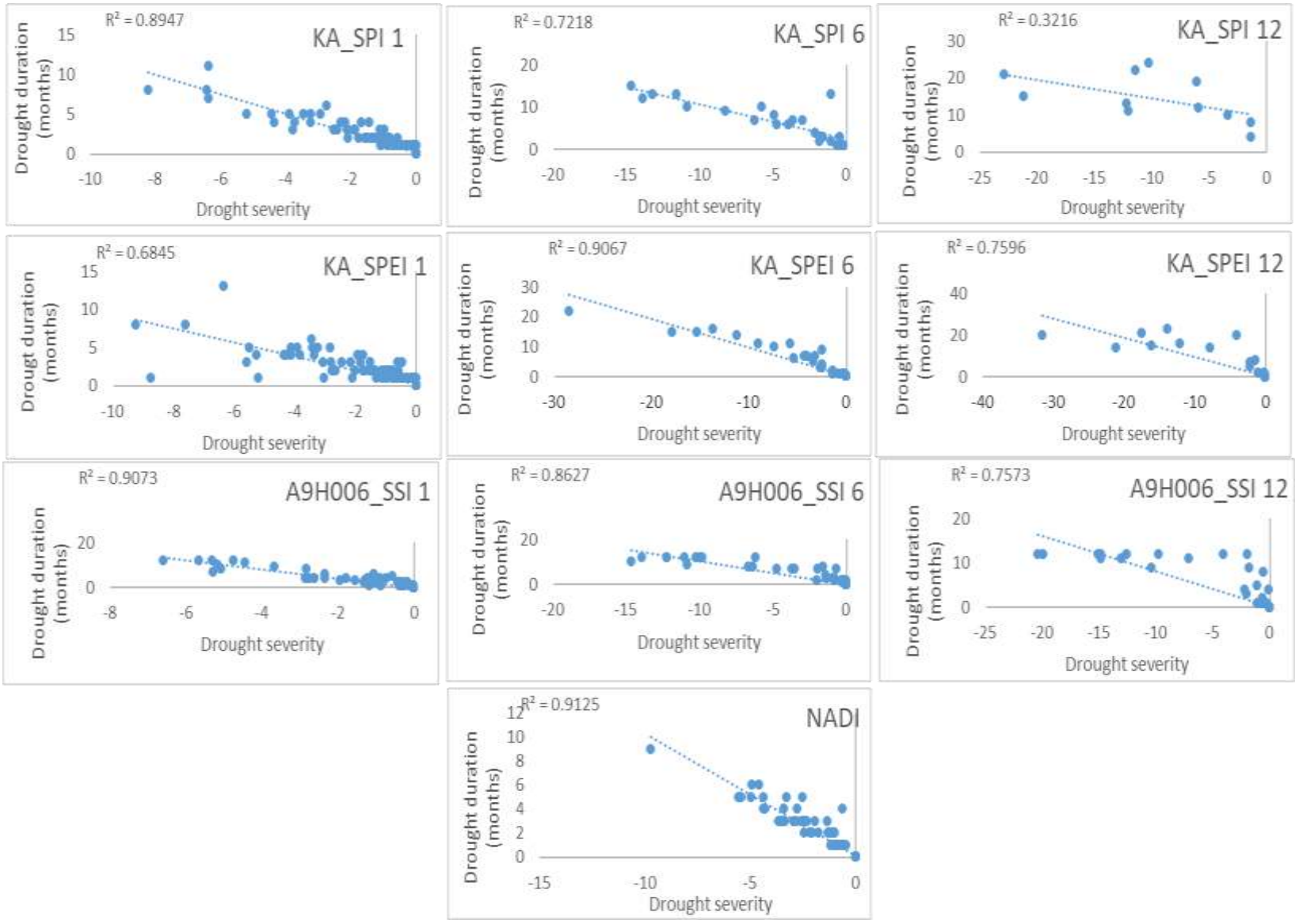

Figure 5.3: Duration-severity curves.

5.3.2 Evaluation of Indices

The 1- month timescale was the only timescale used for index evaluation since NADI was only computed at that timescale. The total weighted scores for each respective index are tabulated in Table 5.2. The rationale for the raw scores of each decision criterion as reflected in Table 5.2 are discussed in the sub-sections below.

Table 5.2: Indices scores based on weighted evaluation criteria.

Drought index	Raw scores (1-5)					Total weighted scores
	Robustness	Tractability	Sophistication	Transparency	Extendibility	
SPI	2	5	2	5	5	106
SPEI	5	4	5	4	4	129
SSI	5	5	4	5	2	125
NADI	4	2	3	3	2	84

5.3.2.1 Robustness

Robustness indicates the usefulness of a drought index over a wide range of physical conditions, taking into consideration some measure of variability. An ideally robust index must be responsive as opposed to being temperamental (i.e. liable to unreasonable changes) (Keyantash and Dracup, 2002). Raw scores of five, four, and two were assigned to SPEI & SSI, NADI, and SPI, respectively (Table 5.2). SPEI and SSI were not temperamental and their response was quite positive in detecting historical drought in the LRC. The SSI, NADI, and SPI agreed with the SPEI historical drought detection, however, NADI was ranked lower in detecting 1992 followed by SPI and subsequently by the SSI for the same drought year. The raw score assignment for NADI agrees with those suggested by Barua (2010) while making use of the linear ADI in that the index is not liable to unreasonable changes. Although NADI gives an overall catchment water availability, for this study, it undermined a major historical drought compared to the rest of the other indices. Studies such as Kim *et al*. (2009) have reported that SPI tends to overestimate small rainfall scarcity even if excessive rainfall occurs just before the period of interest. SPI was therefore assigned a raw score of two since it is

rainfall dependent and does not give an overall view of catchment water availability. Further to the latter coupled with its temperamental nature resulted in SPI low raw score assignment.

5.3.2.2 Tractability

Tractability indicates the practical aspects of an index. Keyantash and Dracup (2002) indicated that a tractable index requires a low level of numerical computations and sparsely observed data. The raw scores of five, four, five, and two were assigned to SPI, SPEI, SSI, and NADI respectively (Table 5.2). Of the four indices, SPI and SSI are the more practical, computation is easier compared to SPEI and NADI and they also require fewer input variables (i.e. rainfall and streamflow) and hence the two were assigned the highest raw scores. The computation of NADI is quite rigorous and requires advanced statistical skills coupled with more hydro-climatic variables while SPEI only requires rainfall and evapotranspiration and the computation is less complex. Therefore, making NADI was found to be less tractable with a raw score of two.

5.3.2.3 Transparency

Transparency considers the clarity of the objective behind a respective drought index (Keyantash and Dracup, 2002). This is an important decision criterion because a pragmatic index should not be only understood by the scientific community but by all stakeholders affected by drought events. The easier to understand indices are usually those that require less input data variables and for this study, including SPI and SSI, which were both assigned a raw score of five (see Table 5.2). Although SPEI had two input variables, challenges may arise if evaporation data is not available, the index is deemed easier to understand by different stakeholders compared to NADI with more input variables with quite involving computations. The SPEI and NADI were assigned raw scores of four and two respectively as indicated in Table 5.2.

5.3.2.4 Sophistication

The sophistication decision criteria consider the conceptual merits of drought characterisation (Keyantash and Dracup, 2002). The latter study further indicated that a drought measurement technique may be less understood but may be sophisticated from a proper perspective. Although linear ADI with similar characteristics to NADI was the least tractable and transparent, it was found useful in drought characterisation (i.e. defining drought duration,

intensity, and severity) by Barua (2010) while for this study it underestimated a major historical drought (1991/92) including the most recent 2014/16 and thus it was assigned a raw score of three. In characterising drought for this study, SPEI, SPI, and SSI showed the best strength as they were all able to detect the most severe drought in the catchment and were assigned raw scores of five and four respectively (see Table 5.2). For the case of SPI, it was the least sophisticated and was therefore assigned a raw score of two.

5.3.2.5 Extendibility

Extendibility describes the degree to which an index may be extended across time to alternate drought scenarios (Keyantash and Dracup, 2002). Historical data was used for all the indices considered in this study (i.e. rainfall, streamflow, soil moisture, and temperature). However, if modeled future long-term data is made available, the extension of an index is possible. Raw scores of five, four, two, and two were assigned to SPI, SPEI, SSI, and NADI respectively (Table 5.2). That is because the computation of SPI and SPEI is relatively less complex and some of their future data variables are already available in certain platforms. On the other hand, for the computation of SSI, streamflow should be forecasted first and this requires modeling skills and can be quite challenging. For the case of NADI, the index requires soil moisture data as one of its input variables, which may make forecasting future drought challenging.

5.3.2.6 Overall comparative index evaluation

As indicated in Table 5.2, the overall index evaluation of the drought indices is in terms of the total weighted score. The SPEI, SSI, SPI, and NADI showed an overall score of 129, 125, 106, and 84 respectively. This study, therefore, showed that the SPEI was the better index while comparing it to SPI, SSI, and NADI, making it more suitable for drought assessment and monitoring in the study area. For historical drought detection, SPEI modeled better the characteristics and showed the severity of the 1991/92 drought. Further to the 1991/92 drought, the index also demonstrated the severity of the prolonged 2014/16 drought and suggested that the severity and intensity superseded that of the 1991/92 drought. This was also shown by SSI at 1- month timescale. The lowest ranking index was the NADI. Due to its complexity in index computation coupled with the data required to carry out the computations. Although Barua (2010) found that ADI (where NADI is derived) was the best performing index in his study, the author determined that in data-scarce catchments, other indices may perform better than ADI. Because of the many data variables required to compute NADI, it makes it difficult for

the different stakeholders to understand the index. The second-ranking was SSI. The index is easy to understand with minimal data requirements and the computation is not rigorous. Since the index is solely dependent on streamflow, it is disadvantaged in the scoring system. Although it did not rank the highest, SPEI was still considered to reflect water deficiency in the hydrological system at longer timescales. Based on Table 5.2 the SPEI was found to be superior compared to the other indices.

5.4 Chapter summary

Drought indices are often developed for specific regions and therefore it is important to assess index usefulness in a region it has not been developed to determine its suitability. This chapter was therefore dedicated to drought characterisation and index evaluation for their strength in detecting hydrological drought in the study area. Drought characterisation was conducted using the four indices (SPI, SPEI, SSI, and NADI) for the following periods; 1986 - 1996, 1996 – 2006, and 2006 - 2016. The characterisation was based on drought duration, intensity, frequency, magnitude, and severity. An increased drought duration was observed between 1986 - 1996 while the shortest duration was observed between 1996 - 2006. SPI showed the highest severity followed by SPEI, NADI, and then the SSI. The study found that lower drought severity corresponded to much-reduced drought intensity and this was realised in all timescales. Further, this study found that drought intensity increases with an increasing timescale (i.e. 1-month timescale indicated an average severity for SSI was -7.29 while the 12- month showed the same as -16.62). The relationship between drought severity and duration revealed a strong linear relationship across all the indices at all timescales. The same indices that were used for characterisation were evaluated for their suitability for drought assessment in the LRC. Making use of the decision criteria by Keyantash and Dracup (2002), the indices were evaluated. According to the raw scores of each of the five criteria SPEI ranked the highest with a total weight score of 129 followed by the SSI with a score of 122 and then the SPI with a score of 106 and lastly the NADI with a score of 76. Because SPEI ranked the highest of all the four indices evaluated, it was regarded as the best index that better assessed historical drought conditions on the LRC. Although this is the case, this study is hydrological, and hydrological drought manifests through reduced streamflow which can be evident when the meteorological timescale is increased. The SPEI is therefore used in the prediction of drought for the LRC.

6 APPLICATION OF DROUGHT PREDICTION MODELS

Chapter overview, Case study data used, Drought prediction, Results, and discussion, Summary

6.1 Chapter overview

The significance of drought prediction in water resources management in mitigating the negative impacts of drought has been well articulated in the previous chapters. Drought indices are believed to be more functional than raw data in decision making (Hayes, 2003) and thus, such indices have been widely used in drought prediction studies. From Chapter 5 (section 5.3.2.6), SPEI was found to be the best overall index in drought assessment and characterisation in the LRC. Thus, SPEI at 1-, 6- and 12- month's timescale was used in the application of drought models. To improve prediction accuracy, the SPEI time series was decomposed using the Ensemble Empirical Mode Decomposition (EEMD) and further prediction combinations were attempted. Two prediction approaches were used (i.e. statistical and machine learning). The statistical approach yielded four models while machine learning only resulted in three. Models applied in this chapter were based on Autoregressive Moving Average (ARIMA), Generalised Additive Models (GAM), and the deep learning Long Short-Term Memory neural network (LSTM). Hybrid models were also applied i.e. EEMD-GAM, EEMD-ARIMA-GAM, and EEMD-LSTM. Further, prediction combinations were conducted which summed up the means of all the models (note that statistical models were not combined with machine learning) for the case study.

Test for model performance was achieved by employing the Mean Error (ME), Mean Absolute Error (MAE), Root Mean Square Error (RMSE), Mean Percentage Error (MPE), and Mean Absolute Percentage Error (MAPE) while the linear relationship between predicted values and target values was determined using the coefficient of determination ($R^2_{adjusted}$). This chapter begins with a description of the case study data used in the modeling process, followed by a detailed methodology of model applications for both statistical and machine learning approaches. The findings of the study on the model application and uncertainty analysis based on prediction intervals are presented followed by a chapter summary.

6.2 Case study data used

Rainfall and temperature were the two hydro-meteorological variables used in the formulation of SPEI for the LRC. The SPEI monthly time series at 1-, 6-, and 12- month's timescales were used for models to be applied in this study. The time series contained data from 1986 to 2016.

6.3 Application of drought prediction models

Statistical and machine learning techniques were applied to predict drought in the LRC. A flowchart showing the sequential flow of application of these models is presented in Figure 6.1. The figure shows all the steps followed in applying these models, which is divided, into four stages (i.e. Decomposition, Components prediction, ensemble prediction, and prediction combinations). An overview of each stage is given below and the details are later discussed under several sub-sections.

The first stage of the modeling process is the decomposition, which was achieved by the EEMD, which extracted seven IMF's, and one residual from the SPEI time series. The IMF's were then predicted in stage two; statistical and machine learning models achieved the component prediction. The choice of the appropriate model for both learning techniques were based on the modeler's preference. The Generalised Additive Models was selected for statistical learning while LSTM was used for machine learning. These techniques have not been adequately documented in the literature regarding drought studies. Further, LSTM is a deep learning neural network that has shown to improve prediction accuracy. Maier *et al.* (2010) indicated that model input variables are generally determined using an iterative process, while Barua (2010) added that they could also be based on prior knowledge and the availability of data within the area of study. Potential input variables are selected from probable input variables using correlation techniques amongst others and the same input is further pre-processed before they can be utilised in the prediction process. Stage two is the component prediction stage, calibration, and model parameters are determined.

Stage three presents the final predicted results output of each IMF. All the IMFs including the residuals were accumulated and resulted in a predicted single value for each month of SPEI time series. This process is termed an ensemble (of size 8) prediction since it represents the sum of all the predicted IMFs including the residuals. In the fourth stage, the prediction combination was done where all the model means were averaged using quantile regression

averaging. The model application is completed by validating the calibrated models in the fifth stage. The model validation was done to investigate how the different models predicted the target values that were not used in the calibration stage.

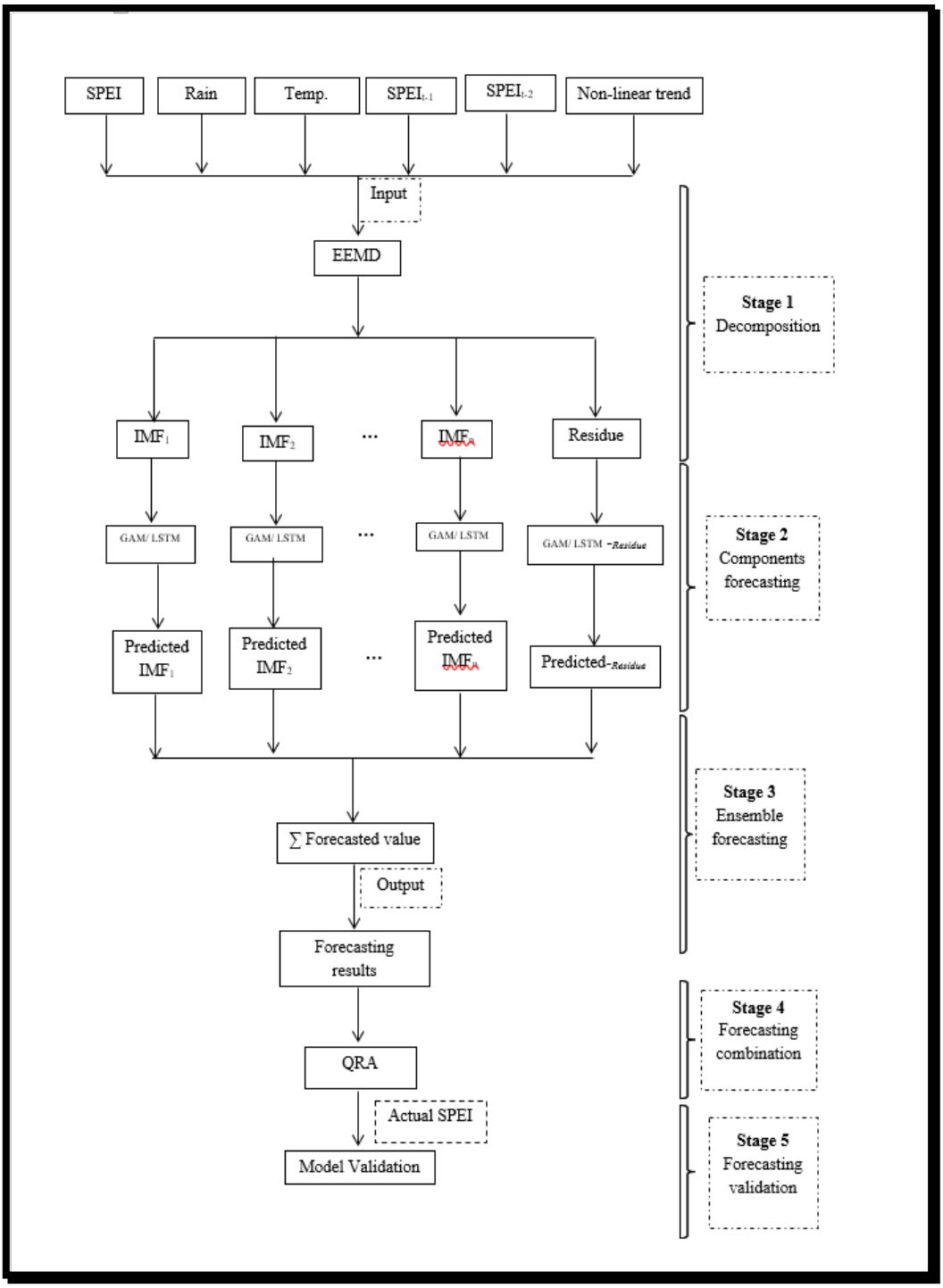

Figure 6.1 Drought prediction framework.

6.3.1 Time series decomposition

The merits and basis of EEMD have thoroughly been discussed in Chapter 2. To successfully decompose the SPEI time series using EEMD, the following steps were followed:

1. White noise $w_i(t)$ was added to the original signal time series $spei(t)$, the new time series was computed as:

$$SPEI_i(t) = spei(t) + w_i(t), \quad (6.1)$$

2. $SPEI_i(t)$ was decomposed into seven IMFs with one residual using the EMD algorithm;
3. Steps 1 and 2 were repeated with different white noise, adding to the signal time series each time;
4. The mean of the ensemble corresponding IMFs of the decompositions was obtained as the results.

In the first step of the EEMD, the determination of the ensemble times and the amplitude of the added noise is of importance. Wu and Haung (2009) suggested the amplitude of adding noise to 0.2 after comparing the results of the actual signal analysis and this was used in this study. Adding the white noise results in;

$$\varepsilon_n = \frac{\varepsilon}{\sqrt{N\prime}}, \quad (6.2)$$

where, N' is the number of ensemble times, ε is the amplitude of the added noise while ε_n is the error of the final standard deviation, which is given by the difference between the original signal time series and the corresponding IMFs.

6.3.2 Input variables selection and data pre-processing

Statistical correlation tests and gradient boosting were used to determine input variables selection for this study. Studies such as Maity and Kumar (2008) and Tran *et al*. (2009) have successfully applied correlation test for variable selection. Only variables that were highly correlated to the SPEI and each IMF were selected as potential input for drought prediction. Gradient boosting constructs additive regression models by sequentially fitting a simple parameterized function (base learner) to current "pseudo"-residuals by least-squares at each iteration (Friedman, 2002). Studies such as Sankaran *et al*. (2008) successfully used Stochastic Gradient Boosting to investigate the relationship between predictor variables in regulating the woody cover in African savannas. By denoting $\{y_i, X_i\}_1^N$ as the entire training set sample then

$\{\pi(i)\}_1^L$ is the random permutation of the targets $\{1, \dots, N\}$. A random sub-sample of size $\tilde{N} < N$ is given by $\{\tilde{y}_{\pi(i)m}, X_{\pi(i)}\}_1^{\tilde{N}}$. Friedman (2002) gives the gradient boosting algorithm used in this study as shown in Figure 6.2.

$$F_0(X) = \arg min_\gamma \sum_{i-1}^{N} \Psi(y_i, \gamma)$$

For $m = 1$ to M do:

$$\{\pi(i)\}_1^L = rand\_perm\{i\}_1^N$$

$$\tilde{y}_{\pi(i)m} = -\left[\frac{\partial \Psi\left(y_{\pi(i)}, F(X_{\pi(i)})\right)}{\partial F(X_{\pi(i)})}\right]_{F(X)=F_{m-1}(X)}, i = 1, \tilde{N}$$

$$\{R_{lm}\}_1^L = L - terminal\ node\ tree\ \left(\{\tilde{y}_{\pi(i)m}, X_{\pi(i)}\}_1^{\tilde{N}}\right)$$

$$\gamma_{lm} = \arg min_\gamma \sum_{X_{\pi(i)\epsilon R_{lm}}} \Psi\left(y_{\pi(i)}, F_{m-1}(X_{\pi(i)}) + \gamma\right)$$

$$F_m(X) = F_{m-1}(X) + \nu . \gamma_{lm} 1(X \epsilon R_{lm})$$

Figure 6.2: Gradient boosting algorithm. (Friedman, 2002)

The smaller the fraction f, the more the random samples used in successive iterations will differ, thereby introducing more overall randomness into the procedure. Using the value is roughly equivalent to drawing bootstrap samples at each iteration. Using $\tilde{N} = f \cdot N$ also reduces the computations by a factor of f. However, making the value of f smaller reduces the amount of data available to train the base learner at each iteration. This then causes the variance associated with the individual base learner estimates to increase. Table 6.1 shows the potential input variables used in this study. It should be noted that SPEI was a potential input variable while considering the IMFs and the residual while it was a response variable in the un-decomposed model application.

Table 6.1: Potential predictor variables for model application.

Predictor variable	Description
SPEI 1	Computed SPEI time series at 1- month timescale.
SPEI 6	Computed SPEI time series at 6- month timescale.
SPEI 12	Computed SPEI time series at 12- month timescale.
Rain	Mean monthly station rainfall time series in the study area.
Temperature	Max, Min and Mean monthly station temperature in the study area.
Lag1	A lagged time series data set produced by back shifting 1- month lags.
Lag2	A lagged time series data set produced by back shifting 2- month lags.
Non-linear trend	An extracted trend from the actual SPEI time series.

6.3.3. Statistical learning model application (Generalised Additive Models - GAMs)

6.3.3.1 The generalised additive model without auto-correlated errors

Let y_t be SPEI on month t, where $t = 1, \dots, n$ with the corresponding covariates $x_{t1}, x_{t2}, \dots, x_{tp}$, where p represents the number of variables. The generalised additive model is then written as follows:

$$y_t = \beta_0 + \sum_{j=1}^{p} s_j(X_t\beta_j) + \varepsilon_t, \qquad (6.3)$$

where, y_t is the response variable, X_t is the dependent variable, β_0 is the intercept, β_j is a parameter, s_j is an unknown parameter and ε_t is the error term. Equation (6.3) is estimated using penalised cubic splines (Wood, 2006; Goude *et al*., 2014), which is expressed in terms of Equation (6.4).

$$\min_{sj} \left[\sum_{t=1}^{n}\left(y_t - \beta_0 - \sum_{j=1}^{p} s_j(x_{tj})\right)^2 + \sum_{j=1}^{p} \lambda_j\left(\int (f''(x))^2 dx\right)\right]. \qquad (6.4)$$

The degree of smoothness is controlled by the penalty parameter $\Lambda = (\lambda_j, j = 1, \dots, p)$, which determines the roughness of the function estimate to the data. It is optimised using the generalised cross-validation criterion (GCV) and easily implemented in the package 'mgcv' (Wood, 2006; 2017). For small values of λ_j, the smoothness is rough. The smooth function, s_j is given by Equation (6.5), which can be explained as the sum of basis functions, $b_i(x)$ and their regression coefficients β_i.

$$s_j(x) = \sum_{i=1}^{q} \beta_i\, b_i(x), \qquad (6.5)$$

where, q denotes the basis dimension.

6.3.3.2 The generalised additive model with auto-correlated errors

Let y_t be SPEI as defined above, which gives the generalised additive model with autocorrelated errors are given in Equations (6.6) and (6.7), respectively.

$$y_t = \beta_0 + \sum_{j=1}^{p} s_j(X_t\beta_j) + \varepsilon_t, \quad (6.6)$$

where variables and parameters are as defined in section 6.3.3.1. Time-series observations are normally auto-correlated. To correct for autocorrelation, it is normally advised to use time series, regression models. This study, therefore, assumes that the error terms ε_t are auto-correlated and follow a seasonal autoregressive moving average (SARMA) model given in Equation 6.7.

$$\emptyset(B)\Phi(B)\varepsilon_t = \theta(B)\Theta(B)\, v_t, \quad (6.7)$$

where, $\emptyset(B)$ is the non-seasonal autoregressive operator, $\theta(B)$ is the nonseasonal moving average operator and the corresponding seasonal autoregressive and seasonal moving operators are $\Phi(B)$ and $\Theta(B)$ respectively; v_t denotes a white noise series. By expressing Equation (6.6) in terms of ε_t and substituting in Equation (6.7), we get Equation (6.8).

$$\emptyset(B)\Phi(B)\left[y_t - \left\{\beta_{0t} + \sum_{i=1}^{p} s_j(X_t\beta_j)\right\}\right] = \theta(B)\Theta(B)v_t. \quad (6.8)$$

6.3.4 Machine learning model application (Long Short-Term Memory – LSTM)

6.3.4.1 Selection of machine learning model structure

Artificial Neural Network (ANN) machine learning technique was used in this study, due to its strength of analysing large data that do not exhibit a linear relationship. Studies such as Fausett (1994); Samaransinghe (2006); Mishra *et al*., (2007) developed ANN-based models for application in the fields of engineering and science. For drought prediction, the Recursive Multi-step and Direct Multi-step Neural Networks are commonly used (e.g. Mishra and Desia, 2006; Kim and Valdes, 2003; Mishra *et al*., 2007; Ochoa-Rivera *et al*., 2007). However, this study applied a deep learning approach of ANN prediction which is based on an improved multilayer perceptron, which is somewhat different from these traditional ANNs. Deep learning uses a cascade of multiple processing layers to learn features or representations of data with different levels of abstractions (Lecun *et al*., 2015). To predict SPEI at 1-, 6- and 12- month timescales, this study used the Long Short-Term Memory (LSTM) Recurrent Neural Network

(RNN). The LSTM was successfully used in modeling land and surface temperature and satellite imagery disturbances in Zhang *et al*. (2018) and Kong *et al*. (2018), respectively.

6.3.4.1.1 Long Short-Term Memory Neural Network

Donahue *et al*. (2017) describe the LSTM cell used in this study in detail. The LSTM structure is as shown in Figure 6.3 and contains the forget date (f_t), input gate (i_t), input modulation gate (m_t), output gate (o_t), a memory cell (c_t), and the hidden state (h_t). Each of the gates acts on the received signal, and then block or pass on information based on its strength and import, which they filter with their own sets of weights. The weights modulate input and hidden states are then adjusted through recurrent networks learning processes. The cells learn when to allow data to enter, leave, or be deleted through the iterative process of making guesses, back-propagating error, and adjusting weights via gradient descent.

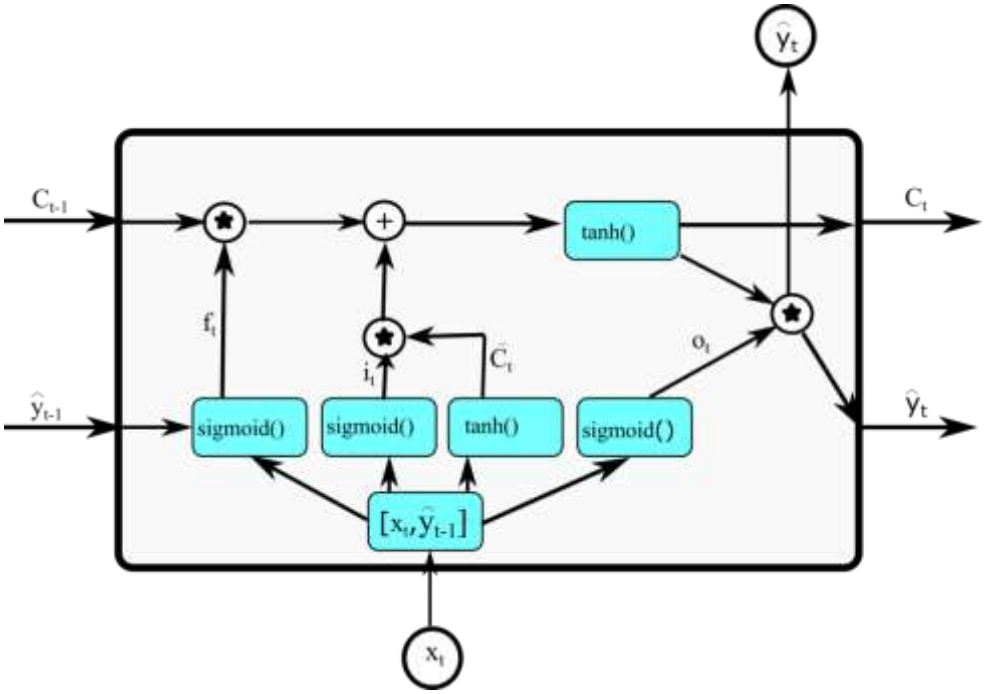

Figure 6.3: The structure of the LSTM cell unit.

The first step is to determine whether information from the cell state has been forgotten or remembered and this is determined by a sigmoid layer in the forget gate and is computed using Equation (6.9).

$$f_t = S(W_f.[\hat{y}_{t-1}, x_t] + b_f), \tag{6.9}$$

In the second step, a decision is made whether the new information needs to be stored in the cell state and this step consists of two parts. Firstly, a sigmoid layer (i.e. forget gate) determines which values are used for updating after which, a $tanh$ layer is used to generate a new candidate value $\hat{C}_t$ which is added to the cell state. Secondly, the two are combined to create an update to the state. The latter are computed using Equations (6.10) and (6.11).

$$i_t = S(W_i.[\hat{y}_{t-1}, X_t] + b_i], \tag{6.10}$$

$$\hat{C}_t = \tanh(W_C.[\hat{y}_{t-1}, X_t] + b_C). \tag{6.11}$$

Step three involves the updating of the old cell state C_{t-1}. The old cell state C_{t-1} is multiplied by f_t to remove redundant information that is not of interest. It is added to $\hat{C}_t$ to obtain a new candidate value, which is scaled by the number required to update each state value, which is computed using Equation (6.12):

$$C = f_t.C_{t-1} + i_t.\hat{C}_t, \tag{6.12}$$

Step four is the final stage and the sigmoid layer is run to determine what part of the cell state is going to be an output. Then the cell state is put through $tanh$ function, which is multiplied by the output of the sigmoid gate and is achieved by Equations (6.13) and (6.14).

$$o_t = S(W_o.[\hat{y}_{t-1}, X_t] + b_o), \tag{6.13}$$

$$\hat{y}_t = o_t.\tanh(\hat{C}_t) \tag{6.14}$$

where in Equations (6.9) to (6.13), X_t is the input vector, $\hat{y}_{t-1}$ is the previous hidden state, W and $\hat{y}$ are the weight matrices and S is the logistic sigmoid function, *tanh* is the hyperbolic tangent function and b is the bias vector.

A sliding time window-based method described by Cheng *et al*. (2016) is used to obtain several samples for training LSTM from a single historical SPEI at 1-, 6- and 12- month timescales. For a time series (x_1, x_2, . . . , x_n) with *n* time steps, assuming the size of the time window is l (l < n), the first sample is input subsequence (x_1, x_2, . . . , x_l) for output x_{t+1}. The time window slides one time-step ahead at a time to generate one training sample. The subsequence (x_{t-l}, . . . , x_{t-2}, x_{t-1}) in the time window corresponds to the output x_t one time-step ahead. Thus, *n - l + 1* samples are obtained for training the LSTM network. For the LSTM hidden layers in this study,

a dropout layer with a dropout rate of 0.5 is added to prevent over-fitting (Srivastava *et al*., 2014). In addition, the mean square error (MSE) loss function and the Adam optimiser (Kingma and Ba, 2014) are used for LSTM training. With an *l-step* sliding time window, the output y_{t+1} is predicted using the input sequence $(x_{t-l+1}, \ldots, x_{t-1}, x_t)$. A strategy to implement prediction of *n* steps is performed iteratively using the predictive outputs of the previous steps to compose the input sequence to the next step. Therefore, the output y_{t+n} would be predicted using the input sequence $(x_{t+n-l}, \ldots, x_t, y_{t+1}, \ldots, y_{t+n-1})$.

The LSTM model summary at 1-, 6- and 12- month timescales are presented in Appendix C (Figures C7, C8, and C9) and consists of one LSTM and one dense layer. The number of LSTM parameters varies from SPEI to the Residual at all timescales while the dense layer parameters remain at 33 in all timescales. The variables with the same numbers of trainable parameters indicate that they consist of the same number of input variables. This is determined by the number of input variables selected as identified by GBM to influence each target value. No non-trainable parameters are identified in the calibration stage.

To determine whether there is underfitting or overfitting, training and testing loss are determined at each epoch. The LSTM learning curves for each timescale are shown in Appendix C (Figures C10, C11, and C112). The epochs (number of iteration) was set at 300. It was found that the number of training and testing losses decreases with an increased number of epochs at all timescales for all the models. Both training and testing losses stabilise around the same point, which according to Bouktif *et al*. (2018) indicated a good fit.

6.3.5 Prediction combination

The study employed Quantile Regression Averaging (QRA) prediction combination techniques, first introduced by (Nowotarski and Weron, 2015). The prediction combination was done for statistical learning models, machine learning models, and the best performing statistical and machine learning hybrid models. The QRA is based on predicting the response variable against the combined predictions, which are treated as independent variables. SPEI is denoted by $y_{t,\tau}$ as indicated in the GAM sections above and the methods used to predict the next observation $y_{t,\tau}$ which is dented by $y_{t+1}, y_{t+2}, \ldots, y_{t+m}$. Using $j = 1, \ldots, M$ methods, the combined prediction are given by the following.

$$\hat{y}_{t,\tau}^{QRA} = \beta_{0,\tau} + \sum_{j=1}^{k} \beta_{j,\tau}\, \hat{y}_{tj,\tau} + \varepsilon_{t,\tau},\ \tau \in (0,1), \qquad (6.15)$$

where, $\hat{y}_{tj}$ is the predictive from method j, $\hat{y}_{t,\tau}^{QRA}$ is the combined prediction at quantile τ and $\varepsilon_{t,\tau}$ is the error term. Equation (6.16) gives the solution of the parameter estimates.

$$\arg\min_{\beta} \sum_{t=1}^{n} \rho_{\tau} \left(\hat{y}_{t}^{QRA} - \beta_0 - \sum_{j=1}^{m} \beta_j \hat{y}_{tj}\right), \tag{6.16}$$

where, ρ_{τ} is the pinball loss function. The QRA prediction is then compared with prediction based on a weighted average of the prediction using Equation (6.17):

$$\hat{y}_{t,\tau}^{c} = \sum_{j=1}^{M} \omega_{jt} \hat{y}_{jt,\tau}, \tag{6.17}$$

Where, ω_{jt} is the weight assigned to the prediction at time *t* using method *j*.

6.3.6 Test for model performance

The performance of the applied models for this study was based on their Root Mean Square Error (RMSE), Mean Error (ME), Mean Absolute Error (MAE), Mean Percentage Error (MPE), and the Mean Absolute Percentage Error (MAPE). The detailed models underpinning these measures of performances are documented in Chapter 2, sub-section 2.8.

6.3.7 Determination of prediction intervals

The Prediction Intervals (PIs) are determined for the best performing statistical (GAM) and machine learning (LSTM) models. Various indices are used to evaluate the reliability of PIs, for this, study the Prediction Interval Coverage Probability (PICP) and the Prediction Interval Normalised Average Width (PINAW) are used and their details can be obtained in Sun *et al*. (2017). The PICP and PINAW are computed using Equations (6.18) and (6.19), respectively.

$$PICP = \frac{1}{m} \sum_{i=1}^{m} I_{ij}, \tag{6.18}$$

where, m is the number of prediction and *I* is a binary variable defined as;

$$I_{ij} = \begin{cases} 1, & if\ y_i \in \left(UL_{ij}, LL_{ij}\right), \\ 0, & otherwise \end{cases}$$

The PICP is valid if it is greater than or equal to the predetermined level of confidence. The PINAW is used to check if the required value is covered by the PI and is computed using Equation (6.19).

$$PINAW = \frac{1}{m\left(\max(y_{ij}) - min(y_{ij})\right)} \sum_{i=1}^{m} \left(UL_{ij} - LL_{ij}\right), j = 1, \ldots, n. \tag{6.19}$$

If the PICP is valid and accurate, then the PINAW is expected to be small (Sun *et al*., 2017).

6.4 Results and discussions

6.4.1 Exploratory data analysis

Figure 6.4 shows the SPEI time series plot of density, normal quantile to quantile (Q – Q), and the box plots at 1-, 6- and 12- month timescales before decomposition. To determine the normality SPEI data, Anderson-Darling tests were carried out and the results are presented in Figure 6.5 for SPEI 1- month timescale while Table 6.2 shows the results statistics for all the timescales. For the case study results of SPEI 6- and 12- month timescales, see Appendix C (Figures C1 and C2). The initial visual interpretation of the Q-Q plot (Figure 6.4) suggested the departure of SPEI data from normality while the detailed statistical distribution fit test Probability-Probability Plot (P-P) showed that the data is normally distributed at all the timescales. Altman and Bland (1995); Oztuna *et al*. (2006) and Field (2009) reported that although visual inspection of normality is used, it is often unreliable with no guarantees of the results. Johnson SB, Error, and Dagun (4P) distributions were the best fit for SPEI 1-, 6- and 12- month timescales respectively.

From Figure 6.4, it can be concluded that the distribution of the SPEI data at 6- and 12- month timescales are bimodal while the 1- month timescale exhibited a unimodal distribution. The current study made use of EEMD to decompose the SPEI time series at different timescales. Time series decomposition was deemed necessary because environmental variables are non-stationary and exhibit a certain complexity. These complexities, according to Labat (2010) and Montzka *et al*. (2009) are due to the interrelated physical factors and compounded by the effects of a changing climate. In a study by Di *et al*. (2014), hydrological time series complexity was measured using Lempel-Ziv Complexity theory and it was found that decomposition greatly reduced the complexity of the time series and improved the prediction accuracy (Nazir *et al*., 2019). Seven independent IMFs and one residual were obtained for each SPEI timescale (see Figures 6.6 for SPEI 1- and Appendix C (Figures C3 and C4) for SPEI 6- and 12- respectively). The IMF's exhibit an oscillation characteristic from high to low frequencies while the residual maintains the trend of the time series.

Table 6.3 shows the statistics of the original SPEI time series together with that of each IMFs and the residual component at all the timescales considered in this study. The variance of the

actual data ranged between 0.799 and 1.147 for both the training and testing data while the decomposed IMFs showed lower values compared to the actual data. The study found that IMF 1 was characterised by a larger variance compared to the last IMF, while the residual was higher than that of the last IMF. The variance behaviour was also found for the standard deviation. The test of both the actual data the IMFs was much lower than the training set. The standard deviation and variance results obtained in this study are comparable to Zhang *et al*. (2018), which showed similar behaviour while comparing statistics of decomposed and actual data. The majority of the kurtosis values for both the actual and decomposed SPEI were found to be much smaller while the skewness ranged between -0.01417 and 1.1959.

The 12- month timescale had the highest skewness with 66.67% of the data negatively skewed while 1- and 6- timescales had 38.89% and 50% negative skewness respectively. These findings according to Microsoft (1996) indicate that SPEI 12- distribution is characterised by an asymmetrical tail extending more towards the negative followed by SPEI 6- while SPEI 1- data showed to be positively skewed. Normally distributed data produces a skewness of zero with possibilities of small variations (Brown, 1997). The skewness results obtained in this study indicate that the data is approximately asymmetrical since 74.07% of the data are greater than 0.1. Although Brown (1997) suggested that a skewness statistic of 0.01819 was acceptable for normally distributed data, this study adopted a skewness statistic of 0.1 since it is a variation from Brown (1997) suggestion is less than 10%.

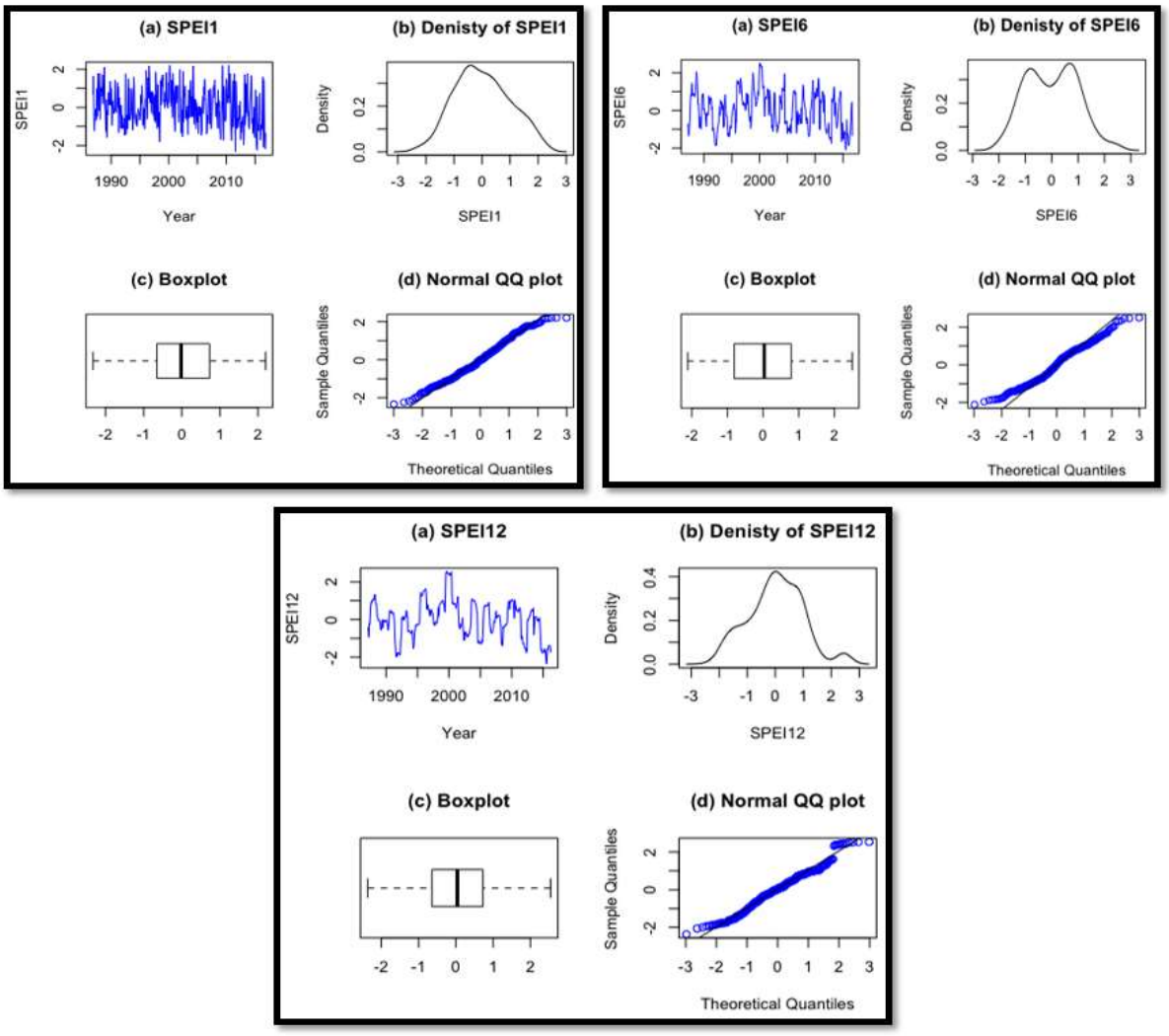

Figure 6.4: SPEI empirical results for SPEI 1, SPEI 6, and SPEI 12.

Table 6.2: Five best-fit distributions statistics results from Anderson-Darling test.

	Distribution	Rank	Statistic
SPEI 1	Johnson SB	1	0.36984
	Gen. Extreme	2	0.46404
	Burr (4P)	3	0.59691
	Weibull (3P)	4	0.60388
	Beta	5	0.68164
SPEI 6	Error	1	0.91662
	Johnson SB	2	1.1468
	Gen. Gamma (4P)	3	1.2168
	Kumaruswamy	4	1.2168
	Dagum (4P)	5	1.2455
SPEI 12	Dagum (4P)	1	0.75992
	Log-Logistic (3P)	2	1.2606
	Normal	3	1.3187
	Error	4	1.3207
	Error function	5	1.234

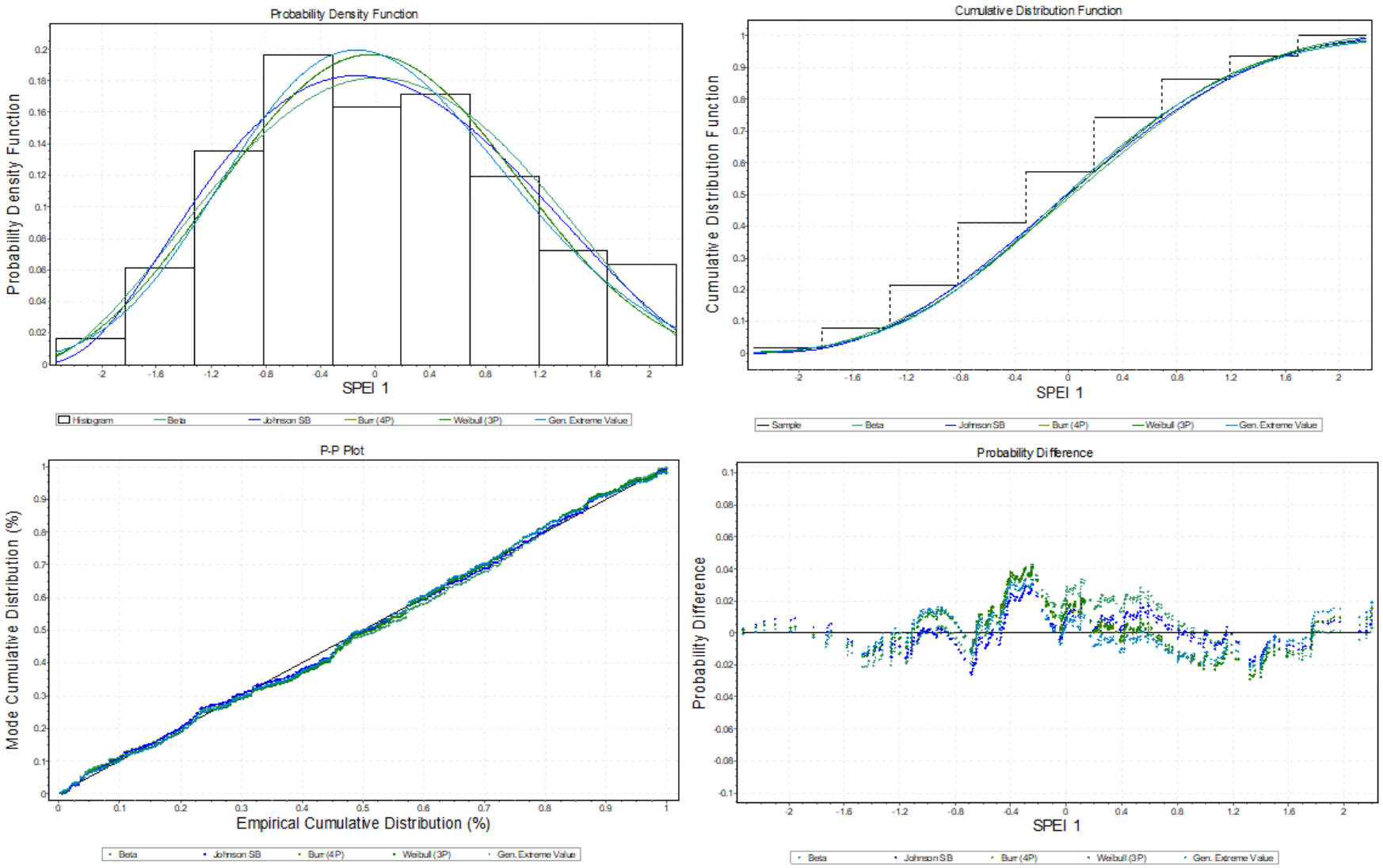

Figure 6.5: Statistical distribution fit test results for SPEI 1.

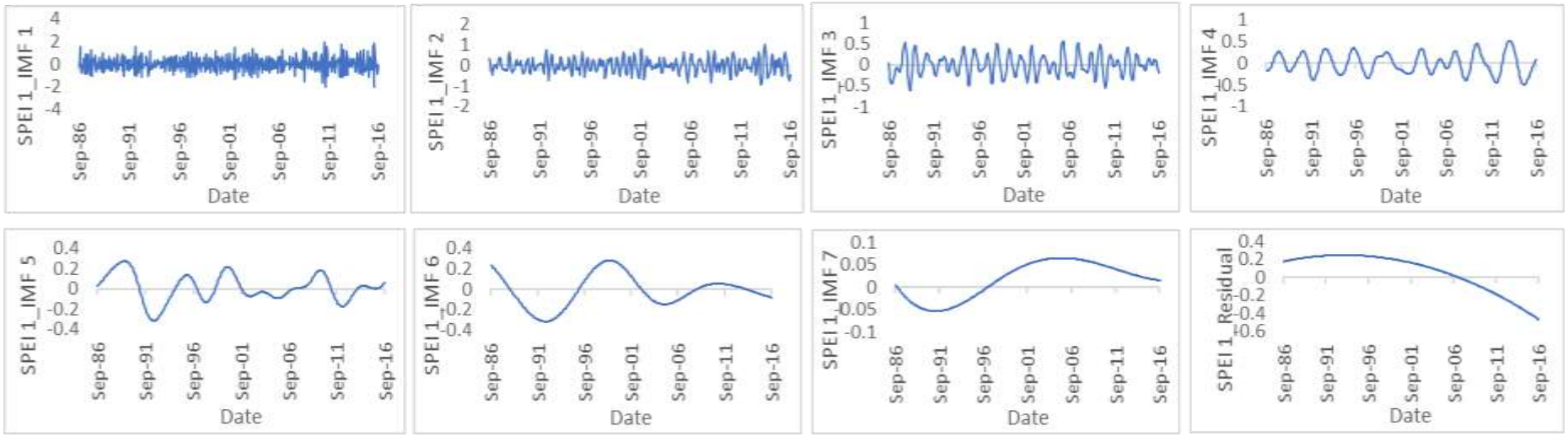

Figure 6.6: Sample IMFs for SPEI 1.

6.4.2 Variable selection

Variable selection was achieved using gradient boosting. The main objective of a variable selection procedure is to identify the correct predictor variables, which have an important influence on the response variable and could provide robust model prediction (Haque *et al*., 2018). Variable selection was conducted for each SPEI time series and IMFs including the residual at the different timescales. Figure 6.7 shows the relative importance of different predictor variables as selected by gradient boosting. Figure 6.7 shows results for SPEI 1- timescale, the IMFs, and the residual, while the results of SPEI 6- and 12- are presented in Appendix C (Figures C5 and C6, respectively). The relative importance values are the means of 50 model runs, each based on a randomly selected subset of 90% of the data (Sankaran *et al*., 2007).

Table 6.3: Summary statistics of the original and the decomposed time series.

Time scale	Time series	Period	Min.	Max.	Mean	SD	Variance	Skew.	Kurt.
SPEI1	Actual dataset	Train	-1.81278	2.19896	0.148561	0.910605	0.829202	0.221582	-0.64457
		Test	-2.32907	2.199187	-0.82	1.070987	1.147013	0.277515	-0.67855
	IMF1	Train	-1.36737	1.499639	-0.00234	0.616641	0.380246	0.060363	-0.72371
		Test	-2.00883	1.954978	-0.00585	0.783791	0.614329	0.205315	0.006426
	IMF2	Train	-0.82817	0.843964	-0.01036	0.315931	0.099812	-0.27299	0.05817
		Test	-0.93602	1.020698	-0.0061	0.399217	0.159374	0.02349	-0.47482
	IMF3	Train	-0.61475	0.57066	-0.01001	0.25657	0.065828	0.068829	-0.67494
		Test	-0.56767	0.497348	0.001743	0.233017	0.054297	0.066488	-0.32031
	IMF4	Train	-0.39727	0.349118	0.000626	0.203401	0.041372	0.023372	-1.20691
		Test	-0.49732	0.518653	-0.00515	0.297948	0.088773	0.173266	-1.1085
	IMF5	Train	-0.31629	0.271511	0.007903	0.151258	0.022879	-0.14936	-0.60484
		Test	-0.1748	0.183806	-0.01343	0.090346	0.00816	-0.06964	-0.11953
	IMF6	Train	-0.31537	0.282087	-0.02241	0.188362	0.03548	0.110488	-1.24838
		Test	-0.10642	0.053169	-0.04002	0.047042	0.002213	-0.44244	-1.08256
	IMF7	Train	-0.05362	0.065376	0.00398	0.043949	0.001931	0.129717	-1.55465
		Test	0.015715	0.064241	0.007856	0.015912	0.000253	-0.02776	-1.40831
	Residual	Train	0.022217	0.246122	0.18953	0.060794	0.003696	-1.18926	0.337862
		Test	-0.46694	0.019302	0.019302	0.142496	0.020305	-0.1954	-1.16856
SPEI6	Actual dataset	Train	-1.88287	2.502429	0.165879	0.953006	0.908221	0.143209	-0.59864
		Test	-2.11441	1.696328	0.119342	0.953183	0.908556	0.149464	-1.12683
	IMF1	Train	-0.86447	1.0222214	0.001508	0.26408	0.068858	0.193554	1.359236
		Test	-1.00061	1.063124	-0.00257	0.35038	0.122766	0.098206	0.499751
	IMF2	Train	-0.78712	0.643729	-0.00216	0.242107	0.058616	-0.05015	0.480301
		Test	-0.77676	0.67489	0.001258	0.280518	0.07869	-0.20288	-0.27622
	IMF3	Train	-0.69784	0.867707	-0.0066	0.411532	0.169359	0.0176451	-1.14614
		Test	-0.71143	0.845515	-0.00268	0.4023	0.161846	0.324342	-0.89305
	IMF4	Train	-0.73816	0.72446	0.014992	0.394933	0.155972	-0.03329	-1.20204
		Test	-0.84534	0.745929	-0.00529	0.467398	0.218461	-0.03972	-1.14763
	IMF5	Train	-0.67003	0.610197	-0.02455	0.337414	0.113848	-0.17639	-0.60507
		Test	-1.159	0.276158	-0.08311	0.140341	0.019696	0.689158	-0.8109
	IMF6	Train	-0.21202	0.336629	-0.00915	0.198007	0.39207	0.541607	-1.28458
		Test	-0.16457	0.091232	0.01288	0.076898	0.005913	-0.63264	-0.80111
	IMF7	Train	-0.01218	0.044395	0.019121	0.021761	0.000474	-0.21805	-1.65539
		Test	0.008134	0.034692	0.022095	0.008333	0.0000694	0.321258	-1.22907
	Residual	Train	0.038626	0.245892	0.181124	0.058455	0.003417	-0.68193	-0.73303
		Test	-0.57808	0.035206	0.189559	0.179909	0.032367	-0.22986	-1.15638
SPEI12	Actual dataset	Train	-1.99772	2.539835	0.170487	0.397574	0.952069	0.198231	0.04558
		Test	-2.36548	1.046242	0.138832	0.893879	0.799019	-0.39594	-1.01876
	IMF1	Train	-0.60582	0.491949	0.004402	0.178638	0.031911	-0.00541	0.49103
		Test	-0.49141	0.667998	0.004939	0.185027	0.034235	1.195896	0.187336
	IMF2	Train	-0.49038	0.528846	-0.00741	0.202928	0.04118	-0.3788	0.020563
		Test	-0.51725	0.401521	-0.00058	0.194732	0.39624	-0.01417	-0.39624
	IMF3	Train	-1.01647	0.817369	0.005364	0.365714	0.133747	-0.27986	0.423858
		Test	-0.63599	0.576616	0.003628	0.256241	0.065659	-0.32191	-0.49566
	IMF4	Train	-0.94251	1.038782	0.004179	0.47766	0.228159	0.120488	-0.68228
		Test	-1.04925	0.92727	-0.0094	0.53429	0.285466	-0.9953	-0.05535
	IMF5	Train	-0.73644	0.630692	-0.02485	0.390485	0.152479	-0.09351	-0.95628
		Test	-0.19096	0.336679	-0.07899	0.15719	0.024709	0.679647	-0.61952
	IMF6	Train	-0.32518	0.432001	0.003434	0.264392	0.069903	0.310529	-1.38921
		Test	-0.19777	0.209411	0.028521	0.127616	0.016286	-0.38268	-1.24626
	IMF7	Train	-0.05116	0.07139	-0.00397	0.040052	0.001604	0.470288	-1.18411
		Test	0.000959	0.078755	-0.00286	0.022377	0.000501	-1.14776	0.080774
	Residual	Train	-0.02681	0.286657	0.196453	0.083892	0.007038	-0.83412	-0.3017
		Test	-0.92842	-0.03185	0.203329	0.262974	0.069155	-0.22625	-1.15771

The rain showed to be the most important variable for predicting SPEI 1. For the decomposed IMFs from SPEI 1, the non-linear trend showed to be the most important at IMF 2, 3, 4, 5, 6, and 7 while for IMF 1, SPEI 1 and Lag 1 were most important respectively. For the case of the residual components, non-linear trend and Lag 2 were the most important variables. The non-linear trend is the most important predictor for predicting SPEI at 6-month timescale. Time series components (i.e. trend, seasonality, remainder, etc.) have been successfully used as model input in prediction exercises. For example, Benkachcha *et al*. (2015) used time series components in predicting airline passengers using ANN. Like the 1-month timescale, a non-linear trend was important for most of the IMFs (i.e. 2, 3, 4, 5, 6, and 7) while Lag 1 and Lag 2 respectively mostly influenced IMF 2 and the residual. Taşpınar (2015) reported a significant three consecutive lags (i.e. Lags 1, 2, and 3) as input while predicting daily PM_{10} data. The lagged variable of importance was successfully determined by PCA. The findings of this study regarding the importance of Lags 1 and 2 are therefore comparable with those reported by Taşpınar (2015). The relative importance for SPEI at 6-month timescale was similar to that of SPEI at 12-month timescale; however, Lag 1 mostly influenced both IMF 2 and the residual.

Temperature, which has been reported to play a significant role in the development of drought through its inherent nature to highly influence evaporation was found to be important in the SPEI at 1- and 6- months timescales, IMF 1 and 2 time series at all timescales. Lenton *et al*. (2017) reported that sea surface temperature variability contributed to increased land temperature variability and autocorrelation, which ultimately contributed to persistent droughts in North America and the Mediterranean. Mean temperatures were found to be more dominant compared to the minimum and maximum temperature in predicting SPEI. All predictor variables are significantly different from one another in their relative importance (Sankaran *et al*., 2007). Therefore, thus, all features that appeared to have some relative importance (i.e. ranging from 0 to 100) were selected as input variables into both statistical and machine learning models. The ultimate features selected as input variables for this study are as outlined in Table 6.4.

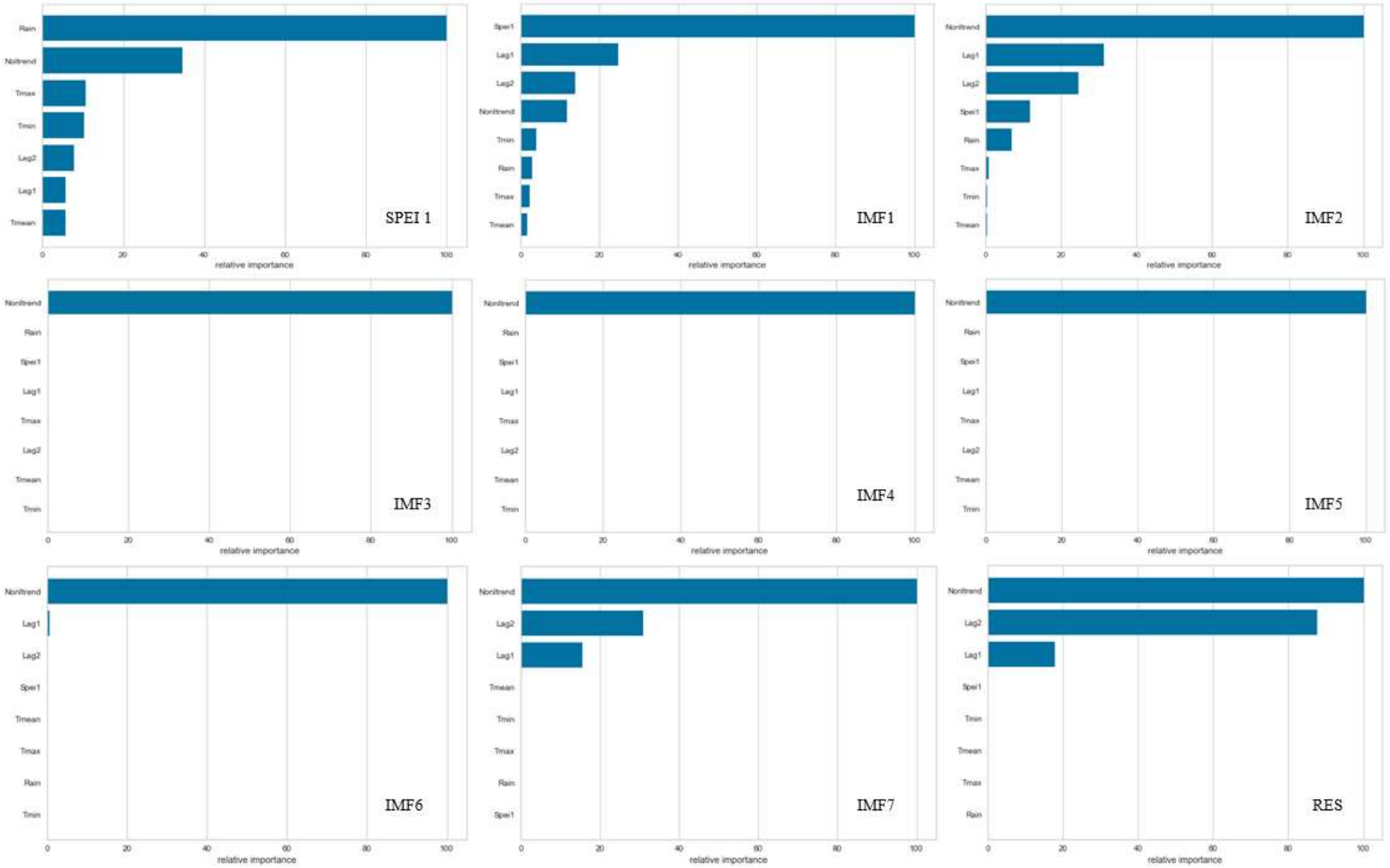

*__SPEI__ - Standardised Precipitation Evaporation Index, __IMF__ - Intrinsic Mode Function, __Res__ – Residual.

Figure 6.7: Sample gradient boosting for the variable of importance (SPEI 1).

Table 6.4: Features used as input variables for model application.

	1-month timescale	6-month timescale	12-month timescale
SPEI	Rain, non-linear trend , $SPEI_{t-1}$ & $SPEI_{t-2}$, Tmax, Tmin, Tmean	Rain, non-linear trend , $SPEI_{t-1}$ & $SPEI_{t-2}$, Tmax, Tmin, Tmean	Non-linear trend , $SPEI_{t-1}$
IMF 1	SPEI, rain, non-linear trend , $SPEI_{t-1}$ & $SPEI_{t-2}$, Tmax, Tmin, Tmean	SPEI, rain, non-linear trend , $SPEI_{t-1}$ & $SPEI_{t-2}$, Tmax, Tmin, Tmean	SPEI, rain, non-linear trend , $SPEI_{t-1}$ & $SPEI_{t-2}$, Tmax, Tmin, Tmean
IMF 2	SPEI, rain, non-linear trend , $SPEI_{t-1}$ & $SPEI_{t-2}$, Tmax, Tmin, Tmean	SPEI, rain, non-linear trend , $SPEI_{t-1}$ & $SPEI_{t-2}$, Tmax, Tmin, Tmean	SPEI, rain, non-linear trend , $SPEI_{t-1}$ & $SPEI_{t-2}$, Tmax, Tmin, Tmean
IMF 3	Non-linear trend	Non-linear trend	Non-linear trend
IMF 4	Non-linear trend	Non-linear trend	Non-linear trend
IMF 5	Non-linear trend	Non-linear trend , $SPEI_{t-1}$	Non-linear trend , $SPEI_{t-1}$
IMF 6	Non-linear trend , $SPEI_{t-1}$	Non-linear trend , $SPEI_{t-1}$	Non-linear trend , $SPEI_{t-1}$
IMF 7	Non-linear trend , $SPEI_{t-1}$ & $SPEI_{t-2}$	Non-linear trend , $SPEI_{t-1}$ & $SPEI_{t-2}$	Non-linear trend , $SPEI_{t-1}$
Residual	Non-linear trend , $SPEI_{t-1}$ & $SPEI_{t-2}$	Non-linear trend , $SPEI_{t-1}$ & $SPEI_{t-2}$	Non-linear trend , $SPEI_{t-1}$ & $SPEI_{t-2}$, SPEI

6.4.3 SPEI prediction

The full range of data from 1986 to 2016 for all variables that appeared in the variable of importance (see Table 6.4) was divided into 2 parts for training and testing the prediction models. For SPEI 1, data from Sep. 1986 to Jul. 2006 was used for training while Aug. 2006 to Sep. 2016 was used for the testing exercise. Data from Feb. 1987 to Jan. 2007 was used to train and Feb. 2007 to Sep. 2016, data was used to test SPEI 6 models. The highest timescale considered in this study (i.e. SPEI 12) training data period ranged from Aug. 1987 to May 2007 and the testing data were between June 2007 and Sep. 2016. Seven potential statistical and machine learning-based models were applied for this study and are shown in Table 6.4. These were applied for SPEI at all time scales and each decomposed IMF was predicted separately. To improve the prediction ability of GAM models, auto-correlated SARIMA errors were used. Quantile regression averaging of the prediction results from GAM and LSTM is fQRA-GAM and fQRA-LSTM respectively as can be seen from Table 6.5. prediction combination, which is the mean of all the applied models, was conducted to improve prediction accuracy.

Table 6.5: Potential drought prediction models.

Model	Description
1	GAM
2	EEMD-GAM
3	EEMD-ARIMA-GAM
4	fQRA-GAM
5	LSTM
6	EEMD-LSTM
7	fQRA-LSTM

6.4.3.1 Results of statistical models

To understand the prediction performance of statistical models, a comparative study was conducted between the four applied models. Figure 6.8 shows the results of models for all timescales considered in this study. The smoothing effect of the GAM models is evident in the predicted results. The GAM provides a flexible specification of response by defining the model in terms of smooth functions as a replacement for the detailed parametric relationships on the covariates (Ravindra *et al.*, 2019). The decomposition of environmental time series is expected to improve the prediction accuracy of models, and this is evident at all timescales that the decomposed GAM performed better than an undecomposed GAM. Although EEMD-GAM predicted SPEI better than GAM, from Figure 6.8A EEMD-GAM is seen to overestimate drought events between 2011 and 2016, with GAM greatly underestimating the target values while EEMD-ARIMA-GAM (i.e. GAM after correcting residual autocorrelation) improved the prediction. Since prediction models are imperfect abstracts of reality (UNESCO, 2005), such behaviour in model outputs is therefore expected as often the models are not perfect. Sigauke *et al*. (2018) found that incorporating corrected residual autocorrelation increased model accuracy and improved the out of sample forecasts. At longer timescales, all GAM based models showed a great improvement in the prediction of SPEI in the LRC.

Figure 6.9 is the scatterplot of the different models based on statistical learning at all the timescales considered in this study. All the models' results show that a positive correlation exists between the modeled output and the actual data. The GAM, EEMD-GAM, and EEMD-ARIMA-GAM predicted results showed the lowest correlation at 1-, 6- and 12- month timescales respectively. The fQRA(GAM) showed the highest correlations at 1- and 6- month timescales while for the 12- month, GAM showed the highest correlation. The high correlation showed by fQRA(GAM) is due to that fQRA is made up of a mean combination of all the models, therefore, all the models' strength results in fQRA being superior compared to the other models applied in this study.

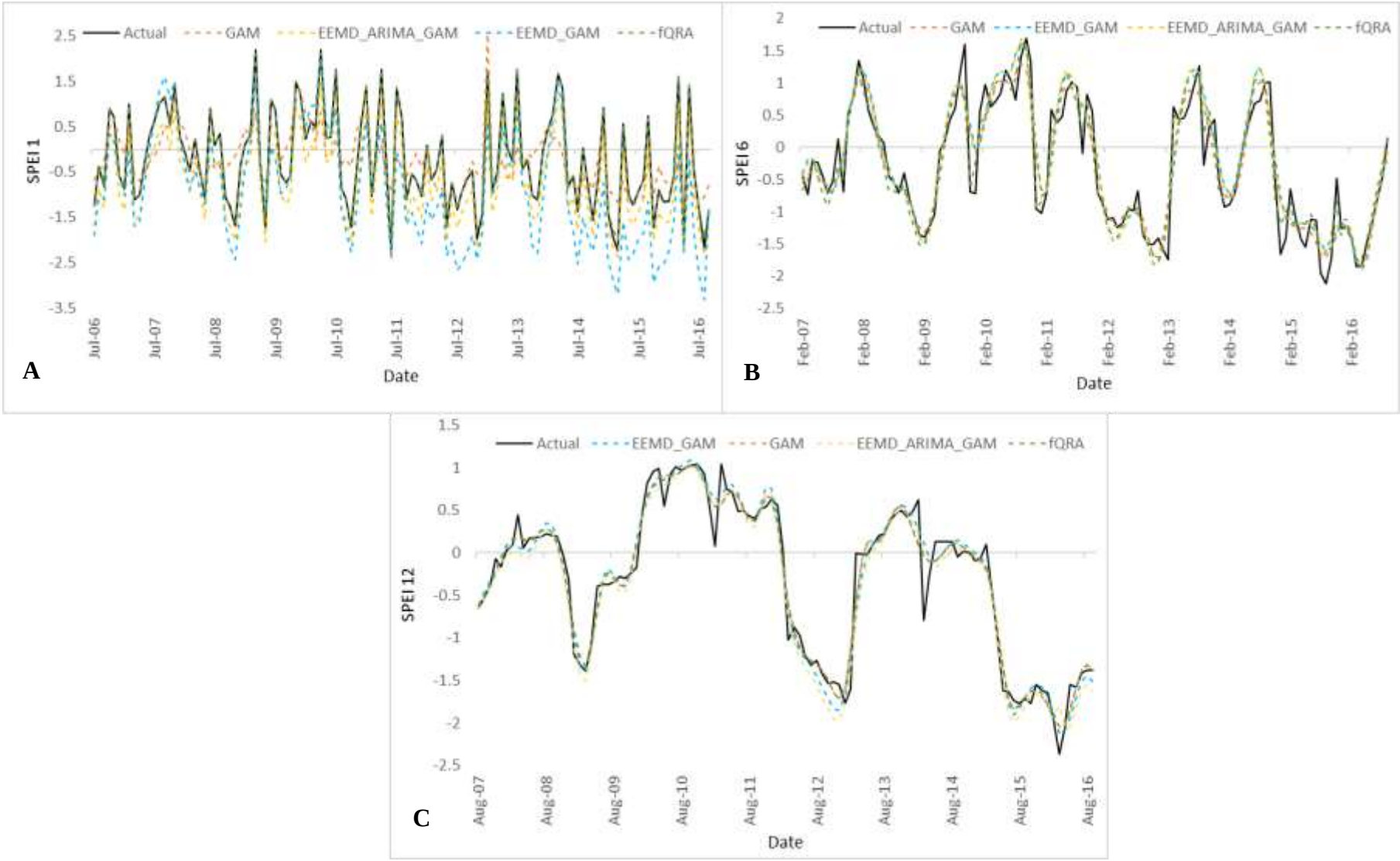

Figure 6.8: GAM prediction models results for SPEI 1-, 6- and 12- month timescales.

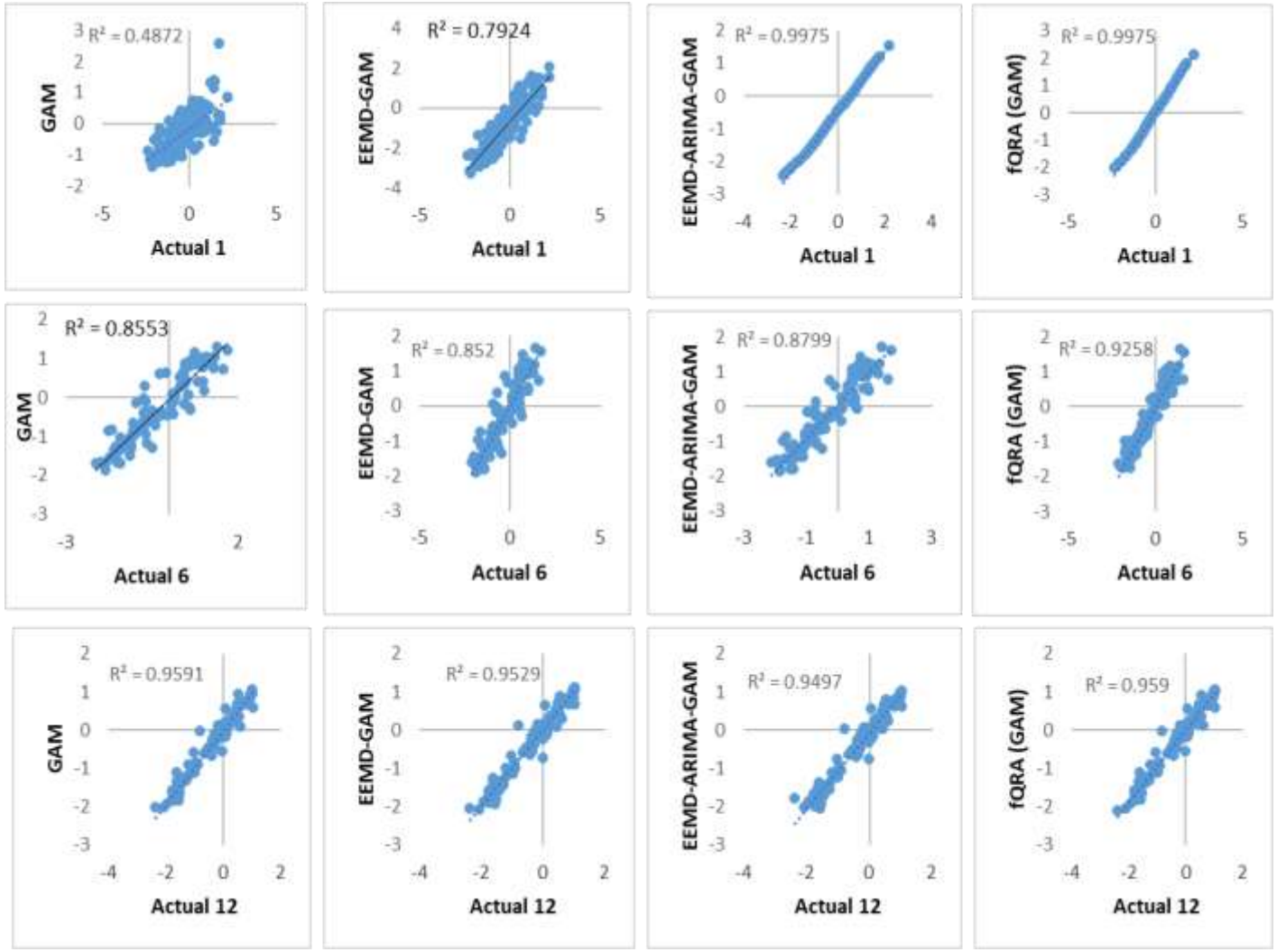

Figure 6.9: Scatterplot of the GAM, EEMD-GAM, EEMD-ARIMA-GAM, and fQRA (GAM) models vs SPEI target values.

6.4.3.2 SPEI prediction using machine learning

Figure 6.10 shows drought prediction models' results based on deep learning neural networks (LSTM) at all timescales of study. All models seemed to follow the actual test data, however, EEMD-LSTM is seen in certain cases to overestimate or underestimate the actual test data at all timescales. The decomposition of environmental time series and prediction combination is expected to improve the prediction accuracy of models, however, for deep learning neural networks that is not the case. An undecomposed LSTM mimicked the test data better than the decomposed LSTM while the prediction quantile regression averaging results performed better than the decomposed LSTM. This is because LSTM-fQRA combines the prediction strength of the deep learning LSTM and the reduced complexity of the time series through decomposition. The results obtained in this study differ from those obtained by Zhang *et al*. (2018) regarding the prediction ability of EEMD-LSTM and LSTM. The study by Zhang *et al*. (2018) found that the hybrid EEMD-LSTM outperformed the LSTM model while the current study found that for predicting SPEI at 1-, 6- and 12- month timescales, LSTM performed better than EEMD-LSTM. The type and number of input variables used during the calibration stage may influence the differing results.

Figure 6.11 is the scatterplot of the different models based on machine learning at all timescales. Like statistical learning, all the models' results show that a positive correlation relationship exists between the modeled output and the actual data. The EEMD-LSTM showed the lowest correlation relationship with the actual data at 1-, 6- and 12- month timescales while the fQRA-LSTM and LSTM showed the highest correlation at the same timescales. Both the LSTM and fQRA-LSTM found an R^2 of 0.9997 at 1- month timescale and 0.9996 for both 6- and 12- month timescales. The fitted line of the predicted results is close to the 45° line to the horizontal and this indicates a probable high performance of a model. A correlation cannot, however, be the single determinant of the prediction model accuracy. The use of R and R^2 should not be utilised alone to measure the accuracy of predictive models for numerical data as they can present biased, insufficient, or misleading results (Murphy and Epstien, 1989; Kessler and Neas, 1994; Legates and McCabe, 1999; Li and Heap, 2008). Therefore, further analysis of model performance was conducted using statistical evaluation metrics.

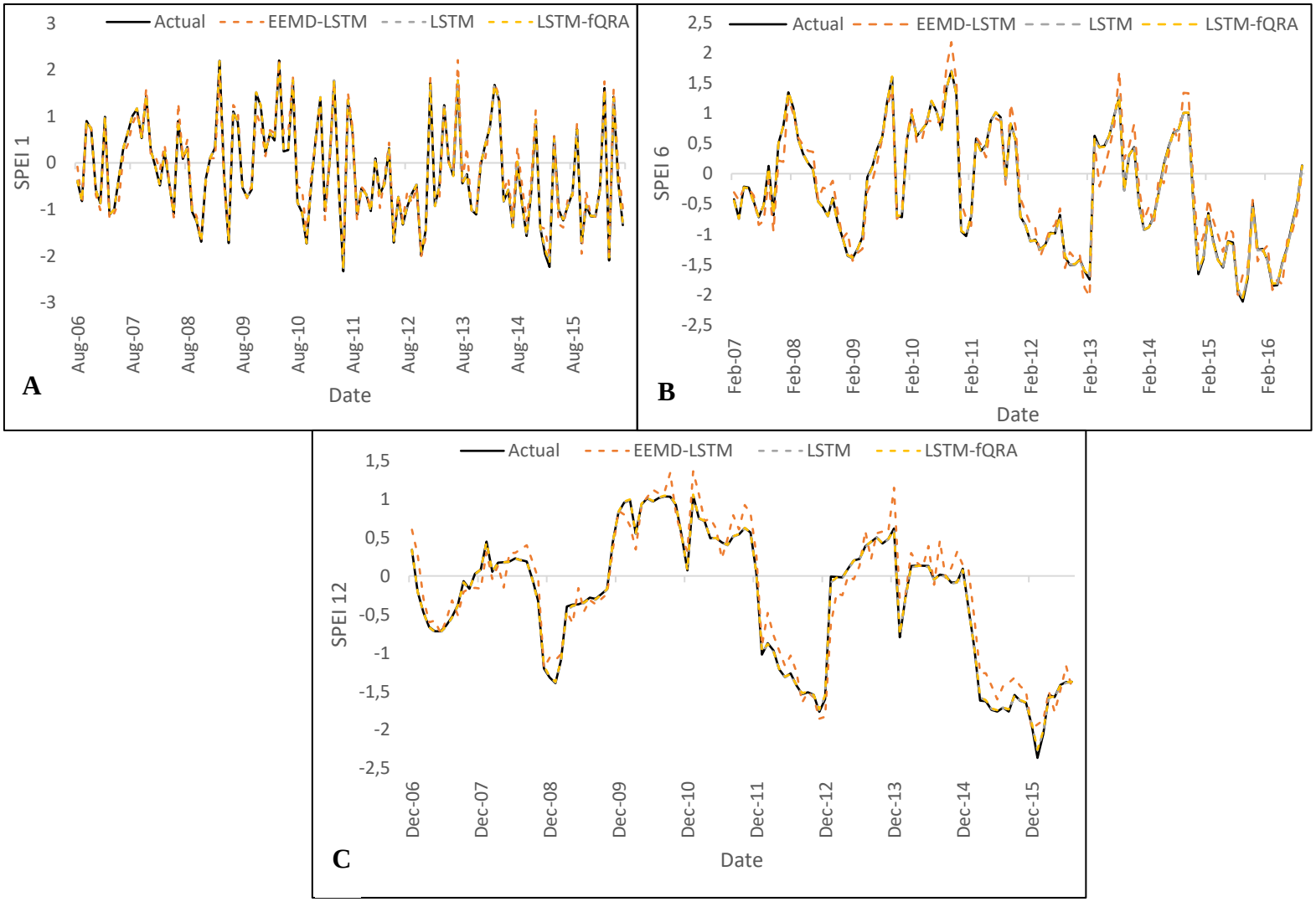

Figure 6.10: LSTM drought prediction model results for SPEI 1-, 6- and 12- timescales.

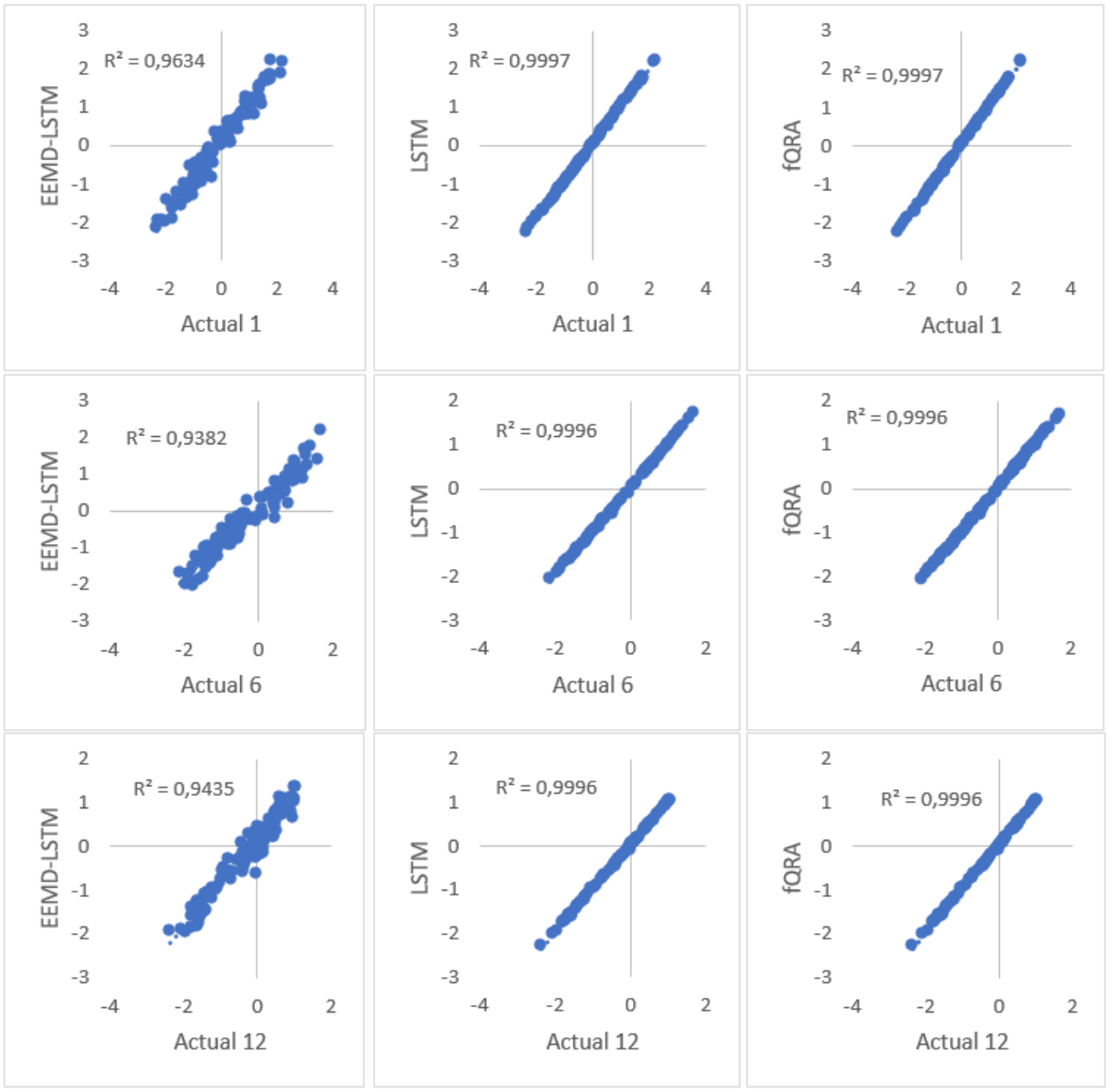

Figure 6.11: Scatterplot of the LSTM, EEMD-LSTM and fQRA (LSTM) models vs SPEI.

6.4.4 Model performance comparative analysis

As there is no consensus on the most appropriate metric for model error performance, Chai and Draxler (2014) recommended a combination of evaluation metrics. Therefore, the prediction performance of both statistical learning (GAM) and machine learning (LSTM) models in this study were further conducted using five statistical evaluations (i.e. ME, RMSE, MAE, MPE, and MAPE) to measure the models' performance. The evaluation of both statistical and machine learning SPEI time series outputs at 1-, 6- and 12- months timescales are shown in Table 6.6. At 1- month timescale, machine learning outperformed statistical learning techniques. From Table 6.6 the smallest RMSE for statistical learning was found to be fQRA-GAM model as 0.0599 while machine learning was an fQRA-LSTM with an RMSE of 0.0199.

This, therefore, showed that at 1- month timescale, machine learning was the best performing learning technique. The ME, MAE, MAPE, MPE further support the RMSE findings between the applied models' results. It is shown in Table 6.6 that the better performing model showed the least errors showed by all the performance measures. Every statistical measure condenses a large number of data into a single value; it only provides one projection of the model errors emphasizing a certain aspect of the error characteristics of the model performance (Chai and Draxler, 2014). Figure 6.11 shows the models that indicated the least errors in the model performance for both GAM and LSTM based models at SPEI 1-, 6- and 12- month timescales. At all timescales, LSTM based models outperformed GAM based models. It is evident from both Table 6.6 and Figure 6.12 that the prediction combinations (fQRA) improved model performance of both statistical and machine learning at all timescales while the decomposition was useful in improving GAM performance as this was not in the case for LSTM based models.

Table 6.6: Performance evaluation of the applied models.

Learning technique	Timescale	Model	ME	RMSE	MAE	MPE	MAPE
Statistical Learning	1	GAM	0.0177	0.7676	0.6127	-3.8647	231.728
		EEMD-GAM	0.6805	0.8829	0.7410	-47.4685	275.233
		EEMD-ARIMA-GAM	0.4718	0.481	0.4718	-135.946	280.609
		fQRA (GAM)	-0.0116	0.0599	0.03369	11.971	17.099
	6	GAM	-0.0016	0.3644	0.2694	19.774	57.438
		EEMD-GAM	-0.0563	0.3818	0.2833	13.330	57.293
		EEMD-ARIMA-GAM	-0.0599	0.3449	0.2595	10.227	51.763
		fQRA (GAM)	0.0030	0.2609	0.2057	8.053	37.699
	12	GAM	0.0021	0.1809	0.1199	-63.013	123.075
		EEMD-GAM	0.0067	0.1978	0.1373	-128.169	181.563
		EEMD-ARIMA-GAM	0.0851	0.2221	0.162	-77.719	183.636
		fQRA (GAM)	0.0032	0.1811	0.1194	-67.49	127.262
Machine learning	1	LSTM	-0.0135	0.0135	0.0165	1.1088	4.9365
		EEMD-LSTM	-0.0540	0.2085	0.1627	14.0429	60.5617
		fQRA (LSTM)	-0.0029	0.0199	0.0112	-2.2083	3.691
	6	LSTM	0.0082	0.0203	0.0150	-0.2712	3.4515
		EEMD-LSTM	-0.0465	0.2430	0.2037	6.7900	40.0487
		fQRA (LSTM)	-8.79e-5	0.0190	0.0126	-0.0722	2.3933
	12	LSTM	0.0049	0.0186	0.0127	-1.3798	20.8003
		EEMD-LSTM	-0.0809	0.2235	0.1812	-81.3093	188.065
		fQRA (LSTM)	-0.0026	0.0184	0.0105	-4.4569	12.3226

*__ARIMA__-Auto Regressive Moving Average, __EEMD__-Ensemble Empirical Mode Decomposition, __GAM__-Generalised Additive Models, __LSTM__-Long Short Term Memory, __fQRA__-prediction Quantile Regression Averaging.

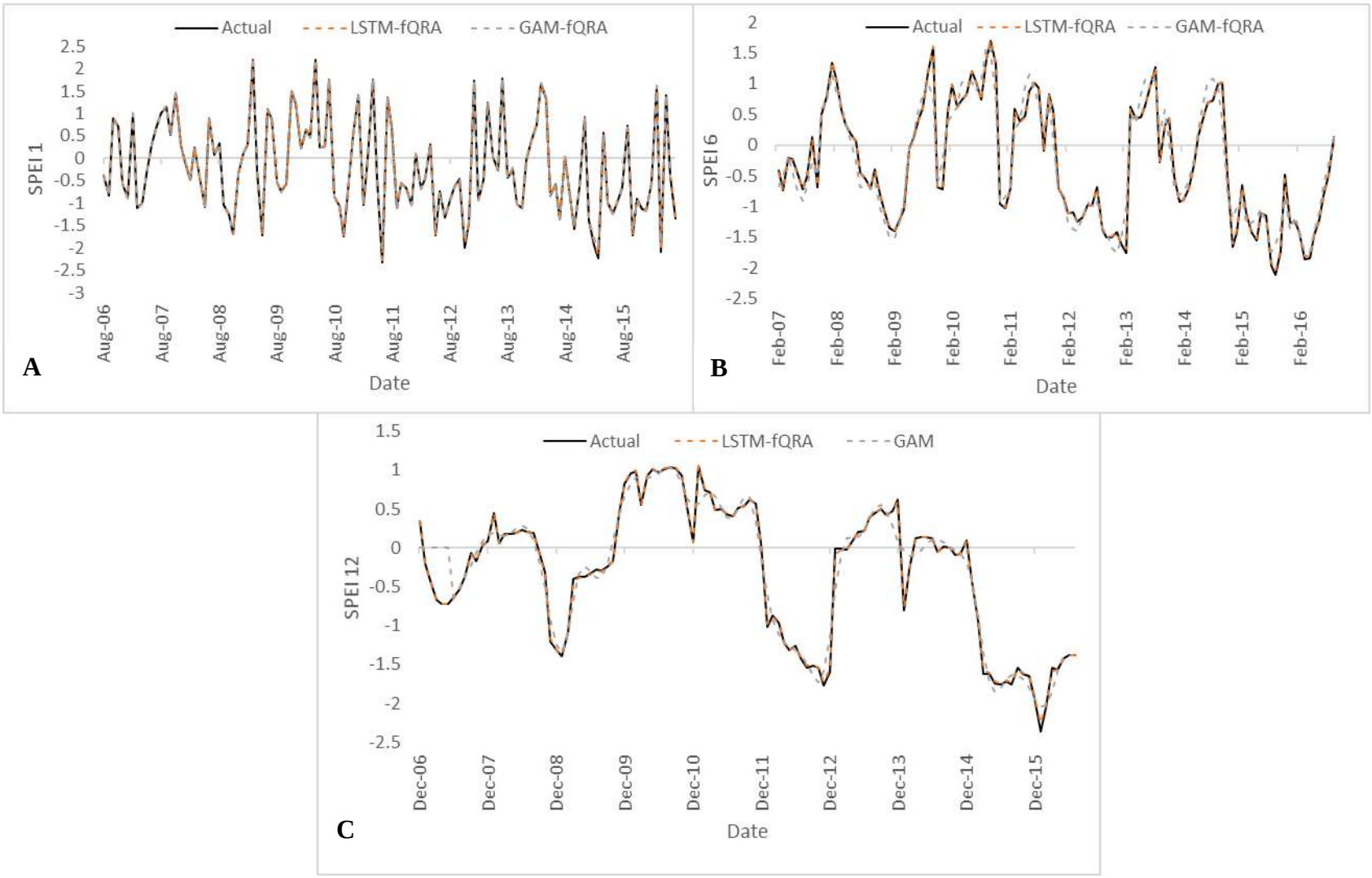

Figure 6.12: Best performing GAM and LSTM models at SPEI 1-, 6- and 12- month timescales.

The density plots from the best performing statistical (GAM) and machine learning (LSTM) techniques models superimposed with actual SPEI data at all timescales are presented in Figure 6.13. The LSTM models plot showed the best fit of the densities at all timescales while the GAM densities were fairly good at all timescales. Table 6.7 shows the pinball loss scores for the best GAM and LSTM for all timescales. Since the pinball loss score for LSTM-fQRA is smaller than that of GAM-fQRA, LSTM-fQRA is a better model. This was realised in all the timescales, with SPEI 1- GAM showing to be the best compared to the other GAM timescales. For the case of LSTM, SPEI 12- showed the least pinball loss score followed by SPEI 1- and 6- month timescales. Pinball loss provides a comprehensive score for probabilistic prediction performance and is consistent with the objective function of quantile regression instead of focusing on a single aspect (Wang *et al*., 2016). The same study further showed that pinball scores were reduced by an average of 4.39% through probabilistic prediction ensembles.

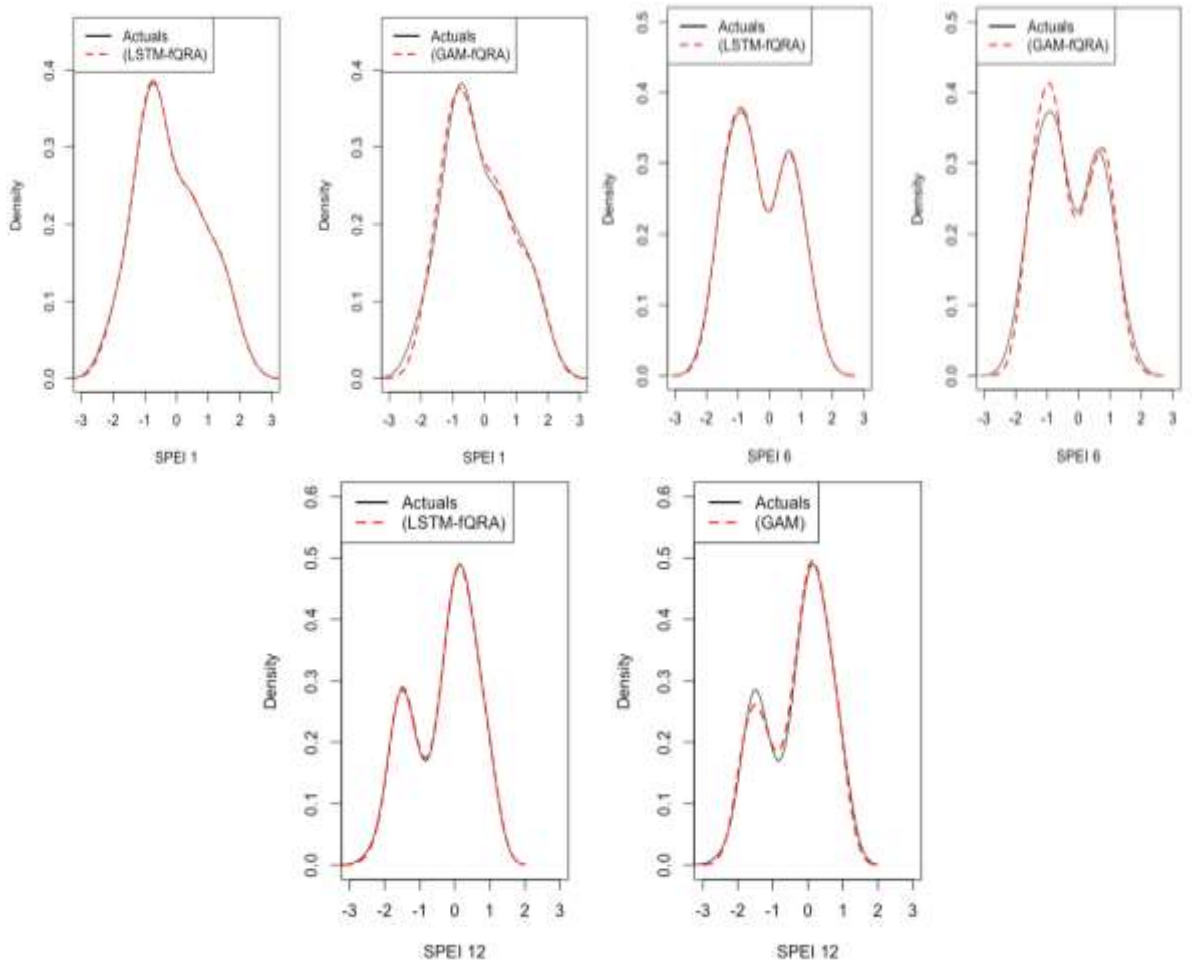

Figure 6.13: Best performing GAM and LSTM models' density at SPEI 1-, 6- and 12- month timescales.

Table 6.7: Best performing models pinball loss scores.

Index timescale	LSTM pinball loss	GAM pinball loss
SPEI 1	0.00561523	0.0161798
SPEI 6	0.006276735	0.1028351
SPEI 12	0.005472007	0.05992876

6.4.5 Evaluation of model uncertainty

Uncertainty analysis in this study was only carried out for the best performing statistical (GAM) and machine learning (LSTM) models. This was achieved by constructing an empirical prediction interval (PI) at all timescales. The prediction intervals were used to find the Prediction Interval Widths (PIWs), Prediction Interval Normalised Widths (PINAWs), Prediction Interval Coverage Probability (PICP) and determined the number of prediction below and above the PI for each best performing GAM and LSTM model. The lower and the upper intervals are shown in Figure 6.14 for the best performing GAM and LSTM based model at 1-, 6- and 12- month timescale.

The summary statistics of PIWs for the best performing GAM, LSTM, and Mean* models for Prediction Interval Nominal Confident (PINC) values of 95% are shown in Table 6.8. The Mean* are the endpoints interval averages; these are simple and robust in combination point prediction (Gaba *et al*., 2017). The skewness at 1- and 6- month timescales are to the right in all the models (positive skewness) while the 12- month timescale is showing left skew with all models reporting a negative skewness. The LSTM at 12- month timescale showed the smallest standard deviation, which is indicative of a narrower model. Therefore, at both 1- and 6- month timescales, GAM model is narrower compared to the Mean* and LSTM.

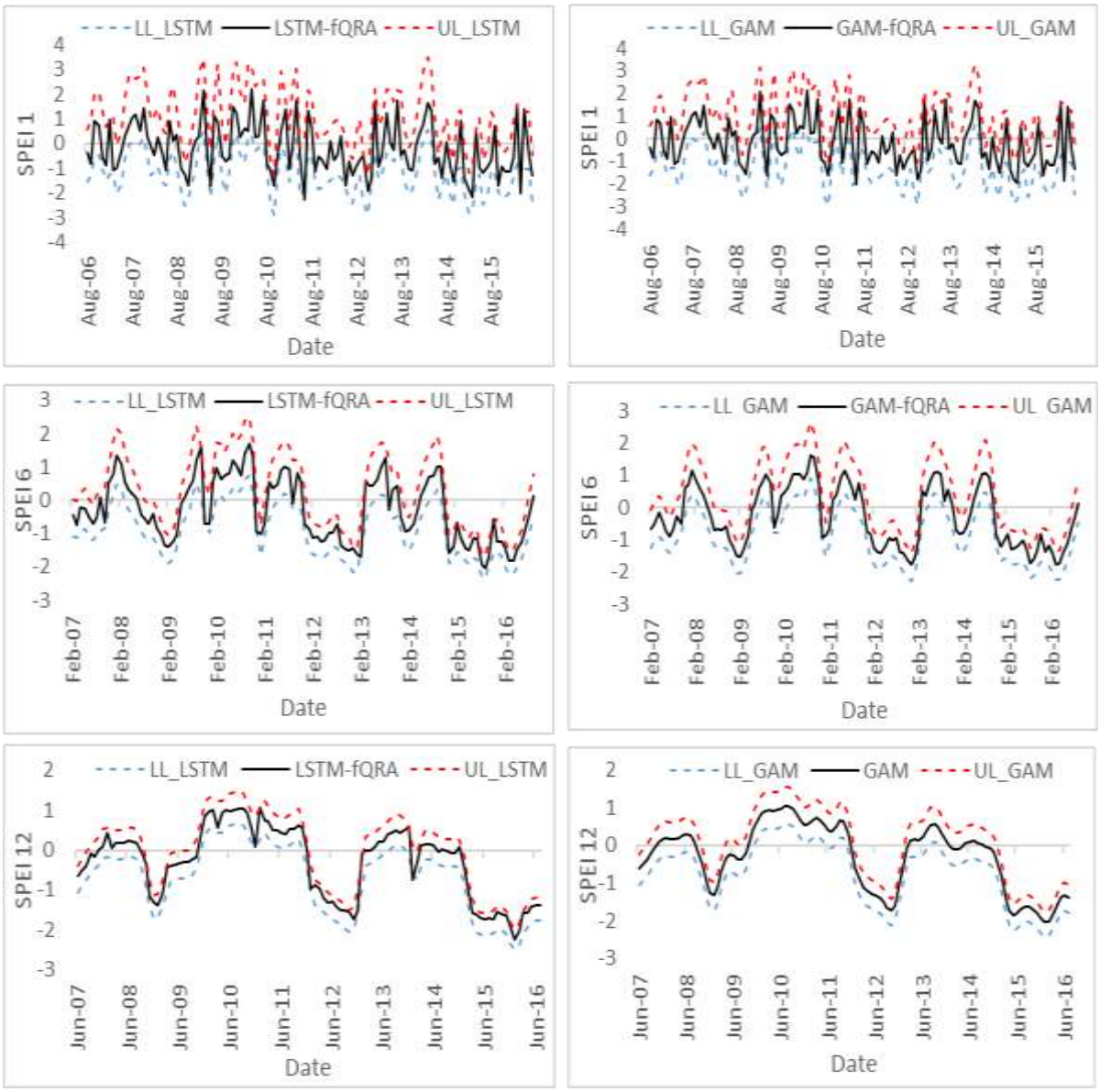

Figure 6.14: SPEI 1-, 6- and 12- month timescales 95% prediction limits.

Table 6.8: Models PIWs statistics.

		Mean	Median	Min.	Max.	SD	Skew.	Kurt.
SPEI 1	GAM	2.254	2.237	1.868	2.662	0.196	0.123	-0.810
	LSTM	2.278	2.257	1.614	2.953	0.329	0.188	-0.762
	Mean*	2.266	2.247	1.741	2.808	0.263	0.120	-0.781
SPEI 6	GAM	1.260	1.219	0.890	1.721	0.224	0.179	-1.263
	LSTM	1.194	1.167	0.664	1.320	0.297	0.091	-1.208
	Mean*	1.227	1.196	0.795	1.734	0.259	0.122	-1.263
SPEI 12	GAM	0.851	0.875	0.675	0.986	0.088	-0.448	-1.047
	LSTM	0.692	0.715	0.530	0.814	0.079	-0.413	-1.011
	Mean*	0.771	0.795	0.603	0.900	0.083	-0.433	-0.104

Mean* - Combination interval prediction, SD – Standard deviation

A comparative evaluation of all models (i.e. GAM, LSTM, and Mean* limits) using PI indices for PINC value of 95% is shown in Table 6.9. The LSTM-fQRA showed a valid PICP at 1-month timescale, GAM-fQRA showed a valid PICP at 6- month timescale while at 12- month timescale; no valid PICP was obtained since all the models had the same value. It should be noted that, although the PICP was not valid at a 90% confidence level, the difference was not greater than 1.8%. Khosravi *et al*. (2010) accepted metamodel PICP close to a 90% confidence level. At 1- and 12- month timescales, LSTM-fQRA has the smallest PINAW while Mean* showed the same at 6- month timescale. The performance of LSTM-fQRA seems to be best in conducting drought prediction compared to the other models. It is the only model that had a PICP of exactly 95% at 1- month timescale and a reasonable variation at 6- and 12- month timescales. The model further showed the lowest PINAW at two timescales (i.e. 6- and 12-month). The smaller the PINAW, the better the detecting ability it can reach, as a result, a smaller PINAW and a larger PICP are desirable in constructing a PI (Pang *et al*., 2018).

Table 6.9: Comparative evaluation of models using prediction interval indices.

Index timescale		LSTM-fQRA	GAM- fQRA	Mean*
1	PICP	0.950	0.942	0.942
	Mean* PIW	2.28	2.25	2.266
	PINAW	1.65	2.75	2.054
6	PICP	0.94	0.948	0.966
	Mean* PIW	1.19	1.26	1.227
	PINAW	1.82	1.52	1.307
12	PICP	0.936	0.936	0.936
	Mean* PIW	0.69	0.85	0.771
	PINAW	2.44	2.74	2.592

6.5 Implications of the study findings

Due to the impacts of a changing climate, extreme events have been shown to increase in both frequency and magnitude. Extremes have also been reported in the Limpopo River Basin of southern Africa within which the study area is located (Alemaw and Kileshye-Onema, 2014). Further, drought trends analysis in this study has shown that drought is increasing and becoming more intense in the LRC. When considering the difference between precipitation and evaporation as a function of global temperature changes, the subtropics generally display an overall trend towards drying (IPCC, 2018). Increased temperatures are likely to impact surface water resources negatively, such that reduction in the availability of water resources at 2°C of global warming is projected to be greater than 1.5°C (IPCC, 2018). Apart from the natural

factors, anthropogenic factors such as exponential population growth also play a significant role in pressure exerted on water resources at the catchment level.

Hydrological extremes such as drought impact negatively on economies, the environment, biodiversity, water resources, and communities and their livelihoods. Droughts, more so when they occur in series, significantly erode poor people's assets and further undermine their livelihoods in terms of labour productivity, housing, infrastructure, and social networks (Olsson *et al*., 2014). Although studies such as Stagge *et al*. (2015) have correlated drought events to drought impacts, Haro-Monteagudo *et al*. (2017) indicated that this only provides insight once a drought event has passed. Drought prediction is therefore a significant practice, as the correlation between the prediction and potential impacts can be drawn. This study applied seven specialised drought prediction models. These models demonstrated their potential to forecast future drought conditions in a semi-arid LRC. The prediction tools were formulated based on drought indices time series (i.e. SPEI), therefore, these tools have the potential not to only predict drought but also flood events. This is because the SPEI time series depicts both periods of water excess and deficit in the environment. This, therefore, makes these prediction tools versatile and increases their usefulness in hydrological extremes prediction as they have the capability of predicting intense drought and extreme floods.

The two best performing models after uncertainty analysis can be incorporated into already existing Early Warning Systems (EWS) programmes from SAWS and DWS for drought risk reduction. Drought risk assesses the impacts on human activities, economy, and environmental systems intending to identify appropriate strategies to mitigate potential impacts (Jenkins, 2013). The EWS anticipate the effects that drought may have on a system to trigger necessary mitigation measures (Rossi *et al*., 2008). Therefore, by incorporating LSTM-fQRA and GAM-fQRA as prediction tools in drought EWS in the LRC and catchments with similar characteristics to those of the LRC, is likely to improve the reliability of these EWS since the prediction tools were subjected to uncertainty analysis. These improved EWS have the potential to aid in reducing the impact of climate extremes on communities and the catchments economy.

The EWS plays a significant role in ensuring equitable water allocation during periods of drought induces water deficit. When water authorities (i.e. national, provincial, local water manager) are knowledgeable of a probable drought event in the coming rainfall season, they

are better placed at triggering management strategies that are in line with the available water resources. The abstractions of water from the Luvuvhu River for agricultural purposes, for instance, must be closely monitored during drought periods together with the management of the major reservoirs in the catchment (i.e. Albasini, Nandoni, and Vondo dams). Proper management of these important water resources is only possible if the authorities are aware of what is likely to come in the next season. Although applied for semi-arid environments, these tools are applicable in arid and humid environments. This, however, would require a determination of features of importance, since drought development is affected by different features in different areas. The prediction tools presented in this study are tailored for the LRC and will add into existing decision support tools such as GCM based models for operational seasonal forecasts generated by the South African Weather Service and other climate centres.

6.6 Chapter summary

This chapter presented drought prediction models as applied in this study. The two learning approaches used were statistical (GAM) and machine learning (LSTM). As indicated in Chapter 5, only the highest scoring index was considered in drought prediction. SPEI scored the highest and was found to be the best index to assess drought in the LRC. Seven models were applied based on SPEI time series at 1-, 6- and 12- month timescales. Due to the complexity of the environmental time series, this study conducted a time series decomposition to reduce the complexities and improve prediction accuracy. Variable selection was conducted to determine their important influence in the SPEI time series. It was found that rainfall, non-linear trend, and lags 1 & 2 time-series were most important in predicting an SPEI time-series, and this was realised across all the timescales. The training and testing period varied between the timescales. All model predictions were combined to improve drought prediction accuracy. The R^2 was used to determine a correlative relationship between the target and predicted values while five statistical measures were used to determine the model performance. At 1- and 6-month timescales, the prediction combination showed to be the best GAM model while for the case of LSTM the same was realised in all timescales. The study also found that the correlation between target values and LSTM and LSTM-fQRA was the same at 0.9997 at 1- month and 0.9996 at 6- and 12- month timescales. Further statistical evaluations showed that LSTM-fQRA was the better model compared to an undecomposed LSTM (i.e. RMSE of 0.0199 for LSTM-fQRA over 0.0241 for LSTM). The best performing GAM and LSTM based models were used to conduct uncertainty analysis, which was based on the prediction interval. The PICP and

PINAW results indicated that LSTM-fQRA was the best model to predict the SPEI time series at all timescales.

7 THESIS CONCLUSIONS AND RECOMMENDATIONS

Conclusions, Limitations, and Recommendation of the study

7.1 Conclusion

This study aimed to apply drought prediction models based on statistical and machine learning techniques using a semi-arid catchment in north-eastern South Africa as a case study. The LRC was selected for its significant role as an economic hub of Limpopo Province since the Levubu valley is one of the largest agricultural producers in the country. To achieve the main objective, this study formulated three specific objectives that were based on drought assessment, characterisation of historical drought events & evaluation of drought indices, and then applied hybrid models based on statistical and machine learning techniques to predict drought.

For the case of drought assessment, all the indices detected major historical drought events that have been reported in the study area, although the precipitation based indices were the only ones that categorised the 1991/92 drought as extreme at 6- and 12- month timescales in two stations while the streamflow index and NADI underestimated the event. The indices further showed that the most prevalent drought event in the LRC was mild drought. Extreme drought events were the least showed at 6.42%, 1.08%, 1.56%, and 4.4% for SPI, SPEI, SSI, and NADI respectively. Considering the MK trend test, the standardised indices detected a negative trend that showed that drought severity increased in the study area throughout the study period while NADI showed a positive upward trend which depicts a decreased drought severity throughout the study period. There was therefore a need to further characterise the drought events in terms of magnitude, duration, frequency, and severity as detected by these indices to get a better understating of their performance in detecting and assessing drought conditions in the study area. The study found that there was no distinct pattern of spatial variability of drought events in the study area, and this may have been influenced by the density of stations that were concentrated in the upper reaches of the catchment.

Drought characterisation was based on drought duration, intensity, frequency, magnitude, and severity. An increased drought duration was observed between 1986 - 1996 while the shortest duration was observed between 1996 - 2006 followed by 2006 - 2016. SPI showed the highest severity followed by SPEI, NADI, and then the SSI. The study found that lower drought severity corresponded to much-reduced drought intensity and this was realised in all timescales.

Further, drought intensity was shown to increase with an increasing timescale (i.e. 1- month timescale showed an average severity for SSI at -7.29 while the 12- month showed the same as -16.62). The relationship between drought severity and duration revealed a strong linear relationship across all indices at all timescales. Drought indices were evaluated for their strength in detecting hydrological drought and suitability for drought assessment in the LRC. Making use of the decision criteria, indices were evaluated. According to the raw scores of each of the five criteria SPEI ranked the highest with a total weight score of 129, SSI scored 122, and then the SPI with a score of 106, and lastly the NADI with a score of 76. Since SPEI ranked the highest of all the four indices evaluated, it was regarded as the best index to assess and characterise historical drought conditions on the LRC.

A total of seven models were applied based on SPEI time-series at 1-, 6- and 12- month timescales. Because of the complexity of the environmental time series, this study conducted a time series decomposition to reduce the complexities and improve prediction accuracy. Variable selection was conducted to determine their important influence in the SPEI time series. It was found that rainfall, non-linear trend and lags one and two of the SPEI time series were more important in predicting an SPEI time-series and this was realised across all the timescales. The training and testing period varied between the timescales since the length differed respectively. Predictions from the different learning approaches were combined to further improve drought prediction accuracy. The R^2 was used to determine a correlative relationship between the target and predicted values while five statistical measures were used to determine the model performance. At 1- and 6- month timescales, the prediction combination was shown to be the best GAM model while for the case of LSTM the former was found in all timescales. The study also found that the correlation between target values and LSTM and LSTM-fQRA predicted values were the same at 0.9997 at 1- month and 0.9996 at 6- and 12- month timescales. Further statistical evaluations showed that LSTM-fQRA was the better model compared to an undecomposed LSTM (i.e. RMSE of 0.0199 for LSTM-fQRA over 0.0241 for LSTM). Only the best performing GAM and LSTM based models were used to conduct uncertainty analysis, which was based on the prediction intervals. The PICP and PINAW results indicated that LSTM-fQRA was the best model to predict SPEI time-series at all timescales. This, therefore, indicates that deep learning neural network models are better in predicting drought in environments characterised by semi-arid conditions. The models can be incorporated into early warning systems for drought risk reduction.

The study hypothesised that a multivariate index (NADI) was better in drought assessment and characterisation compared to univariate indices. Considering the evaluation criteria, NADI scored the lowest with a weight of 76 while SPEI scored 126. Therefore, the study rejected the null hypothesis thereby accepting the alternative hypothesis based on the index evaluation results. The second hypothesis was that drought severity increases with an increase in the timescale. The second hypothesis was found to be true and therefore the study rejected the alternative hypothesis. This was further found to correlate with what has been reported in the literature. This study further hypothesised that hybrid models are more effective in predicting drought conditions compared to individual models. This study found that hybrid models performed better at 1- and 6- month timescales for statistical learning while machine learning showed the same for all timescales. For the case of statistical learning, at 12- month timescale, the null hypothesis was rejected for GAM based models since hybrid models outperformed a single GAM. However, for machine learning, LSTM rejected the alternative hypothesis at all timescales. The overall conclusion is that hybrid models are better for drought prediction given that the majority of the timescales based on both statistical and machine learning rejected the alternative hypothesis.

7.2 Limitations of the study and Recommendations

Based on the findings of this study, some limitations were realised and recommendations for further studies and operations were suggested. The first major limitation of the study was in the formulation of NADI. Long-term soil moisture data is one of the input variables required for formulating the index and this is not readily available in South Africa. This study, therefore, used Giovanni satellite-based MERRA-2 model data as a soil moisture proxy to formulate NADI. Satellite-based data have their inherent limitations in capturing the accuracy of variables such as soil moisture in this case. This study, therefore, recommends that there be continuous monitoring of soil moisture in South Africa to enable an effective assessment of drought at all components of the hydrological cycle. This should be available in an open access repository to enable access by academics, researchers, students, and agricultural practitioners, and any other interested stakeholders.

Weather stations with quality rainfall and temperature data are clustered in the upper reaches of the LRC, with the lower reaches having major inconsistent gaps while some stations were no longer operational. The quality of streamflow data for the majority of the catchment was

found to be also poor and inconsistent. Although there are not many economic activities in the lower reaches of the catchment, there is a need to monitor environmental changes as this gives an overall picture of the catchment health. This study, therefore, recommends the refurbishment of the non-operating stations and the establishment of new stations in the middle and lower reaches of the catchment. This will enable researchers and planners to get a better spatial and temporal variability of drought conditions in the catchment. Further to the latter, this will enable a better impact assessment study and for the planning of resource allocations during drought events.

Studies of hydrological extremes characterisation (i.e. frequency, spatial extent, and severity) have been well documented in the literature, however, a detailed analysis of compound extremes (occurrence of multiple events with extreme impacts) of drought can yield useful data that can be used together in early warning systems of drought. This study, therefore, recommends such studies in semi-arid catchments of developing nations to manage drought risk. Although LSTM had been compared to RNN in other areas of studies including environmental time series, such has not been done for a drought time series specifically. This study recommends that this be done also for a drought time series in future studies. The predicted outputs of deep learning techniques should also be compared against the current systems used to predict drought at national and provincial levels in South Africa. Dynamic models should also be used in conjunction with machine learning techniques to predict drought conditions in future studies. The level of uncertainty for the best performing GAM and LSTM based models was achieved using prediction interval indices (i.e. PICP, PIW, and PINAW) in this study. A robust uncertainty analysis using a bootstrapping procedure is therefore recommended for further studies. This should be compared to the findings from prediction interval indices. Future research can further assess drought conditions making use of extreme value theory via the copula approach. While making use of downscaled hydro-meteorological variables, operational forecasts using LSTM-fQRA (the best performing model in non-operational forecasting) can be achieved. This was not the scope of the current study; however, such a study has the potential to yield reliable results on future drought conditions based on deep learning neural networks. This can also translate into better future water management in the catchment during drought periods.

REFERENCES

Abad, M. B. J., Zade, A. H., Rohina, A., Delbalkish, H. and Mohagher, S. S. (2013) The effect of climate change on flow regime in Basher river using two meteorological and hydrological standards. *International Journal of Agriculture and Crop Sciences*, **5**, pp.2852-2857.

Abadan, S. and Shabri, A. (2014) Hybrid empirical mode decomposition-Arima for forecasting price of rice. *Applied Mathematical Sciences*, **8(63)**, pp.3133–3143.

Abramowitz, M. and Stegun, I.A. (Eds) (1965) Handbook of Mathematical functions. New York: Dover-USA.

Adamowski, J. and Sun, K. (2010) Development of a coupled wavelet transform and neural network method for flow forecasting of non-perennial rivers in semi-arid watersheds. *J. Hydrol*., **390**, pp.85-91. DOI: 10.1016/j.jhydrol.2010.06.033.

Adhyani, N.L., June, T and Sopaheluwakan, A. (2017) Exposure to Drought: Duration, Severity and Intensity (Java, Bali and Nusa Tenggara), IOP *Conf. Ser.: Earth Environ. Sci*. **58** 012040.

Alexander, L.V., Zhang, X., Peterson, T.C., et al. (2006) Global observed changes in daily climate extremes of temperature and precipitation. *J. Geophys. Res*., **111**, D05109. http://dx.doi.org/10.1029/ 2005JD006290.

Alemaw, B.F. and Kileshye-Onema, J.M. (2014) Evaluation of drought regimes and impacts in the Limpopo basin, *HESSD*,**11**, dio:10.5184/hessd-11-199–222.

Allen, K.J., Ogden, J., Buckley, B.M., Cook, E.R. and Baker, P.J. (2011) The potential to reconstruct broadscale climate indices associated with southeast Australian drought from Athrotaxis species, Tasmania. *Clim. Dyn*. **37,** pp.1799-1821.

Alley, W.M., 1984. The Palmer drought severity index: limitations and assumptions. *Journal of Climate and Applied Meteorology*, **23**, pp.1100–1109.

Altman, D.G. and Bland, J.M. (1995) Statistics notes: the normal distribution. Bmj.; **310(6975)**, pp.298.

Amiri, G.G. and Asadi, A. (2009) Comparison of different methods of wavelet and wavelet packet transform in processing ground motion records. *Int. J. Civil Eng*., **7**, pp.248-257.

Association for Rural Advancement (AFRA) **(**1993) Drought relief and rural communities. Special Rep. No. 9. Pietermaritzburg, South Africa.

Awass, A.A. (2009). Hydrological drought analysis-occurrence, severity and risks, the case of Wabi Shebele River Basin, Ethiopia. *PhD thesis,* Universität Siegen.

Bacanli, U. G., Firat, M. and Dikbas, F. (2008) Adaptive neuronfuzzy inference system for drought forecasting. Stochastic Environ. *Res. Risk Assess*., **23**, pp.1143–1154.

Barnston, A. G., 1992: Correspondence among the correlation, RMSE, and Heidke forecast verification measures: Refinement of the Heidke score. *Wea. Forecasting*, **7**, pp.699-709.

Barua, S., Ng, A. W. M. & Perera, B. J. C. (2012) Drought assessment and forecasting: A case study on the Yarra River catchment in Victoria, Australia", Australian Journal of Water Resources, **15(2)**, pp. 95-108, http://dx.doi.org/10.7158/W10848.2012.15.2.

Barua, S. (2010) Drought assessment and forecasting using a nonlinear aggregated drought index. *PhD thesis*, Victoria University, Australia.

Baudoin, M.A., Vogel, C., Nortje, K. and Naik, M. (2017) Living with drought in South Africa: lessons learnt from the recent El Niño drought period. *Int. J. Disaster Risk Reduction,* **23** pp.128–137. https://doi.org/10.1016/j.ijdrr.2017.05.005.

Begueria, S., Vicente-Serrano, S.M., Reig, F. and Latorre, B. (2013) Standardized precipitation evapotranspiration index (SPEI) revisited: parameter fitting, evapotranspiration models, tools, datasets and drought monitoring. *Int. J. Climatol.* **34**, pp.3001-3023.

Belayneh, A. and Adamowski, J. (2013) Drought forecasting using new machine learning methods, *Journal of Water and Land Development,* 18(I-IV), pp.3-12.

Benkachcha, S., Benhra, J. and El-Hassani, H. (2015) Seasonal Time Series Forecasting Models based on Artificial Neural Network, *International Journal of Computer Applications*, **116(20),** pp.0975 – 8887.

Benson, C and Edward J. Clay. 1998. 'The impact of drought on Sub-Saharan African economies: a preliminary examination'. *World Bank Technical Paper 401*. Washington, D.C.: World Bank.

Berger, A., Yin, Q., Nifenecker, H. and Poitou, J. (2017) Slow-down of global surface air temperature increase and acceleration of ice melting, *Earth's Future*, **5**, pp.811–822, doi:10.1002/2017EF000554

Bezdan, J., Bezdan, A., Blagojevic, B., Mesaroš, M., Pejic, B., Vraneševic, M., Pavic, D. and -Đoric, E.N. (2019) SPEI-Based Approach to Agricultural Drought Monitoring in Vojvodina Region, *Water*, **11**, pp.1481.

Biggs, R., Bohensky, E., Desanker, P.V., Fabricius, C., Lynam, T., Misselhorn, A.A., Musvoto, C., Mutale, M., Reyers, B., Scholes, R.J., Shikongo, S. and van Jaarsveld, A.S. (2004) Nature supporting people: The Southern African Millennium Ecosystem Assessment, Council for Scientific and Industrial Research (CSIR), Pretoria, South Africa, pp.58.

Botai, C.M., Botai, J.O., Dlamini, L.C., Zwane, N.S and Phaduli, E. (2016). Characteristics of Droughts in South Africa: A Case Study of Free State and North West Provinces, *Water*.

Brown, J. D. (1997) Statistics corner: Questions and answers about language testing statistics: Skewness and kurtosis. Shiken 1 (1), pp.20-23. Available online at www.jalt.org/test/bro_1.htm. [16 Aug. 1997].

Bouktif, S., Fiaz, A., Ouni, A. and Serhani, M.A. (2018) Optimal deep learning LSTM for electric load forecasting using features selection and genetic algorithm: Comparison with machine learning approaches, *Energies* **2018**, *11*(7), 1636; https://doi.org/10.3390/en11071636.

Chai1, T and Draxler, R. R. (2014) Root mean square error (RMSE) or mean absolute error (MAE)? – Arguments against avoiding RMSE in the literature. Geosci. Model Dev., **7**, pp.1247–1250. doi:10.5194/gmd-7-1247-2014.

Chai, T., Kim, H.-C., Lee, P., Tong, D., Pan, L., Tang, Y., Huang, J., McQueen, J., Tsidulko, M., and Stajner, I. (2013) Evaluation of the United States National Air Quality Forecast Capability experimental real-time predictions in 2010 using Air Quality System ozone and NO2 measurements, *Geosci. Model Dev.*, **6**, pp.1831–1850, doi:10.5194/gmd-6-1831-2013.

Chatfield, C. (2003). The analysis time series, an introduction, Chapman and Hall press, USA.

Chen, S-M., Lu, W-X, Wang, H. and Kang Z. (2014). Using Wavelet analyses to determine drought characteristics: A case study of Western Jilin Province, China. *Res. J. Appl. Sci. Eng. and Tech.*, **8(5)**, pp.578-584.

Cheng, M., Xu, Q., Lv, J., Liu, W., Li, Q. and Wang, J. (2016) MS-LSTM: A multi-scale LSTM model for BGP anomaly detection. In Proceedings of the 2016 IEEE 24th International Conference on the Network Protocols (ICNP), Singapore, pp.1–6.

Chikobvu, D. and Sigauke, C. (2012) Regression-SARIMA modelling of daily peak electricity demand in South Africa, *Journal of Energy in Southern Africa*, **23(3)**, pp.23-30. ISSN1021-447X.

Chikoore, H. (2016) Drought in southern Africa: structure, characteristics and impacts, Unpublished PhD thesis submitted to the University of Zululand, pp.203.

Cook, B.I., Mann, M.E., D'Odorico,P. and Smith,T.M. (2004) Statistical simulation of the NAO on European winter surface temperatures: applications to phenological modeling. J. Geophys. Res., **109**, pp.16106, doi:10.1029/2003JD004305.

Coughlin, K. T., and K. K. Tung (2004), 11-year solar cycle in the stratosphere extracted by the empirical mode decomposition method. *Adv. Space Res.*, **34**, pp.323–329.

Crochemore, L., Ramos, M. H., Pappenberger, F. and Perrin, C. (2017) Seasonal streamflow forecasting by conditioning climatology with precipitation indices. *Hydrology and Earth System Sciences*, **21(3)**, 1573–1591. https://doi.org/10.5194/hess-21-1573-2017.

Cunnane, C. (1989). "Statistical distributions for flood frequency analysis." Operational Hydrol. Rep. No.33, WMO-No. 718, World Meteorological Organization, Geneva, Switzerland.

Cutore, P., Di Mauro G. and Cancelliere, A. (2009) Forecasting Palmer Index using neural networks and climatic indexes. *Journal of Hydrologic Engineering*, **14(6)**, pp.588–595.

Dahmen, E.R., Hall, M.J. and International Institute for Land Reclamation and Improvement. (1990) Screening of hydrological data: tests for stationarity and relative consistency Wageningen, Netherlands.

Dai, A., K. E. Trenbert, and T. Qian (2004), A global dataset of Palmer Drought Severity Index for 1870–2002: Relationship with soil moistureand effects of surface warming, J. Hydrometeorol., **5(6)**, pp.1117–1130, doi:10.1175/JHM-386.1.

Dalezios, N.R., Loukas, A., Vasiliades, L. and Liakopoulos, E. (2000) Severity-duration-frequency analysis of droughts and wet periods in Greece. *Hycirol Sci. J.* **45(5)**, pp.751-770.

Dallas, H.F. and Rivers-Moore, N. (2013) Ecological consequences of global climate change for freshwater ecosystems in South Africa. *S Afr J Sci*. **110(5/6)**, pp.11, http://dx.doi.org/10.1590/ sajs.2014/20130274.

Dayal, K., Deo, R., Apan, A.A. (2017) Drought Modelling Based on Artificial Intelligence and Neural Network Algorithms: A Case Study in Queensland, Australia. *Journal of Hydrologic Engineering*, **23(1)**, https://doi.org/10.1061/(ASCE)HE.1943-5584.0001593.

Department of Water Affairs and Forestry [DWAF, (2004)] Luvuvhu/Letaba Water Management Area: Internal Strategic Perspective. DWAF Report No.P WMA 02/000/00/0304.

Department of Water and Sanitation [DWS; (2013)] Monthly Multi-Site Stochastic Streamflow Model: User Guide. Department of Water Affairs, South Africa.

DEAT (Department of Environmental Affairs and Tourism) (2004) *National Climate Change Response Strategy*, viewed 07 April 2011, from http://unfccc.int/files/meetings/ seminar/application/pdf/sem_sup3_south_africa.pdf.

Deser, C., Phillips, A., Bourdette, V. and Teng, T. (2012) Uncertainty in climate change projections: the role of internal Variability. *Clim Dyn.*, **38**, pp.527–546, DOI 10.1007/s00382-010-0977-x.

De Stefano, L., Urquijo, J., Kampragkou, E. and Assimacopoulos, D. (2015) Lessons learnt from the analysis of past drought management practices in selected European regions: experience to guide future policies. *Eur. Water*, **49**, pp.107–117.

Di, C., Yang, X., and Wang, X. (2014) A Four-Stage Hybrid Model for Hydrological Time Series Forecasting. *PLoS One*, **9 (8)**, e104663. http://dx.doi.org/10.1371/journal.pone.0104663.

Donahue, J.; Hendricks, L.A.; Rohrbach, M.; Venugopalan, S.; Guadarrama, S.; Saenko, K.; Darrell, T. (2017) Long-Term Recurrent Convolutional Networks for Visual Recognition and Description. IEEE Trans. *Pattern Anal. Mach. Intell*., **39**, pp.677–691.

DWAF (Department of Water Affairs and Forestry, South Africa) (1994) *Water Supply and Sanitation Policy White Paper. Water – An Indivisible National Asset.* Department of Water Affairs and Forestry, Pretoria.

DWA (Department of Water Affairs, South Africa) (2004) Directorate: National Water Resource Planning. Internal strategic perspective Luvuvhu/Letaba Water Management Areas. Department of Water Affairs, Pretoria, Report No. PWMA 01/000/00/0304.

Durdu, O.F. (2010) Application of Linear Stochastic Models For Drought Forecasting in The Buyuk Menderes River Basin, Western Turkey, *Stochastic Environmental Research and Risk Assessment*, doi:10.1007/s00477-010-0366-3.

D'Arrigo, R., and R. Wilson (2008), El Ni~no and Indian ocean influences on Indonesian drought: Implications for forecasting rainfall and crop productivity, *Int. J. Climatol*., **28(5)**, pp.611–616, doi:10.1002/joc.

Edosaa, D.C., Woyessa, Y.E. and Welderufael, W.A., 2016. Spatiotemporal analysis of drought using self-calibrating Palmer Drought Severity Index in the central region of South Africa. *Theor App Climato.* **126,** pp.643-657.

Edwards, D. C., and McKee, T. B. (1997) Characteristics of 20th century drought in the United States at multiple time scales. Climatology Report Number 97-2, Department of Atmospheric Science, Colorado State University, Fort Collins.

El-Jabi, N., Turkkan, N. and Caissie, D. (2013) Regional climate index for floods and drought using Canadian Climate Model (CGCM3.1), *American Journal of Climate Change*, **2**, pp.106-115, doi:10.4236/ajcc.2013.22011.

Emergency Event Database; EM-DAT. (2010) Global "number killed" and "number affected" by drought between 1900–2009. Brussels, Belgium: Université Catholique de Louvain.

Engelbrecht, F.A., McGregor, J.L. and Engelbrecht, C.J. (2009) Dynamics of the Conformal-Cubic Atmospheric Model projected climate-change signal over southern Africa. *Int. J. Climatol*., **29**, pp.1013-1033. doi:10.1002/joc.1742

Entekhabi, D., Rodriguez-Iturbe, I. and Castelli, F. (1996) Mutual interaction of soil moisture state and atmospheric processes. *J. of Hydrology*, **184 (1996)**, pp.3-17.

Engelbrecht, F., Adegoke, J., Bopape, M.J., Naidoo, M., Garland, R., Thatcher, M., McGregor, J., Katzfey, J., Werner, M., Ichoku, C. and Getebe, C. (2015) Projections of rapidly rising surface temperatures over Africa under low mitigation. *Environ. Res. Lett.*, **10(8)** 085004. https://doi. org/10.1088/1748-9326/10/8/085004.

Engelbrecht, F.A., McGregor, J.L. and Engelbrecht, C.J. (2009) Dynamics of the Conformal-Cubic Atmospheric Model projected climate-change signal over southern Africa. *Int. J. Climatol*., **29**, pp.1013-1033. doi:10.1002/joc.1742.

Fallah, S.N., Deo, R.C., Shojafar, M., Conti, M. and Shamshirband, S. (2018) Computational Intelligence Approaches for Energy Load Forecasting in Smart Energy Management Grids: State of the Art, Future Challenges, and Research Directions, *Energies*, **11**, pp.596; doi:10.3390/en11030596.

Farahmand, A. and AghaKouchak, A. (2015) A generalized framework for deriving nonparametric standardized drought indicators. *Advances in Water Resources*, 76(2015), 140-145. http://dx.doi.org/10.1016/j.advwatres.2014.11.012

Fausett, L. (1994) Fundamentals of neural networks: architectures, algorithms, and applications, Prentice-Hall, Inc. Upper Saddle River, New Jersey, USA.

Fessant, F. and Midenet, S. (2002) Self-Organising Map for Data Imputation and Correction in Surveys. *Neural Comput & Applic*., **10**, 300–310.

Feyen, L. and Dankers, R. (2009) Impact of global warming on streamflow drought in Europe. *Journal of Geophysical Research*, **114**, pp.17, doi: 10.1029/2008jd011438.

Field, A. (2009) Discovering statistics using SPSS. 3rd ed. London: SAGE publications Ltd. pp. 822.

Fleig, A. K., Tallaksen, L. M., Hisdal, H. and Demuth, S. (2006) A global evaluation of streamflow drought characteristics. *Hydrology and Earth System Sciences*, **10**, pp.535–552, doi: 0.5194/hess-10-535-2006.

Folguera, L., Zupan, J., Cicerone, D. and Magallanes, J.F. (2014) Self-organizing maps for imputation of missing data in incomplete data matrices. *Chemometrics and Intelligent Laboratory Systems*, **143**, 146–151, https://doi.org/10.1016/j.chemolab.2015.03.002.

FAO (2004) Drought impact mitigation and prevention in the Limpopo River Basin: A situation analysis, Food and Agricultural Organisation, Rome, Italy, pp.160.

Foster, G. and Rahmstorf, S. (2011) Global temperature evolution 1979–2010, *Environ. Res. Lett*., **6 (2011)**, pp.8.

Fuchs B, Svoboda M, Nothwehr J, Poulsen C, Sorensen W, Guttman N. (2012) A New National Drought Risk Atlas for the U.S. from the National Drought Mitigation Center. http://www.clivar.org/sites/default/files/Fuchs.pdf.

Friedman, J.H. (2002) Stochastic Gradient Boosting. *Computational Statistics and Data Analysis*, **28**, pp.367–78. doi:10.1016/S0167-9473(01)00065-2.

Gaba A., Tsetlin, I. and Winkler, R.L. (2017). Combining interval forecasts. *Decision Analysis*, **14(1)**, pp.1-20.

Gao, B.C. (1996) NDWI—A Normalized Difference Water Index for Remote Sensing of Vegetation Liquid Water from Space. *Remote Sensing of Environment*, **58**, pp.257-266.

Gebre, S.L. and Getahan, Y.S. (2016) Analysis of climate variability and drought frequency events on Limpopo River Basin, South Africa, *Hydrol.Current.Res*. **7:3**, DOI:10.4172/2157-7587.1000249.

Gilles, J. (2013) Empirical Wavelet Transform. *IEEE Transactions on Signal Processing*. **61(16)**, pp.3999-4010. doi 10.1109/TSP.2013.2265222

Glaser, A.N. (2000) High Yield Biostatistics. 1st Ed. New Delhi, India: Lippincott Williams and Wilkins.

Gokhale, M.Y. and Khanduja, D.K. (2010) Time domain signal analysis using wavelet packet decomposition approach. *Int. J. Commun. Netw. Syst. Sci*., **3**, pp.321-329. DOI:10.4236/ijcns.2010.33041.

Gommes R. (2006), Non-parametric crop yeild forecasting. A didactic case study for Zimbabwe. In remote sensing support to crop yeild forecast and area estimates. ISPRS Archives XXXVI-8/W48 Workshop proceedings, pp.79-84.

Goude, Y., Nedellec, R. and Kong, N. (2014) Local short and middle term electricity load forecasting with semi-parametric additive models. IEEE Transactions on Smart Grid, **5(1)**, pp.440- 446.

Gringorten, I. (1963) A Plotting Rule for Extreme Probability Paper. *Journal of Geophysical Research*. **68**, pp.813-814. 10.1029/JZ068i003p00813.

Gu, Y., Brown, J.F., Verdin, J.P. and Wardlow, B. (2007) A five-year analysis of MODIS NDVI and NDWI for grassland drought assessment over the central Great Plains of the United States. *Geophys. Res. Lett*., **34**, L06407, doi:10.1029/2006GL029127.

Guttman, N. B., 1991: A sensitivity analysis of the Palmer Hydrologic Drought Index. *Water Resour. Bull.*, **27**, pp.797–807.

Guttman, N. B. J. R. Wallis, and J. R. M. Hosking, 1992: Spatial comparability of the Palmer Drought Severity Index. *Water Resour. Bull.*, **28**, pp.1111–1119.

Hao, Z., Xia, Y., Luo, L., Singh, V. P., Ouyang, W., and Hao, F. (2017) Toward a categorical drought prediction system based on U.S. Drought Monitor (USDM) and climate forecast. *Journal of Hydrology*, **551**, pp.300–305. https://doi.org/10.1016/j.jhydrol.2017.06.005

Hao, Z., Hao, F., Singh, V. P., Ouyang, W., and Cheng, H. (2017) An integrated package for drought monitoring, prediction and analysis to aid drought modeling and assessment. *Environmental Modelling and Software*, **91**, pp.199–209. https://doi.org/10.1016/j.envsoft.2017.02.008.

Hao, Z., Hao, F., and Singh, V.P. (2016) A general framework for the multivariate multi-index drought prediction based on multivariate ensemble streamflow predictions (ESP). *Journal of Hydrology*, **539**, pp.1 –10. https://doi.org/10.1016/j.jhydrol.2016.04.074.

Hao, Z., AghaKouchak, A., Nakhjiri, N., and Farahmand, A. (2014) Global integrated drought monitoring and prediction system. *Scientific Data*, **1**, 140001. https://doi.org/10.1038/sdata.2014.1.

Haque, M., Rahman, A., Hagare, D. and Chowdhury, R.K. (2018) A Comparative Assessment of Variable Selection Methods in Urban Water Demand Forecasting, *Water*, **10**, pp.419, doi:10.3390/w10040419.

Hargreaves, G.H. and Samani, Z.A. (1985) Reference crop evapotranspiration from temperature. *Appl. Eng. Agric.*, **1**, pp.96-99

Haro-Monteagudo, D., Solera, A. and Joaquin, A. (2017) Drought early warning based on optimal risk for forecast in regulated river systems: Application to the Jucar River Basin (Spain). *Journal of Hydrology*, **544**, pp.36-45.

Hastie, T. and Tibshirani, R. (1986) Generalized additive models (with discussion). *Statist. Sci.*, **1**, pp.297–318.

Hastie, T. and Tibshirani, R. (1990) Generalized Additive Models. London: Chapman and Hall.

Hawker, D. (2015) South Africa crisis map: What we need to know, e.TV News Channel (ENCA) news article, South Africa, https://www.enca.com/south-africa/sa-water-crisis-map-what-you-need-know. (Accessed on 26/10/2016).

Hawkins, E. and Sutton, R. (2011) The potential to narrow uncertainty in projections of regional precipitation change. *Clim Dyn.*, **37**, pp.407. https://doi.org/10.1007/s00382-010-0810-6.

Hayes, M., Svoboda, M., Wall. N. and Widhalm, M. (2010) The Lincoln declaration on drought indices: universal meteorological drought index recommended. *Bull Am Meteorol Soc*, **92**, 485–488. doi:10.1175/2010BAMS3103.1.

Hayes, M.J. (2003) Drought indices, National Drought Mitigation Center, University of Nebraska-Lincoln [http://www.drought.unl.edu/whatis/indices.htm#spi], (accessed February 24, 2009).

Heddinghaus, T. R., and P. Sabol (1991), A review of the Palmer Drought Severity Index and where do we go from here? paper presented at 7th Conference on Applied Climatology, American Meteorological Society, Boston, Mass.

Heim Jr., R. (2002) A review of twentieth-century drought indices used in the United States, *Bulletin of the American Meteorological Society*, **83**, pp.1149–1165.

Hisdal, H., Tallaksen, L. M., Clausen, B., Peters, E., and Gustard, A. (2004) Hydrological Drought Characteristics, chap. 5, pp.139–198, in: Hydrological drought: processes and estimation methods for streamflow and groundwater, Developments in water science; **48**, edited by Tallaksen, L. M., and Van Lanen, H. A. J., Elsevier Science B.V., Amsterdam, the Netherlands.

Hu, Y., Li, F., Li, H. and Liu, C. (2017) An enhanced empirical wavelet transform for noisy and non-stationary signal processing. *Digital Signal Processing*, **60(2017)**, pp.220-229. http://dx.doi.org/10.1016/j.dsp.2016.09.012.

Huang, J. S. M., Wood, A., Schubert, S., Peters-Lidard, C., Wood, E., Pulwarty, R. and Barrie, D. (2016) Research to advance national drought monitoring and prediction capabilities, NOAA Interagency Drought Task Force. NOAA/Modeling Analysis Predictions and Projections (pp. 29).

Huang, Y., F.G. Schmitt, Z. Lu and Y. Liu, (2009). Analysis of daily river flow fluctuations using empirical mode decomposition and arbitrary order Hilbert spectral analysis. *J. Hydrol*., **373**, pp.103-111. DOI: 10.1016/j.jhydrol.2009.04.015.

Huang, N. E., and Z. Wu (2008), A review on Hilbert-Huang transform: Method and its applications to geophysical studies. *Rev. Geophys*., **46**, RG2006, doi:10.1029/2007RG000228.

Huang, N.E., Wu, M.L.C., Long, S.R., Shen, S.S., Qu, W., Gloersen, P. and Fan, K.L. (2003) A confidence limit for the empirical mode decomposition and Hilbert spectral analysis. No. 2037, *Proceedings of the Royal Society of London A: Mathematical, Physical and Engineering Sciences*, pp. 2317-2345

Huang, N. E., Shen, Z. and Long, S.R. (1998) The empirical mode decomposition and the Hilbert spectrum for nonlinear and non-stationary time series analysis. *Proceedings of the Royal Society of London, Series A*, **454, pp.**903-995.

Humphrey, G.B., Gibbs, M.S., Dandy, G.C. and Maier, H.R. (2016) A hybrid approach to monthly streamflow forecasting: Integrating hydrological model outputs into a Bayesian artificial neural network. *Journal of Hydrology*, **540**, 623–640. https://doi.org/10.1016/j.jhydrol.2016.06.026.

Hyndman, R.J. and Athanasopoulos, G. (2018) Forecasting: Principles and practice, (2nd ed.), OTexts.

Hochreiter, S. and Schmidhuber, J. (1997) Long Short-Term Memory. *Neural Computation* **9(8)**, pp.1735-1780.

IPCC (2018) Global Warming of 1.5°C. An IPCC Special Report on the impacts of global warming of 1.5°C above pre-industrial levels and related global greenhouse gas emission pathways, in the context of strengthening the global response to the threat of climate change, sustainable development, and efforts to eradicate poverty [Masson-Delmotte, V., P. Zhai, H.-O. Pörtner, D. Roberts, J. Skea, P.R. Shukla, A. Pirani, W. Moufouma-Okia, C. Péan, R. Pidcock, S. Connors, J.B.R. Matthews, Y. Chen, X. Zhou, M.I. Gomis, E. Lonnoy, T. Maycock, M. Tignor, and T. Waterfield (eds.)].

Inbar M. (2007) Importance of drought information in monitoring and assessing land degradation, In Sivakumar M.V.K. and Ndiangui N. (ed.), Climate and Land Degradation, Springer, 253-266.

Intergovernmental Panel on Climate Change (IPCC), (2013) Intergovernmental Panel on Climate Change (IPCC) Climate change 2013: the physical science basis, T.F. Stocker, D. Qin, G.-K. Plattner, M. Tignor, S.K. Allen, J. Boschung, A. Nauels, Y. Xia, V. Bex, P.M. Midgley (Eds.), Contribution of Working Group I to the Fifth Assessment Report of the Intergovernmental Panel on Climate Change, Cambridge University Press, Cambridge, United Kingdom and New York, NY, USA (2013).

Intergovernmental Panel on Climate Change (IPCC: 2007) Climate variability 2007-synthesis Report. Contribution of working Groups, I, II and III The 4th assessment report of the intergovernmental panel on climate variability, Pachauri, R. K. and Resinger, A. Eds, IPCC Secretariat, Geneva.

Jahangir, A.T.M., Sayedur, R.M. and Saadat, A.H.M. (2013) *International Journal of Geomatics and Geosciences*, **3(3)**, pp.511-524.

Jenkins, K. (2013) Indirect economic losses of drought under future projections of climate change: A case study for Spain. *Nat. Hazard*, **69**, pp.1967-1986.

Kabanda, T. A. (2004). Climatology of long term drought in the northern region of the Limpopo Province of South Africa (*Unpublished PhD thesis*). School of Environmental Sciences, University of Venda, South Africa.

Kagoda, P. A. and Ndiritu, J. G. Celiwe Ntuli, C. and Beason Mwaka, B. (2010) Application of radial basis function neural networks to short-term streamflow forecasting, *Physics and Chemistry of the Earth*, **35 (2010)**, pp.571–581.

Kang, H.M. and Yusof, F. (2012). Application of Self-Organising Map (SOM) in missing daily rainfall data in Malaysia. International Journal of Computer Applications (0975-888), **48(5)**, pp.23-28

Karamouz, M. Rasouli, K. and Nazi, S. (2009). Development of a hybrid index for drought prediction: case study, *Journal of Hydrologic Engineering*, **14(6)**, pp.617-627.

Karl, T. R., and R. R. Heim Jr. (1990), Are droughts becoming more frequent or severe in the United States, *Geophys. Res. Lett.*, **17(11)**, pp.1921–1924, doi:10.1029/GL017i011p01921.

Karl, T.R., and Knight, R.W. (1985) Atlas of monthly Palmer Hydrological Drought Indices (1931–1983) for the contiguous United States, *National Climatic Data Center Historical Climatology Series 3-7*, Asheville, NC, pp.319. [Available from National Climatic Data Center, Federal Building, 151 Patton Ave., Asheville, NC 28801-5001.]

Karl, T.R. (1983) Some spatial characteristics of drought duration in United States. *J.Climate Appl. Meteor*., **22**, pp.1356-1366.

Karl, T. R. (1986) The sensitivity of the Palmer Drought Severity Index and Palmer's Z-Index to their calibration coefficients including potential evapotranspiration, J. Clim. Appl. Meteorol., 25, 77–86, doi:http:// dx.doi.org/10.1175/1520-0450(1986)025<0077:TSOTPD>2.0.CO;2

Karl, T.R., Melillo, J.M. and Peterson, T.C. (2009) Global climate change impacts in the United States. Cambridge Univ. Press, Cambridge, UK.

Karthikeyan and D.N. Kumar, (2013) Predictability of non-stationary time series using wavelet and EMD based ARMA models**.** *Journal of Hydrology*, **502**, pp.103-119.

Kedadouche, M., Thomas, M. and Tahan, A. (2016) A comparative study between Empirical Wavelet Transforms and Empirical Mode Decomposition Methods: Application to bearing defect diagnosis. *Mechanical Systems and Signal Processing*, **81(2016)**, pp.88-107. http://dx.doi.org/10.1016/j.ymssp.2016.02.049.

Kessler E, Neas B (1994) On correlation, with applications to the radar and rain-gauge measurement of rainfall. *Atmospheric Research*, **34**, pp.217–229.

Keyantash, J.A. and Dracup, J.A. (2004) An aggregate drought index: Assessing drought severity based on fluctuations in the hydrologic cycle and surface water storage. *Water Resources Research,* **40**: doi: 10.1029/2003WR002610. issn: 0043-1397.

Khan, Md. M.H., Muhammad, Nur S. and El-Shafie, Ahmed. (2018). Wavelet-ANN versus ANN-Based Model for Hydrometeorological Drought Forecasting. *Water*, **10**, pp.998. 10.3390/w10080998

Khosravi, A., Nahavandi, S. and Creighton, D. A. (2010) prediction interval-based approach to determine optimal structures of neural network metamodels. *Expert Syst*, **37**, pp.2377–2387.

Kiem, A.S. and Austin, E.A. (2013) Drought and the future of rural communities: Opportunities and challenges for climate change adaptation in regional Victoria, Australia. *Global Environmental change,* **23**, pp.1307–1316.

Kim, D.W., Byun, H.R. and Choi, K.S. (2009) Evaluation, modification, and application of the Effective Drought Index to 200Year drought climatology of Seoul, Korea, *J. Hydrol*., **378**, pp.1–12, doi:10.1016/j.jhydrol.2009.08.021.

Kim, T.W. and Valdes, J.B. (2003) Nonlinear model for drought forecasting based on a conjunction of wavelet transforms and neural networks, Journal of Hydrologic Engineering **8(6)**, pp.319-328.

Kingma, D.P. and Ba. J. (2014) Adam: A method for stochastic optimization, In: *arXiv preprint arXiv*, pp.1412.6980.

Kisi, O., Shiri, J. and Nazemi, A.H. (2011) A waveletgenetic programming model for redicting shortterm and long-term air temperatures. *J. Civil Eng. Urbanism*, **1**, pp.25-37.

Kjeldsen, T. R., Lundorf, A. and Rosbjerg, D. (2000) Use of a two-component exponential distribution in partial duration modelling of hydrological droughts in Zimbabwean rivers. *Hydrol. Set J.*, **45(2)**, pp.265-298.

Kohonen, T. (2001) Self-Organizing Maps. Number 30 in Springer Series in Information Sciences. Springer-Verlag, Berlin, 3rd edition.

Kolusu, S.R., Shamsudduha, M., Todd, M.C. Taylor, R.G. Seddon, D., Kashaigili, J.J., Ebrahim, G.Y., Cuthbert, M.O., Sorensen, J.P.R., Villholth, K.G., MacDonald,A.M. and MacLeod, D.A. (2019) The El-Niño event of 2015–2016: climate anomalies and their impact on groundwater resources in East and Southern Africa. *Hydrol. Earth Syst. Sci*., **23**, pp.1751–1762.

Kong, Y., Huang Q., Wang, C., Chen, J.,Chen J. and He, D. (2018) Long Short-Term Memory Neural Networks for Online Disturbance Detection in Satellite Image Time Series, *Remote Sens*., **10**, pp.452; doi:10.3390/rs10030452.

Kramer, M.A. (1991) Nonlinear Principal Component Analysis Using Autoassociative Neural Networks. *AlChE Journal*, **37(2)**, pp.233-243.

Kruger, A.C. and Nxumalo, M.P. (2017) Historical rainfall trends in South Africa: 1921–2015, *Water SA*, **43(2)**.

Kumar, V. and Panu, U. S. (1997) Predictive assessment of severity of agricultural droughts based on agro-climatic factors. *J. Am. Wat. Resour. Assoc.,* **33(6)**, pp.1255-1264.

Kumar, V. & Panu, U. S. (1994) On application of pattern recognition in drought classification. In: *Proc. Annual Coif. of the Canadian Society.*

Kundzewicz ZW, Mata LJ, Arnell NW, Döll P, Kabat P, Jiménez B, et al. Freshwater resources and their management. Climate change impacts, adaptation and vulnerability. Contribution of Working Group II to the Fourth Assessment Report of the Intergovernmental Panel on Climate Change. Cambridge: Cambridge University Press; 2007.

Labat, D. (2010) Cross Wavelet Analyses of Annual Continental Freshwater Discharge and Selected Climate Indices. *Journal of Hydrology*, **385**, pp.269-278. doi.org/10.1016/j.jhydrol.2010.02.029.

Landman, W.A., DeWitt, D., Lee, D.E., Beraki, A. and Lötter, D., (2012) Seasonal rainfall prediction skill over South Africa: one-versus two-tiered forecasting systems. *Weather and Forecasting*, **27(2)**, pp.489-501.

Le, M.H., Perez, G.C., Solomatine, D. and Nguyen, L. B. (2016) Meteorological Drought Forecasting Based on Climate Signals Using Artificial Neural Network–A Case Study in Khanhhoa Province Vietnam. *Procedia Engineering*, **154**, 1169-1175.

Lecun, Y. Bengio, Y. and Hinton, G. (2015) Deep learning, *Nature*, **521**, pp.436–444.

Legates, D.R. and McCabe, G.J. (1999) Evaluating the use of "goodness-of-fit" measures in hydrologic and hydroclimatic model validation, *Water Resources Research,* **35(9),** pp.233–241.

Lenton, T.M., Vasilis Dakos, V., Bathiany, S. and Scheffer, M. (2017) Observed trends in the magnitude and persistence of monthly temperature variability, *Scientific Reports*, **7**: 5940, DOI:10.1038/s41598-017-06382-x.

Levey, K.M. and Jury, M.R. (1996) Composite interseasonal oscillation of convection over southern Africa. *J. Climate*, **9**, pp.1910-1920.

Li J, Heap A (2008) A Review of Spatial Interpolation Methods for Environmental Scientists, *Geoscience Australia*, **23**, pp.137.

Li, W., Hou, M., Chen, H. and Chen, X. (2012) Study on drought trend in south China based on standardized precipitation evapotranspiration index. *J. Nat. Disasters.* **21,** 84–90.

Lin, S. J. (2004) A vertically Lagrangian finite-volume dynamical core for global models. Mon. Wea. Rev., 132, 2293–2307.

Linting, M., Meulman, J.J., Groenen, P.J.F. and van der Kooij, A.J. (2007) Nonlinear principal components analysis: Introduction and application. *Psychological methods,* **12(3)**, pp.336-358. DOI: 10.1037/1082-989X.12.3.336

Liu, W., Cao, S. and Chen, Y. (2016) Seismic time-frequency analysis via Empirical wavelength transform. *IEEE Geosci. And Remote sensing letters*, **13(1)**, pp.28-32.

Liu, Z., Ding, J., Lin, J. and Huang, Y. (2018) A rolling bearing fault diagnosis-optimized scale-space representation for the Empirical Wavelet Transform. *Shock and Vibration*, **2018**, pp.1-22.

Lindesay, J.A. (1988) Southern African rainfall, the Southern Oscillation and a Southern Hemisphere semi-annual cycle. *J.Climatol*, **8**, pp.19-30.

Lohani, V. K. & Lognathan, G. V. (1997) An early warning system for drought management using the Palmer drought severity index. *Nordic Hydro/.,* **29(t)**, pp.21-40.

Lorenzo-Lacruz, J., Vicente-Serrano, S.M., Lopez-Moreno, J.I., Begueria, S., Garcia-Ruiz, J.M. and Cuadrat, J.M. (2010) The impact of droughts and water management on various hydrological systems in the headwaters of the Tagus River (Central Spain). *J. Hydrol*. **386,** pp.13-26.

Loucks, D.P. and Van Beek, E. (2005) Water Resources Systems Planning and Management: An Introduction to Methods, Models and Applications Studies And Reports in Hydrology. Unesco. University of Michigan. ISBN, 9231039989.

Lugina, K.M., Groisman, P.Y., Vinnikov, K.Y., Koknaeva, V.V. and Speranskaya, N.A. (2006) Monthly surface air temperature time series area-averaged over the 30-degree latitudinal belts of the globe, 1881-2005. In *Trends: A Compendium of Data on Global Change*. Carbon Dioxide Information Analysis Center, Oak Ridge National Laboratory, U.S. Department of Energy, Oak Ridge, Tenn., U.S.A. doi: 10.3334/CDIAC/cli.003.

Lukamba (2010) Natural disasters in African countries: what can we learn about them? Journal of Transdisciplinary Research in Southern Africa., **6(2)**, pp.478-495.

Ma W, Sun X, Song Y, Tao F, Feng W, et al. (2013) Applied Mixed Generalized Additive Model to Assess the Effect of Temperature on the Incidence of Bacillary Dysentery and Its Forecast. *PLoS ONE,* **8(4)**: e62122. doi:10.1371/journal.pone.0062122.

Ma, X., Xu, J, Luo, Y., Aggarwal, S. P. and Li, J. (2009). Response of hydrological processes to land-cover and climate variability in Kejie watershed, south-west China, *Journal of Hydrological processes*., **23**, pp.1179-1191.

Maca, P. and Pech, P. (2016) Forecasting SPEI and SPI drought indices using the Integrated Artificial Neural Networks. *Comput. Intell. Neurosc*., 3868519

Maier, A. R., Jain, A., Dandy, G. C. and Sudheer, K. P. (2010). Methods used for development of neural networks for the prediction of water resource variables in river systems: current status and future directions, *J. Environmental modelling*. **25(8)**, pp.891-909.

Maier, H.R. and Dandy, G.C. (2000) Neural networks for the prediction and forecasting of water resources variables: a review of modelling issues and applications. *Environ. Modell. Softw*., **15 (1)**, pp.101–124.

Maity, R. and Kumar, D.N. (2008) Basin-scale stream-flow forecasting using the information of large-scale atmospheric circulation phenomena, *Hydrological Processes*, **22 (5)**, pp.643-650.

Malherbe, J., Engelbrecht, F.A. & Landman, W.A. (2013) Projected changes in tropical cyclone climatology and landfall in the Southwest Indian Ocean region under enhanced anthropogenic forcing. *Clim Dyn*, **40**, pp2867–2886. doi.org/10.1007/s00382-012-1635-2.

Manikandan S. (2011) Measures of central tendency: The mean. *Journal of pharmacology & pharmacotherapeutics*, **2(2)**, 140–142. https://doi.org/10.4103/0976-500X.81920

Mann, H.B. (1945) Non-parametric tests against trend. *Econometrica.*, **13(3)**, pp.245-259.

Maponya, P. and Mpandeli, S. (2012) Impact of drought on food scarcity in Limpopo province, South Africa, *African Journal of Agricultural Research*, **7(37)**, pp.5270-5277.

Marinozzi, A., Martinelli, N., Panascı, M., Cancilleri, F., Franceschetti, E., Vincenzi, B., DiMartino, A. and Denaro, V. (2009) Italian translation of the Manchester-Oxford Foot Questionnaire, with re-assessment of reliability and validity. *Quality of Life Research*, **18**, 923–927.

Masih I., Maskey S., Mussá F.E.F. and Trambauer, P. (2014) A review of droughts on the African continent: a geospatial and long-term perspective. *Hydrol. Earth Syst. Sci*. **18,** pp.3635-3649.

Masupha, T.E, Moeletsi, M.E. and Tsubo, M. (2016) Dry spells assessment with reference to the maize crop in the Luvuvhu River catchment of South Africa. *Phys. Chem. Earth*, Parts A/B/C, **92**, pp.99-111.

Mavhura, E., Manatsa, D. and Mushore, T. (2015) Adaptation to drought in arid and semi-arid environments: case of the Zambezi Valley, Zimbabwe. *Jàmbá: Journal of Disaster Risk Studies*, **7(1)**, pp.7. http:// dx.doi.org/10.4102/jamba. v7i1.144.

Maydeu-Olivares, A. and García-Forero, C. (2010) Goodness of fit testing. In Peterson, P., Baker, E., & McGaw, B. (Eds). International Encyclopedia of Education (3rd ed.), pp. 190-196). Oxford: Elsevier.

Mazloumi, E., Rose, G., Currie, G. and Moridpour, S. (2011) *Engineering Applications of Artificial Intelligence*, **24**, pp.534–54.

McIntyre, N., Wheater, H. and Lees, M. (2002) Estimation and propagation of parametric uncertainty in environmental models. *Journal of Hydroinformatics*. **4(3)**, 177-197

McKee, T.B., Doesken, N.J. and Kleist, J. (1993) The relationship of drought frequency and duration of time scales. Eighth Conference on Applied Climatology, *American Meteorological Society*, Jan. 17-23, 1993, Anaheim CA, pp.179-186.

McKeen, S. A., Wilczak, J., Grell, G., Djalalova, I., Peckham, S., Hsie, E., Gong, W., Bouchet, V., Menard, S., Moffet, R., McHenry, J., McQueen, J., Tang, Y., Carmichael, G. R., Pagowski, M., Chan, A., Dye, T., Frost, G., Lee, P. and Mathur, R. (2005) Assessment of an ensemble of seven realtime ozone forecasts over eastern North America during the summer of 2004, *J. Geophys. Res*., **110**, D21307, doi:10.1029/2005JD005858.

Mckellar, N., New, M. and Jack C. (2014) Observed and modelled trends in rainfall and temperature for South Africa: 1960-2010. *S. Afr. J. Sci*. **110 (7/8)**.

Microsoft [Computer software]. (1996). Excel. Redmond, WA: Microsoft Corporation.

Mishra, A.K. and Desai, V.R. (2006). Drought forecasting using feed-forward recursive models. *Journal of Ecological Modelling*, **198**, pp.127-138.

Mishra, A.K. and Desai, V.R. (2005) Drought forecasting using stochastic models. *Stoch. Environ. Res. Risk Ass*., **19**, pp.326-339.

Mishra, A.K., Singh, V.P. and Desai, V.R. (2009) Drought characterization: a probabilistic approach. *Stochastic Environ. Res. Risk Assessm*., **23(1)**, pp.41-55.

Mishra A.K. and Singh, V.P (2009) Analysis of drought severity-area-frequency curves using a general circulation model and scenario uncertainty, *Journal of Geophysical Research*, **114**, D06120, doi:10.1029/2008JD010986.

Mishra, A.K., Desai, V.R. and Singh, V.P. (2007) Drought forecasting using a hybrid stochastic and neural net-work models. *Journal of Hydrological Engineering*, **12(6)**, pp.626-638.

Mishra, S.S. and Nagarajan, R. (2011) Spatio-temporal drought assessment in Tel river basin using Standardized Precipitation Index (SPI) and GIS. *Geomatics, Natural Hazards and Risk*, **2(1)**, pp.79-93.

Mishra, A. K. and Singh, V. P. (2010) A Review of Drought Concepts. *Journal of Hydrology*, **391(1-2)**, pp.202-216.

Monacelli, G. (2005) Drought assessment and forecasting. WMO, Technical Report, 26.IV.2005. Italy, **88**.

Monahan, A.H. (2000) Nonlinear principal component analysis by Neural Networks: Theory and Application to the Lorenz System. *American Meteorology Society*, **13**, pp.821-835.

Monahan, A.H. (2001) Nonlinear principal component analysis: Tropical Indo-Pacific Sea Surface Temperature and Sea Level Pressure. *American Meteorology Society*, 1, 219-233.

Montzka, SA, BD Hall and JW Elkins (2009), Accelerated increases observed for hydrochlorofluorocarbons since 2004 in the global atmosphere. *Geophys. Res. Lett*. **136**, Art. No. L03804, issn: 0094-8276, ids: 404SV, doi: 10.1029/2008GL036475.

Morid, S., Smakhtin, V. and Bagherzadeh, K. (2007). Drought forecasting using artificial neural networks and networks and time series of drought indices. *International Journal of climatology.*, **27(15)**, pp.2103-2111.

Mosad, A. and Alazba A.A. (2015) Drought forecasting using stochastic models in a hyper-arid climate. *Atmosphere.* **6,** pp. 410-430.

Mosase, E. and Ahlablame, L. (2018) Rainfall and temperature in Limpopo River Basin, southern Africa: Means, variation and trends from 1979 to 2015, *Water*, **(10)**, pp.364, doi:10.339/w10040364.

Mpandeli, N. S. and Maponya, P. I. (2013) Coping with climate variability in Limpopo Province, South Africa. *Peak Journal of Agricultural Sciences*, **1(4)**, pp.54-64.

Mulualem, G.M. and Liou, Y. (2020) Application of Artificial Neural Networks in Forecasting a Standardized Precipitation Evapotranspiration Index for the Upper Blue Nile Basin. *Water*, **12**, 643; doi:10.3390/w12030643.

Murphy. A.H., and Epstein, E. (1989) Skill scores and correlation coefficients in model verification. *Monthly Weather Review*, **117,** pp.572–581.

Musyoki, A., Thifhufhelwi, R. and Murungweni, F.M. (2016) The impact of and responses to flooding in Thulamela Municipality, Limpopo Province, South Africa, *Jàmbá: Journal of Disaster Risk Studies*, **8(2)**, pp.10. http://dx.doi. org/10.4102/jamba.v8i2.166.

M'Marete, C.K. (2003) Climate and water resources in the Limpopo Province. In: Nesamvuni ,A.E., Oni, S.A., Odhiambo, J.J.O. and Nthakheni, N.D. (eds.) *Agriculture as the Cornerstone of the Economy in the Limpopo Province*. A study commissioned by the Economic Cluster of the Limpopo Provincial Government under the leadership of the Department of Agriculture. 1-49.

Myeni, L., Moeletsia, M.E. and Clulowb, A.D. (2019) Present status of soil moisture estimation over the African continent. *Journal of Hydrology: Regional Studies*, **21**, p.14-24. doi.org/10.1016/j.ejrh.2018.11.004.

Mzezewa, J., Misi, T. and van Rensberg, L.D. (2010) Characterisation of rainfall at a semi-arid ecotope in the Limpopo Province (South Africa and its implication for sustainable crop production. *Water SA*, **36(1)**, pp.19-26.

Nash, J. E. and Sutcliffe, J. V. (1970) River flow forecasting through conceptual models: Part I - a discussion of principles. *Hydrol*. **10**, pp.282-290.

Naumann, G., Alfieri, L., Wyser, K., Mentaschi, L., Betts, R. A., Carrao, H., Spinoni, J., Vogt, J. and Feyen, L. (2018). Global changes in drought conditions under different levels of warming. *Geophysical Research Letters*, **45**, pp.3285–3296. https://doi.org/ 10.1002/2017GL076521

Nazir, H.M., Hussain, I., Faisal, M., Shoukry, A.M., Gani, S. and Ahmad, I. (2019) Development of multidecomposition hybrid model for hydrological time series analysis. *Complexity*, Article **2782715**.

Ngaka, M.J. (2012) Drought preparedness, impact and response: A case of the Eastern Cape and Free State provinces of South Africa', *Jàmbá: Journal of Disaster Risk Studies*, **4(1)**, pp.10. http://dx.doi. org/10.4102/jamba.v4i1.47.

Nicholson, S.E. and Entekhabi, D. (1987) Rainfall variability in equatorial and southern Africa: Relationship with seas surface temperatures along the southwestern coast of Africa, *J.Clim. and Appl. Meteorol*., **26**, pp.561-578.

Nourani, V., Parhizkar, M. Khanghah, T.R. Baghanam, A.H. and Sharghi, E. (2012) Wavelet-based feature extraction of rainfall-runoff process via self organizing map. *Proceedings of the 12th WSEAS International Conference on Applied Computer Science*, (ACS' 12), Greece, pp.101-106.

Nowotarski, J. and Weron, R. (2015) Computing electricity spot price prediction intervals using quantile regression and forecast averaging. *Comput. Stat*., **30**, 791–803.

Nury, A.H. and Hasan, K. (2016) analysis of drought in northwestern Bangladesh using standardized precipitation index and its relation to Southern oscillation index. *Environ. Eng. Res.*, **21(1)**, pp.58-68. http://dx.doi.org/10.4491/eer.2015.115

Nyakudya, I.W. and Stroosnijder, L. (2011) 'Water management options based on rainfall analysis for rainfed maize (Zea mays L.) production in Rushinga district, Zimbabwe', *Agricultural Water Management*, **98(10)**, pp.1649–1659, viewed 10 January 2014, from http://linkinghub.elsevier.com/retrieve/pii/S0378377411001338.

Ochoa-Rivera, J.C. (2008) Prospecting droughts with stochastic artificial neural networks. *J. Hydrol*., **352**, pp.174–180.

Ochoa-Rivera, J.C., Andreu, J. and García-Bartual, R. (2007) Influence of inflows modeling on management simulation of water resources system, *Journal of Water Resources Planning and Management*, **133(2)**, pp.106-116.

Odiyo, J.O., Makungo, R. and Nkuna, T.R. (2015) Long-term changes and variability in rainfall and streamflow in Luvuvhu River Catchment, South Africa. *S. Afr J Sci*. **111(7/8)**, pp.9.

Olesen, J.E., Trnka, M., Kersebaum, K.C., Skjelvag, A.O., Seguin, B., Peltonen-Sainio, P., Rossi, F., Kozyra, J. and Micale, F. (2011) Impacts of adaptation of European crop

production systems to climate change. *Eur. J. Agron.* **34**, 96–112. doi:10.1016/j.eja.2010.11.003.

Olsson, L., Opondo, M., Tschakert, P., Agrawal, A., Eriksen, S.H., Ma, S., Perch, L.N. and Zakieldeen, S.A. (2014) Livelihoods and poverty. In: Climate Change 2014: Impacts, Adaptation, and Vulnerability. Part A: Global and Sectoral Aspects. Contribution of Working Group II to the Fifth Assessment Report of the Intergovernmental Panel on Climate Change [Field, C.B., V.R. Barros, D.J. Dokken, K.J. Mach, M.D. Mastrandrea, T.E. Bilir, M. Chatterjee, K.L. Ebi, Y.O. Estrada, R.C. Genova, B. Girma, E.S. Kissel, A.N. Levy, S. MacCracken, P.R. Mastrandrea, and L.L. White (eds.)]. Cambridge University Press, Cambridge, United Kingdom and New York, NY, USA, pp. 793-832.

Ozger, M., Mishra, A.K. and Singh, V.P. (2011) Estimating Palmer Drought Severity Index using wavelet fuzzy logic model based on meteorological variables. *Int. J. Climatol.* **31**, 2021-2032. DOI: 10.1002/joc.2215.

Oztuna, D., Elhan, A.H. and Tucca,r E. (2006) Investigation of four different normality tests in terms of type 1 error rate and power under different distributions. *Turkish Journal of Medical Sciences*. **36(3)**, pp.171-6.

Palmer, W.C. (1965) Meteorological Drought. Research Paper. 45,U.S. Weather Bureau, Washington, D.C., pp.58.

Pan, Y., Pohlen, T. and Manago, S. (2013) Hybrid Neural Network Model in Forecasting Aggregate U.S. Retail Sales. In: *Advances in Bussiness Management Forecasting*, Emerald, **9**, pp. 153–170

Pang, J.D., Liu, D., Peng, Y. and Peng, X. (2018) Optimize the Coverage Probability of Prediction Interval for Anomaly Detection of Sensor-Based Monitoring Series, Sensors, **18**, pp.967; doi:10.3390/s18040967.

Panu, U.S. and Sharma, T.C. (2002) Challenges in drought research: some perspectives and future directions. *Hydrol. Sci.*, **7(S)**, pp.S19-S30.

Paulo A. A., Ferreira, E, Coelho, C. and Pereira L. S. (2005) Drought class transition analysis through markov and log linear model; an approach to early warning system, *Journal of agricultural water management*, **77(1-3)**, pp.59-81, http://dx.doi.org/10.1016/j.agwat.2004.09.039, accessed on 25/03/2014.

Paulo A. A., Pereira L. S. (2007) Prediction of SPI drought class transitions using Markov chains, *Journal of water resources management*, **21(10)**, pp.1813-1827, http://dx.doi.org/10.1007/s11269-006-9129-9 accessed on 24/03/2014.

Paulo A. A. and Pereira L. S. (2008) Stochastic Prediction of drought class transitions, *Journal of water resources management*, **22(9)**, pp.1277-1296, http://dx.doi.org/10.1007/s11269-007-9225-95, accessed on 24/03/2014.

Peng, S., Liu, W., Wang, W. Shao, Q.,Jiao, X., Yu, Z., Xing, W., Xu, J., Shang, Z. and Luo, Y. (2013). Estimating the effect of climatic variability and human activities on stream flow in the Hutuo River Basin, China, *Journal of Hydrologic Engineering*, **18(4)**, pp.422-430.

Peng, G., Li, P., Zhao, B., Xu, R., Zhao, G., Sun, W. and Mu, X. (2017). Use of double mass curves in hydrologic benefit evaluations. *Hydrological Processes*. **31**. 10.1002/hyp.11377.

Peters, E., Bier, G., Van Lanen, H.A.J. and Torfs, P.J.J.F. (2006) Propagation and spatial distribution of drought in a groundwater catchment. *Journal of Hydrology*, **321**, pp.257–275, doi: 10.1016/j.jhydrol.2005.08.004.

Peters, E. (2003) Propagation of drought through groundwater systems: illustrated in the Pang (UK) and Upper-Guadiana (ES) catchments, *Ph.D. thesis*, Wageningen University, Wageningen, the Netherlands.

Pirnia, A., Golshan, M., Darabi, H., Jan Adamowski, J. and Rozbeh, S. (2019) Using the Mann–Kendall test and double mass curve method to explore stream flow changes in response to climate and human activities. *Journal of Water and Climate Change* **10 (4)**, 725–742.

Ramulifho, P., Ndou, E., Thifhulufhelwi, R. and Dalu, T. (2019) Challenges to Implementing an Environmental Flow Regime in the Luvuvhu River Catchment, South Africa, *Int. J. Environ. Res. Public Health*, **16**, pp.3694.

Rana, A., Moradkhani, H. and Qin, Y. (2016) Understanding the joint behavior of temperature and precipitation for climate change impact studies. *Theor. Appl Climatol,* **129**, pp.321 doi:10.1007/s00704-016-1774-1.

Ravindraa, K., Rattana, P., Morb, S. and Aggarwalc, A.N. (2019) Generalized additive models: Building evidence of air pollution, climate change and human health, *Environment International*, **132**, doi.org/10.1016/j.envint.2019.104987.

Ravikumar, K. and Tamilselvan, S. (2014) On the use of wavelets packet decomposition for time series prediction. *Applied Math. Sci*., **8**, pp.2847-2858.

Redmond, K. (1991) Climate monitoring and indices. In *Proceeding of the Seminar and Workshop: Drought Management and Planning*, 30 May–June 1 1990, Denver, CO; 29–33.

Refsgaard, J.C., and Henriksen, H.J. (2004). Modelling guidelines-terminology and guiding principles. *Advances in Water Resources*. **27(1)**, 71-82.

Refsgaard, J.C., van der Sluijs, J.P., Hojberg, A.L. and Vanrolleghem, P.A. (2007). Uncertainty in the environmental modelling process - a framework and guidance. *Environmental Modelling and Software.* **22**, 1543-1556

Reichle, R. H. (2012) The MERRA-land data product. NASA GMAO Office Note3 (version1.2), pp.33 [Available online at https://gmao.gsfc.nasa.gov/pubs/docs/Reichle541.pdf.

Ripley, B.D. (1994) Neural networks and flexible regression and discrimination. *In Statistics and Images 2*, ed. K. V. Mardia, volume 2 of *Advances in Applied Statistics*, Abingdon: Carfax, pp.3-57.

Ross, S. (2017) Testing Statistical Hypotheses. 10.1016/B978-0-12-804317-2.00009-6. In book: Introductory Statistics, pp.381-432. SBN**,** 978-0-12-804317-2.

Rossi, G., Nicolosi, V. and Cancelliere, A. (2008) Recent methods and techniques for managine hydrological droughts. In: Lopez-Francos, A. (Ed.). CIHEAM, 2009. P.251-266. International Conference on drought management: Scientific and Technological Innovation, 2009/06/12-14, Zaragoza (Spain).

Rouault, M. and Richard, Y. (2005) Intensity and spatial extent of droughts in southern Africa, *Geophysical Research Letters*, **32**, L15702, doi:10.1029/2005GL022436.

Safavi, H.R. and Malek Ahmadi, K., 2015. Prediction and assessment of drought effects on surface water quality using artificial neural networks: case study of Zayandehrud River,

Iran. *Journal of Environmental Health Science and Engineering*, **13(1)**, 68. doi:10.1186/s40201-015-0227-6.

Samarasinghe, S. (2006) Neural networks for applied sciences and engineering: from fundamentals to complex pattern recognition, Auerbach Publications, New York.

Sánchez-Lugo, A., Berrisford, P., Morice, C., and Argüez, A. (2018). Temperature [in *State of the Climate in 2018*]. *Bulletin of the American Meteorological Society*, **99(8)**, pp.S11–S12.

Sang, Y-F., Sun, F., Singh, V.P., Xie, P. and Sun, J. (2012) A discrete wavelet spectrum approach to identifying 1 non-monotonic trend pattern of hydroclimate data. *Hydrol. Earth Syst. Sci. Discuss*., doi:10.5194/hess-2017-6.

Sankaran, M., Ratnam, J. and Hanan, N. (2008) Woody cover in African savannas: the role of resources, fire and herbivory. *Glob. Ecol. Biogeogr*. **17,** pp.236–245. doi:10.1111/j.1466-8238.2007.00360.x.

Savage, N. H., Agnew, P., Davis, L. S., Ordóñez, C., Thorpe, R., Johnson, C. E., O'Connor, F. M., and Dalvi, M. (2013) Air quality modelling using the Met Office Unified Model (AQUM OS24-26): model description and initial evaluation, *Geosci. Model Dev*., **6**, 353–pp.372, doi:10.5194/gmd-6-353-2013.

Scheffran, J., Marmer, E. and Show, P. (2012) Migration as a contribution to resilience and innovation in climate adaptation: social networks and co-development in North West Africa, *applied geography*, **33**, pp.119-127.

Schubert, S. D., Stewart, R. E., Wang, H., Barlow, M., Berbery, E. H., Cai, W. and Lyon, B. (2016) Global meteorological drought: A synthesis of current understanding with a focus on SST drivers of precipitation deficits. *Journal of Climate*, **29(11)**, pp.3989–4019. https://doi.org/10.1175/ JCLI-D-15-0452.1.

Seo, Y. and Kim, S. (2016) Hydrological Forecasting Using Hybrid Data-Driven Approach. *American Journal of Applied Sciences*, **13(8)**, pp.891.899.

Seo, Y. (2015) River stage forecasting model combining wavelet packet transform and artificial neural network. *J. Environ. Sci. Int.*, **24**, pp.1023-1036. DOI: 10.5322/JESI.2015.24.8.1023.

Seo, Y., Kim, S., Kisi O. and Singh, V.P. (2015) Daily water level forecasting using wavelet decomposition and artificial intelligence techniques. *J. Hydrol*., **520**, pp.224-243. DOI: 10.1016/j.jhydrol.2014.11.050.

Shafer B.A. and Dezman, L.E. (1982) Development of a Surface Water Supply Index (SWSI) to Assess the Severity of Drought Conditions in Snowpack Runoff Areas. *Proceedings of the Western Snow Conference*, Colorado State University, Fort Collins, pp.164-175.

Sharda V, Srivasta P, Kalin L, Ingram K, Chelliah M (2012) Development of community water deficit index (CWDI) -Drought forecasting tool for small to mid-size communities of south-eastern united states. *Journal of Hydrologic Engineering*, **7**, pp.846-858.

Shatanawi, K., Rahbeh, M., Shatanawi, M. (2013) Characterizing, monitoring and forecasting of drought in Jordan River basin, *Journal of water resources and protection,* **5**, pp.1192-1202.

Sheffield, J. and Wood, E. (2011) Drought; Past Problems and Future Scenarios, Earthscan, London, UK, Washington DC, USA.

Sherval, M., Askew, L.E. and McGuirk, P.M. (2014) Manifestations of Drought. In A.C. Michalos (Ed.), Encyclopedia of Quality of Life and Well-Being Research (pp. 3756-3761). Dordrecht, Netherlands: Springer.

Shin, H. and Salas, J.D. (2000), Regional drought analysis based on neural networks. *J. Hydrol. Engng.,* **5(2)**, pp.145-155.

Shiau, J., Modarres, R. and Nadarajah, S. (2012) Assessing Multi-site Drought Connections in Iran Using Empirical Copula. *Environ Model Assess*, **17**, pp.469–482.

Shuttelworth (1993) Evaporation, In: Maidment, D.R. (Ed.) Hanbook of Hvdrolo McGraw-Hill Book Company, New York City, New York, 4.1-4.53.

Sifundza, L.S., van der Zaag, P. and Masih, I. (2019) Evaluation of the responses of institutions and actors to the 2015/2016 El Niño drought in the Komati catchment in Southern Africa: lessons to support future drought management. *Water SA*, **45(4)**, pp.547-559.

Sigauke, C., Nemukula, M.M. and Daniel Maposa, D. (2018) Probabilistic Hourly Load Forecasting Using Additive Quantile Regression Models, *Energies*, ***11*(9)**, pp.2208.

Sigauke C. and Chikobvu D. (2012). Short-term peak electricity demand in South Africa. *African Journal of Business Management*, **6(32)**, pp. 9243-9249.

Simpson GL (2018) Modelling Palaeoecological Time Series Using Generalised Additive Models. *Front. Ecol. Evol*. **6**, pp.149. doi: 10.3389/fevo.2018.00149

Singh, M. (2006) Identifying and assessing drought hazard and risk in Africa. Regional conference on insurance and reinsurance for natural catastrophe risk in Africa. Casablanca, Morocco, November 14/12/2005.

Smakhtin, V. U. (2001) Low flow hydrology: A review. *Journal of Hydrology*, **240**, pp.147–186, doi: 10.1016/S0022- 1694(00)00340-1.

Sohn, S.J., Joong-Bae, A. and Chi-Yung, T. (2013) Six month–lead downscaling prediction of winter to spring drought in South Korea based on a multimodel ensemble. *Geophys. Res. Lett.* **40,** pp.579–583.

Solaiman TA (2011) Uncertainty estimation of extreme precipitations under climatic change: a non-parametric approach, *PhD Thesis*, Department of Civil and Environmental Engineering, University of Western Ontario.

Solomon, S. (2010) Water: The epic struggle for wealth, power and civilization, HarpeCollins, ISBN: 0060548312, 9780060548315, pp.624.

Srivastava, N., Hinton, G., Krizhevsky, A., Sutskever, I. and Salakhutdinov, R. (2014) Dropout: A Simple Way to Prevent Neural Networks from Overfitting, *J. Mach. Learn. Res*., **15**, pp.1929–1958.

Stagge, J.H., Kohn, I., Tallaksen, L.M. and Stahl, K (2015) Modeling drought impacts occurrence based on meteorological drought indices in Europe. *Journal of Hydrology*, **530**, pp.37-50.

Stahl, K., and Demuth, S. (1999) Linking streamflow drought to the occurrence of atmospheric circulation patterns. *Hydrological Sciences Journal*, **44**, pp.467–482, doi: 10.1080/02626669909492240.

Stahl, K., Tallaksen, L., Hannaford, J. and van Lanen, H. (2012) Filling the white space on maps of European runoff trends: Estimates from a multi-model ensemble, *Hydrol. Earth Syst. Sci*., **16**, 2035–2047.

State of Rivers Report (2001) South African River Health Programme: Letaba and Luvuvhu River Systems. DWAF, Resource Quality Services. WRC Report no. 165/01. Water Research Commission.

Sun, X., Wang, Z. and Hu, J. (2017) Prediction interval construction for by product gas flow forecasting using optimized twin extreme learning machine, *Math. Probl. Eng*.

Tadross, M., Suarez, P., Lotsch, A., Hachigonta, S., Mdoka, M., Unganai, L., Lucio, F., Kamdonyo, F. and Muchinda, M. (2007). Changes in growing-season rainfall characteristics and downscaled scenarios of change over southern Africa: implications for growing maize. Regional expert meeting report, pp.193-204. www.csag.uct.ac.za/~mtadross

Tallaksen, L.M., and Van Lanen, H.A.J. (2004). Hydrological drought: processes and estimation methods for streamflow and groundwater, Developments in water science; eds, **48**, Elsevier Science B.V., Amsterdam, the Netherlands.

Tallaksen, L. M. (2000) Streamflow drought frequency analysis, in: Drought and Drought Mitigation, edited by: Vogt, J. V. and Somma, F., Advances in Natural and Technological Hazards Research, Kluwer Academic Publishers, Dordrecht, the Netherlands, **14**, pp.103–117.

Tan, C., Yang, J. and Li, M. (2015) Temporal-Spatial variation of drought indicated by SPI and SPEI in Ningxia Hui Autonomous Region, China. *Atmosphere,* **6**, pp.1399-1421. doi:10.3390/atmos6101399

Tang, B., Dong, S. and Song, T. (2012) Method for eliminating mode mixing of empirical mode decomposition based on the revised blind source separation. *Signal Processing,* **92 (1)**, pp.248–258.

Taşpınar, F. (2015) Improving artificial neural network model predictions of daily average PM10 concentrations by applying principle component analysis and implementing seasonal models, *Journal of the Air & Waste Management Association*, **65(7)**, pp.800-809, DOI: 10.1080/10962247.2015.1019652.

Tate, E. L. and Freeman, S. N. (2000) Three modelling approaches for seasonal streamflow droughts in southern Africa: the use of censored data. *Hydrol. Sci. J.*, **45(1)**, pp.27–42.

Tennant, W.J. and Hewitson, B.C. (2002) Intra-seasonal Rainfall Characteristics and their Importance to the Seasonal Prediction Problem. *Int. J. Climatol*., **22**, pp.1033-1048.

Thompson, D.W.J., Wallace, J.M., Jones, P.D. and Kennedy, J.J. (2009) Identifying Signatures of Natural Climate Variability in Time Series of Global-Mean Surface Temperature: Methodology and Insights. *Journal of Climate*, **22**, pp.6120- 6140.

Thornton, P.K., Ericksen, P.J., Herrero, M. and Challinor, A.J. (2014) Climate variability and vulnerability to climate change: a review, *Global Change Biology*, **20**, pp.3313–3328, doi: 10.1111/gcb.12581

Torrence, C. and G.P. Compo, 1998. A practical guide to wavelet analysis. B. Am. Math. Soc., **79**, pp.61-78.

Trenberth, K.E., P.D. Jones, P. Ambenje, et al. (2007) Observations: Surface and Atmospheric Climate Change. In: Climate Change 2007: The Physical Science Basis. Contribution of Working Group I to the Fourth Assessment Report of the Intergovernmental Panel on Climate Change [Solomon, S., D. Qin, M. Manning, Z. Chen, M. Marquis, K.B. Averyt, M. Tignor and H.L. Miller (eds.)]. Cambridge University Press, Cambridge, United Kingdom and New York, NY, USA.

Trambauer, P., Werner, M., Winsemius, H.C., Maskey, S., Dutra, E. and Uhlenbrook, S. (2015) Hydrological drought and skill assessment for the Limpopo River Basin, southern Africa, *Hydrol. Earth Syst. Sci.*, pp.1695-1711.

Tran, H. D. Perera, B. J. C. and Ng, A. W. M. (2009). Comparison of structural deterioration models for storm water drainage pipes, *computer aided civil and infrastructure engineering*, **24(2)**, pp.145-156.

Tshililo, F.P. (2017) Rainy season characteristics with reference to maize production for the Luvuvhu River Catchment, Limpopo Province, South Africa, Unpublished Masters dissertation submitted to the University of Kwazulu-Natal, pp.112.

Tychon, B., Pecheur, C. and Ozer, P. (2007) The NDWI as a drought index applied to Belgium and Heilongjiang in Belgian and Chinese crop growth monitoring systems: Comparison, adaptation and Improvement, *Tychon B. (ed), FUL, Arlon, Belgium*, pp.111-120.

Tyson, P.D. (1986) Climatic change variability in southern Africa, Oxford University Press, Cape Town, pp.220.

United Nations (UN: 2008) Trends in sustainable development, agriculture, rural development, land desertification and drought. Department of economic and social affairs, United Nations, New York.

United Nations Development Programme (UNDP: 2012) Kenya: adapting to climate variability in Arid and Semi-Arid Lands (KACCAL), Project report.

UNESCO (2005) Water resource systems planning and management. Chap. 9: Model sensitivity and Uncertainty Analysis, pp.255-287. ISBN 92-3-103998-9

UNESCO (2007) Africa Review Report on Drought and Desertification, Fifth Meeting of the Africa Committee on Sustainable Development, Addis Ababa, Ethiopia, pp.65.

Unganai, L.S. (1994) Drought and Southern Africa: A Note from the Harare Regional Drought Monitoring Centre, *Drought Network News (1994-2001).* Paper 85. http://digitalcommons.unl.edu/droughtnetnews/85.

Usman, M.T. and Reason, C.J.C. (2004) Dry spell frequency and their variability over southern Africa, *Clim Res*., **26**, pp.199-211.

Vallam, P., Qin, X.S. and Yu, J.J. (2014) Uncertainty quantification of hydrologic model. *APCBEE Procedia,* **10(2014)**, pp.219-233.

van Lanen, H., Wanders, N. Tallaksen, L.M. and van Loon, A.F. (2013) Hydrological drought across the world: Impact of climate and physical catchment structure, *Hydrol. Earth Syst. Sci*., **17(5)**, 1715–1732, doi:10.5194/hess-17-1715-2013.

Van Lanen, H. A. J., Fendeková, M., Kupczyk, E., Kasprzyk, A., and Pokojski, W. (2004) Flow Generating Processes. chap. 3, 53–96, In: Hydrological drought: processes and estimation methods for streamflow and groundwater, Developments in water science; 48, edited by Tallaksen, L. M., and Van Lanen, H. A. J., Elsevier Science B.V., Amsterdam, the Netherlands.

Van Loon A.F. (2013) On the propagation of drought. How climate and catchment characteristics influence hydrological drought development and recovery, *PhD thesis*, Wageningen University, Wageningen, NL, pp.198, ISBN 978–94–6173–501–0.

Van Vliet, M.T.H. and Zwolsman, J.J.G., (2008) Impact of summer droughts on the water quality of the Meuse river. *Journal of Hydrology*, **353(1–2)**, 1–17. doi:10.1016/j.jhydrol.2008.01.001.

Vetter, S. (2009) Drought, change and resilience in South Africa's arid and semi-arid rangelands. *S. Afr J Sci*., **105**, pp.29–33.

Vicente-Serrano, S.M., Begueria, S. and Lo´pez-Moreno, J.I. (2010a) A Multiscalar Drought Index Sensitive to Global Warming: The Standardized Precipitation Evapotranspiration Index. *J. of Climate*. **23,** pp.1696-1718.

Vicente-Serrano, S.M., Lasanta, T. and Gracia, C. (2010b) Aridification determines changes in leaf activity in Pinus halepensis forests under semiarid Mediterranean climate conditions. *Agric. For. Meteorol.***150,** pp.614-628.

Vicente-Serrano, S.M., Chura, O., Lopez-Moreno, J.I., Azorin-Molina, C., Sanchez-Lorenzo, A., Aguilar, E., Moran-Tejeda, E., Trujillo, F., Martinez, R. and Nieto, J.J. (2014) Spatio-temporal variability of droughts in Bolivia, *Int. J. Climatol.*, **35**, pp.3024-3040. DOI: 10.1002/joc.4190

Vogel, C. H. (1994) T'he impact of extreme drought events. Human Sciences Research Council Rep., Pretoria, South Africa, pp.36.

Wang, W-C., Chau, K-W., Xu, D-M. and Chen, X-Y. (2015) Improving Forecasting Accuracy of Annual Runoff Time Series Using ARIMA Based on EEMD Decomposition. *Water Resour Manage,* **29**, pp.2655-2675. doi 10.1007/s11269-015-0962-6.

Wang, L., Chen, W. and Zhou, W. (2014) Assessment of future drought in Southwest China based on CMIP5 multimodel projections. *Adv. Atmos. Sci.*, 31(5), 1035–1050, doi: 10.1007/s00376-014-3223-3.

Wijesekera, N.T.S. and Perera, L.R.H. (2012) Key Issues of Data and Data Checking for Hydrological Analyses - Case Study of Rainfall Data in the Attanagalu Oya Basin of Sri Lanka. *Engineer*, **xxxxv(02)**, pp. 1-12.

Wilhite, D.A. (2005) The Role of Disaster Preparedness in National Planning with Specific Reference to Droughts. In: Sivakumar M.V., Motha R.P., Das H.P. (eds) Natural Disasters and Extreme Events in Agriculture. Springer, Berlin, Heidelberg

Wilhite, D.A. (1993) Planning for drought, in D.A. Wilhite (ed.), *Drought assessment, management and planning*: *Theory and case studies*, pp.87−108, Kluwer Academic Publishers, Boston. http://dx.doi.org/10.1007/978-1-4615-3224-8_6.

Wilhite, D.A. and Glantz, M.H. (1987) Understanding The Drought Phenomenon The Role of Definitions. In Wilhite, D.A., Easterling, W.E. and Wood, D.A., Eds., Planning for Drought Toward a Reduction of Social Vulnerability, Westview Press, Boulder, CO, 11-30.

Wilhite, D. A., and Glantz, M. H. (1985) Understanding the drought phenomenon: the role of definitions, *Water International*, **10**, pp.111–120, doi: 10.1080/02508068508686328.

Willmott, C. and Matsuura, K. (2005) Advantages of the Mean Absolute Error (MAE) over the Root Mean Square Error (RMSE) in assessing average model performance, *Clim. Res*., **30**, pp.79–82.

Willmott, C. J., Matsuura, K., and Robeson, S. M. (2009) Ambiguities inherent in sums-of-squares-based error statistics, Atmos. Environ., **43**, pp.749–752.

World Meteorological Organisation (WMO) (2012) Standardized Precipitation Index: User Guide, Geneva 2, Switzerland.

Wood, S. (2006) Generalized Additive Models. Chapman & Hall/CRC: New York.

Wood S.N., Goude, Y. and Shaw, S. Generalised additive models for large data sets, *Appl. Statist*. **64(1)**, pp.139–155

Wood, S. (2017) P-splines with derivative based penalties and tensor product smoothing of unevenly distributed data. *Statistics and Computing*, **27**, pp.985–989.

Wu, Z.H. and Huang, N.E. (2009) Ensemble empirical mode decomposition: A noise-assisted data analysis method. *Adv. Adaptive Data Analy*., **1**, pp.1-41. DOI: 10.1142/S1793536909000047.

Wu, J.D. and Tsai, Y.J. (2011) Speaker identification system using empirical mode decomposition and an artificial neural network. *Expert systems with applications*, **38(2011)**, pp.6112-6117

Xu, Z., Huang, B. & Li, K. (2010), An alternative envelope approach for empirical mode decomposition, *Digital Signal Processing: A Review Journal*, **20**(1), pp.77–84.

Yang, Y., T. R. McVicar, R. J. Donohue, Y. Zhang, M. L. Roderick, F. H.S. Chiew, L. Zhang, and J. Zhang (2017), Lags in hydrologic recovery following an extreme drought: Assessing the roles of climate and catchment characteristics, *Water Resour. Res*., **53**, doi:10.1002/2017WR020683.

Yevjevich, V. (1972) Stochastic Processes in Hydrology, Water Resources Publication, Highlands Ranch, Colorado, USA.

Yevjevich, V. (1967) An objective approach to definitions and investigations of continental hydrologic droughts. Colo. State Univ. Fort Collins Hydrol. Pap., pp.23

Yi, Y., Kimball, J.S., Jones, L.A., Reichle, R.H. and McDonald, K.C. (2011) Evaluation of MERRA Land Surface Estimates in Preparation for the Soil Moisture Active Passive Mission. *J. Clim*., **24**, 3797–3816.

Zhang, G.P. (2003). Time series forecasting using a hybrid ARIMA and neural network model. *Neurocomputing*, **50**, pp.159-175.

Zhang, X., Lai., K.K. and Wang, S-Y (2008) A new approach for crude oil price analysis based on Empirical Mode Decomposition. *Elsevier Journal of Energy Economics*, **30**, pp.905-908.

Zhang, Z., Lu, W.X., Chu, H.B., Cheng, W.G. and Zhao, Y. (2014) Uncertainty analysis of hydrological model parameters based on the bootstrap method: A case study of the SWAT model applied to the Dongliao River Watershed, Jilin Province, North-eastern China. *Sci China Tech Sci*, **57**, pp.219-229. doi: 10.1007/s11431-013-5385-0

Zheng, J., Pan, H., Yang, S. and Cheng, J. (2017) Adaptive parameterless empirical wavelet transform based time-frequency analysis method and its application to rotor rubbing fault diagnosis. *Signal Processing*, **130(2017)**, pp.305-314. http://dx.doi.org/10.1016/j.sigpro.2016.07.023.

Zhang, X., Zhang, Q., Zhang , G., Nie, Z., Gui, Z. and Que, H. (2018) A Novel Hybrid Data-Driven Model for Daily Land Surface Temperature Forecasting Using Long Short-Term Memory Neural Network Based on Ensemble Empirical Mode Decomposition, *Int. J. Environ. Res. Public Health*, **15**, pp.1032; doi:10.3390/ijerph15051032.

Zoljoodi, M. and Didevarasl, A. (2013). Evaluation of spatio-temporal variability of droughts in Iran using Palmer Drought Severity Index and its precipitation factors through (1951-2005), *Atmosphere and Climate Sciences Journal*, **3**, pp.193-207.

APPENDICES

Appendix A: Chapter 4

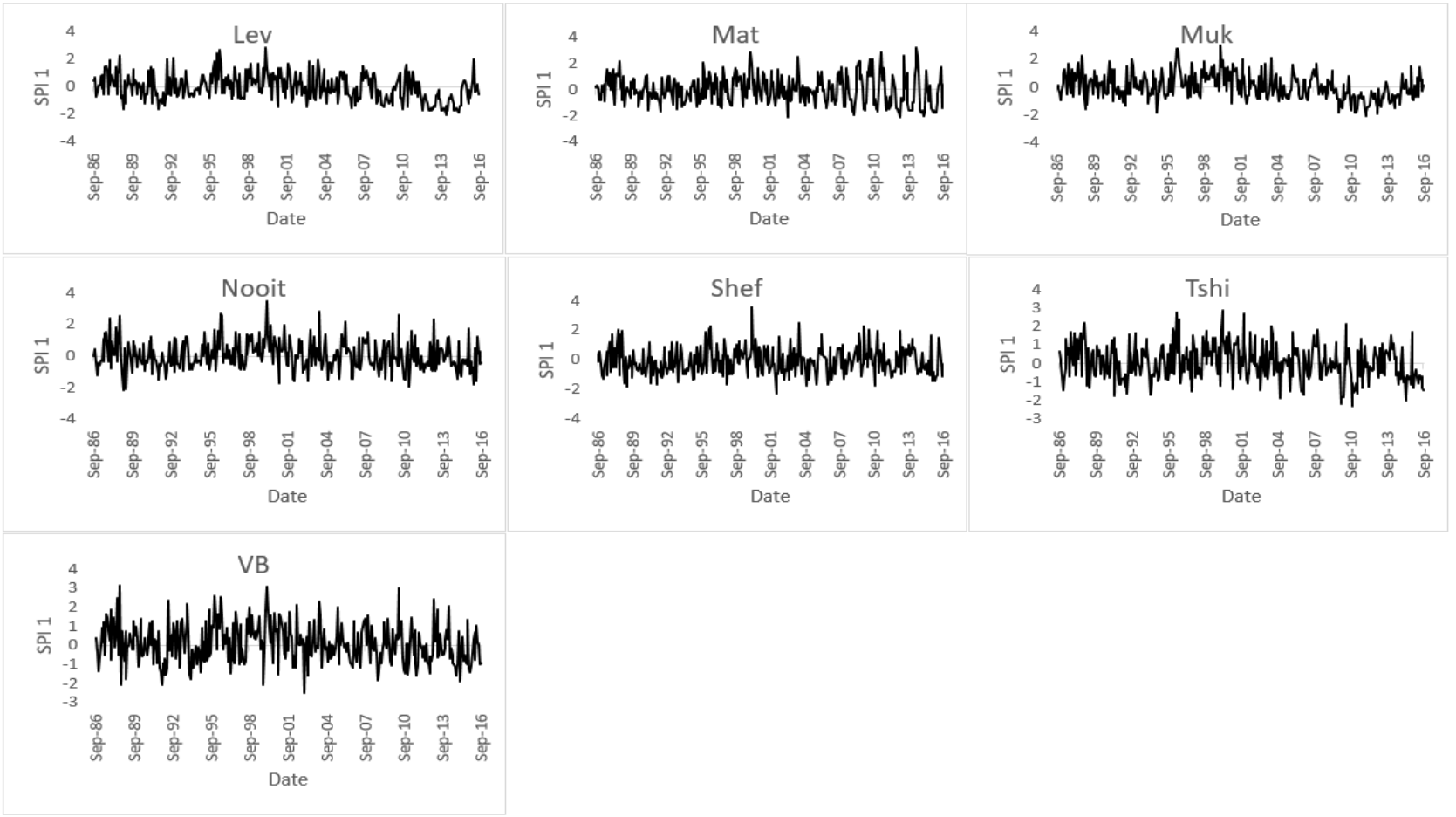

Figure A1: SPI 1 time series.

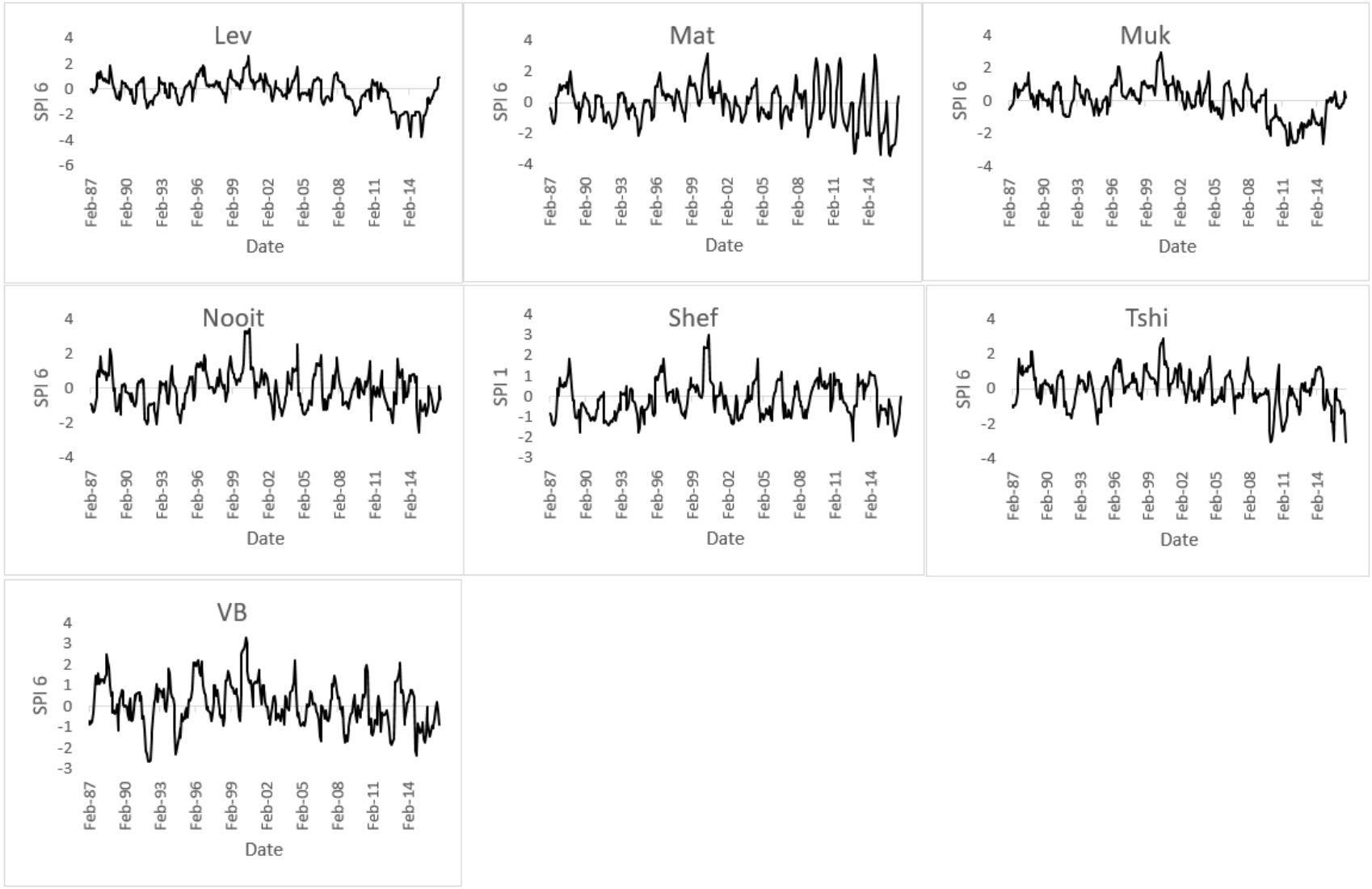

Figure A2: SPI 6 time series.

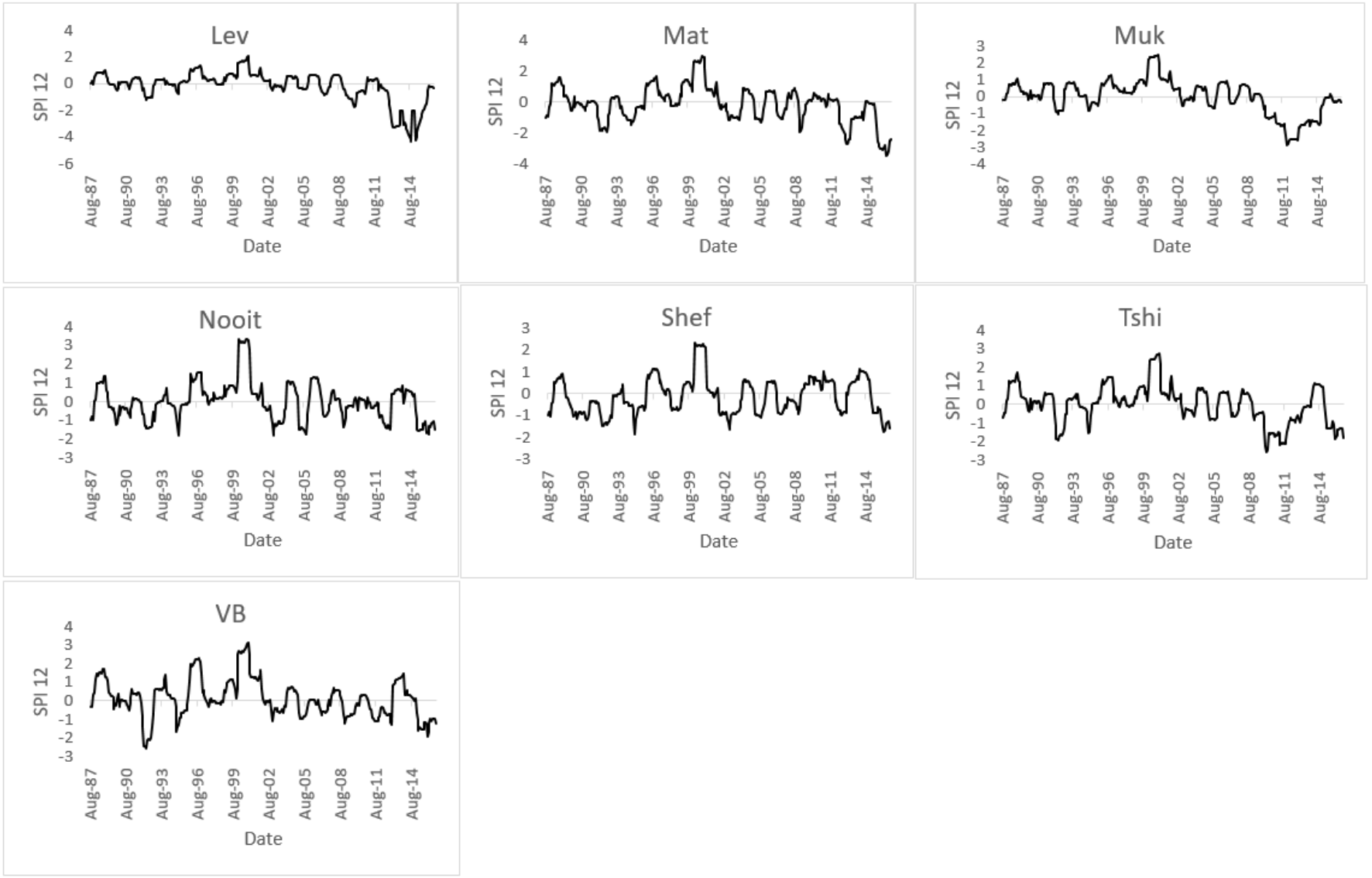

Figure A3: SPI 12 time series.

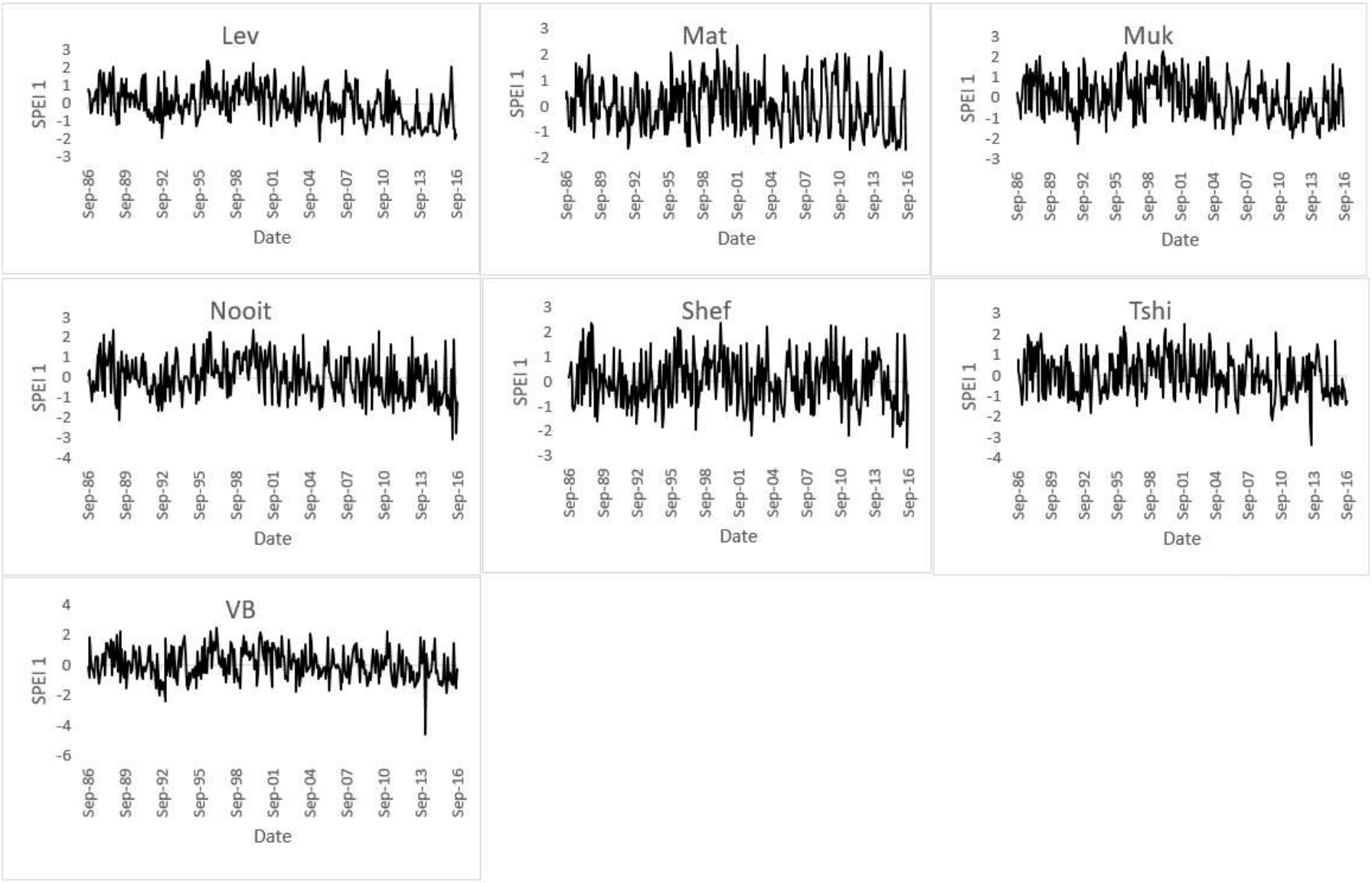

Figure A4: SPEI 1 time series.

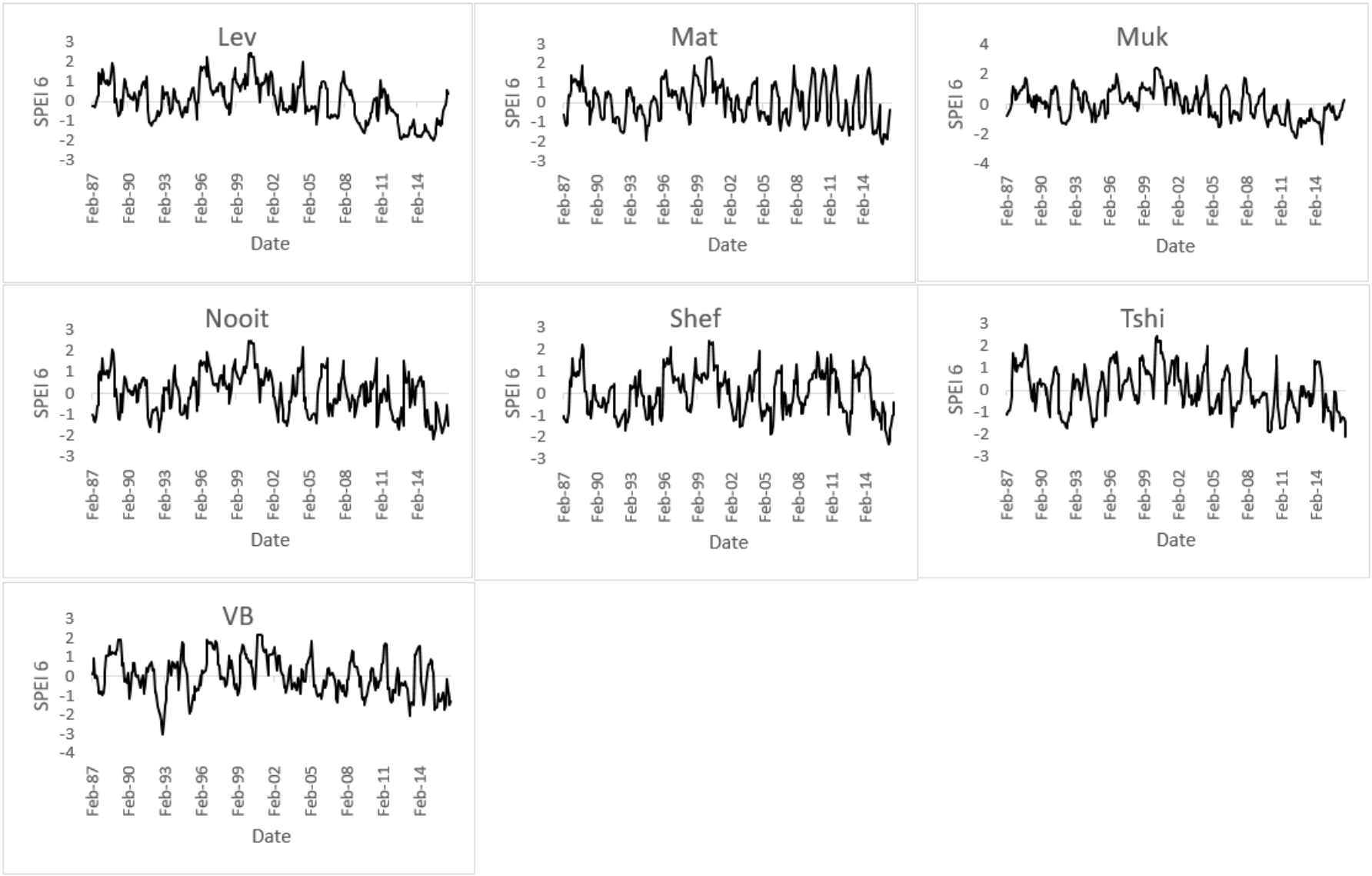

Figure A5: SPEI 6 time series.

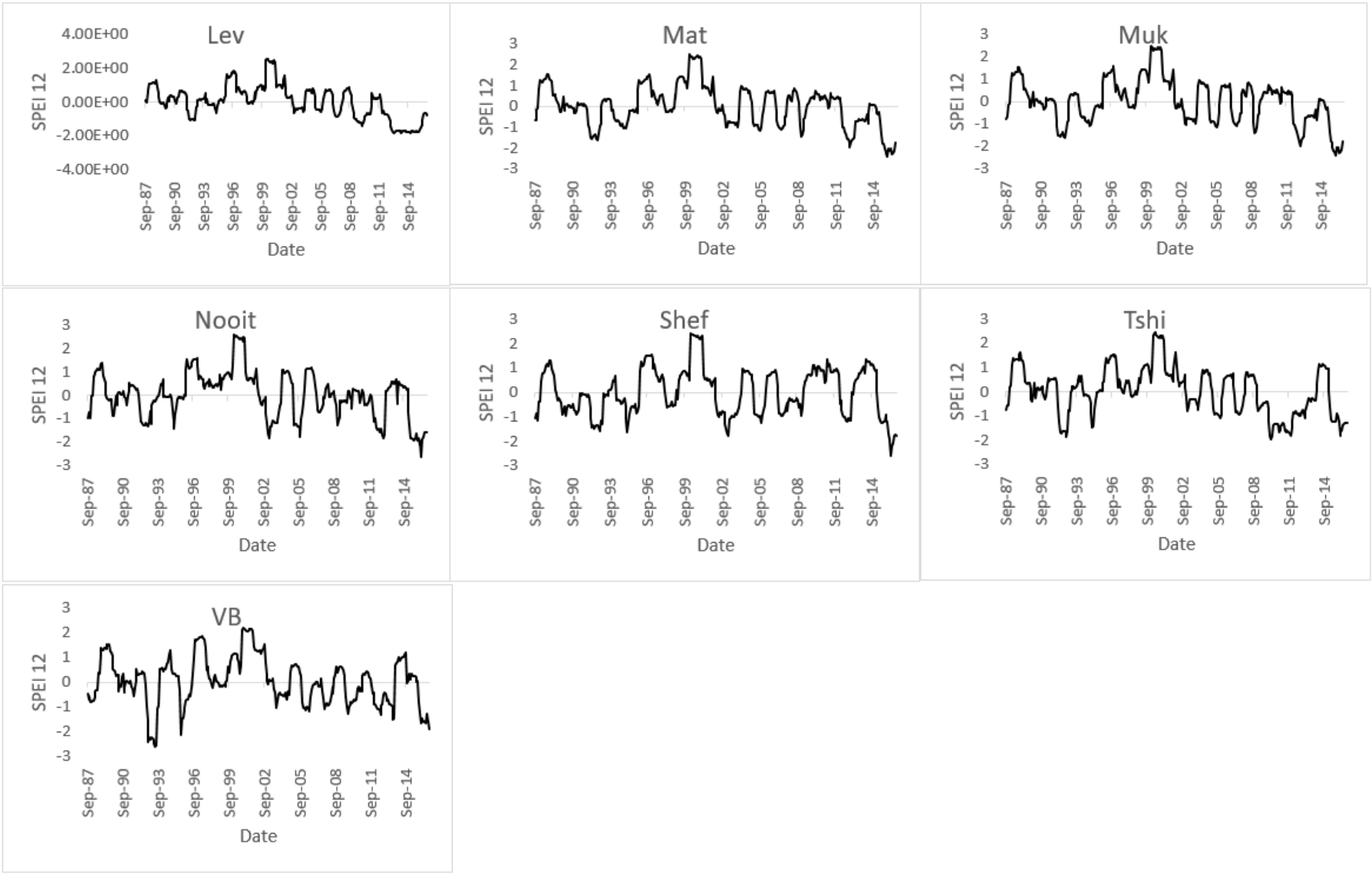

Figure A6: SPEI 12 time series.

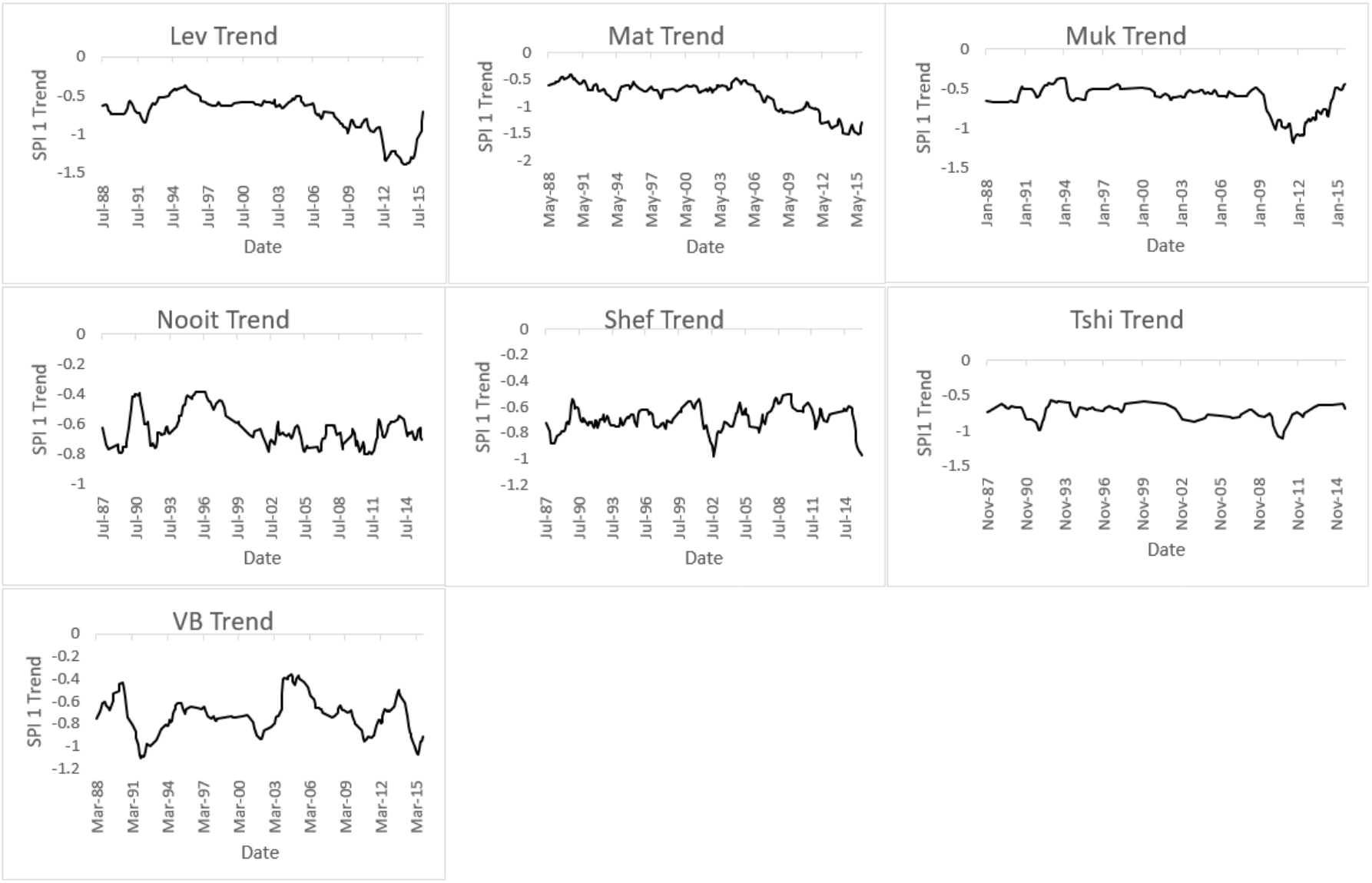

Figure A7: SPI 1 non-liner trend.

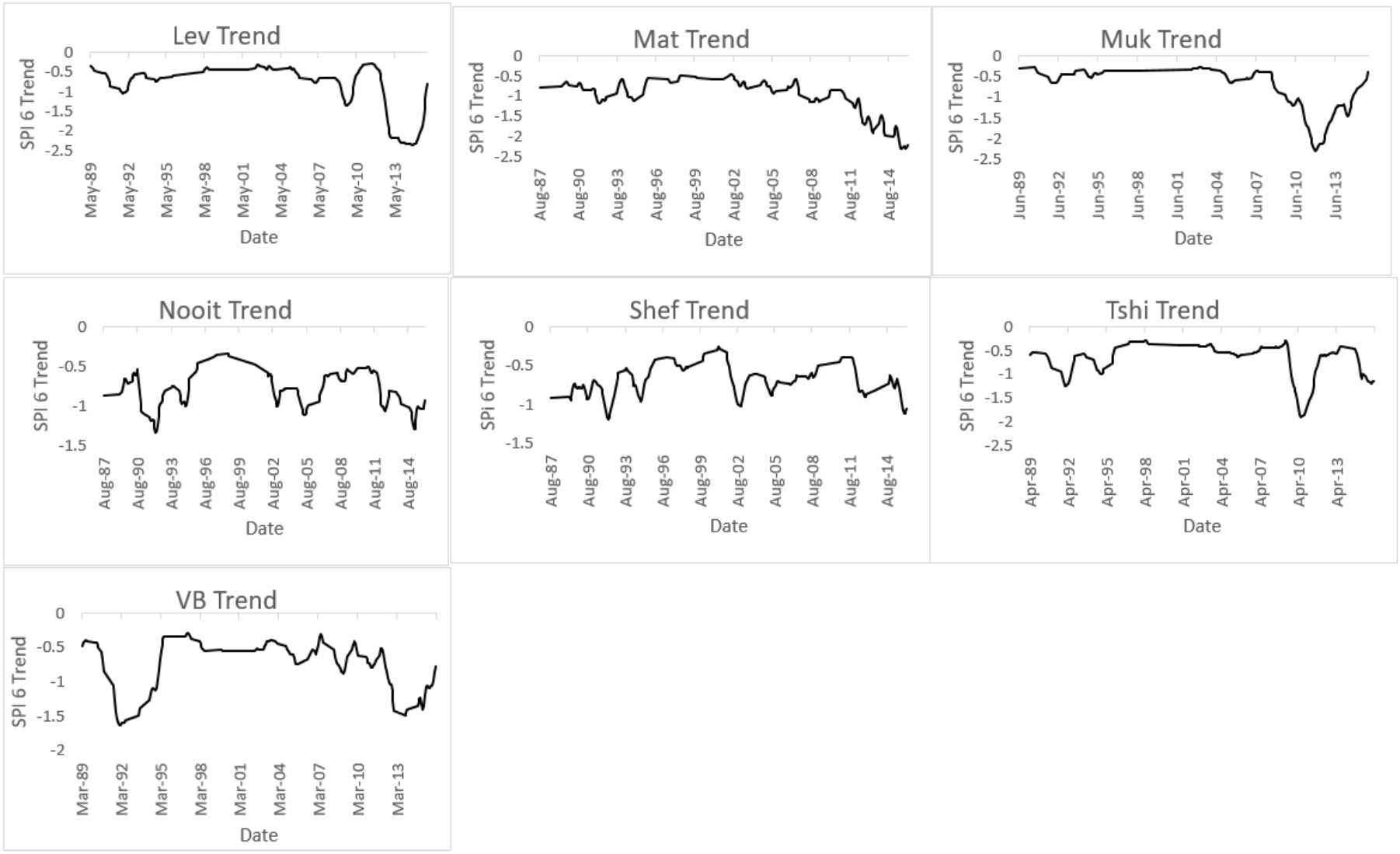

Figure A8: SPI 6 non-linear trend.

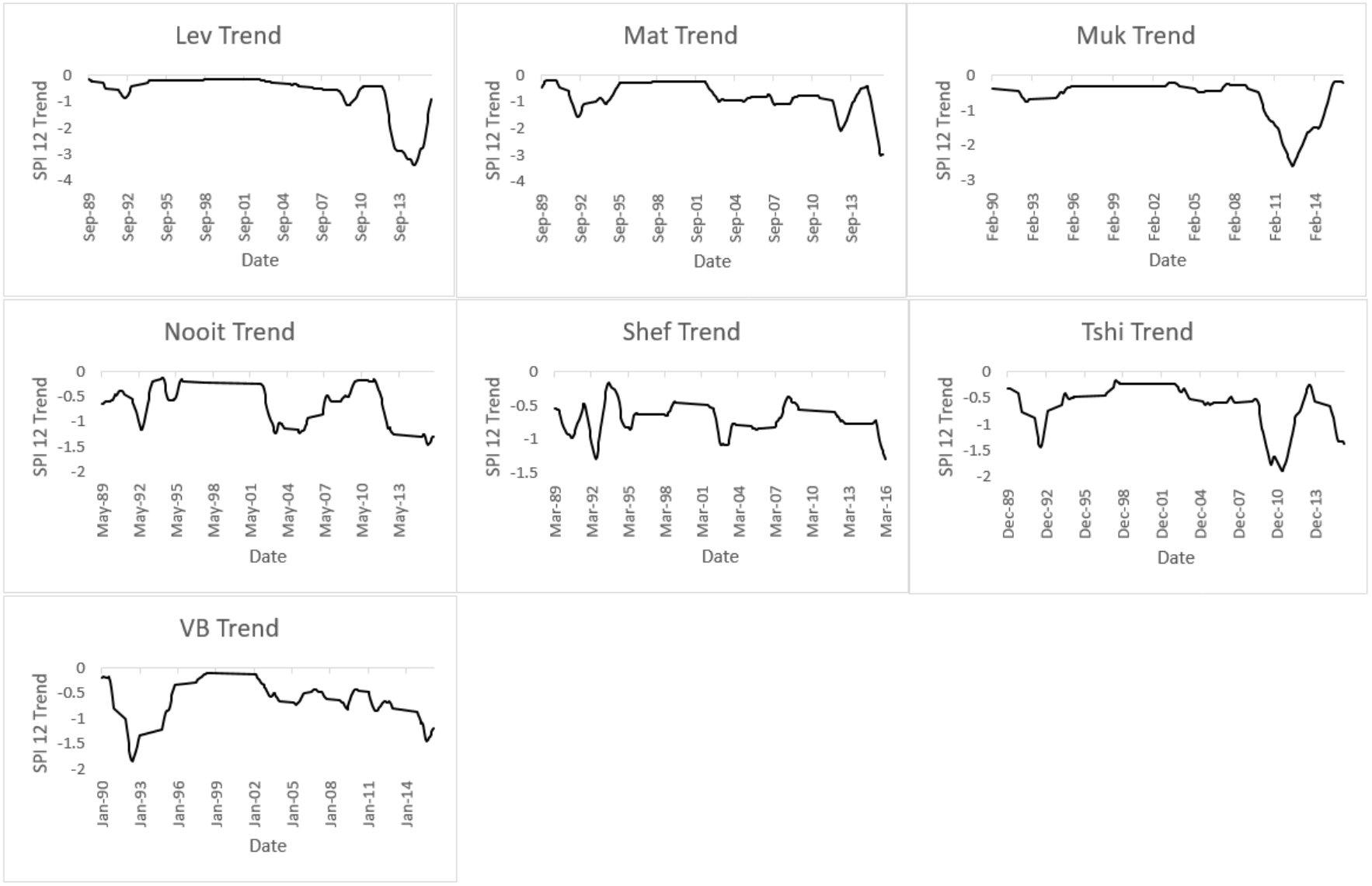

Figure A9: SPI 12 non-linear trend.

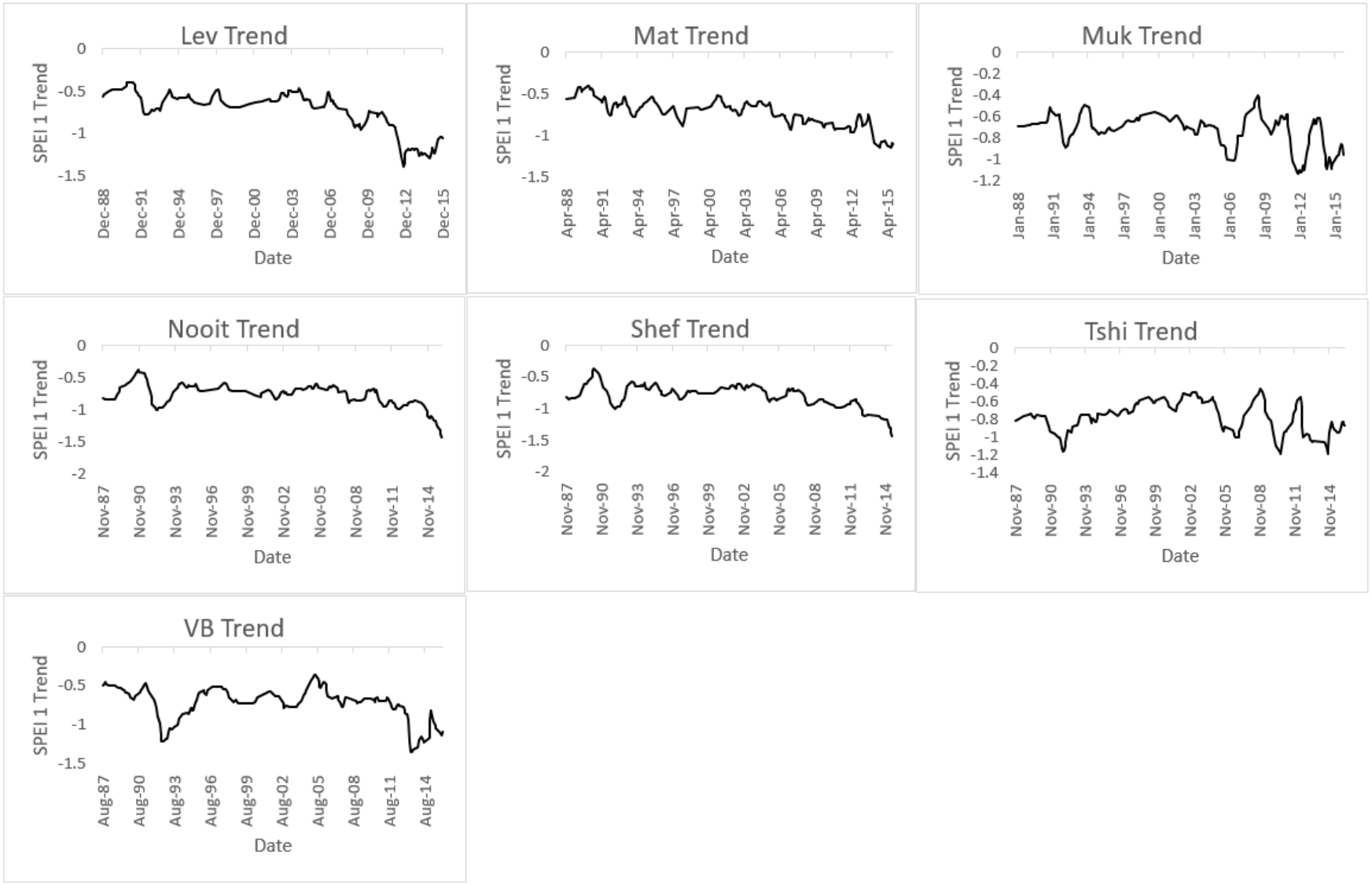

Figure A10: SPEI 1 non-linear trend.

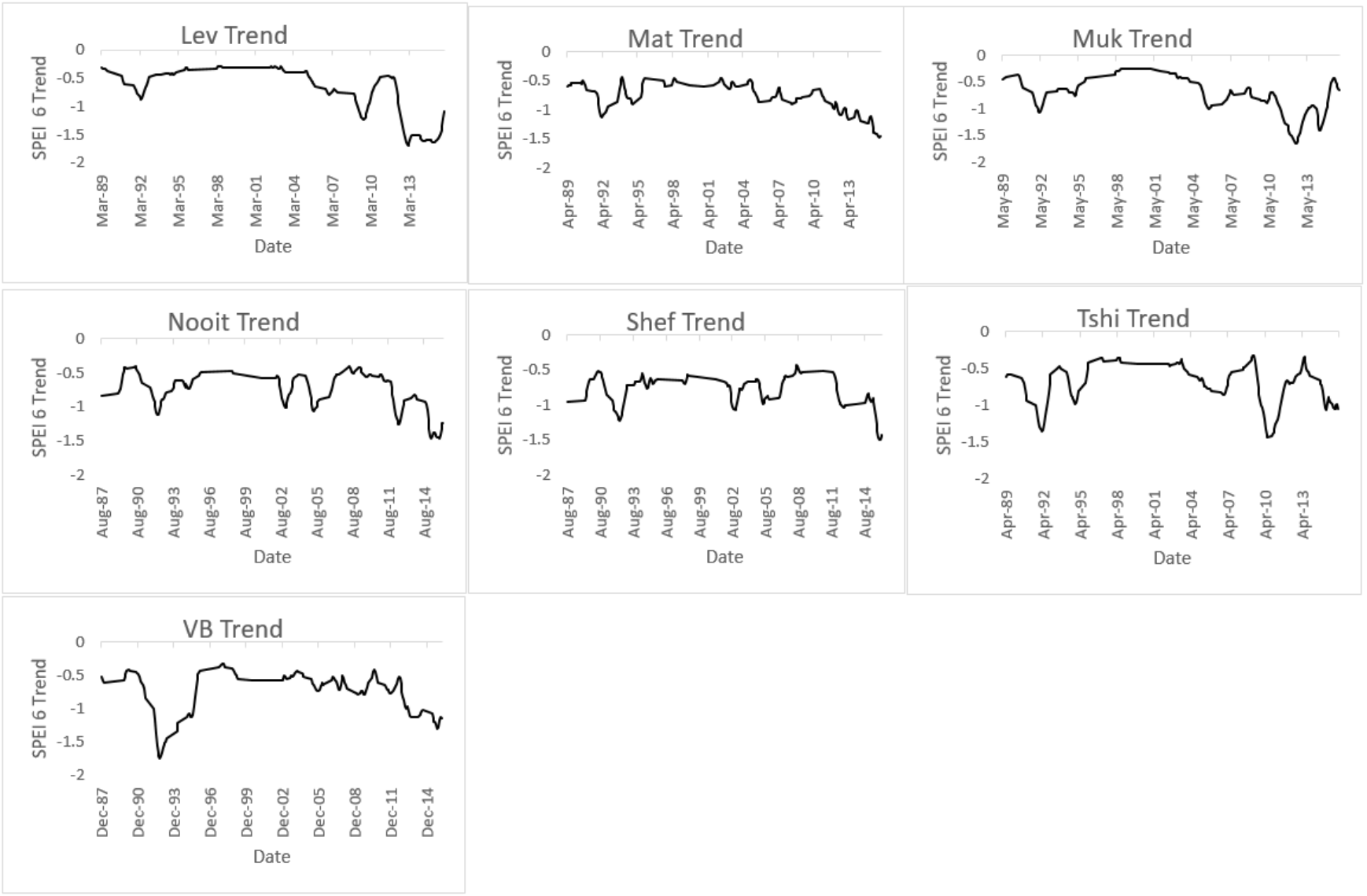

Figure A11: SPEI 6 non-linear trend.

Figure A12: SPEI 12 non-linear trend.

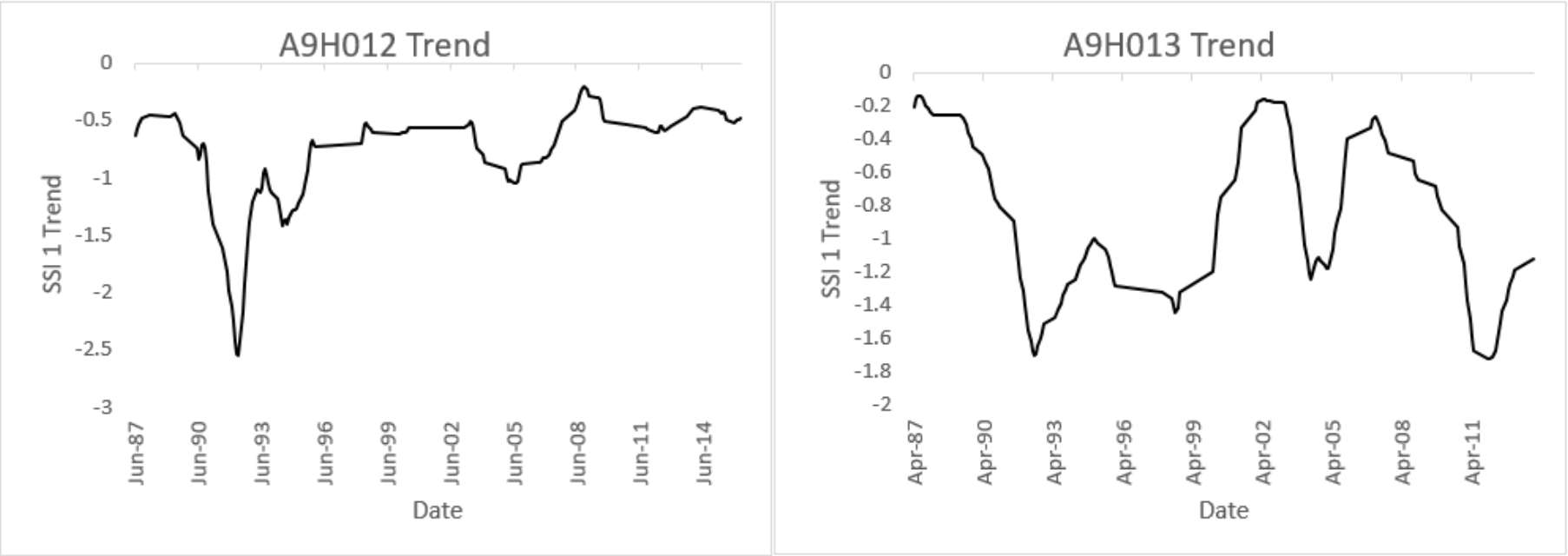

Figure A13: SSI 1 non-linear trend.

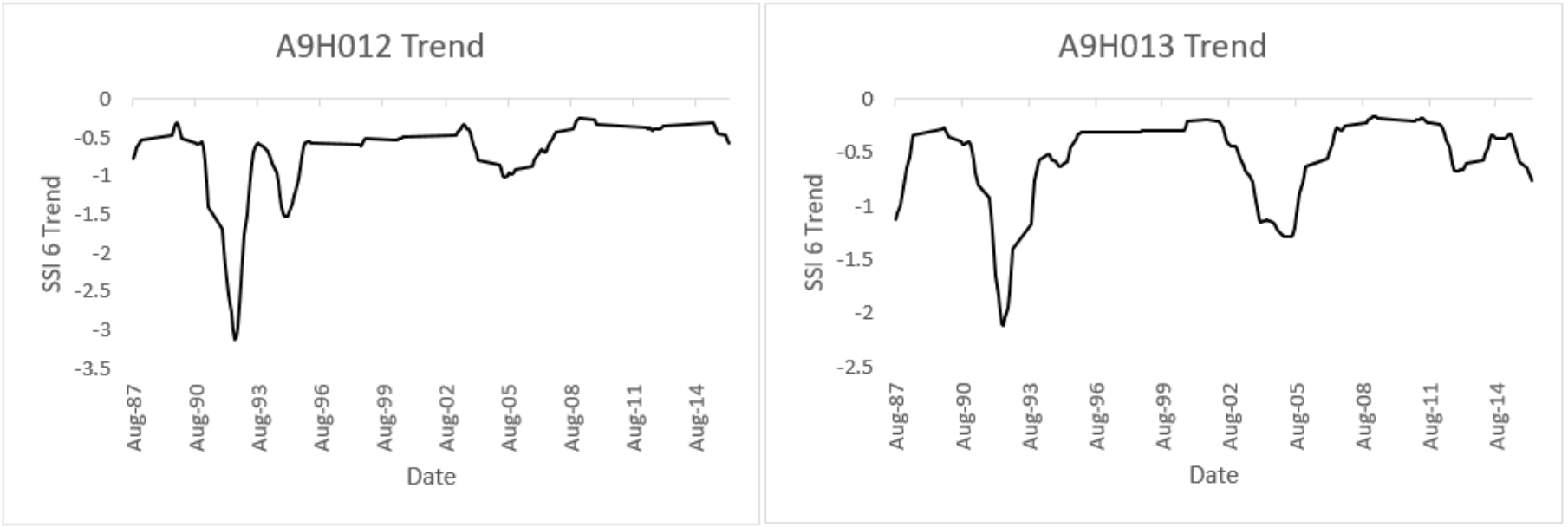

Figure A14: SSI 6 non-linear trend.

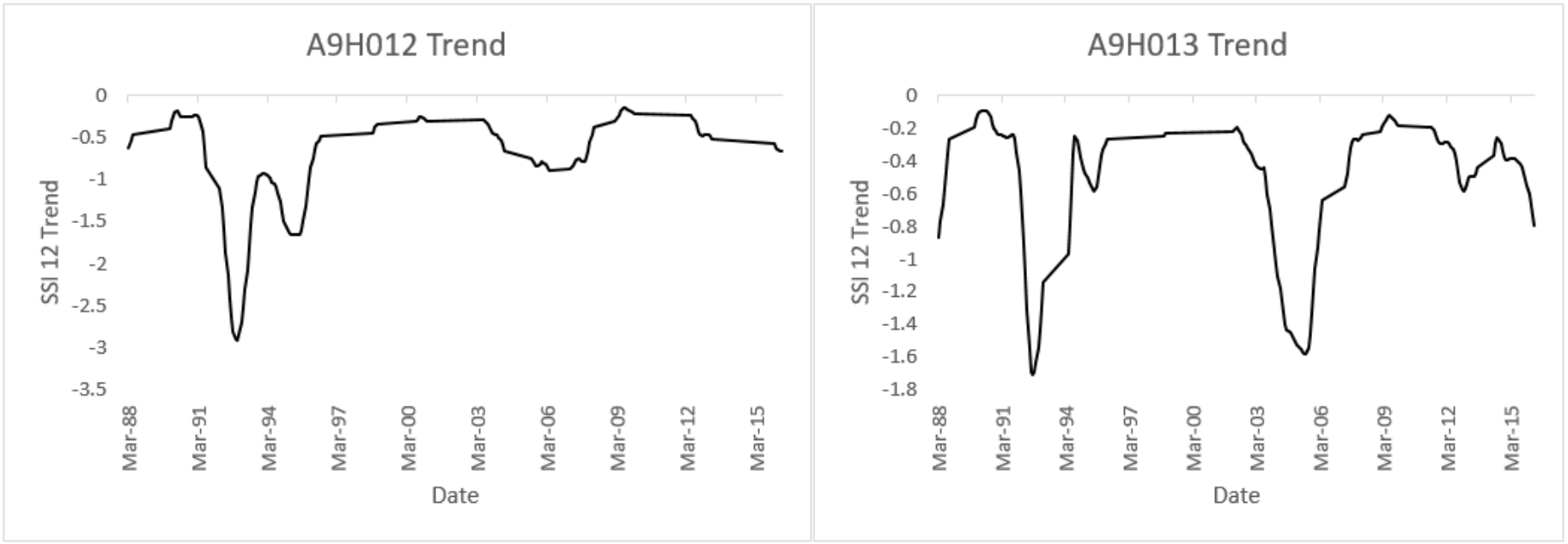

Figure A15: SSI 12 non-linear trend.

Appendix B: Chapter 5

Table B1: Duration, Severity and Intensity of drought events for different periods as per SPI, SPEI, SSI, and NADI.

			1986-1996						1996-2006						2006-2016					
Station	**Drought indicator**		**Longest**		**Strongest**		**Highest**		**Longest**		**Strongest**		**Highest**		**Longest**		**Strongest**		**Highest**	
			Year	**D**	**Year**	**S**	**Year**	**I**	**Year**	**D**	**Year**	**S**	**Year**	**I**	**Year**	**D**	**Year**	**S**	**Year**	**I**
Lev	**SPI**	**1**	1991 - 1992	15	1991 - 1992	-11.25	1989	-1.22	1998+ 2003	5	1998	-4.022	2001	-1.45	2012 - 2015	40	2012 - 2015	-50.77	2011	-1.435
		6	1991 - 1992	15	1991 - 1992	-12.94	1991 - 1992	-0.862	2004 - 2005	10	2004 - 2005	-3.94	1998 - 1999	-0.427	2011 - 2016	55	2011 - 2016	-91.34	2011 - 2016	-1.661
		12	1992 - 1993	13	1992 - 1993	-10.28	1992 - 1993	-0.791	2002 - 2003	15	2002 - 2003	-3.75	2002 - 2003	-0,25	2012 - 2016	57	2012 - 2016	-116.62	2012 - 2016	-2.046
	SPEI	**1**	1991 - 1992	12	1991 - 1992	-6.628	1991 - 1992	-1.411	1998+ 2002 - 2004	3	2005	-3.036	2001	-1.252	2012 - 2013	17	2012 - 2013	-19.125	2016	-1.639
		6	1991 - 1992	13	1991 - 1992	-11.025	1991 - 1992	-0.848	2004 - 2005	14	2004 - 2005	-6.504	2004	-0.511	2011 - 2016	57	2011 - 2016	-74.443	2011 - 2016	-1.306
		12	1994 - 1995	14	1992 - 1993	-10.669	1992 - 1993	-0.821	2002 - 2004	16	2002 - 2004	-6.187	2005	-0.434	2012 - 2016	57	2012 - 2016	-80.179	2012 - 2016	-1.407
Mat	**SPI**	**1**	1994	9	1994	-7.06	1995	-0.72	2005	6	1998	-4.32	1997	-1.47	2012 - 2016	8	2014 - 2015	-11.22	2013 - 2014	-1.186
		6	1993 - 1995	17	1991 - 1992	-16.54	1991 - 1992	-1.103	2004 - 2005	14	2004 - 2005	-11.34	2001	-0.83	2006 - 2007	13	2015 - 2016	-25.54	2015 - 2016	-2.322
		12	1990 - 1993	36	1990 - 1993	-22.67	1993 - 1995	-0.718	2002 - 2004	24	2002 - 2004	-16.11	2005	-0.951	**2011 - 2016**	54	2011 - 2016	-85.01	2011 - 2016	-1.574
	SPEI	**1**	1994	9	1994	-6.311	1995	-0.916	1999+ 2005	5	2005	-4.063	1997	-1.515	2015 - 2016	12	2015 - 2016	-12.560	2016	-1.661
		6	1993 - 1994	18	1991 - 1992	-15.656	1991 - 1992	-0.979	2004 - 2005	15	2004 - 2005	-10.089	2001	-0.702	2014 - 2016	21	2014 - 2016	-28.695	2014 - 2016	-1.366
		12	1993 - 1995	25	1991 - 1992	17.256	1991 - 1992	-1.233	2001 - 2003	22	2001 - 2003	-13.157	2005	-0.844	2012 - 2014	27	2014 - 2016	-32.116	2014 - 2016	-1.606
Muk	**SPI**	**1**	1991 - 1992	8	1991 - 1992	-5.2	1994	-1.47	2005	7	2005	-3.98	2003	-0.815	2010 - 2013	35	2010 - 2013	-35.72	2010 - 2013	-1.021
		6	1991 – 1992+ 1995	12	1991 - 1992	-7.9	1991 - 1992	-0.658	2003	6	2003	-1.76	2004	-0.43	2009 - 2014	62	2009 - 2014	-97.77	2009 - 2014	-1.578
		12	1994 - 1995	14	1992	-7.53	1992	-0.685	2002 - 2003	10	2002 - 2003	-2.29	2002 - 2003	-0.229	2009 - 2015	71	2009 - 2015	-103.17	2009 - 2015	-1.453
	SPEI	**1**	1991 - 1992	11	1991 - 1992	-9.468	1994	-1.391	2005	7	2005	-6.627	1997	-1.399	2013 - 2014	14	2013 - 2014	-13.685	2016	-1.346
		6	1991 - 1992	14	1991 - 1992	-13.489	1991 - 1992	-0.964	2004 - 2005	14	2004 - 2005	-11.790	2004 - 2005	-0.842	2011 - 2015	42	2011 - 2015	-50.521	2011 - 2015	-1.203
		12	1993 - 1995	25	1993 - 1995	-13.91	1993 - 1995	-0.556	2002 - 2003	16	2002 - 2003	-11.764	2005 - 2006	-0.843	2012 - 2014	27	2015 - 2016	-32.116	2015 - 2016	-1.606
Nooit	**SPI**	**1**	1991	7	1991	-4.92	1993	-0.99	2002 - 2003	6	2002 - 2003	-4.99	2001	-1.063	2011 - 2012	10	2011 - 2012	-5.78	2001	-1.46
		6	1991 - 1992	15	1991 - 1992	-19.91	1991 - 1992	-1.327	2004 - 2005	14	2004 - 2005	-14.22	2004 - 2005	-1.016	2011 - 2012	14	2014 - 2015	-15.97	2014 - 2015	-1.331
		12	1980 - 1991	24	1991 - 1993	-15.42	1987	-0.88	2002 - 2004	24	2002 - 2004	-20.07	2005 - 2006	-1.255	2010 - 2012	28	2014 - 2016	-26.93	2014 - 2016	-1.347
	SPEI	**1**	1991	7	1992	-5.103	1989	-1.178	2002 – 2003+ 2005	6	2002 - 2003	-4.667	2001	-1.355	2011 - 2012	10	2011 - 2012	08.929	2016	-3.061
		6	1991 - 1993	17	1991 - 1993	-17.789	1991 - 1993	-1.046	2004 - 2005	15	2004 - 2005	-13.71	2004 - 2005	-0.914	2014 - 2016	25	2014 - 2016	-33.703	2011 - 1012	-1.14
		12	1992 - 1993	21	1992 - 1993	-15.614	1992 - 1993	-0.744	2002 - 2004	23	2002 - 2004	-19.449	2002 - 2004	-0.846	2015 - 2016	20	2015 - 2016	-35.25	2015 - 2016	-1.768
Shef	**SPI**	**1**	1991 - 1992	15	1991 - 1992	-8.82	1987 - 1988	-1.08	2005	8	2005	-3.84	1997+ 2000	-1.16	2015	8	2015 - 2016	-8.04	2015 - 2016	-1.34
		6	1989 - 1991	28	1989 - 1991	-21.25	1987	-1.134	2004 - 2005	15	2004 - 2005	-13.1	2004 - 2005	-0.873	2014 - 2016	24	2014 - 2016	-22.4	2014 - 2016	-0.933
		12	1990 -1993	56	1990 -1993	-40.25	1987	-0.762	2002 - 2006	36	2002 - 2006	-32.43	2002 - 2006	-0.901	2007 - 2009	26	2012 - 2016	-22.23	2012 - 2016	-1.112
	SPEI	**1**	1994	7	1994	-4.615	1991	-1.351	2001 - 2001	6	2005	-5.639	2003	-1.310	2015	8	2015 - 2016	-10.295	2011	-2.182
		6	1991 - 1992	17	1991 - 1992	-19.879	1991 - 1992	-1.169	2004 - 2005	16	2004 - 2005	-14.476	2004 - 2005	-0.905	2014 - 2016	25	2014 - 2016	-28.901	2014 - 2016	-1.156

		12	1989 - 1993	50	1989 - 1993	-32.079	1987 1988	-0.8	2002 - 2004	25	2002 - 2004	-22.881	2002 - 2004	-0.915	2007 - 2009	24	2015 - 2016	-28.626	2015 - 2016	-1.507
Tshi	**SPI**	**1**	1991 - 1992	8	1991 - 1992	-7.68	1991	-1.75	1998	5	1998	-2.78	2004	-1.85	2015	4	2009	-3.99	2009	-1.995
		6	1991 - 1992	13	1991 - 1992	-15.58	1991 - 1992	-1.199	2004 - 2005	10	2004 - 2005	-5.89	2005	-5.43	2008 - 2010	24	2008 - 2010	-21.12	2010 - 2011	-1.585
		12	1990 - 1993	17	1990 - 1993	-18.31	1990 - 1993	-1.077	2002 - 2004	15	2002 - 2004	-5.38	2005	-0.693	2008 -2012	60	2008 -2012	-63.43	2015 - 2016	-1.288
	SPEI	**1**	1992	8	1991	-9.242	1991	-1.303	1998	5	1998	-3.453	1997	-1.445	2015 - 2016	12	2015 - 2016	-10.405	2013	-2.808
		6	1991 -1992	15	1991 -1992	-17.854	1991 -1992	-1.190	2004 - 2005	14	2004 - 2005	-10.490	2004 - 2005	-0.749	2008 - 2010+ 2014 - 2016	25	2014 - 2016	-16.957	2010 - 2011	-1.302
		12	1994 - 1995	16	1992 - 1993	-18.502	1992 - 1993	-1.322	2003 - 2004	15	2005 - 2006	-8.644	2005 - 2006	-0.786	2009 - 2013	60	2009 - 2013	-59.997	2015 - 2016	-1.272
VB	**SPI**	**1**	1994	11	1991 - 1992	-10.66	1988	-2.08	1998	5	1998	-3.61	2002	-2.48	2014	8	2014	-7.02	2010	-1.173
		6	1994 - 1995	13	1991 - 1992	-19.81	1991 - 1992	-1.651	2004 - 2005	10	2004 - 2005	-6.95	2004 - 2005	-0.695	2014 - 2016	22	2014 - 2016	-25.24	2014 - 2016	-1.147
		12	1991 - 1992	14	1991 - 1992	-22.86	1994 - 1995	-0.782	2002 - 2004	21	2002 - 2004	-8.73	2005	-0.665	2006 - 2010	29	2014 - 2016	-26.05	2014 - 2016	-1.133
	SPEI	**1**	1995	11	1992	-11.708	1992	-1.464	2005 - 2006	11	2005 - 2006	-4.46	2003	-1.037	2012 - 2013	11	2012 - 2013	-9.114	2016	-1.162
		6	1992 - 1993	14	1992 - 1993	-21.654	1992 - 1993	-1.547	2005 - 2006	14	2005 - 2006	-9.763	2005 - 2006	-0.697	2015 - 2016	17	2015 - 2016	-20.782	2015 - 2016	-1.223
		12	1992 - 1993	14	1992 - 1993	-26.058	1992 - 1993	-1.861	2003 - 2004	16	2003 - 2004	-8.535	2003 - 2004	-0.534	2011 - 2013	24	2011 - 2013	-20.484	2015 - 2016	-1.187
A9H012	**SSI**	**1**	1992	15	1992	-32.7	1992	-2.18	2005	11	2005	-12.29	2005	-1.117	2015 - 2016	10	2015 - 2016	-5.72	2007	-1.375
		6	1992 - 1996	53	1992 - 1996	-73.1	1992 - 1996	-1.379	2003 - 2005	22	2003 - 2005	-15.52	2003 - 2005	-0.706	2006 - 2007	14	2006 - 2007	-8.62	2016	-0.716
		12	1992 - 1996	53	1992 - 1996	-81.06	1992 - 1996	-1.529	2003 -2004	13	2003 -2004	-5.46	2003 -2004	-0.42	2007 - 2008	13	2007 - 2008	-9.66	2007 - 2008	-0.743
A9H013	**SSI**	**1**	1992	17	1992	-23.52	1992	-1.384	2005	35	2005	-32.7	2005	-0.934	2015 - 2016	12	2015 - 2016	-11.94	2015 - 2016	-0.995
		6	1988	16	1988	-14.78	1991 - 1992	-1.896	2004 - 2006	25	2004 - 2006	-28.65	2004 - 2006	-1.146	2012 - 2013	16	2012 - 2013	-8.76	2015 - 2016	-0.932
		12	1989 - 1993	40	1989 - 1993	-25.31	1989 - 1993	-0.633	2002 - 2006	52	2002 - 2006	-46.68	2002 - 2006	-0.894	2011 - 2016	58	2011 - 2016	-15.27	2011 - 2016	-0.527

Table B2: Drought frequency for different periods as per SPI, SPEI, SSI, and NADI.

			1986-1996				1996-2006				2006-2016			
Station	**Drought indicator**	**Timescale**	**Year**	**D**	**D_{total}**	**F (%)**	**Year**	**D**	**D_{total}**	**F (%)**	**Year**	**D**	**D_{total}**	**F (%)**
KA	SPI	1	1994	11	120	9,2	2004 - 2005	6	122	4,9	2012	8	109	7,3
		6	1992 - 1995	13	115	11,3	2004 - 2006	13	120	10,8	2011 - 2012	15	121	12,4
		12	1989 - 1990	19	108	17,6	2002 - 2004	24	120	20,0	2015- 2016	21	121	17,4
	SPEI	1	1994	13	120	10,8	1998 + 2003	5	122	4,1	2012	8	109	7,3
		6	1991 - 1992	15	115	13,0	2004 - 2005	16	120	13,3	2014 - 2016	22	121	18,2
		12	1994 - 1995	23	108	21,3	2003 - 2004	16	120	13,3	2015 - 2016	20	121	16,5
A9H006	SSI	1	1991 - 1995	58	120	48,3	2004 - 2005	15	122	12,3	2011 - 2012	17	109	15,6
		6	1990 - 1996	69	115	60,0	2004 - 2005	14	120	11,7	2014 - 2016	21	121	17,4
		12	1989 - 1995	82	108	75,9	1996 - 1998	22	120	18,3	2015 - 2016	14	121	11,6
	NADI	1	1987 - 1988	9	120	7,5	2005	5	122	4,1	2008	5	119	4,2
Lev	SPI	1	1991 - 1992	15	120	12,5	1998+ 2003	5	122	4,1	2012 - 2015	40	109	36,7
		6	1991 - 1992	15	115	13,0	2004 - 2005	10	120	8,3	2011 - 2016	55	121	45,5
		12	1992 - 1993	13	108	12,0	2002 - 2003	15	120	12,5	2012 - 2016	57	121	47,1
	SPEI	1	1991 - 1992	12	120	10,0	1998+ 2002 - 2004	3	122	2,5	2012 - 2013	17	109	15,6
		6	1991 - 1992	13	115	11,3	2004 - 2005	14	120	11,7	2011 - 2016	57	121	47,1
		12	1994 - 1995	14	108	13,0	2002 - 2004	16	120	13,3	2012 - 2016	57	121	47,1
Mat	SPI	1	1994	9	120	7,5	2005	6	122	4,9	2012 - 2016	8	109	7,3
		6	1993 - 1995	17	115	14,8	2004 - 2005	14	120	11,7	2006 - 2007	13	121	10,7
		12	1990 - 1993	36	108	33,3	2002 - 2004	24	120	20,0	2011 - 2016	54	121	44,6
	SPEI	1	1994	9	120	7,5	1999+ 2005	5	122	4,1	2015 - 2016	12	109	11,0
		6	1993 - 1994	18	115	15,7	2004 - 2005	15	120	12,5	2014 - 2016	21	121	17,4
		12	1993 - 1995	25	108	23,1	2001 - 2003	22	120	18,3	2012 - 2014	27	121	22,3
Muk	SPI	1	1991 - 1992	8	120	6,7	2005	7	122	5,7	2010 - 2013	35	109	32,1
		6	1991 – 1992+ 1995	12	115	10,4	2003	6	120	5,0	2009 - 2014	62	121	51,2
		12	1994 - 1995	14	108	13,0	2002 - 2003	10	120	8,3	2009 - 2015	71	121	58,7
	SPEI	1	1991 - 1992	11	120	9,2	2005	7	122	5,7	2013 - 2014	14	109	12,8
		6	1991 - 1992	14	115	12,2	2004 - 2005	14	120	11,7	2011 - 2015	42	121	34,7
		12	1993 - 1995	25	108	23,1	2002 - 2003	16	120	13,3	2012 - 2014	27	121	22,3
Nooit	SPI	1	1991	7	120	5,8	2002 - 2003	6	122	4,9	2011 - 2012	10	109	9,2
		6	1991 - 1992	15	115	13,0	2004 - 2005	14	120	11,7	2011 - 2012	14	121	11,6
		12	1980 - 1991	24	108	22,2	2002 - 2004	24	120	20,0	2010 - 2012	28	121	23,1

		1	1991	7	120	5,8	2002 – 2003+ 2005	6	122	4,9	2011 - 2012	10	109	9,2
		6	1991 - 1993	17	115	14,8	2004 - 2005	15	120	12,5	2014 - 2016	25	121	20,7
	SPEI	12	1992 - 1993	21	108	19,4	2002 - 2004	23	120	19,2	2015 - 2016	20	121	16,5
		1	1991 - 1992	15	120	12,5	2005	8	122	6,6	2015	8	109	7,3
		6	1989 - 1991	28	115	24,3	2004 - 2005	15	120	12,5	2014 - 2016	24	121	19,8
	SPI	12	1990 -1993	56	108	51,9	2002 - 2006	36	120	30,0	2007 - 2009	26	121	21,5
		1	1994	7	120	5,8	2001 - 2001	6	122	4,9	2015	8	109	7,3
		6	1991 - 1992	17	115	14,8	2004 - 2005	16	120	13,3	2014 - 2016	25	121	20,7
Shef	SPEI	12	1989 - 1993	50	108	46,3	2002 - 2004	25	120	20,8	2007 - 2009	24	121	19,8
		1	1991 - 1992	8	120	6,7	1998	5	122	4,1	2015	4	109	3,7
		6	1991 - 1992	13	115	11,3	2004 - 2005	10	120	8,3	2008 - 2010	24	121	19,8
	SPI	12	1990 - 1993	17	108	15,7	2002 - 2004	15	120	12,5	2008 -2012	60	121	49,6
		1	1992	8	120	6,7	1998	5	122	4,1	2015 - 2016	12	109	11,0
		6	1991 -1992	15	115	13,0	2004 - 2005	14	120	11,7	2008 - 2010+ 2014 - 2016	25	121	20,7
Tshi	SPEI	12	1994 - 1995	16	108	14,8	2003 - 2004	15	120	12,5	2009 - 2013	60	121	49,6
		1	1994	11	120	9,2	1998	5	122	4,1	2014	8	109	7,3
		6	1994 - 1995	13	115	11,3	2004 - 2005	10	120	8,3	2014 - 2016	22	121	18,2
	SPI	12	1991 - 1992	14	108	13,0	2002 - 2004	21	120	17,5	2006 - 2010	29	121	24,0
		1	1995	11	120	9,2	2005 - 2006	11	122	9,0	2012 - 2013	11	109	10,1
		6	1992 - 1993	14	115	12,2	2005 - 2006	14	120	11,7	2015 - 2016	17	121	14,0
VB	SPEI	12	1992 - 1993	14	108	13,0	2003 - 2004	16	120	13,3	2011 - 2013	24	121	19,8
		1	1992	15	120	12,5	2005	11	122	9,0	2015 - 2016	10	109	9,2
		6	1992 - 1996	53	115	46,1	2003 - 2005	22	120	18,3	2006 - 2007	14	121	11,6
A9H012	SSI	12	1992 - 1996	53	108	49,1	2003 -2004	13	120	10,8	2007 - 2008	13	121	10,7
		1	1992	17	120	14,2	2005	35	122	28,7	2015 - 2016	12	109	11,0
		6	1988	16	115	13,9	2004 - 2006	25	120	20,8	2012 - 2013	16	121	13,2
A9H013	SSI	12	1989 - 1993	40	108	37,0	2002 - 2006	52	120	43,3	2011 - 2016	58	121	47,9

*D – Duration, D_{total} – period total duration, F – Frequency

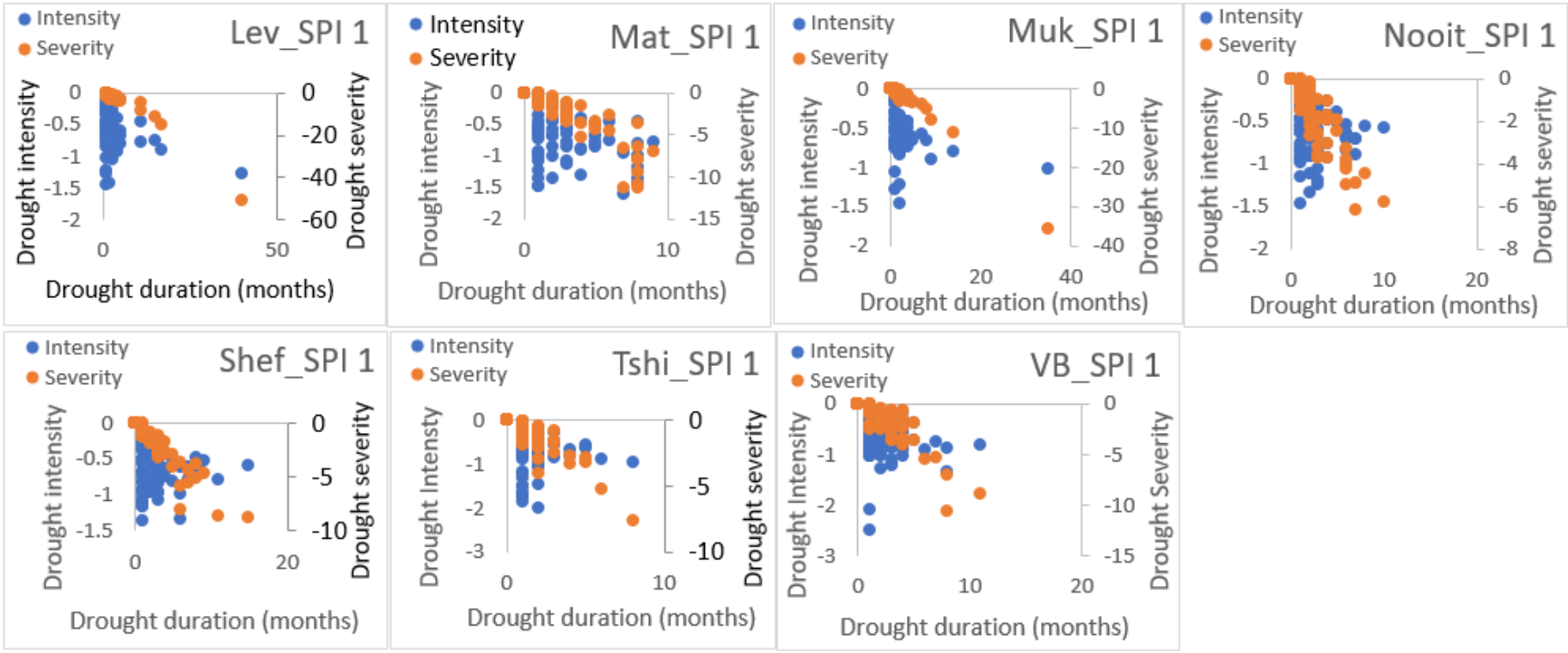

Figure B3: SPI 1 Drought-intensity-severity curves.

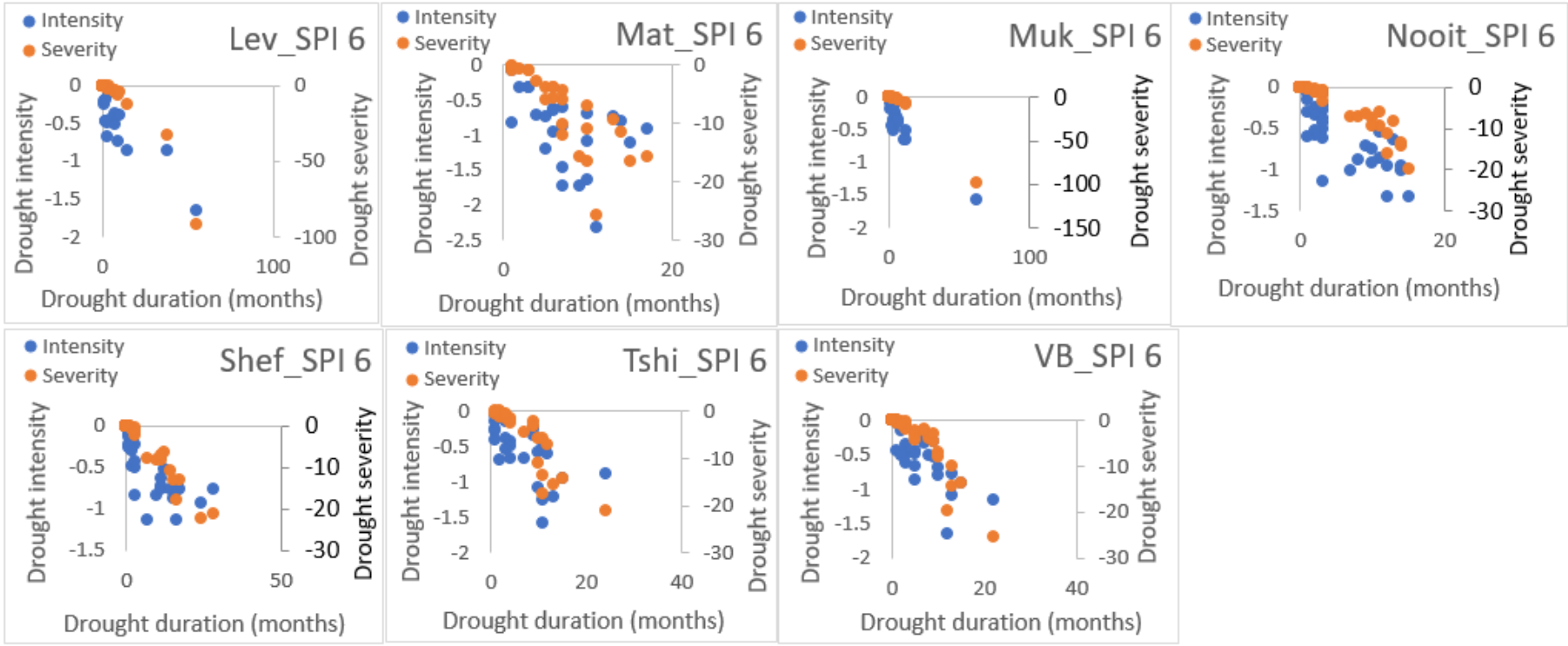

Figure B4: SPI 6 Drought-intensity-severity curves.

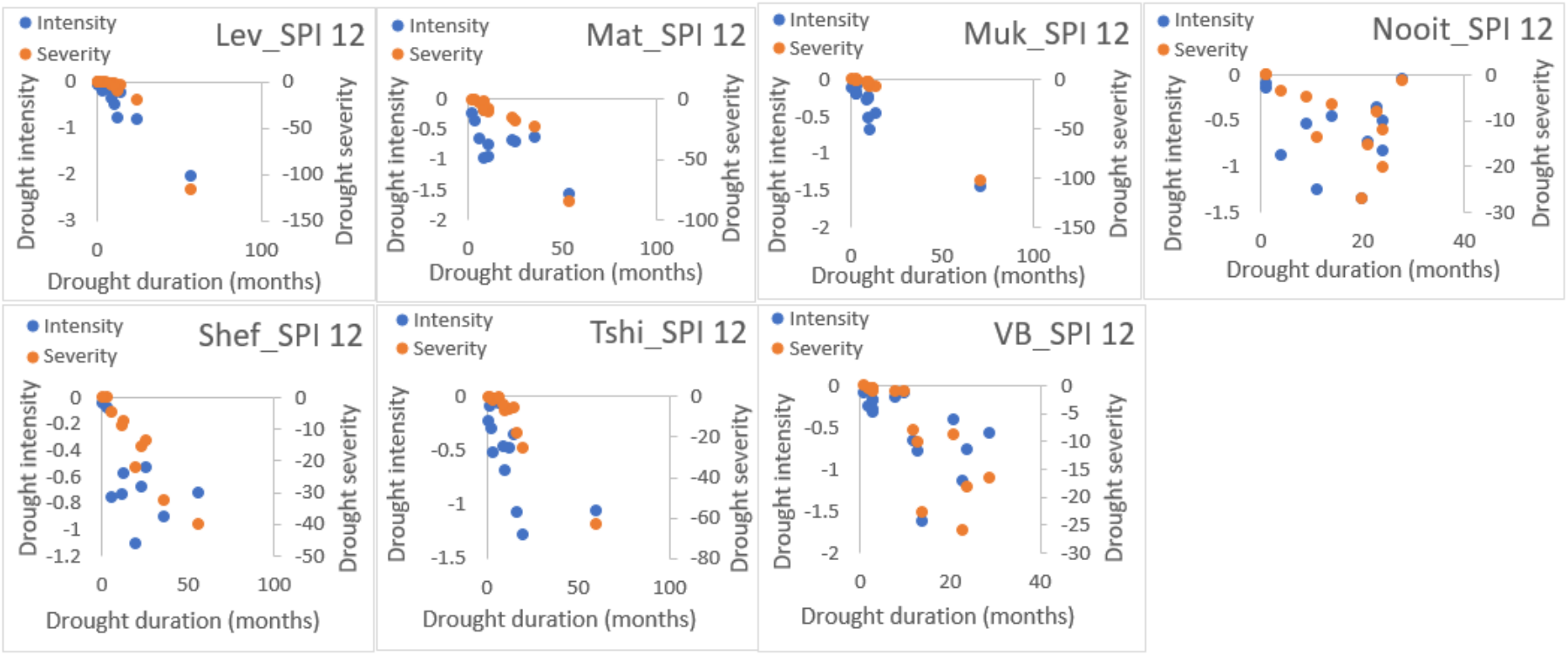

Figure B5: SPI 12 Drought-intensity-severity curves.

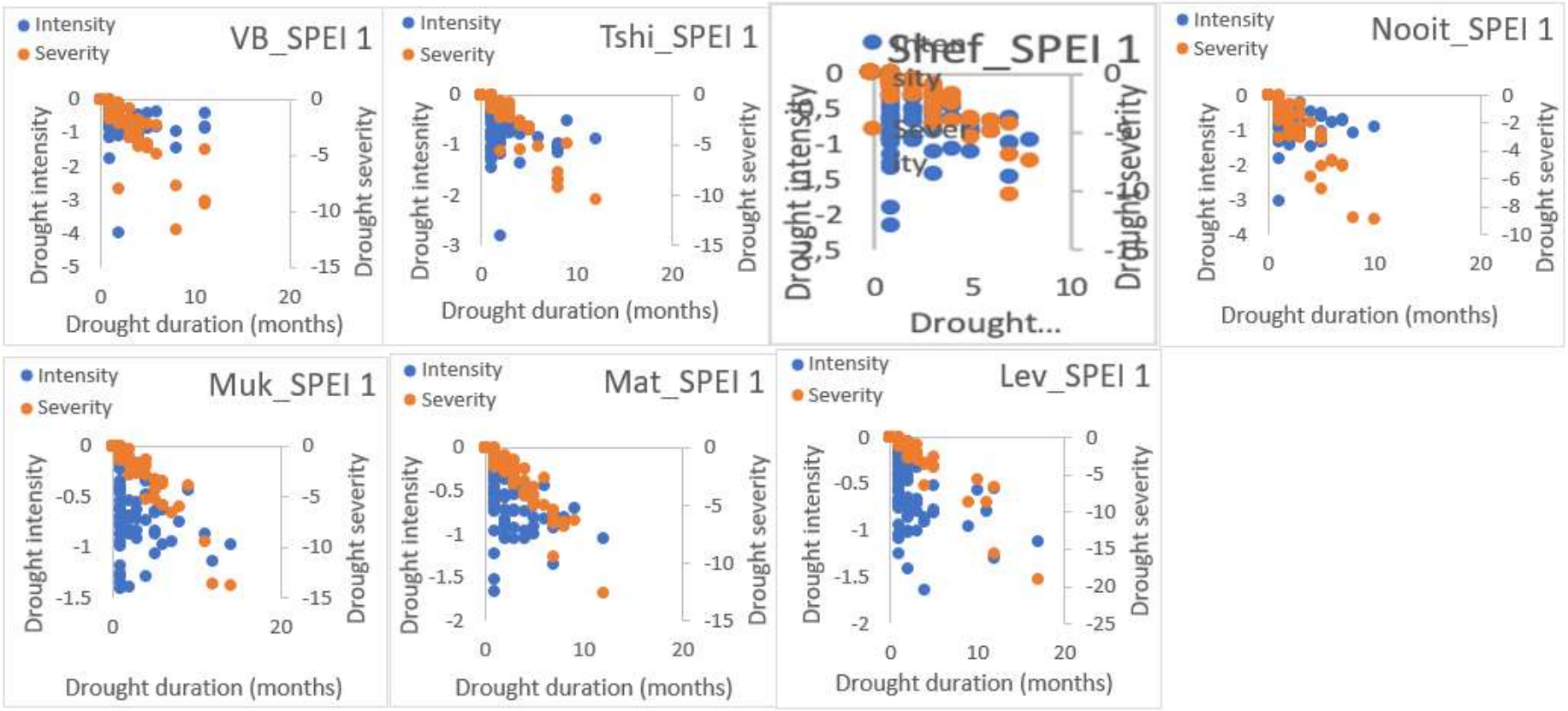

Figure B6: SPEI 1 Drought-intensity-severity curves.

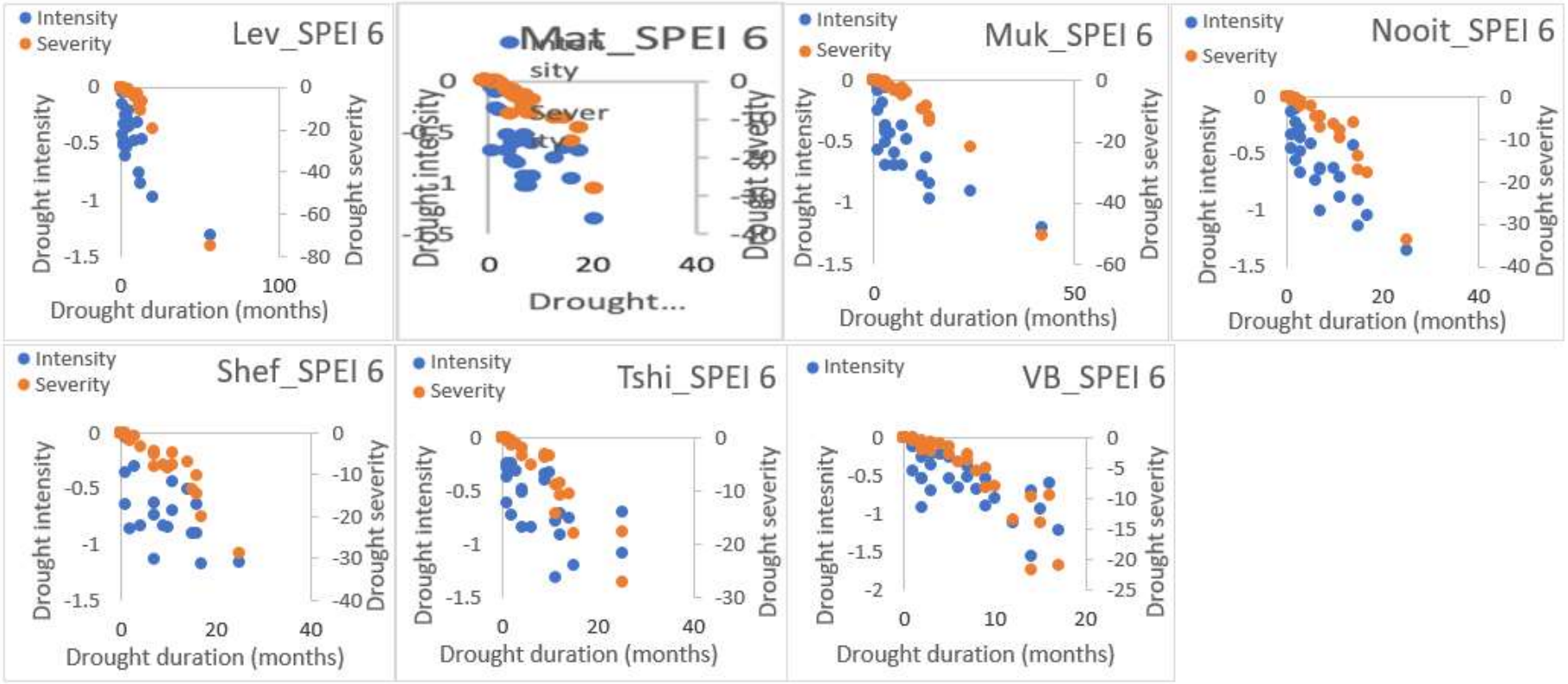

Figure B7: SPEI 6 Drought-intensity-severity curves.

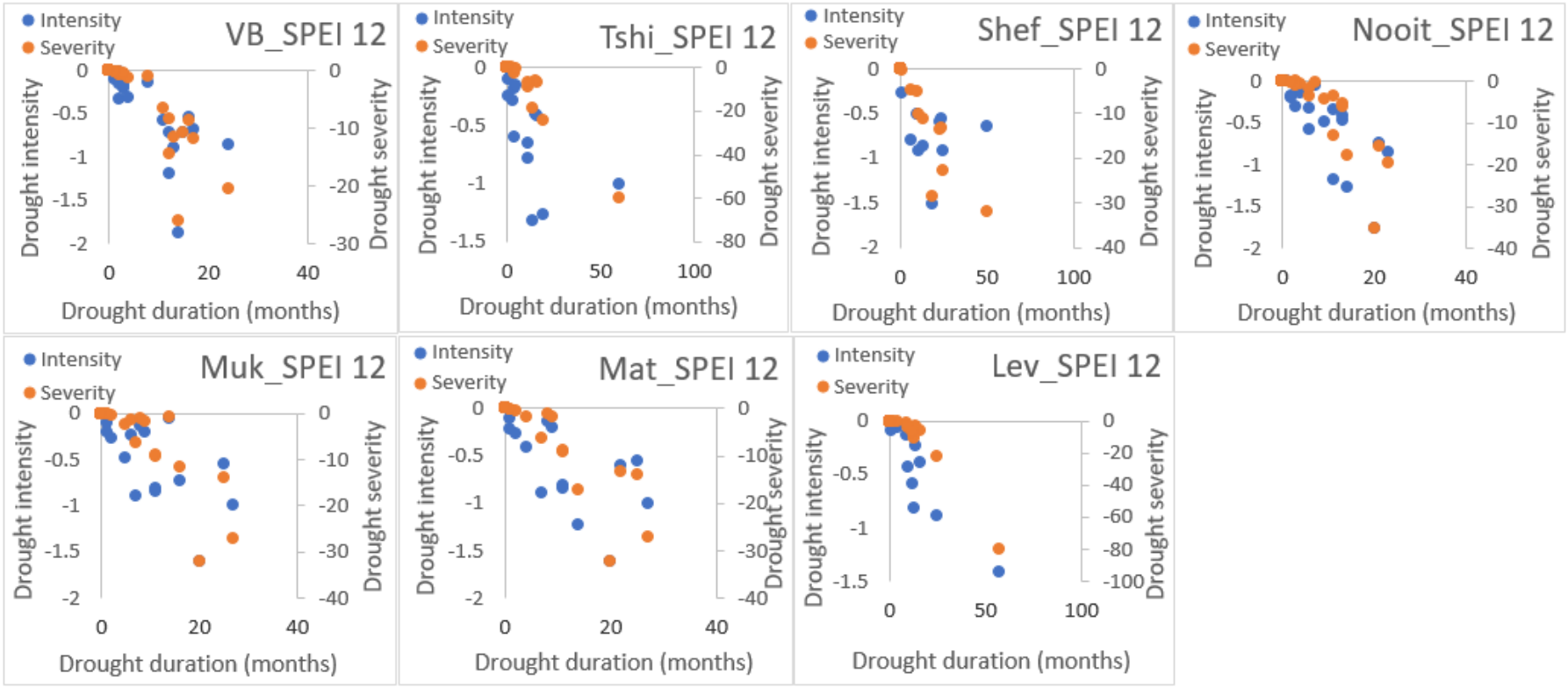

Figure B8: SPEI 12 Drought-intensity-severity curves.

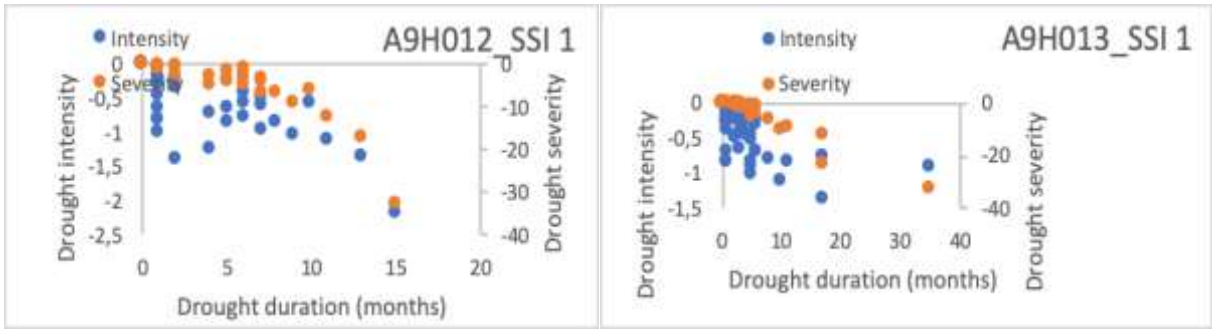

Figure B9: SSI 1 Drought-intensity-severity curves.

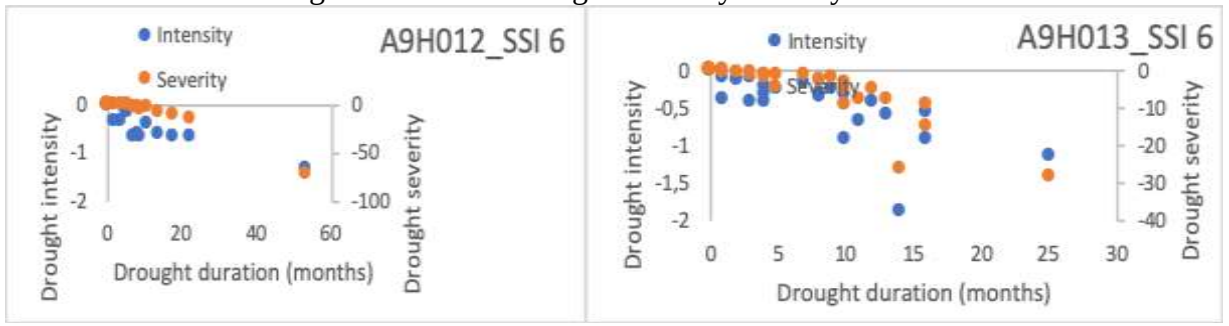

Figure B10: SSI 6 Drought-intensity-severity curves.

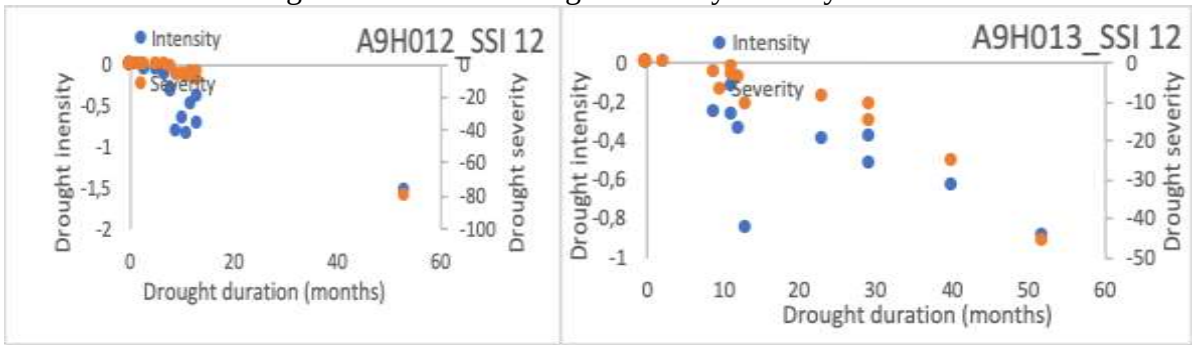

Figure B11: SSI 12 Drought-intensity-severity curves.

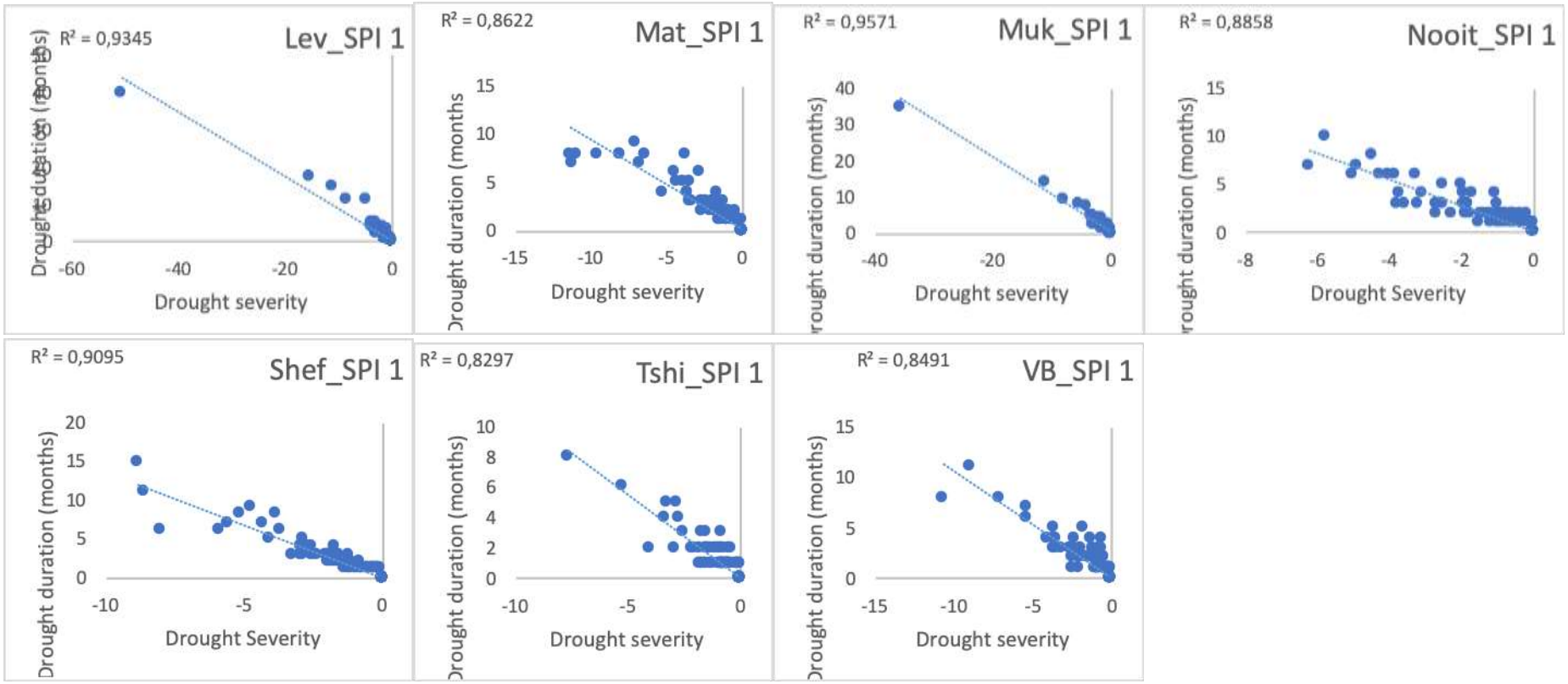

Figure B12: SPI 1 duration-severity curves.

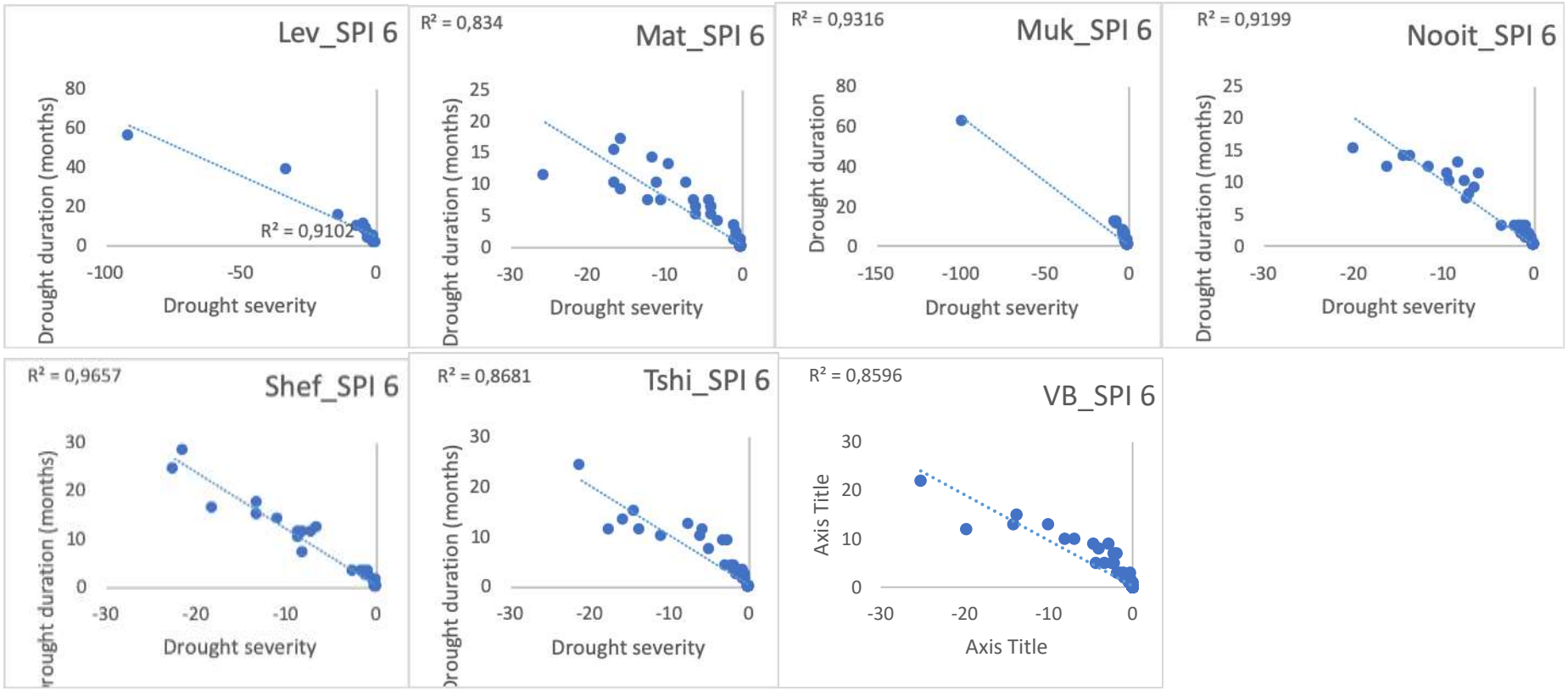

Figure B13: SPI 6 duration-severity curves.

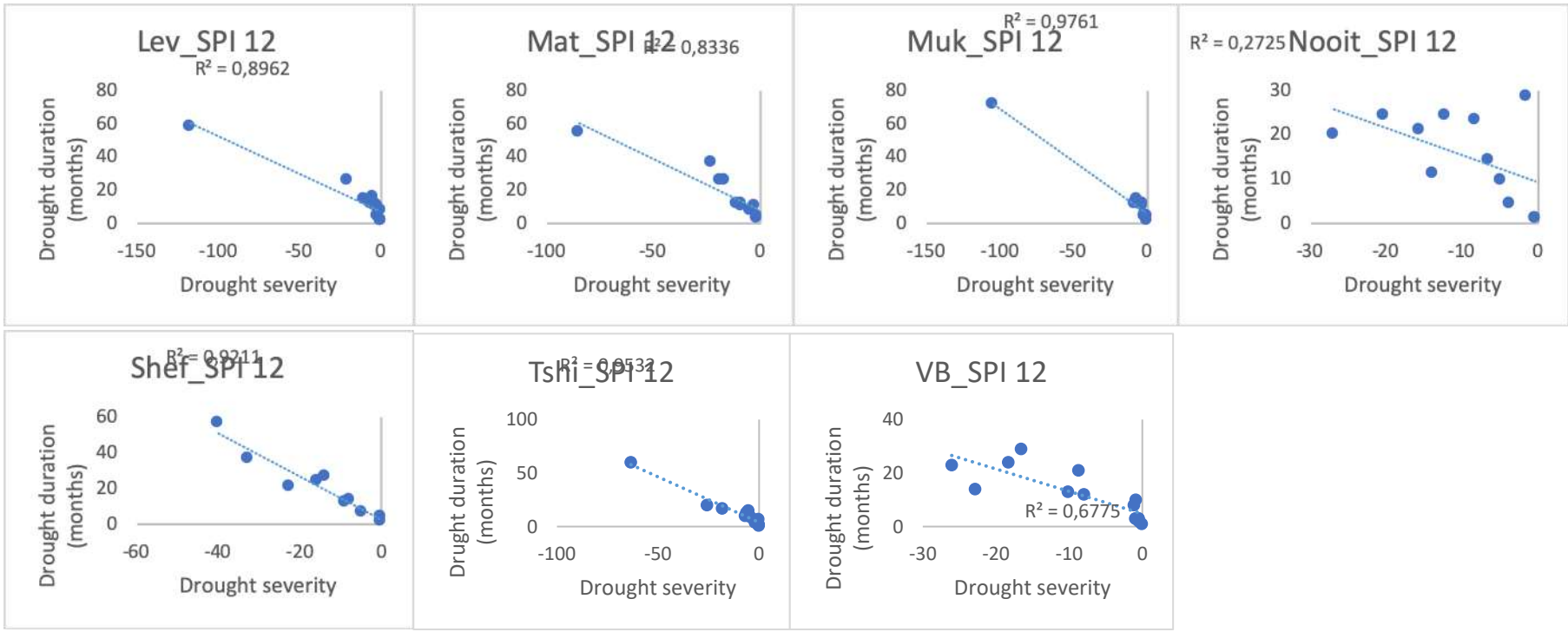

Figure B14: SPI 12 duration-severity curves.

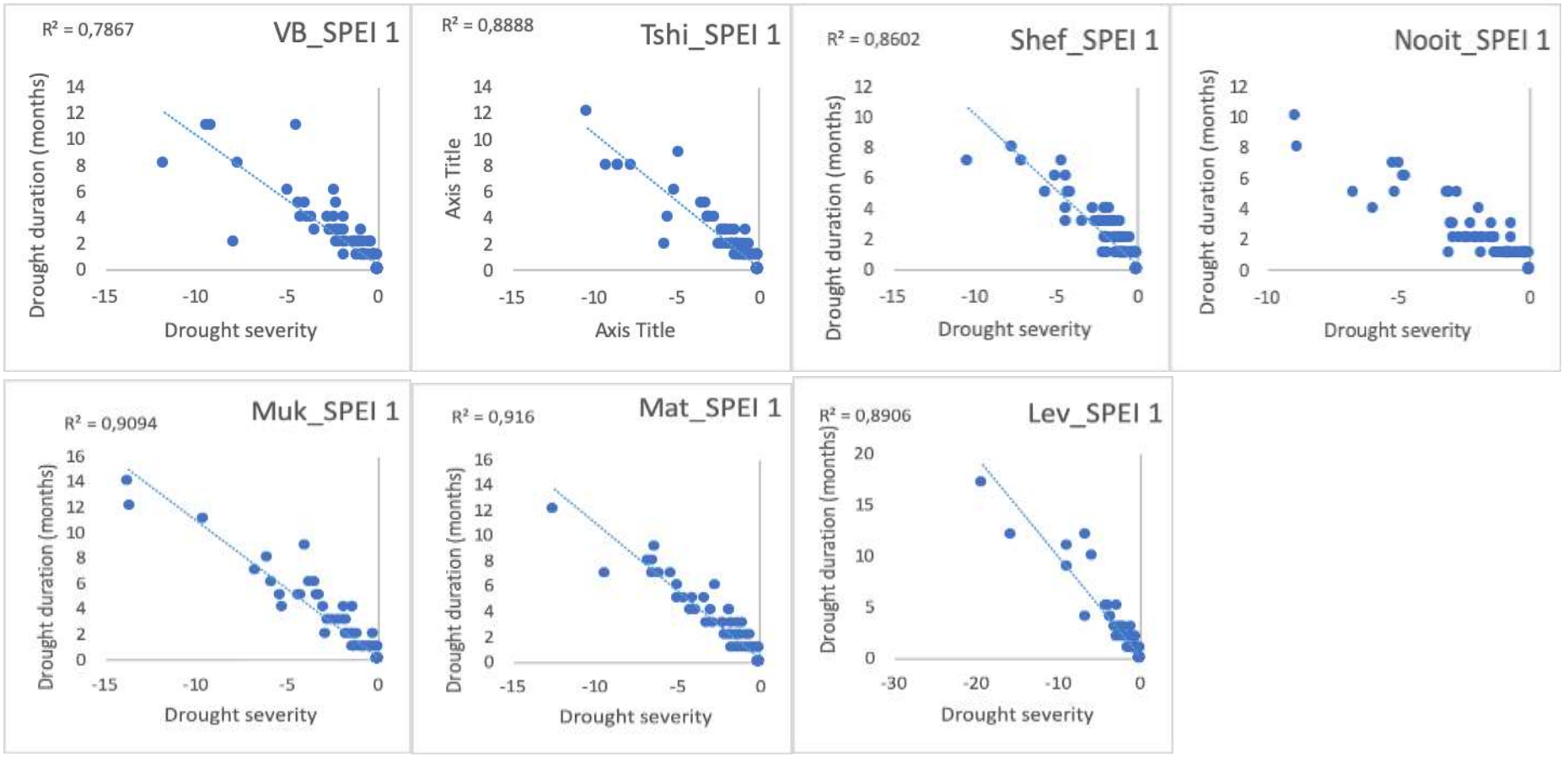

Figure B15: SPEI 1 duration-severity curves.

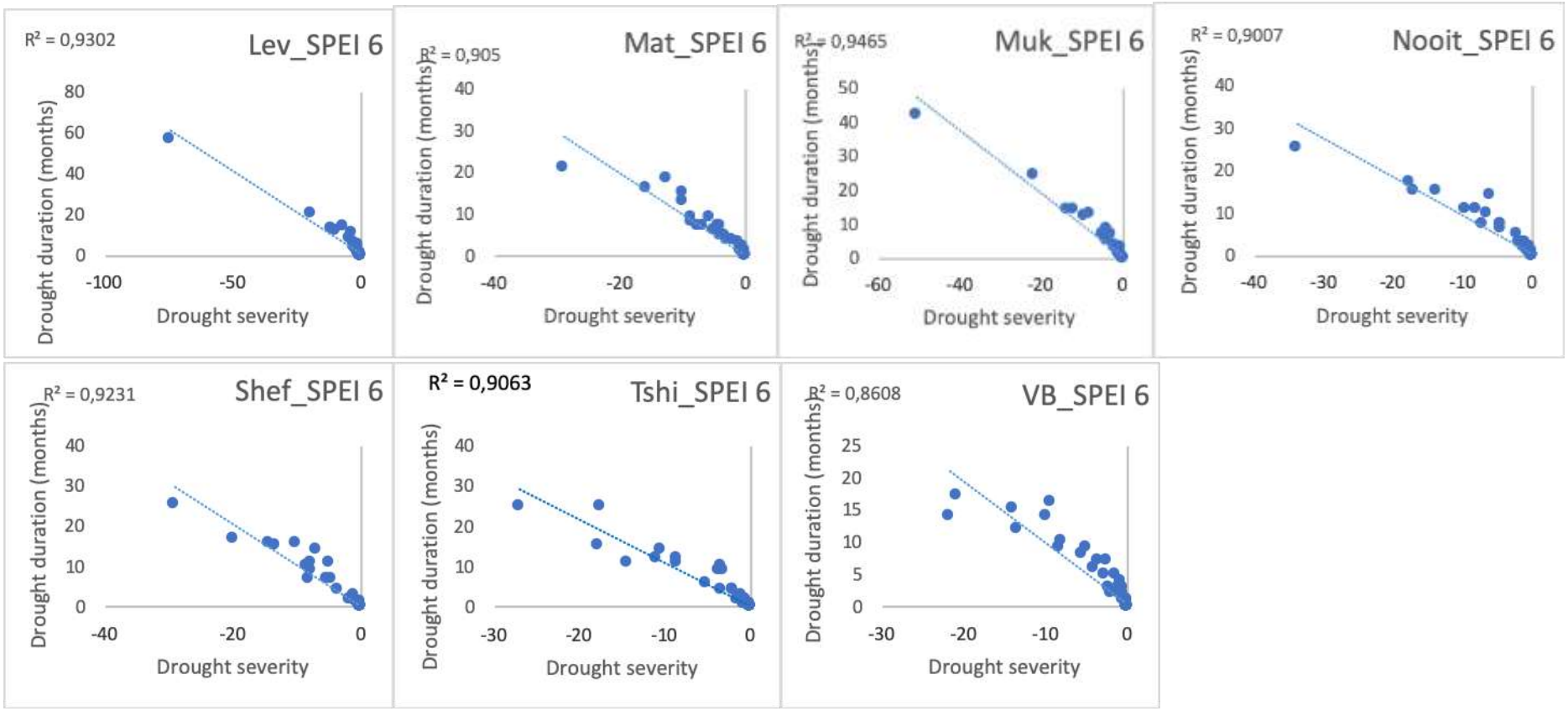

Figure B16: SPEI 6 duration-severity curves.

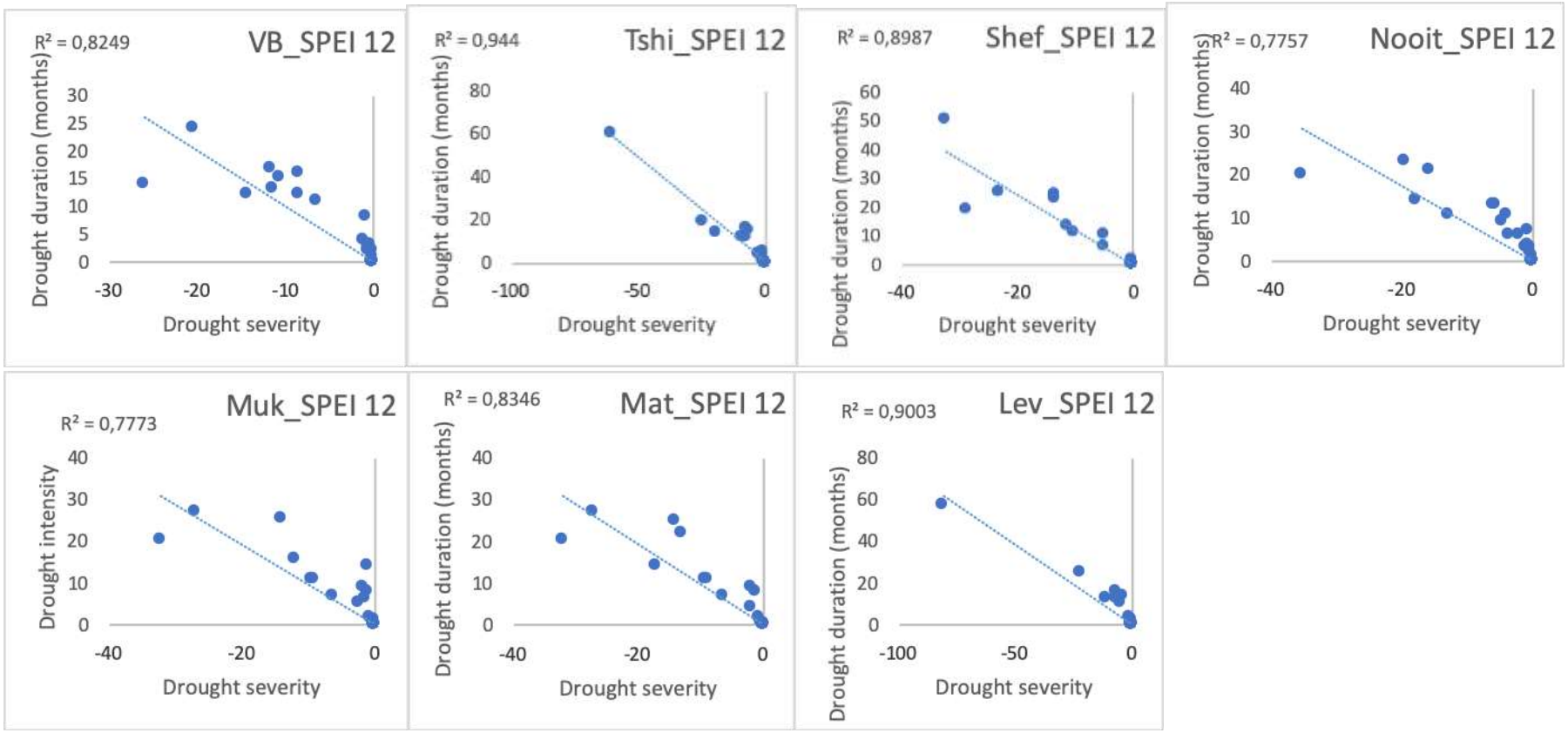

Figure B17: SPEI 12 duration-severity curves.

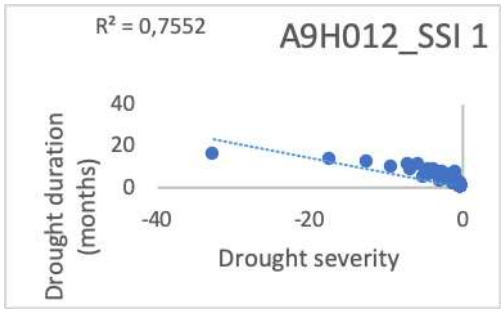

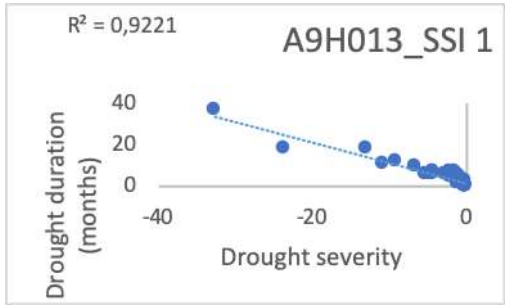

Figure B18: SSI 1 duration-severity curves.

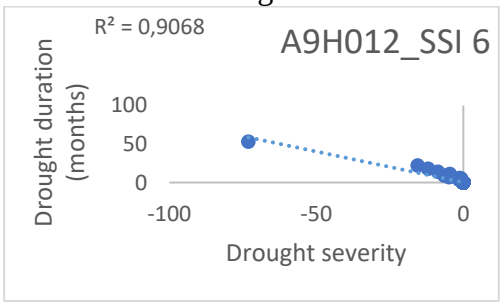

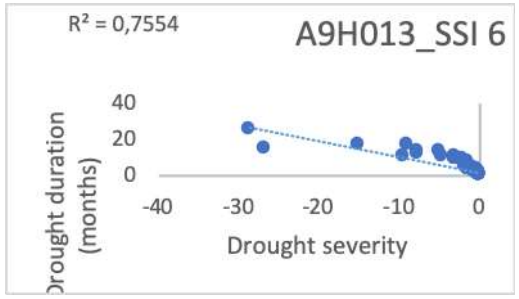

Figure B19: SSI 6 duration-severity curves.

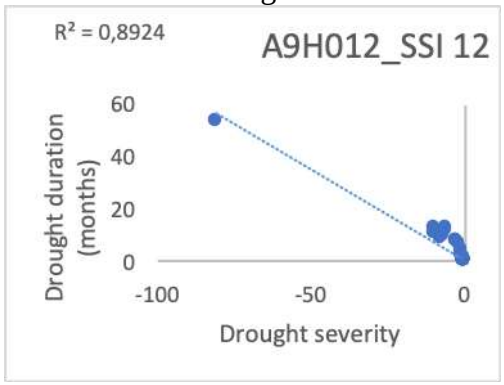

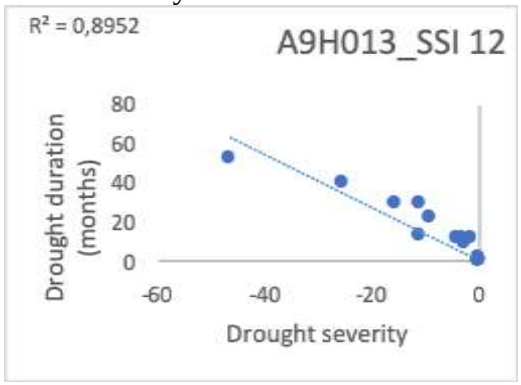

Figure B20: SSI 12 duration-severity curves.

Appendix C: Chapter 6

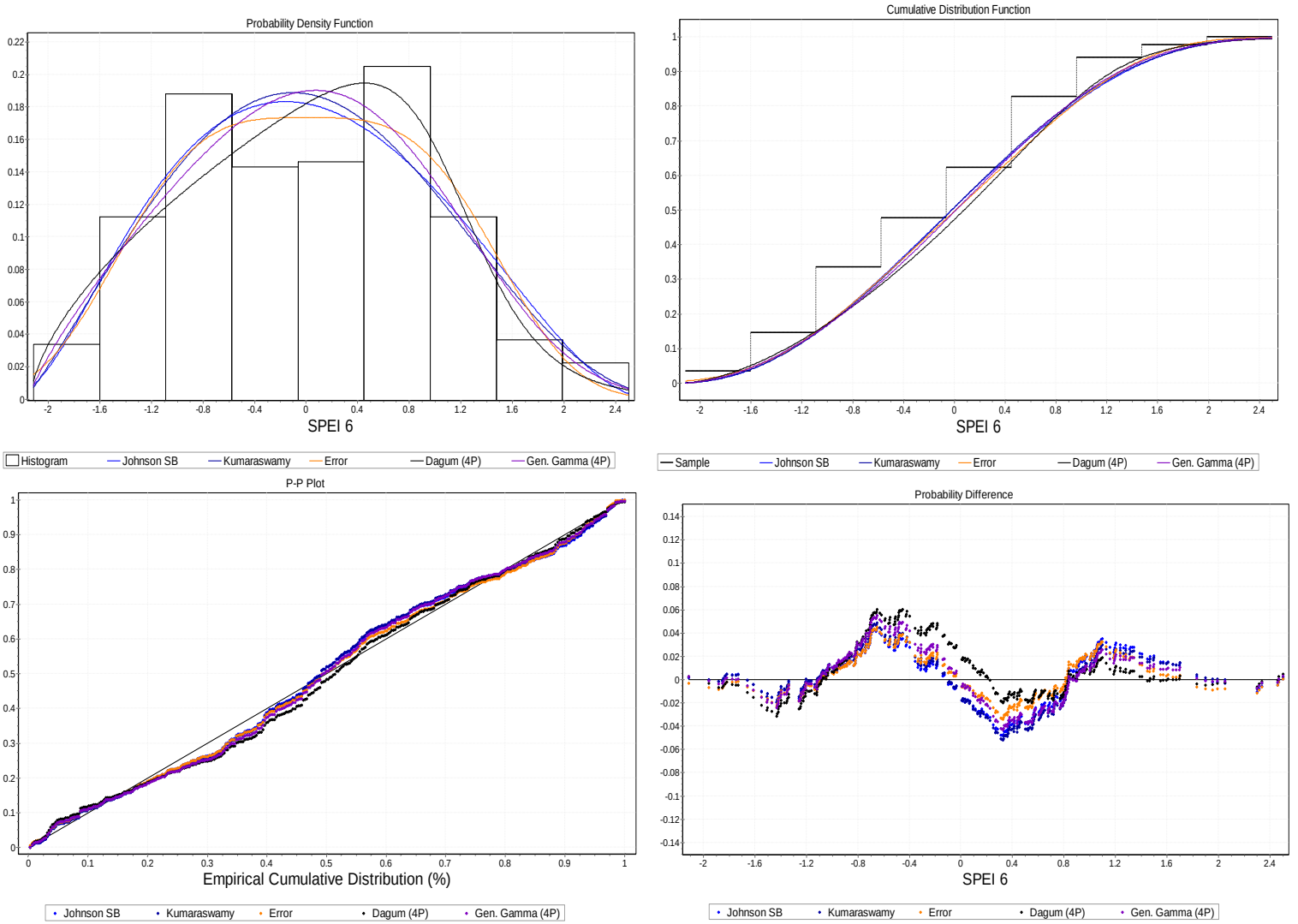

Figure C1: Anderson-Darling test results for SPEI 6.

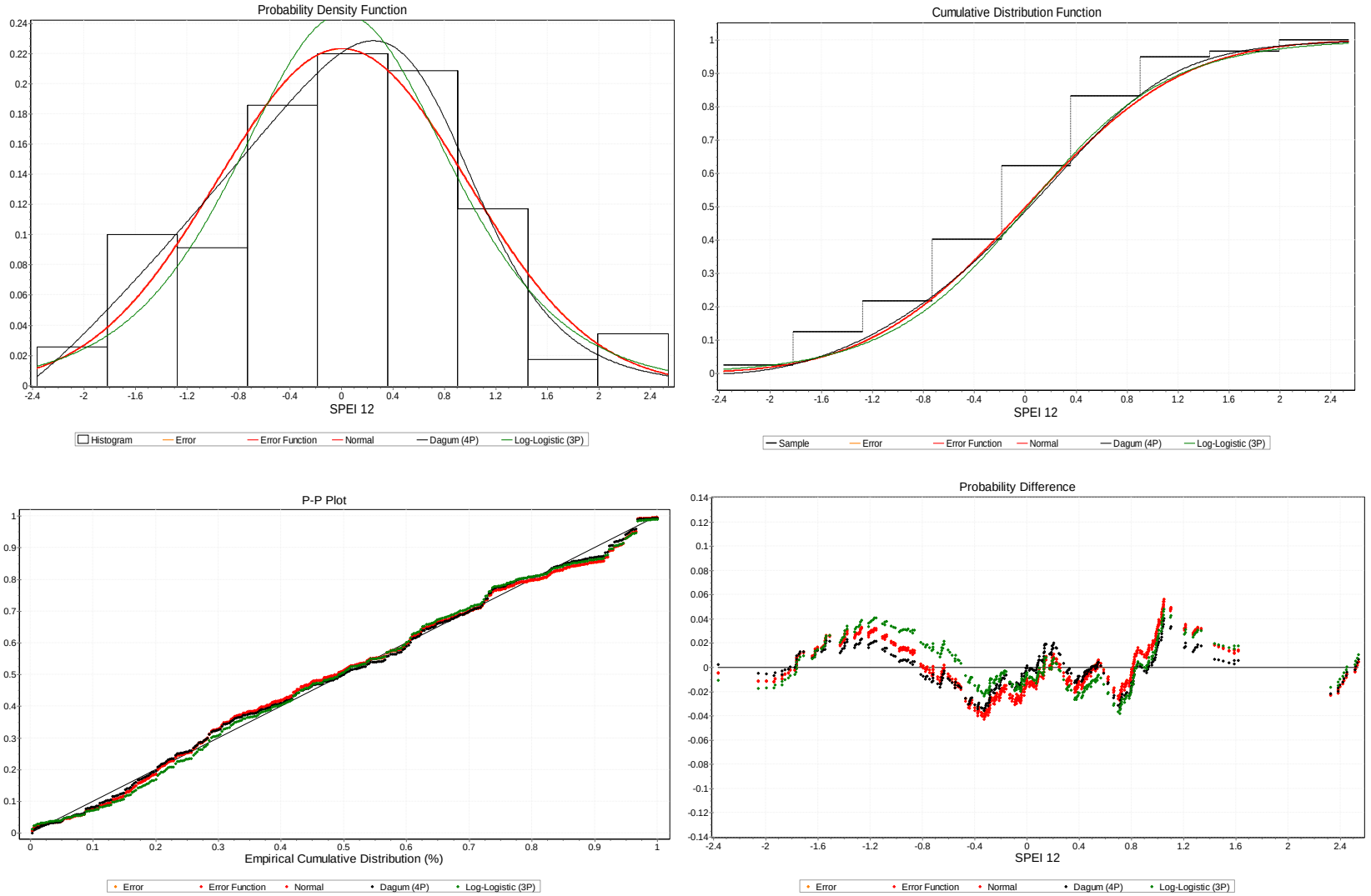

Figure C2: Anderson-Darling test results for SPEI 12.

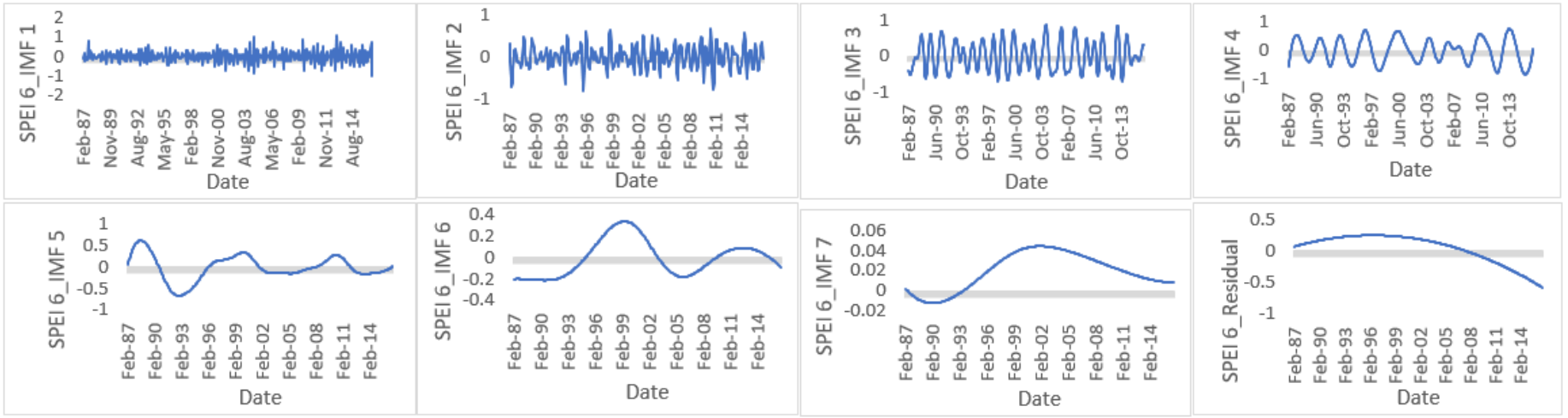

Figure C3: Sample IMFs for SPEI 6

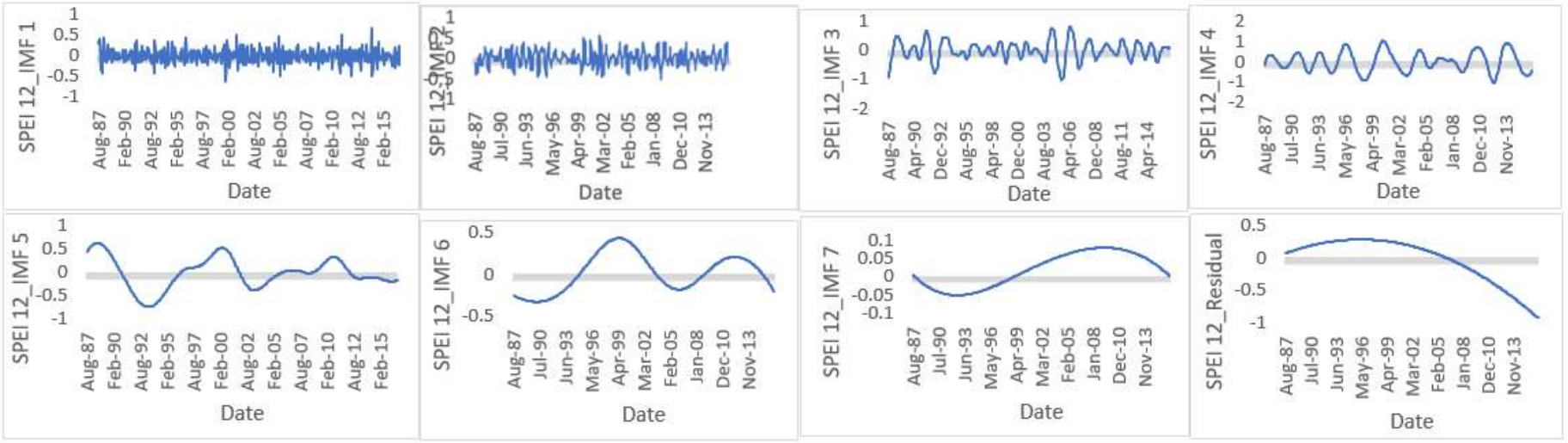

Figure C4: Sample IMFs for SPEI 12.

Figure C5: Sample gradient boosting for variable of importance (SPEI 6).

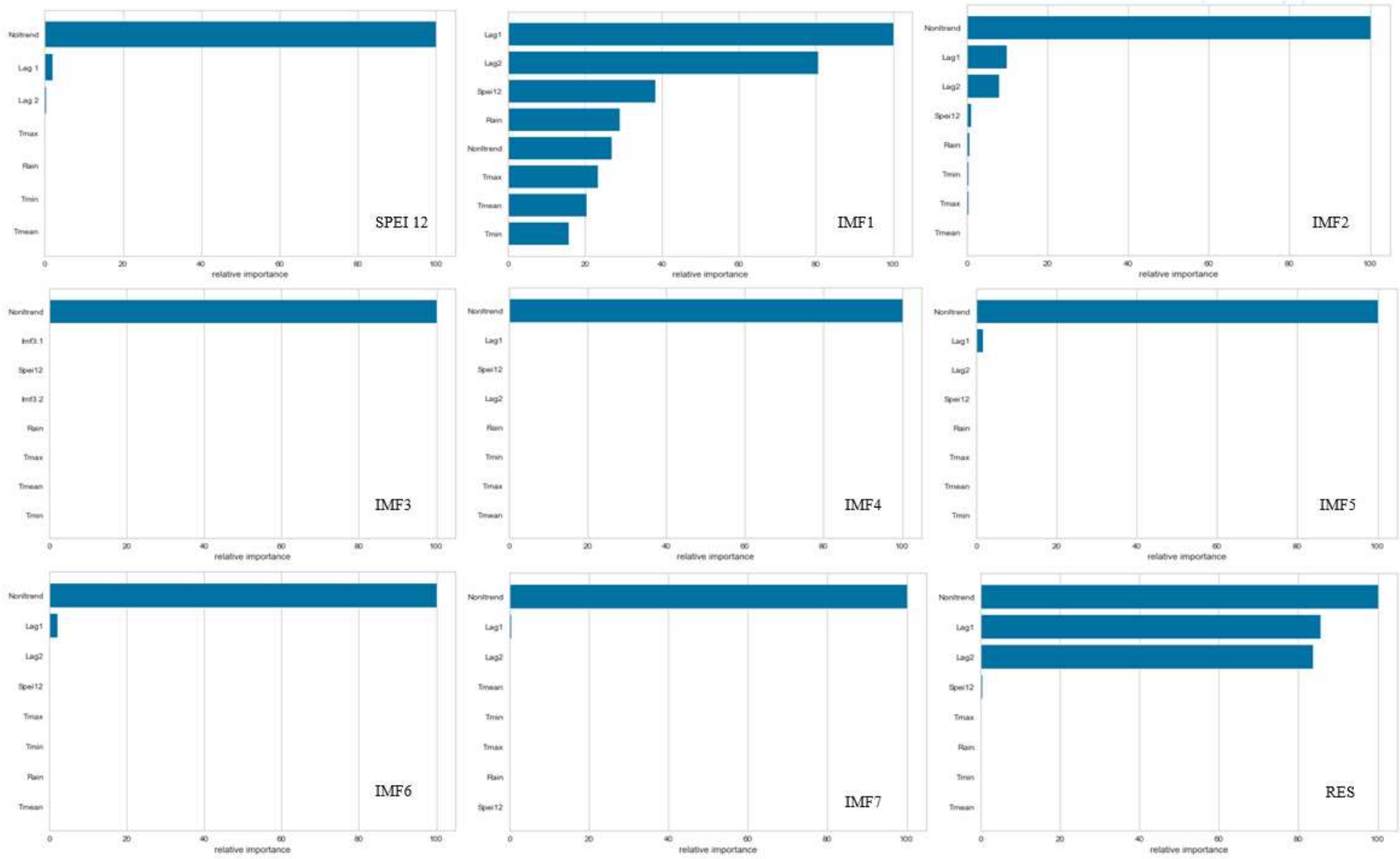

Figure C6: Sample gradient boosting for variable of importance (SPEI 12).

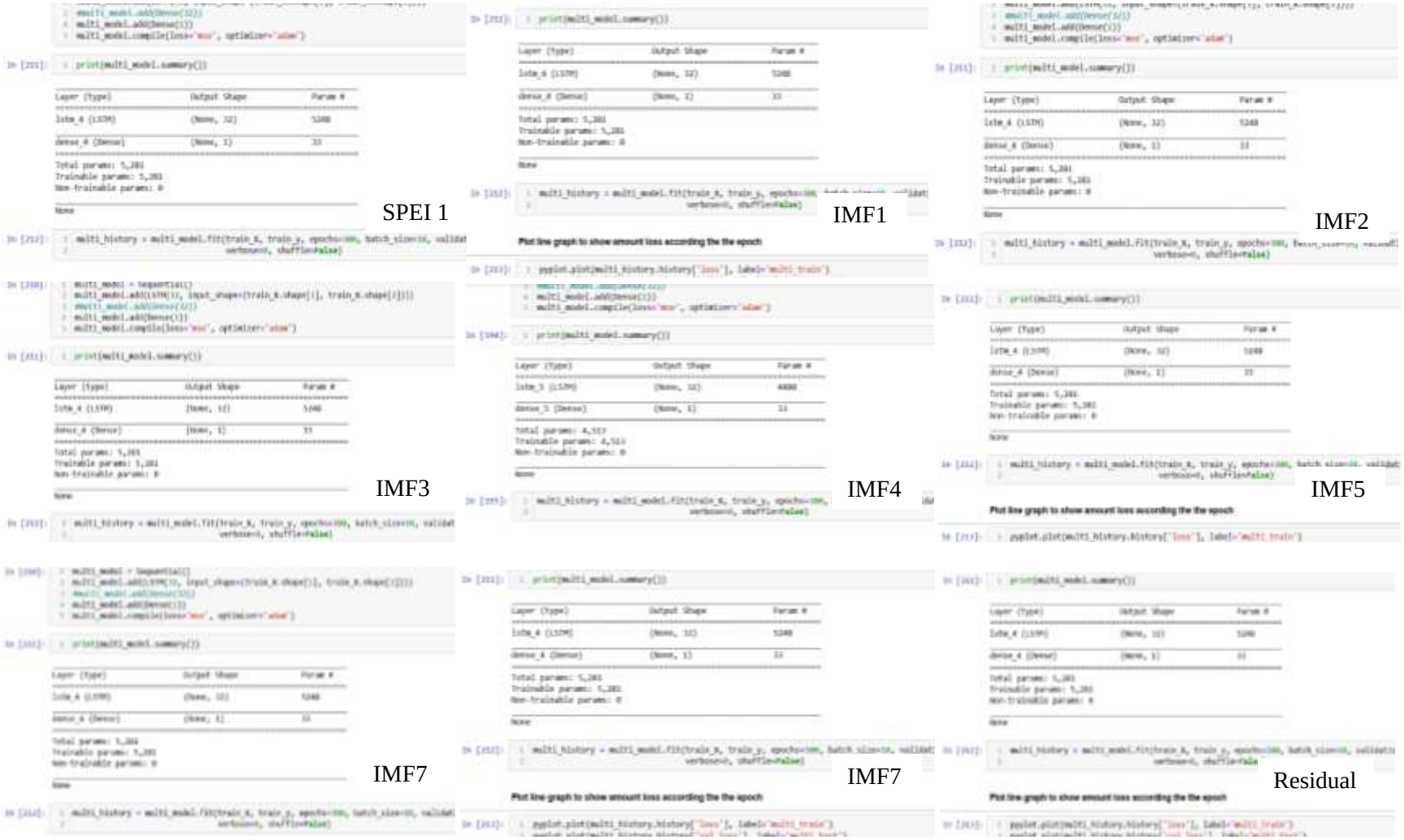

Figure C7: LSTM model summary for SPEI 1.

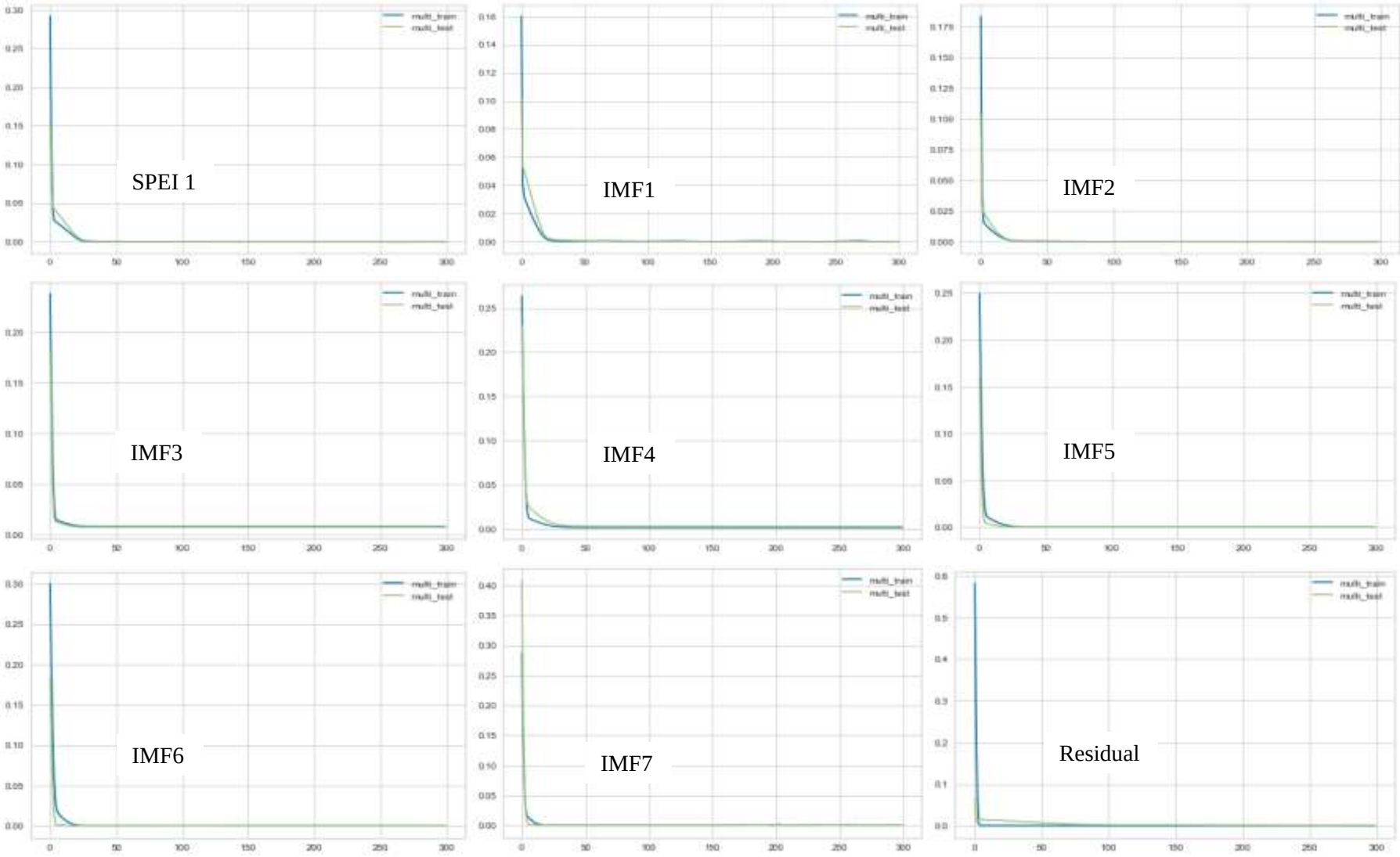

Figure C8: LSTM learning curve at SPEI 1.

Figure C9: LSTM model summary for SPEI 6.

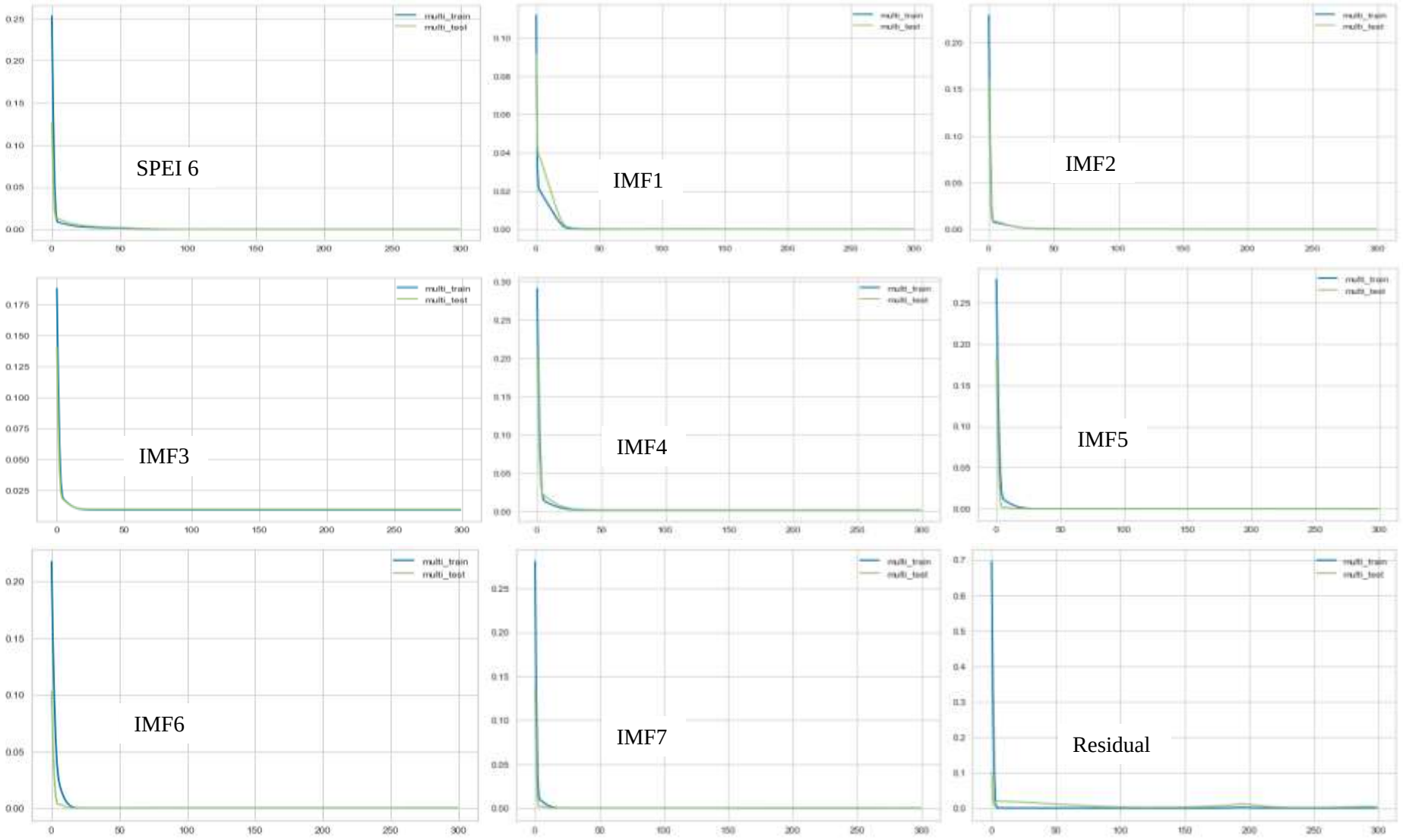

Figure C10: LSTM learning curve at SPEI 6.

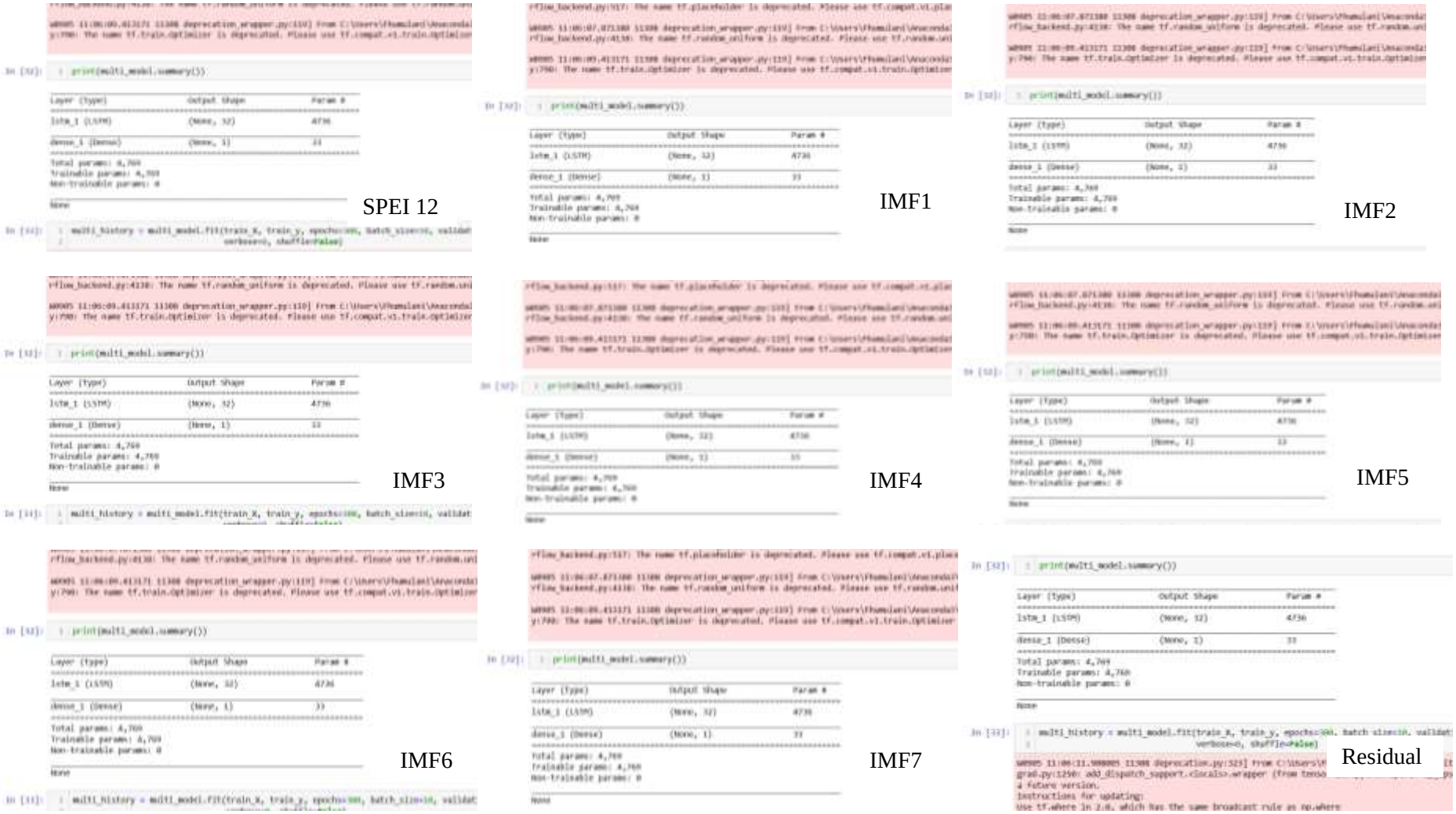

Figure C11: LSTM model summary for SPEI 12.

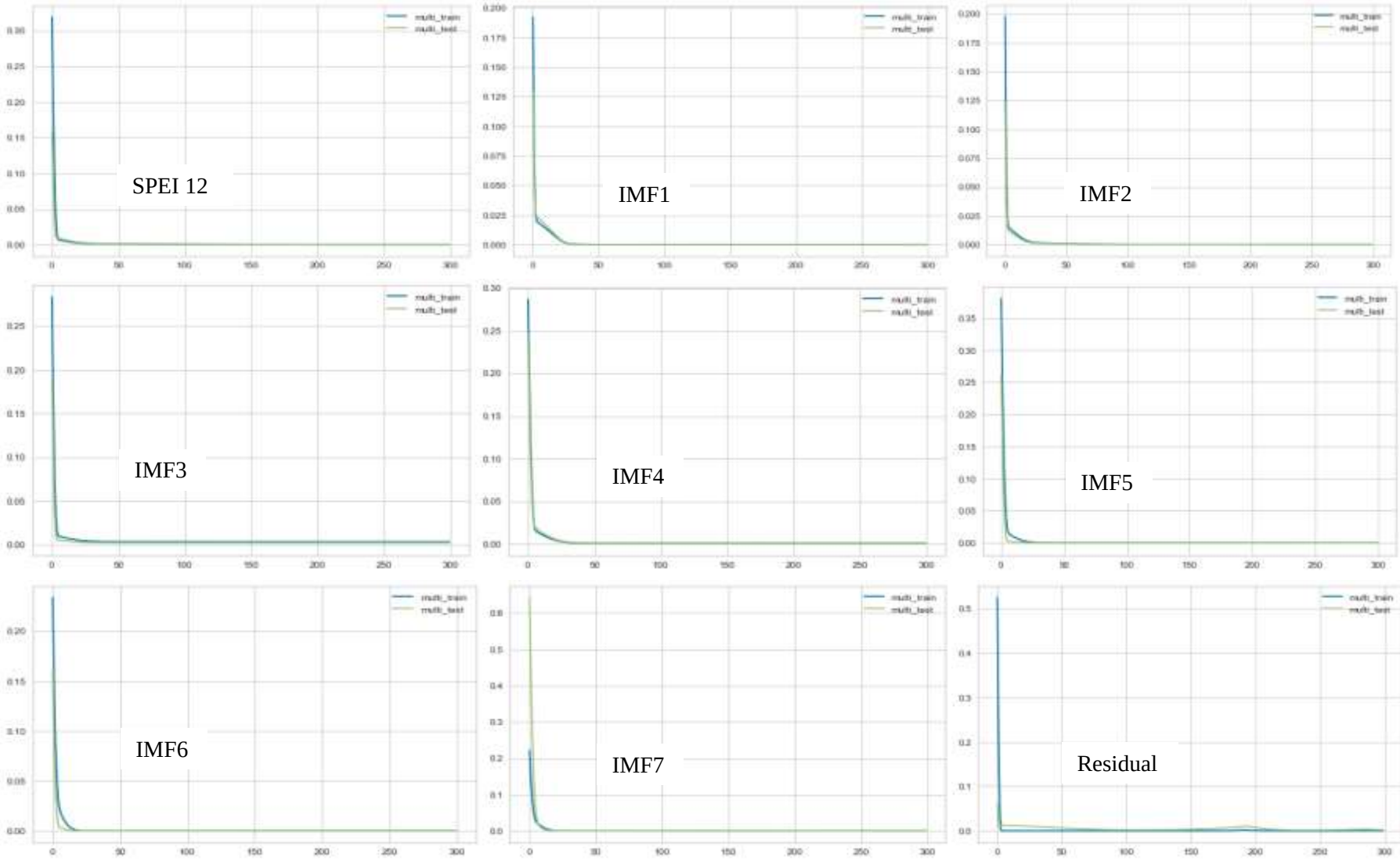

Figure C12: LSTM learning curve at SPEI 12.